MODELING OF ENHANCED COALBED METHANE RECOVERY FROM AMASRA COALBED IN ZONGULDAK COAL BASIN

ÇAĞLAR SINAYUÇ

JULY 2007

MODELING OF ENHANCED COALBED METHANE RECOVERY FROM
AMASRA COALBED IN ZONGULDAK COAL BASIN

A THESIS SUBMITTED TO
THE GRADUATE SCHOOL OF NATURAL AND APPLIED SCIENCES
OF
MIDDLE EAST TECHNICAL UNIVERSITY

BY

ÇAĞLAR SINAYUÇ

IN PARTIAL FULFILLMENT OF THE REQUIREMENTS
FOR
THE DEGREE OF DOCTOR OF PHILOSOPHY
IN
PETROLEUM AND NATURAL GAS ENGINEERING

JULY 2007

Approval of the thesis:

**"MODELING OF ENHANCED COALBED METHANE RECOVERY
FROM AMASRA COALBED IN ZONGULDAK COAL BASIN"**

submitted by **ÇAĞLAR SINAYUÇ** in partial fullfillment of the requirements for
the degree of **Doctor of Philosophy** in **Petroleum and Natural Gas
Engineering** by,

Prof. Dr. Canan ÖZGEN   _____
Dean, Graduate School of **Natural and Applied Sciences**

Prof. Dr. Mahmut PARLAKTUNA.   _____
Head of Department, **Petroleum and Natural Gas Engineering**

Prof. Dr. Fevzi GÜMRAH   _____
Supervisor, **Petroleum and Natural Gas Engineering, METU**

Examining Committee Members:

Prof. Dr. Ender OKANDAN   _____
Petroleum and Natural Gas Engineering, METU

Prof. Dr. Fevzi GÜMRAH   _____
Petroleum and Natural Gas Engineering, METU

Prof. Dr. Mahmut PARLAKTUNA   _____
Petroleum and Natural Gas Engineering, METU

Prof. Dr. Tevfik GÜYAGÜLER   _____
Mining Engineering, METU

Prof. Dr. Ülkü MEHMETOĞLU   _____
Chemical Engineering, Ankara University

                    Date: _____

I hereby declare that all information in this document has been obtained and presented in accordance with academic rules and ethical conduct. I also declare that, as required by these rules and conduct, I have fully cited and referenced all material and results that are not original to this work.

Çağlar SINAYUÇ

ABSTRACT

MODELING OF ENHANCED COALBED METHANE RECOVERY FROM AMASRA COALBED IN ZONGULDAK COAL BASIN

SINAYUÇ, Çağlar

Ph.D., Department of Petroleum and Natural Gas Engineering

Supervisor: Prof. Dr. Fevzi GÜMRAH

JULY 2007, 343 pages

The increased level of greenhouse gases due to human activity is the main factor for climate change. CO_2 is the main constitute among these gases. Subsurface storage of CO_2 in geological systems such as coal reservoirs is considered as one of the promising perspectives. Coal can be safely and effectively utilized to both store CO_2 and recover CH_4. By injecting CO_2 into the coal beds, methane is released with CO_2 adsorption in the coal matrix and this process is known as enhanced coal bed methane recovery (ECBM).

Zonguldak Coal Basin is one of the Turkey's important coal resources. Since the coal seams in Bartın-Amasra field are found relatively deeper parts of the basin comparing to other places, this basin was not studied detailed enough yet. Bartın-Amasra basin was found convenient for enhanced coalbed methane recovery. The lithologic information taken from the Turkish Hard Coal Enterprise (TTK) was

examined and the depths of the coal seams and the locations of the wells were visualized to perform a reliable correlation between seams existed in the area. According to the correlations, 63 continuous coal layers were found. A statistical reserve estimation of each coal layer for methane was made by using Monte Carlo simulation method. Uncertainty is an important parameter in risk analysis, for this reason the results were determined at probabilities of P10, P50 and P90.

Enhanced coalbed methane recovery was simulated with CMG-GEM module using Coal Layer #26 which has more initial gas in place. The effects of adsorption, cleat spacing, compressibility, density, permeability, permeability anisotropy, porosity and water saturation parameters were examined in enhanced coalbed methane recovery by the simulation runs.

The initial methane in place found in all these coal layers both in free and adsorbed states were estimated using probabilistic calculations resulted in possible reserve (P10) of 72.97 billion scf, probable reserve (P50) of 47.74 billion scf and proven reserves (P90) of 30.46 billion scf. Since the Amasra coal reservoir is not saturated with water, almost 10% of the total gas in place was found to be in the cleats as free gas. Coal layer #26 has an area of 4099 acres, average thickness of 6.23 ft and depth of 545 m (Karadon formation). P50 reserve estimation was 6.47 billion scf in matrix and 0.645 billion scf in fracture.

Although the decrease in cleat porosity was less when shrinkage and swelling effects included, the decrease in cleat permeability as a function of porosity diminished the methane production. Cumulative methane production was enhanced with the injection of carbon dioxide (ECBM) approximately 23% than that of CBM recovery. Although closing the wells to production because of CO_2 breakthrough had a negative effect on methane production initially, there was no difference between ultimate methane productions whether the wells remained open or closed, but more carbon dioxide was sequestered when the production ceased at the wells.

Injected carbon dioxide amount of 5192 tonnes/year in base case was only capable to sequester only 0.3% of the yearly carbon dioxide emission of Zonguldak Çatalağzı Power Plant nearby. Considering the gas in place capacity of the coal layer #26 as 15% of the resource area-A, it can be said that the project aiming ECBM recovery rather than carbon dioxide sequestration would be successful. In spite of water saturated coal reservoirs where the water production is required initially, it can be possible to start immediately the injection of CO_2 with methane production for a dry coal reservoir.

Cleat permeability being one of the most crucial parameter in the coal reservoir affected the rate of methane production. The more free gas was found in higher porosity cleat systems. Although the cumulative methane production was increased when the cleat porosity rose, methane recovery percentages were remained almost constant. The lower the cleat spacing the higher the rate of transfer between fracture and matrix was observed. The rate of gas desorption from the coal matrix and subsequent diffusion to both butt and face cleats was higher than the rate of flow in the face cleats, then production was flow-limited, pressure-driven and was defined by Darcy's Law.

The cumulative CH_4 production was higher when the coal was denser. The change in coal compressibility affected slightly the cleat porosity and therefore the cleat permeability due to the change in reservoir pressure. Langmuir volume is defined as maximum adsorption capacity. Kozlu formation (deeper than Karadon formation) having lower Langmuir volume resulted in higher ultimate recovery because of lower Langmuir pressure than that of Karadon formation. In base case (Karadon formation), although the higher Langmuir volume was used, less methane production was observed. Permeability anisotropy generated the CO_2-CH_4 front in elliptic shape.

Keywords: Coalbed Methane, Enhanced Coalbed Methane, Carbon dioxide Sequestration, Zonguldak

ÖZ

ZONGULDAK KÖMÜR HAVZASI AMASRA KÖMÜR YATAĞINDAN GELİŞTİRİLMİŞ METAN GAZI ÜRETİMİNİN MODELLENMESİ

SINAYUÇ, Çağlar

Doktora, Petrol ve Doğal Gaz Mühendisliği Bölümü

Tez Yöneticisi: Prof. Dr. Fevzi GÜMRAH

TEMMUZ 2007, 343 sayfa

İnsan kaynaklı sera gazlarının artması iklim değişikliğinin ana nedenidir. CO_2 bu gazlar içerisinde başlıcasıdır. Karbon dioksitin kömür gibi jeolojik yapılar içerisinde depolanması umut verici bir yöntemdir. Kömür, karbon dioksitin güvenli olarak depolanması ve metan üretimi için kullanılabilir. Karbon dioksitin kömür damarlarına basılması ile metan serbest kalırken CO_2 kömür matrikslerinde tutunmaktadır. Bu işleme geliştirilmiş kömür yatağı metan üretimi denilmektedir (ECBM).

Zonguldak Kömür Havzası Türkiye'nin en önemli kömür kaynaklarından birisidir. Bartın-Amasra sahasındaki kömür damarları göreceli olarak diğer bölgelere göre daha derinde olduğundan şimdiye kadar detaylı olarak incelenememiştir. Bartın-Amasra sahasının bir bölümü ECBM için uygun bulunmuştur. Türkiye Taş Kömürü Kurumundan (TTK) alınan litolojik bilgiler kullanılarak kömür damarları

arasında korelasyon derinlik ve kuyu lokasyonları ölçekli hale getirilerek gerçekleştirilmiştir. Bu korelasyona göre devamlılığı olan 63 adet kömür katmanı belirlenmiştir. Monte Carlo simülasyon metodu kullanılarak bu katmanların her birinde istatistiksel metan rezerv tahmini yapılmıştır. Bu gibi risk analizi çalışmalarında belirsizlik önemli bir faktördür. Bu yüzden sonuçlar P10, P50 ve P90 olasılık ihtimallerine göre belirlenmiştir.

CMG-GEM Modulü kullanılarak karbondioksit ile ECBM üretimi 26 nolu kömür katmanı modellenerek gerçekleştirilmiştir. Yapılan simülasyonlar ile gazın kömüre tutunması, çatlak sıklığı, sıkıştırılabilirlik, yoğunluk, geçirgenlik, geçirgenliğin yönlere göre değişimi, gözeneklilik ve su doymuşluğu parametrelerinin değişimlerinin etkileri simülasyon yöntemi ile incelenmiştir.

Belirlenen tüm kömür katmanlarında serbest ve tutunmuş olarak bulunan yerinde gaz miktarı tahminsel hesaplamalar ile 2.07 milyar m^3 mümkün rezerv (P10), 1.35 milyar m^3 olası rezerv (P50) ve 0.86 milyar m^3 kanıtlanmış rezerv olarak tahmin edilmiştir. Amasra kömür rezervi su ile doygun olmadığından, toplam yerinde gaz miktarının yaklaşık %10'luk bir kısmı çatlaklarda serbest gaz olarak bulunmuştur. 26 nolu kömür katmanı 16.6 km^2'lik bir alana, 1.9 m ortalama kalınlığa ve 545 m ortalama derinliğe sahiptir ve Karadon formasyonunda bulunmaktadır. P50 rezerv tahmini matrikste 0.18 milyar m^3 ve çatlakta 0.018 milyar m^3 olarak yapılmıştır.

Çatlak gözenekliliğindeki azalma, sıkışma ve şişme etkileri eklendiğinde daha az olmakla beraber, çatlak gözenekliliğine bağlı olarak çatlak geçirgenliğinde oluşan düşüş metan üretimini de azaltmıştır. Karbon dioksit basılması ile metan üretimi CBM üretimine göre %23 oranında daha yüksek gerçekleşmiştir. CO_2 üretiminin başlamasıyla üretim kuyularının kapatılmasının metan üretimine başlangıçta olumsuz etkisi olmakla beraber, kuyuların kapalı veya açık kalması arasında nihai metan üretimi açısından bir fark bulunmamıştır. Ancak üretimin kesilmesi daha fazla CO_2'in bertaraf edilmesini sağlamıştır.

Referans durumda basılan yıllık 5192 ton karbon dioksit ile Zonguldak Çatalağzı Santralının yıllık karbon dioksit emisyonunun sadece % 0.3'lük bir kısmı bertaraf edilebilmiştir. 26 numaralı kömür katmanı yerinde gaz kapasitesinin Amasra A bölgesi toplam kapasitesinin %15'i kadar olması nedeniyle, karbon dioksit depolanması yerine ECBM üretimini hedefleyen bir proje daha uygun bulunmuştur. İlk aşamada su üretimi gerektiren suya doygun kömür rezervlerinin aksine, kuru kömür rezervuarlarında karbon dioksit basılmasına metan üretimi başlar başlamaz geçilebilmiştir.

Çatlak geçirgenliği, kömür rezervlerinin en önemli parametrelerinden biri olarak, metan üretim debisini etkilemiştir. Çatlak gözenekliliği yüksek olan sistemlerde daha fazla serbest gaz olduğu gözlemlenmiştir. Çatlak gözenekliliğindeki artışla beraber toplam metan üretiminin artmasına rağmen, metan üretim yüzdeleri değişmemiştir. Çatlak sıklığı ne kadar az olursa çatlak ile matriks arasındaki akış hızı o denli yüksek olur. Kömür matriksinden gaz salınım hızı ve sonrasında 'butt' ve 'face' olarak adlandırılan çatlaklara difüzyon hızı çatlaktaki akış hızından daha fazla olduğundan üretim akışla sınırlı ya da basınç yönlendirmeli olmuştur ve Darcy kanunu ile tanımlanmıştır.

Kömür yoğunluğu daha fazla olduğunda metan üretimi daha fazla olmuştur. Kömürün sıkıştırılabilirliğindeki değişiklik rezerv basıncındaki değişiklik ile çatlak gözenekliliğini ve dolayısıyla çatlak geçirgenliğini çok az etkilemiştir. Langmuir hacmi maksimum tutunma kapasitesi olarak tanımlanmaktadır. Kozlu formasyonu (Karadon formasyonundan daha derin) daha az Langmuir hacmine sahip olmasına rağmen Langmuir basıncı Karadon formasyonuna göre daha az olduğundan daha fazla nihai metan üretimi olmuştur. Referans durumda (Karadon formasyonu), daha yüksek bir Langmuir hacmi olmasına rağmen, daha az metan üretimi gerçekleşmiştir. Geçirgenliğin yöne bağlı olarak değişmesi durumunda CO_2-CH_4 cephesi elips şeklinde gelişmiştir.

Anahtar Kelimeler: Kömür Yatağı Gazı, Geliştirilmiş Kömür Yatağı Gazı, Karbon dioksit Bertarafı, Zonguldak

To My Family

ACKNOWLEDGMENTS

TABLE OF CONTENTS

LIST OF TABLES

LIST OF FIGURES

LIST OF SYMBOLS

A Cross sectional area, sq ft or m^2

A_c Field area, acre

b Langmuir constant, psia^{-1}

B Slippage factor, psia or kPa

B_{gi} Gas formation volume factor at initial pressure, Mscf/rcf

c_f Pore volume compressibility, 1/psia

C Concentration, lbm-mol/cu ft or kmol/m^3

C_{gi} Initial sorbed gas concentration (dry, ash-free coal), scf/ton

D Diffusivity coefficient, sq ft/D or m^2/s

GtC   Giga Tonne Carbon (1×10^9 tonnes carbon)

h Coal thickness, ft

f_a Ash content, fraction

f_m Moisture content, fraction

k Permeability, md

K Bulk modulus, psia

L Length, ft or m

m_c Mineral matter content, weight fraction (dry)

M Hydraulic conductivity

M Axial modulus, psia

MW Molecular weight, lbm/lbm-mol or kg/kmol

MtC   Mega Tonne Carbon (1×10^6 tonnes carbon)

nc Number of components

G_i Gas in place at initial reservoir conditions, Mscf

G_s Gas storage capacity, scf/ton

G_{si} Multicomponent gas storage capacity of component i, in-situ basis, scf/ton

p	Pressure, psia
$\bar{p}$	Mean pressure, psia
r_c	Capillary radius, ft
P_L	Langmuir pressure constant, psia
R	Gas constant, $10.73 \frac{psi \cdot cu\,ft}{lbm\,mol \cdot °R}$
s_c	Sulfur content, weight fraction (dry)
s_f	Cleat spacing, ft
S_{wfi}	Interconnected fracture water saturation, fraction
q	Volumetric flow rate, cu ft/D or m³/s
Q	Mass flow rate, lbm/D or kg/s
T	Temperature, °R or K
V_L	Langmuir volume constant, scf/ton
V_{Li}	Pure component Langmuir storage capacity of component i, dry, ash-free basis, scf/ton
V_m	Total matrix volume, scf
y	Mole fraction in the free gas (vapor) phase, dimensionless

Greek Letters

∂, d	Partial and total derivative symbol
Δ	Difference operator
μ	Dynamic viscosity, cp or Pa·s
$\bar{\lambda}$	Mean free path, cm or inch
τ	Sorption time, days
$\emptyset$	Effective porosity, fraction
ρ	Density, g/cc
ϵ_L	Strain at infinite pressure
ϑ	Poisson's ratio

Subscript

a	Apparent
ads	Adsorbed gas
c	Coal
f	Fracture
$free$	Free gas
i	Initial
i,j	Index
m	Matrix
∞	Infinite pressure

CHAPTER 1

INTRODUCTION

Global emissions of greenhouse gases (GHG), including carbon dioxide, methane and nitrous oxides, are increasing. These gases accumulate in the earth's atmosphere, trapping heat that could escape into the outer space. Most GHG (with the exception of chlorofluorocarbons and hydro fluorocarbons) originate from the use of fossil fuels, such as oil, gas, and coal, in factories, vehicles, and generating plants. Excluding water vapor, CO_2 from combustion of fossil fuels is the largest single source of anthropogenic GHG emissions (Gentzis, 2000).

World industrial development over the last two centuries has very largely been based on fossil fuels, with their ready availability, ease of use and high energy contents. As adverse environmental effects became clear, new technologies would be developed to counter them. Techniques were developed to reduce emissions of such noxious materials as particulates, sulphur dioxide and carbon monoxide. However, for most of that period it was assumed that the venting of carbon dioxide into the atmosphere was environmentally harmless. It has been only recently, with the advent of fears about climate change that attention has turned to ways of reducing emissions of carbon dioxide (Grimston et al, 2001).

To stabilize the atmospheric concentration of greenhouse gases, a huge reduction of carbon dioxide emissions is required. Although some people believe that this necessitates a considerable reduction in the use of fossil fuels or fuel switching, other options are available that allow the use of fossil fuels and reduce atmospheric emissions of CO_2. Reduction of anthropogenic CO_2 emissions into the atmosphere can be achieved by a variety of means, i.e. reducing energy intensity, reducing carbon intensity and carbon sequestration. The issue of GHG

emissions reduction is complex and requires innovative solutions. GHG emission reductions can be achieved by either reducing fossil fuel use or by using various sinks for long-term GHG storage (Gentzis, 2000).

Although, it has received relatively little attention as a potential method of combating climate change in comparison to energy reduction measures and development of carbon-free energy technologies, sequestration of carbon dioxide in geologic or biospheric sinks has enormous potential. Available technologies, especially of separating and capturing the carbon dioxide from waste stream, have high costs at present, perhaps representing an additional 40–100% onto the costs of generating electricity. In most of the world there are no mechanisms to encourage firms to consider sequestration. Considerable research and development is required to bring down the costs of the process, to elucidate the environmental effects of storage and to ensure that carbon dioxide will not escape from stores in unacceptably short timescales. However, the potential of sequestration should not be underestimated as a contribution to global climate change mitigation measures (Grimston et al, 2001).

Long-term storage of CO_2 can be accomplished by separating CO_2 from flue gases and subsequently injecting it into active or depleted oil and gas fields with enhanced oil recovery (EOR), deep saline aquifers, gas-rich shales, methane hydrate formations, salt caverns, unmineable coalbeds, other geological formations, or the ocean. The successful sequestration strategy will take advantage of most, if not all, of these potential sinks. Oceanic sequestration may be a viable option for the storage of CO_2 from large, stationary sources near the coast; however, it is probably not the best option for CO_2 from sources in the continental interior. Geological sequestration is probably the best option for CO_2 from those sources. Among the geological sequestration options, those that allow the production of a value-added product such as methane (CH_4) or petroleum are the options that are the most attractive and will likely be developed first. These value-added processes include sequestration of CO_2 in gassy coalbeds with the simultaneous recovery of CH_4 and EOR with CO_2. Some of the technologies for

emissions reduction using the above sinks have been applied in the past (mature), while others are in an embryonic stage (immature). Mature technologies include the use of CO_2 in materials and in energy for enhanced oil recovery or EOR purposes. Immature technologies include the use of CO_2 for enhanced gas recovery and the production of biomass fuels. Sequestration of CO_2 from fossil fuel combustion in the subsurface could prevent the CO_2 from reaching the surface for millions of years. Geological sequestration of CO_2 in deep aquifers or in depleted oil and gas reservoirs is a mature technology. Despite the huge quantities of CO_2 that can be sequestered in this way, this approach do not provide any economic benefit (Gentzis, 2000).

CO_2 capture and geological storage could provide a significant Greenhouse Gas (GHG) mitigation option if the cost of capture can be reduced and the public can be assure that geological storage is safe, measurable and verifiable (Wright et al, 2004).

When combusted, methane emits the least amount of CO_2 per unit of energy released among all the fossil fuels. Therefore, there is a synergy between CO_2 sequestration and production of methane that leads to greater utilization of coalbed resources for both their sequestration ability and energy content (Zhu et al, 2003).

Coalbed methane has been recognized as a significant natural gas resource for a long time, (Wei et al, 2005). Coalbed Methane is truly an unconventional gas resource. The most obvious difference between CBM and conventional gas reservoirs is in the gas storage mechanism. Coalbed methane (CBM) reservoirs hold gas primarily as a sorbed phase at liquid-like densities within the micro porous matrix of the coal, not as a free gas as in conventional gas reservoirs. In CBM some free gas exists in the natural fractures or cleats of the coal, but this gas represents only a small fraction of the total gas. CBM recovery is, therefore, primarily recovery of desorbing gas. Desorption maybe accomplished by lowering the overall pressure of the reservoir, as in conventional recovery, or by lowering

the partial pressure of methane in the free gas by injecting a second gas, as in enhanced recovery (Chaback et al, 1996; Roadifer et al, 2003).

Waste CO_2 from CBM-fueled power plants could be injected into CBM reservoirs to produce more methane for the power plant. The 2:1 coal-sorption selectivity for CO_2 over CH_4 supports the feasibility of operating fossil-fueled power plants without atmospheric CO_2 emissions (Gentzis, 2000). Although the CO_2-Enhanced Coalbed Methane technology is being developed in North America, in the future it would have the greatest potential in countries where coal is abundant and natural gas is a high-valued commodity (Wong et al, 2001).

In primary recovery methods, generally by pumping off large volumes of formation water reservoir pressure are lowered and methane desorption from the coal is elicited. Primary production of coalbed methane recovers only 20% to 60% of original gas-in-place, depending on coal seam permeability, gas saturation, and other reservoir properties. Well spacing and other operational practices also will affect recovery efficiency. Primary recovery thus bypasses a sizeable gas resource. New technologies have been proposed for enhanced coalbed methane recovery (ECBM) to recover a larger fraction of gas in place. The two principle variants of ECBM are inert gas stripping using nitrogen injection and displacement desorption employing carbon dioxide injection. Injected CO_2 is preferentially adsorbed (and remains sequestered within the seam) at the expense of the coalbed methane, which is simultaneously desorbed and thus can be recovered as free gas. Nitrogen injection ECBM works using a different physical process by lowering the partial pressure of methane to elicit desorption (Stevens and Riemer, 1998).

As CO_2 is injected into a coal reservoir, it is preferentially adsorbed into the coal matrix, displacing the methane that exists in that space. The displaced methane then diffuses into the cleat system, and migrates to and is produced from production wells. The use of CO_2 for CBM recovery would have the same effect as enhanced oil recovery and is classified as an enhanced coal bed methane recovery (ECBM) method. Coalbeds have large internal surface area and strong

affinity for certain gas species such as CH_4 and CO_2. In CBM reservoirs, most of the total gas exists in an adsorbed state at liquid-like density. Only a small amount of the total gas is in a free phase. Primary recovery using depressurization induces desorption of the CBM by lowering the overall pressure of the reservoir. Primary recovery factors are roughly 50%. Enhanced recovery of coalbed methane (ECBM) by injecting a second gas maintains the overall reservoir pressure, while lowering the partial pressure of CBM in the free gas. Injectants also sweep desorbed gas through the reservoir. Nitrogen is a natural choice as an injection gas because of its availability. Carbon dioxide is also promising because of the additional benefit of greenhouse gas sequestration (Zhu et al, 2003).

In the CO_2-ECBM process, CO_2 is injected and adsorbed into the subsurface coal matrix. The adsorption of CO_2 and displacement of methane are dependent on coal grade, type and especially on coal rank, which represents the maturation of coal, ranging from peak to anthracite (Jikich et al, 2004).

The key reservoir screening criteria for successful application of CO_2-ECBM include laterally continuous and permeable coal seams, concentrated seam geometry, and minimal faulting and reservoir compartmentalization (Stevens and Riemer, 1998). Enhanced coalbed methane reservoir performance is controlled by a complex set of reservoir, geologic, completion and operation parameters and the inter-relationships between those parameters. In order to identify, analyze and mitigate risks associated with any CBM prospect, one must first understand the relative importance of each of these parameters, how their relative importance changes under different constraints, and how they interactively affect ECBM production (Roadifer et al, 2003).

Since planning and improvement are all based on economics and time limitations of a company, calculations of reserves and producible gas amounts must be performed in time and since it is known that there are uncertainties on the variables of calculations a method must be used to assess the uncertainty. Statistical calculations are widely used to make coal reservoir characterization in

petroleum/mining industry via making a generalization of the gas and rock properties.

The subject of this study was to understand the effects and importance of coal reservoir properties in calculation of gas in place amount and to simulate methane production while sequestering CO_2 into a selected coal seam of lease A in Amasra. The coal seams found in a part of Amasra District of the Zonguldak Basin were correlated using the lithologic information. In order to successfully plan the operations of CO_2 injection and CH_4 production, the continuity of the coal layers were taken into account primarily. Gas-in-place estimated in the area by means of Monte Carlo simulation method. The uncertainties of the parameters lead us to make a risk analysis in the field. Gas in place amount of the seams, in matrix and cleats (fracture) system was calculated by statistical approach. It is not hard to say that there is as much uncertainty as we have few data regarding these variables. To be able to make an economic planning and improvement of coal bed methane (CBM) field, facts and limits must be fully understood and defined in terms of coal reservoir structure and petrophysical properties. CMG/GEM simulator was used to model the methane production while injecting CO_2 into a coal seam by running several scenario.

CHAPTER 2

MITIGATION OF GLOBAL WARMING

2.1 Introduction

In the following sections, the global warming, sources for CO_2 emissions and CO_2 sinks are described in detail.

2.2 Global Warming

Global warming is the increase in the average temperature of the Earth's near-surface air and oceans in recent decades and its projected continuation. Global average air temperature near the Earth's surface raised 0.74 ± 0.18 °C (1.3 ± 0.32 °F) during the past century. Climate models referenced by the Intergovernmental Panel on Climate Change (IPCC) project that global surface temperatures are likely to increase by 1.1 to 6.4 °C (2.0 to 11.5 °F) between 1990 and 2100. The range of values reflects the use of differing scenarios of future greenhouse gas emissions and results of models with differences in climate sensitivity. Although most studies focus on the period up to 2100, warming and sea level rise are expected to continue for more than a millennium even if greenhouse gas levels are stabilized. This reflects the large heat capacity of the oceans. (IPCC, 2007)

Figure 2.1 shows the instrumental record of global average temperatures as compiled by the Climatic Research Unit of the University of East Anglia and the Hadley Centre of the UK Meteorological Office. Data set HadCRUT3 was used which follows the methodology outlined by Brohan et al. (2006). Following the common practice of the IPCC, the zero on this figure is the mean temperature from 1961-1990. (Rohde, 2007)
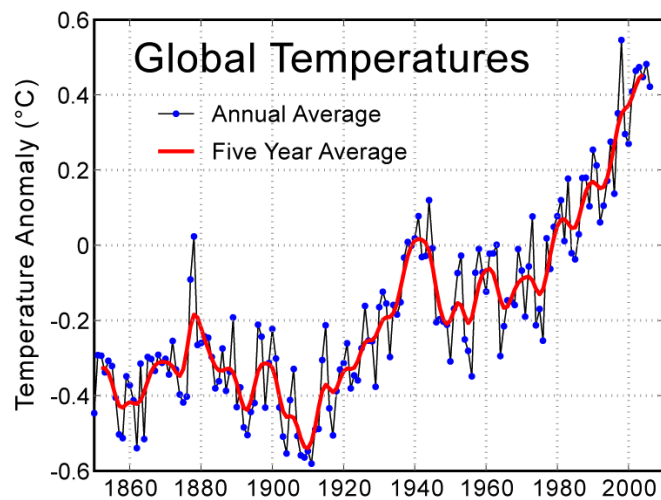
Figure 2.1 Global average temperatures (Rohde, 2007)

Figure 2.2 shows the difference in instrumentally determined surface temperatures between the periods January 1995 through December 2004 and 'normal' temperatures at the same locations, defined to be the average over the interval January 1940 to December 1980. The average increase on this graph is 0.42 °C, and the widespread temperature increases are considered to be an aspect of global warming. (Rohde, 2007)
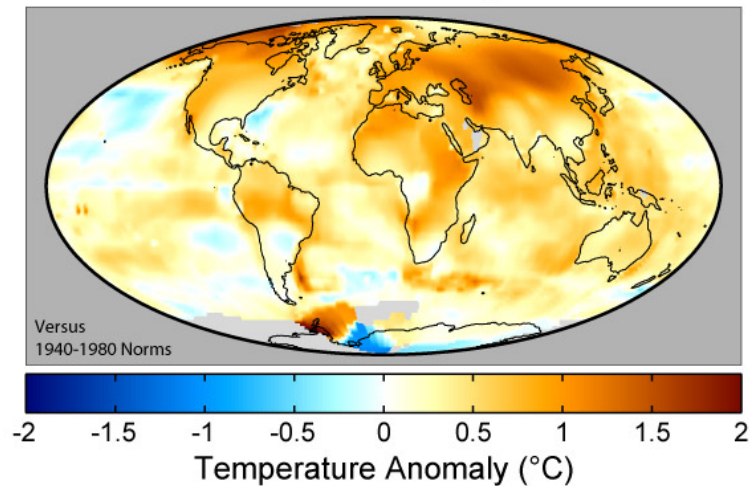
Figure 2.2 Global warming map of 1995-2004 mean temperatures (Rohde, 2007)

2.2.1 The Causes and Results of Global Warming

The climate system varies through natural, internal processes and in response to variations in external forcing factors including solar activity, volcanic emissions, variations in the earth's orbit (orbital forcing) and greenhouse gases. The detailed causes of the recent warming remain an active field of research, but the scientific consensus identifies increased levels of greenhouse gases due to human activity as the main influence. The Intergovernmental Panel on Climate Change (IPCC) concludes, "most of the observed increase in globally averaged temperatures since the mid-20th century is very likely due to the observed increase in anthropogenic (man-made) greenhouse gas concentrations," which leads to warming of the surface and lower atmosphere by increasing the greenhouse effect. This attribution is clearest for the most recent 50 years, for which the most detailed data are available. Contrasting with the scientific consensus, other hypotheses have been proposed to explain some of the observed increase in global temperatures, including: the warming is within the range of natural variation; the warming is a consequence of coming out of a prior cool period, namely the Little Ice Age; or the warming is primarily a result of variances in solar radiation.

An increase in global temperatures can in turn cause other changes, including sea level rise, and changes in the amount and pattern of precipitation. There may also be changes in the frequency and intensity of extreme weather events, though it is difficult to connect specific events to global warming. Other effects may include changes in agricultural yields, glacier retreat, reduced summer stream flows, species extinctions and increases in the ranges of disease vectors. None of the effects of forcing are instantaneous. Due to the thermal inertia of the Earth's oceans and slow responses of other indirect effects, the Earth's current climate is not in equilibrium with the forcing imposed. Climate commitment studies indicate that even if greenhouse gases were stabilized at present day levels, a further warming of about 0.5 °C (0.9 °F) would still occur (Meehl et al, 2005).

2.2.2 Greenhouse Gases

When sunlight reaches the surface of the Earth, some of it is absorbed and warms the Earth. Because the Earth's surface is much cooler than the sun, it radiates energy at much longer wavelengths than does the sun. The atmosphere absorbs these longer wavelengths more effectively than it does the shorter wavelengths from the sun. The absorption of this longwave radiant energy warms the atmosphere; the atmosphere also is warmed by transfer of sensible and latent heat from the surface. Greenhouse gases also emit longwave radiation both upward to space and downward to the surface. The downward part of this longwave radiation emitted by the atmosphere is the 'greenhouse effect' (McGuffie, 2005).

The greenhouse effect was discovered by Joseph Fourier in 1824 and was first investigated quantitatively by Svante Arrhenius in 1896. It is the process by which absorption and emission of infrared radiation by atmospheric gases warms a planet's atmosphere and surface.

Greenhouse gases create a natural greenhouse effect, without which, according to Australian Greenhouse Office mean temperatures on Earth would be an estimated 30 °C (54 °F) lower, so that Earth would be uninhabitable. Thus scientists do not 'believe in' or 'oppose' the greenhouse effect as such; rather, the debate concerns the net effect of the addition of greenhouse gases, while allowing for associated positive and negative feedback mechanisms.

On Earth, the major natural greenhouse gases are water vapor, which causes about 36-70% of the greenhouse effect (not including clouds); carbon dioxide (CO_2), which causes 9-26%; methane (CH_4), which causes 4-9%; and ozone, which causes 3-7%. The atmospheric concentrations of CO_2 and CH_4 have increased by 31% and 149% respectively above pre-industrial levels since 1750. These levels are considerably higher than at any time during the last 650,000 years, the period for which reliable data has been extracted from ice cores. From less direct geological evidence it is believed that CO_2 values this high were last attained

20 million years ago. "About three-quarters of the anthropogenic emissions of CO_2 to the atmosphere during the past 20 years are due to fossil fuel burning. The rest of the anthropogenic emissions are predominantly due to land-use change, especially deforestation." (IPCC, 2007)
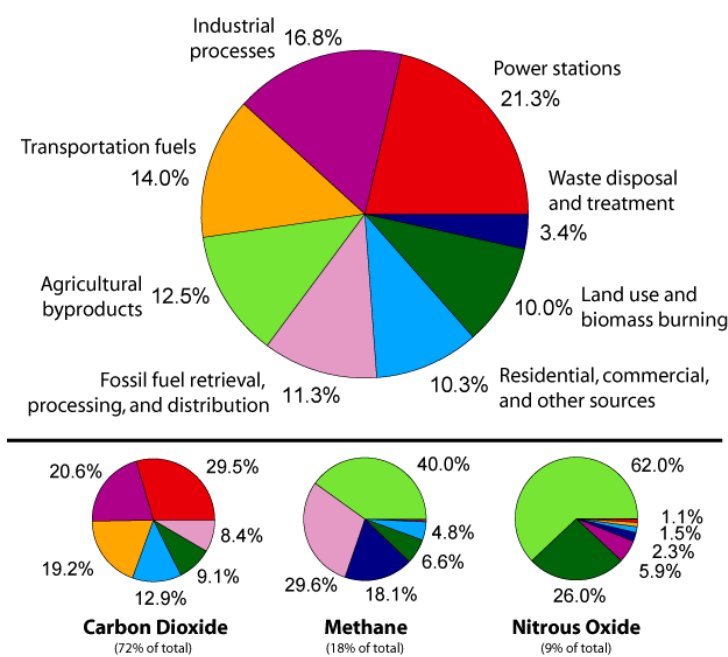
Figure 2.3 Annual man-made greenhouse gas emissions by sector (Rohde, 2007)

Figure 2.3 shows the relative fraction of man-made greenhouse gases coming from each of eight categories of sources, as estimated by the Emission Database for Global Atmospheric Research version 3.2, fast track 2000 project. These values are intended to provide a snapshot of global annual greenhouse gas emissions in the year 2000.

The top panel shows the sum over all greenhouse gases, weighted by their global warming potential over the next 100 years. This consists of 72% carbon dioxide, 18% methane, 8% nitrous oxide and 1% other gases. Lower panels show the comparable information for each of these three primary greenhouse gases, with the same coloring of sectors as used in the top chart. (Rohde, 2007)

The present atmospheric concentration of CO_2 is about 383 parts per million (ppm) by volume (NOAA, 2007).

Future CO_2 levels are expected to rise due to ongoing burning of fossil fuels and land-use change. The rate of rise will depend on uncertain economic, sociological, technological, natural developments, but may be ultimately limited by the availability of fossil fuels. The IPCC Special Report on Emissions Scenarios gives a wide range of future CO_2 scenarios, ranging from 541 to 970 ppm by the year 2100. Fossil fuel reserves are sufficient to reach this level and continue emissions past 2100, if coal, tar sands or methane clathrates (also called methane hydrate) are extensively used. (IPCC, 2007)

2.2.3 Carbon Dioxide Emissions

Average concentrations of CO_2 in the atmosphere reached 358 parts per million by volume (ppmv) in 1994 compared to about 280 ppmv almost 100 years ago (Gentzis, 2000). Emissions of CO_2 will continue to increase over the next decades as overpopulated countries like China and India utilize more and more fossil fuel resources for the production of electrical power (Fyfe et al., 1996).

In the mid-1990s annual carbon dioxide emissions to the atmosphere amounted to 7.4 billion tonnes of carbon (GtC), mostly from fossil fuel combustion. It was estimated that 2.2 GtC were taken up by the oceans and 1.7 GtC by photosynthesis and plant growth, with 3.5 GtC entering the atmosphere as free carbon dioxide (IPCC, 2000).

Fossil-fired power plants emit CO_2 together with other gases such as nitrous oxides (NO_x), oxides sulphur (SO_x), nitrogen (N2), oxygen (O2) and water vapor in the flue gas stream. The CO2 concentration in the flue gas depends on whether the fuel is gas or coal, on particular power station technology and the age of the plant. For example, three fossil-fired power generation technologies such as pulvarized coal fired (PF), natural gas fired combined cycle (NGCC) and

Integrated gasification combined cycle (IGCC) generally release flue gas at different rates per Megawatt hour of electricity produced and have different CO_2 concentration in the flue gas. PF type power plants emit approximately 4 tonnes of flue gas which includes 1 tonne CO_2 per MWh. NGCC type power plants emit 8 tonnes of flue gas. However, CO_2 emission rate is about 0.5 tonnes/MWh. IGCC type power plants emit 9 tonnes of flue gas including 1 tonne of CO_2 per MWh generated (Nguyen and Allinson, 2002).

In 1995 the Intergovernmental Panel on Climate Change produced a 'business as usual' scenario which foresaw annual global emissions of carbon dioxide rising from this 7.4 to 26 GtC in the year 2100. Atmospheric carbon dioxide concentrations would have doubled from pre-industrial revolution levels by 2050, and the rate of increase would grow thereafter.

Similarly, WEC/IIASA (1998) have drawn up three families of scenarios. Even in the most extreme scenario, in which nuclear power undergoes a significant revival and great efforts go into developing and deploying renewables and reducing energy demand, fossil fuels are still producing half of the world's primary energy in 2050, and over 10% more energy than they are today. At the other extreme, more than twice as much energy would be made using fossil fuels as in 1990.

Table 2.1 summarises emissions from the burning of the three principal fossils fuels in different world regions in 1980 and 1998 (IEA, 2000).

Table 2.1 Global carbon dioxide emissions (MtC) by fuel in 1980 and 1998 (Grimston, 2001)

	Natural gas		Oil		Coal		Total	
	1980	1998	1980	1998	1980	1998	1980	1998
North America	339	384	732	771	414	574	1484	1728
Central/South America	22	57	141	180	11	19	173	256
Western Europe	116	206	572	550	335	241	1022	997
Eastern/Central Europe	209	323	415	193	488	284	1111	800
Middle East	53	102	83	159	1	7	137	268
Far East/Oceania	43	144	431	706	503	985	977	1835
Total	812	1264	2432	2658	1807	2202	5051	6124

2.2.4 Mitigation of Global Warming

Remaining scientific uncertainties include the exact degree of climate change expected in the future, and how changes will vary from region to region around the globe. Most national governments have signed and ratified the Kyoto Protocol aimed at combating greenhouse gas emissions.

The broad agreement among climate scientists that global temperatures will continue to increase has led nations, states, corporations and individuals to implement actions to try to curtail global warming or adjust to it. Many environmental groups encourage action against global warming, often by the consumer, but also by community and regional organizations. There has been business action on climate change, including efforts at increased energy efficiency and (still limited) moves to alternative fuels. One important innovation has been the development of greenhouse gas emissions trading through which companies, in conjunction with government, agree to cap their emissions or to purchase credits from those below their allowances.

The world's primary international agreement on combating global warming is the Kyoto Protocol, an amendment to the United Nations Framework Convention on Climate Change (UNFCCC), negotiated in 1997. The Protocol now covers more than 160 countries globally and over 55% of global greenhouse gas emissions. The United States, the world's largest greenhouse gas emitter; Australia; and Kazakhstan have refused to ratify the treaty. China and India, two other large emitters, have ratified the treaty but, as developing countries, are exempt from its provisions.

There is ongoing political and public debate regarding what, if any, action should be taken to reduce or reverse future warming or to adapt to its expected consequences. Mitigation of global warming involves taking actions aimed at reducing the extent of global warming. This is in contrast to adaptation to global

14

warming which involves taking action to minimize the negative effects of global warming.

There are five categories of actions that can be taken to mitigate global warming:

1. Reduction of energy use (per person)
2. Shifting from carbon-based fossil fuels to alternative energy sources
3. Carbon capture and storage
4. Geoengineering including carbon sequestration
5. Birth control, to lessen demand for resources such as energy and land clearing

Strategies for mitigation of global warming include development of new technologies; carbon offsets; renewable energy such as biodiesel, solar power, tidal and ocean energy, geothermal power, and wind power; electric or hybrid automobiles; fuel cells; energy conservation; carbon credits; carbon taxes; enhancing natural carbon dioxide sinks; population control; and carbon capture and storage.

Pacala and Socolow (2004) have proposed a program to reduce CO_2 emissions by 1 billion metric tonnes per year − or 25 billion tonnes over the 50-year period. The proposed 15 different programs, any seven of which could achieve the goal, are:

1. efficient vehicles − increase fuel economy from 30 to 60 mpg for 2 billion vehicles,
2. reduce use of vehicles − improve urban design to reduce miles driven from 10,000 to 5,000 miles per year for 2 billion vehicles,
3. efficient buildings − reduce energy consumption by 25%,
4. improve efficiency of coal plants from today's 40% to 60%,
5. replace 1,400 gigawatts of coal power plants with natural gas,
6. capture and store carbon emitted from 800 gigawatts of new coal plants,
7. capture and reuse hydrogen created by #6 above,

8. capture and store carbon from coal to synfuelsconversion at 30 million barrels per day,

9. displace 700 gigawatts of coal power with nuclear,

10. add 2 million 1 megawatt windmills (50 times current capacity),

11. displace 2,000 gigawatts of coal with solar power (700 times current capacity),

12. produce hydrogen fuel from 4 million 1 megawatt windmills,

13. use biomass to make fuel to displace oil (100 times current capacity),

14. stop de-forestation and re-establish 300 million hectares of new tree plantations,

15. conservation tillage − apply to all crop land (10 times current usage).

The main sources of anthropogenic CO_2 include fossil-fuel utilization, cement production, and land-use changes. Sources of anthropogenic CO_2 can be centralized, as in a power generating station, or diffuse, as in the use of motor vehicles. No single method of CO_2 emissions reductions will be adequate to meet international, national or provincial reduction objectives, since no single method can address the issues related to both large central and diffuse emission generators. Reduction of anthropogenic CO_2 emissions into the atmosphere can be achieved by a variety of means, which has been summarized by Herzog (1998). Three methods can be employed, i.e. reducing energy intensity, reducing carbon intensity and carbon sequestration.

A very attractive and cost effective solution (which will reduce energy intensity) is energy conservation. Solutions are to improve energy and material efficiency or modify industrial processes, which will lead to a lowering of the rate of CO_2 generation. An option to reduce carbon intensity is to increase the use of renewable resources. However, until such energy sources can be developed and applied on a large-scale, fossil energy resources will continue to be the primary energy sources around the globe. During this period, reduction in carbon intensity could be achieved by switching to low carbon alternative fuels (for example switching to natural gas). While most of these options are probably solutions for

the long term, more short and medium term solutions need to be found to deal with the problem of increasing CO_2 emissions. Turkenburg (1997) reported that the issue of emissions reduction is a complex one, and will only be solved by innovative responses that include both reducing the quantities of these gases emitted by anthropogenic activities, and enhancing and using greenhouse gas sinks. For the latter solution, a first step is to describe the attributes of these sinks quantitatively. Reducing CO_2 emissions in order to control the overall levels of CO_2 in the atmosphere has become an international priority in the wake of the Kyoto Protocol. Despite all past and ongoing efforts put into the development of sustainable energy supply, the world still depends heavily on fossil fuels and will continue to do so for years to come. For this reason, technology options are required that will allow for the continued use of fossil fuels without substantial emissions of CO_2. Subsurface storage of CO_2 in geological systems is considered as one promising perspective. This concept can be defended by the basic principle of closed circles: emitted CO_2 originates from fossil fuel, taken from the subsurface, and should therefore be returned to the subsurface.

2.3 Carbon dioxide Sequestration

The term sequestration is used to describe the whole process from separation of the carbon dioxide stream to the final stage of storage/disposal to the selected sink. With exception of the case of vegetative capture of carbon dioxide already in the atmosphere, it therefore consists of three distinct phases.

- Separation of carbon dioxide from the waste stream and capture (S&C), involving carbon removal before combustion, separation of CO_2 from combustion in pure oxygen, and separation of CO_2 from combustion in air.
- Transportation of the carbon dioxide from source to sink.
- Injection and storage of the carbon dioxide in a disposal sink.

Before passing to the application steps of carbon dioxide sequestration it would be useful to describe the properties of CO_2.

17

2.3.1 Properties of Carbon dioxide

The critical point for carbon dioxide is at a temperature of 88 °F (31.18 °C) and a pressure of 1074 psi (73 atm or 7.38 MPa), which is within the range of known reservoir conditions (Figure 2.4) and can be achieved at a depth of only 2480 ft (756 m) under normal hydrostatic pressure. Carbon dioxide has potential to become a supercritical fluid where reservoir temperature exceeds 88 °F (31 °C) and pressure exceeds 1074 psi (73 atm). At normal atmospheric conditions, CO_2 is a thermodynamically very stable gas heavier than air. At these pressure and temperature conditions, CO_2 behaves still like a gas by filling all the available volume, but has a 'liquid' density that increases, depending on pressure and temperature, from 200 to 900 kg/m^3 (Figure 2.5), thus approaching water density (Holloway and Savage, 1993; Hendriks and Blok, 1993).
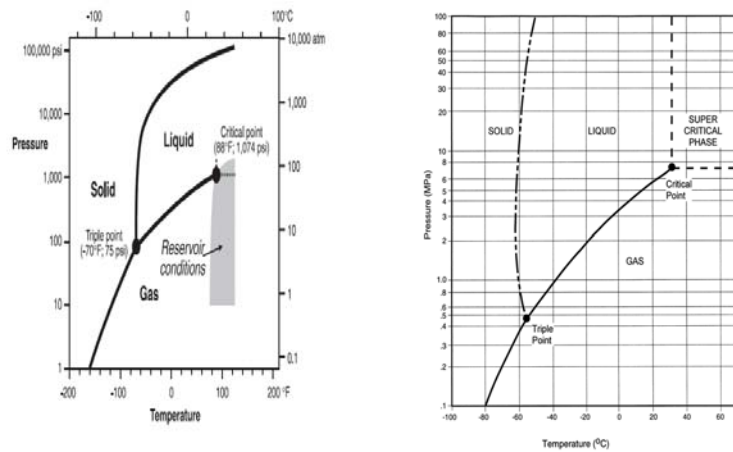
Figure 2.4 Phase diagrams of carbon dioxide
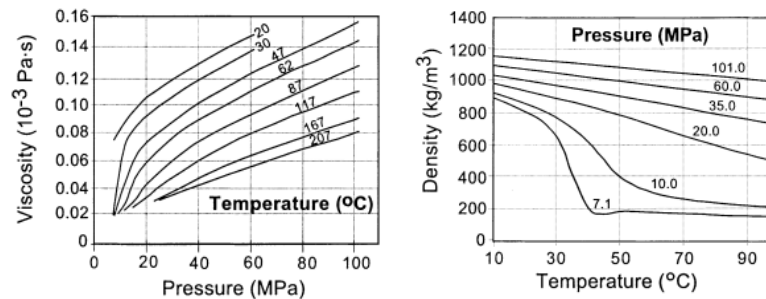
Figure 2.5 CO₂ viscosity and density

CO_2 is a gas, a liquid or in the supercritical phase, with a density and viscosity which approach those of water for low temperature and very high pressure.

2.3.1.1 Interaction of CO_2 with Water

Carbon dioxide is soluble in water; its solubility increases with pressure and decreases with temperature and water salinity (Holloway and Savage, 1993; Koide et.al, 1993a; Koide et.al, 1993b). CO_2 in a supercritical state is immiscible in water (Holloway and Savage, 1993). At low temperatures and elevated pressures, CO_2 forms a solid hydrate heavier than water.

2.3.1.2 Interaction of CO_2 with Coal

Another important property of CO_2 is its affinity to coal, which is almost twice as high as methane, a gas abundantly found in coal beds. Both laboratory experiments and field tests suggest that for two sequestered CO_2 molecules, one CH_4 molecule is produced. Laboratory experiments showed that this exchange ratio of 2:1 could be even larger at pressures higher than 9.6 MPa, where the gaseous CO_2 changes to supercritical CO_2 (Hall et al., 1994). Coal can hold a large volume of carbon dioxide under supercritical reservoir conditions, but little is known about the stability of supercritical carbon dioxide in coalbed methane reservoirs (Kroos et al., 2001).

All these properties of CO_2 and various other criteria play a role in the selection of appropriate methods and sites for CO_2 disposal and sequestration in geological media. Depending on reservoir temperature and original pressure, CO_2 can be stored either as a compressed gas, liquid or in supercritical phase.

2.3.2 Separation and Capture

Carbon dioxide separation is done routinely, but on the basis that the carbon dioxide has a positive value, for example, for increasing yield during oil recovery, or for other commercial reasons, e.g. removal of carbon dioxide from natural gas after extraction to make a pipeline-quality product. Sources that lend themselves

best to separation and capture (S&C) technologies include large-point sources of carbon dioxide.

- Conventional coal-fired power plants.
- Combined cycle gas turbines.
- Advanced power generation systems (enriched air/oxygen, gasified coal, hydrogen turbines or fuel cells).
- Natural gas operations.
- Oil refineries.
- Iron and steel plants.
- Cement and concrete producers.

The concentration of carbon dioxide in waste streams can vary from about 5% to nearly 100%, and pressure can vary from near atmospheric to several tens of atmospheres. The reduction of large volumes of dilutant nitrogen in the technologies using enriched air or oxygen much improves prospects for S&C of carbon dioxide. Dispersed sources of carbon dioxide, especially individual road vehicles and residential buildings, represent a much greater challenge for S&C. However, if road vehicles were to become propelled with hydrogen, using fuel cells or hydrogen turbines, central hydrogen production facilities which allowed for S&C of carbon dioxide may become feasible. Use of electric vehicles would similarly push the carbon dioxide-generating step of the process back to a large facility where S&C may be possible.

Carbon dioxide can be absorbed from gas streams by contact with amine-based solvents or cold methanol. It can be removed by adsorption onto activated carbon or other materials, or by passing the gas stream through special membranes. Advanced methods might include adsorbing carbon dioxide on zeolites or carbon-bonded activated carbon fibers and separating it from flue gases or process gases using inorganic membranes. The most likely options currently identifiable for carbon dioxide S&C research and development include the following (Grimston et al., 2001).

- Chemical and physical absorption.

- Physical and chemical adsorption.

- Low temperature distillation.

- Gas separation membranes.

- Mineralization and biomineralisation.

- Vegetation.

There are two options being investigated to reduce the cost of producing a pure CO_2 waste stream. The first option is efficient, advanced downstream separation technologies; such as use of membranes to produce a pure CO_2 stream from a flue gas. The second option is the use of a pure O_2 stream for combustion, commonly referred to as O_2/CO_2-recycle combustion (Croiset and Thambimuthu, 1998). This option effectively moves the separation (i.e. N_2 from air) upstream in front of the burner. By increasing the oxygen in the feed gas and eventually, by circulating part of the flue gas, a CO_2 concentration of up to 98% by volume can be achieved. Coal combustion at higher oxygen concentration is particularly attractive because not only does it allow reducing the cost of CO_2 separation in the flue gas, but also because it reduces the volume of inert gas, such as nitrogen and thus increases the boiler thermal efficiency.

2.3.3 Transportation

Transportation of carbon dioxide from source to reservoir will depend on distance to be covered. For 'on-site' sequestration carbon dioxide gas may be pumped in pipes. For longer distances, perhaps some tens or hundreds of kilometers, transport as a supercritical fluid by pipeline may be appropriate.

For ocean disposal at distances greater than about 300 km from shore, tankers carrying dry ice or supercritical liquid carbon dioxide may be more economic than pipelines. Pipelines require repressurisation at regular intervals (Fujioka et al., 1997).

2.3.4 Injection and Storage in Sinks

The concentration of CO_2 in the atmosphere is rising and, due to growing concern about its effects, the U.S. and over 160 other countries ratified the Rio Mandate in 1992, which calls for "…stabilization of greenhouse gas concentrations in the atmosphere at a level that would prevent dangerous anthropogenic interference with the climate system". Evidence is mounting that rising levels of atmospheric CO_2, caused primarily by combustion of fossil fuels, will lead to rapid global warming. To address this problem, numerous nations are developing plans for lowering CO_2 emissions to the atmosphere. The principal approaches under consideration are: improving energy efficiency; making greater use of alternative sources of energy; and creating economically viable technologies for capture, separation, and long-term storage of CO_2. The latter strategy, which keeps large masses of CO_2 separate from the Earth's atmosphere for hundreds to thousands of years (a concept commonly known as 'CO_2 sequestration'), is receiving increasing attention because it permits continued use of high-carbon fossil fuels to generate electrical power while ensuring that CO_2 releases to the atmosphere are reduced.

Carbon dioxide sinks can be grouped into three broad classes based on the nature, location and ultimate fate of CO_2 as depicted in Figure 2.6. These groupings are:

- Biosphere sinks, which are active, environmentally sensitive, natural reservoirs for CO_2. The oceans, forests, and soils (agricultural) ecosystems are members of this class.

- Geosphere sinks, which are natural reservoirs for CO_2, but require anthropogenic intervention in order to make use of the sink. Members of this class include oil reservoirs suitable for enhanced oil recovery (EOR), coal beds, depleted oil and gas reservoirs, and deep aquifers.

- Material sinks, which are anthropogenically created/generated pools of carbon. This class includes durable wood products, chemicals and plastics as members.

A number of factors will need to be considered when evaluating the use of a given sink in an integrated portfolio of emissions-reduction mechanisms. These factors include: environmental impact of the proposed sink mechanism; sink CO_2 capacity; retention/residence time of CO_2 in the sink; potential for accelerated leakage of CO_2; rate of CO_2 uptake by the sink; validation of sequestration in the sink; suitability of the sink/match to the emission source and type; and cost of implementation/utilization of the sink mechanism (Gunter et al., 1998).
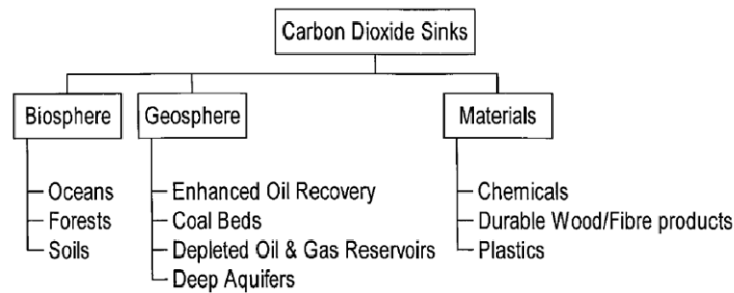
Figure 2.6. Classes of carbon-dioxide sinks (Gunter et al., 1998)

2.3.4.1 Biosphere Sinks

Oceans: Oceans cover approximately 70% of the Earth's surface, and are the largest sinks available for carbon dioxide. Over 39,000 billion tonnes of carbon (GtC, 3.67 tonnes CO_2=1 tonne C) already reside in the ocean, compared with around 760 GtC in the atmosphere and 2500 GtC in the soil and vegetation (IPCC, 2000). The main approaches to ocean disposal of carbon dioxide involved the following (Herzog et al., 1997).

- Dry ice is released at the ocean surface from a ship.
- Liquid carbon dioxide is injected at a depth of about 1000m from a pipe towed by a moving ship and forming a rising droplet plume.
- Liquid carbon dioxide is injected at a depth of about 1000 m from a manifold lying on the ocean bottom and forming a rising droplet plume.
- A dense carbon dioxide-seawater mixture is created at a depth of between 500 m and 1000 m, forming sinking bottom gravity current.

- Liquid carbon dioxide is introduced to a sea floor depression forming a stable 'deep lake' at a depth of about 4000 m.

It is estimated that the oceans could accommodate another 1200 GtC (Watson et al., 1996), with a retention/residence time of several hundred years before re-releases into the atmosphere. The ultimate sequestering capacity of the oceans (determined by choosing a nominal allowable change in the average acidity of all ocean water) has been estimated to be in the range 1000-10,000 GtC (Socolow, 1997). If the injected CO_2 can be incorporated in the general oceanic deep-water circulation, a residence time of up to 1000 yr can be anticipated (Socolow, 1997). However, Ribeiro and Henry (1995) estimated that based on environmental considerations, the global storage capacity in the ocean should be limited to 200-1200 Gt CO_2 or 55-327 GtC (Gunter et al., 1998).

The recent discovery of enormous squids at depths of 2000-5000 meters in the Atlantic, Pacific and the Indian Oceans is an eye-opener, for where large predators roam in significant numbers, there must be higher productivity of smaller animals to support them. Equally important is what lies within the top few centimeters of the sea floor: dense populations of microorganisms whose diversity and functions are barely known. One group of Arachaea living in anoxic sediments fixes 80 percent of the methane produced in the world's oceans. And guess what? Methane is second only to carbon dioxide as a greenhouse gas! How will these organisms respond to the load of jellied CO_2 dumped on top of them? Among the challenges posed will be lower seawater pH, a phenomenon that will also affect larger organisms, causing respiratory distress, reduction of already low metabolic rates, and other physiological problems that will certainly increase morbidity and mortality of benthic animal populations (Greenstone, 2002).

As transportation costs escalate with distance travelled, ocean disposal is likely to be of interest predominantly to those countries with coastal zones and access to ocean depths of greater than 3000 m. There are major environmental concerns associated with the approach. Factors like the effects on ocean chemistry in

immediate vicinity of disposal site and the safety of carbon dioxide plumes on ocean floor, including possible rapid turnover and explosive release of carbon dioxide back into the atmosphere will require serious consideration (Grimstone, 2001).

Forests: The terrestrial biosphere serves as an important source or sink for CO_2. Plants can adsorb large quantities of CO_2 through photosynthesis and carbon is sequestered in woody biomass throughout the life of the tree and after its death. The carbon could be sequestered as long as 500 years. Indeed, forests and plantations are thought to play an important role in regulating atmospheric CO_2 concentrations. The biofixation concept involves sequestering CO_2 from the atmosphere and storing it as carbon either in forest trees or by producing a wood fuel substitute for fossil fuel. The first option involves CO_2 sequestration in long-term forest plantations, whereas the second option involves short-rotation tree cropping to produce a biomass fuel for power generation (Gentzis, 2000).

It is estimated that through sustainable management practices it would be possible to store (globally) an additional 60-87 GtC (Watson et al., 1996) over a 55-year period from 1995 to 2050.

Although terrestrial ecosystems can be managed to reduce GHG emissions and increase carbon sink size considerably in an economically feasible manner, biofixation should be viewed as a temporary solution, from decades to centuries, that allows us time to develop more aggressive solutions for GHG emissions sequestration (Gentzis, 2000).

Soils: The agricultural sector can reduce CO_2 emissions to the atmosphere (Watson et al., 1996) by:
- reducing agriculturally related emissions,
- sequestering carbon in soils through the adoption of sustainable cropping and grazing practices such as:

- o minimizing tilled summer fallow acreage and moving to longer crop rotations,
- o reducing soil tillage which saves energy consumption and reduces soil organics degradation,
- o improving new crop varieties and yields,
- o increasing the amount of Prairie crop land returned to forage crops which
- o provides continuous soil cover, increasing soil carbon,
- o producing biomass to use as a fossil-fuel replacement.

Overall, adoption of these practices could yield between 45 and 122 GtC mitigated on a global cumulative basis over a 50 year period. On an annual basis, the potential is 0.86-2.44 GtC per year (Watson et.al., 1996). It is important to note that this sink has a finite capacity to sequester carbon over a period of 50-100 year, as new equilibrium levels of soil organic matter are established. As with forestry, the most significant challenges facing the use of this sink are stability of the sequestered carbon, and verification as an offset for CO_2 emissions.

2.3.4.2 Material Sinks

These are semi-active, anthropogenically generated carbon reservoirs that have a variety of residences times, related to product life cycles. Carbon-based resources, through human needs and ingenuity, have been turned into products with many different life cycles, for example:

- Durable wood products (furniture, housing, commercial buildings)
- Paper products (books, magazines),
- Durable plastics (automobile parts, appliance parts)

The ability of any one of these sinks to participate in emission reduction strategies will require extensive research on their life cycles and carbon balances. For example, chemical fertilizers are not considered as sinks for carbon as the retention time for CO_2 is too low. If a product can be demonstrated to reduce the

rate of loss of CO_2, then that product could qualify as a material sink. One possible example is structural fiber products such as panel boards developed from agriculture straw. In current farming practice, the straw is either burned or worked back into the soils. By storing the carbon in the structural fiber products, straw burning is eliminated and the CO_2 emissions are avoided. Another way to store the carbon is in wood-based products. Depending on the product, the retention time could be very short such as in the case of consumer paper products or could be relatively long, as would be the case for construction products, in the range of 50-100 yr. At this time, material sinks have not been officially recognized as a mitigation or reduction option. More quantification and life cycle analyses are needed. There are large uncertainties about their capacities as they are affected by consumer needs; and at this stage, capacities cannot be properly evaluated. As such, material sinks may only play a minor role in greenhouse gas mitigation strategies (Gunter et al., 1998).

2.3.4.3 Geosphere Sinks

Geosphere sinks are naturally occurring reservoirs that historically, on a geologic time basis, have been sinks for carbon (with the exception of deep aquifers). Humans have extracted carbon from these sinks to use for energy, thus producing the carbon energy based economy. These same reservoirs, including deep aquifers, can be used to store carbon dioxide thereby removing the CO_2 from active participation in the global carbon balance (Hitchon et al., 1999). These sinks are most suitable for utilization by large CO_2 emission point sources with relatively pure CO_2 waste streams.

Carbon dioxide can be sequestered in geological media by: geological trapping in depleted oil and gas reservoirs, solubility trapping in producing oil reservoirs, adsorption trapping in uneconomic coal beds and in coal bed methane recovery, hydrodynamic trapping in deep aquifers, cavern trapping in salt structures and by mineral immobilization.

The most significant issue that limits the use of geologic sinks as mitigation options is cost. The cost of disposing of CO_2 is made up of three factors: separation costs (i.e. capture/separation of CO_2 from other combustion gases), transportation costs (i.e. compression, pipelines) and injection costs (compression, disposal wells). Efficient, cost-effective transportation and capture/separation technologies will need to be developed to allow large-scale use of geologic sinks. Currently, capture/separation costs represent the largest financial impediment.

Enhanced Oil Recovery: Enhanced oil recovery (EOR) refers to those methods that are used to increase the recovery of oil above the amounts that could be recovered during primary or secondary recovery. The use of CO_2 in miscible floods is a proven technology and its activity continues to increase in the United States (Moritis, 1996). When CO_2 is injected into the reservoir, it dissolves in the oil, thus reducing its viscosity and forces the oil towards the productive well. Inherently, there is always CO_2 co-produced with the oil. However, a portion of the CO_2 will remain in the reservoir. Globally, the EOR-CO_2 sink has an estimated capacity of 20-65 GtC (Watson et al., 1996; IEA, 1995). Use of this sink is restricted to countries that have oil reservoirs suitable for EOR-CO_2 recovery techniques. Use of CO_2 for EOR is capable of sequestering a large quantity of CO_2, resulting in a net reduction in CO_2, but the overall return on investment (either positive or negative) is highly dependent on factors such as the price of oil, price of CO_2 and individual reservoir characteristics.

Depleted Oil and Gas Reservoirs: There are advantages for using depleted oil and gas reservoirs as CO_2 sinks, as the trapping mechanisms and reservoir properties are well known and some of the existing infrastructure can be utilized. There are significant differences in describing 'depleted' oil and gas reservoirs. An abandoned oil reservoir can still have a large quantity of oil remaining in it and it is very unlikely that it will be used as a sink unless some form of enhanced oil recovery is incorporated into the CO_2 disposal scheme. This can be contrasted with an exhausted gas reservoir, where normally up to 90% of the original content would have been removed and the reservoir can genuinely be regarded as depleted

28

and available for CO_2 disposal. The total storage potential of all oil and gas fields in the world is estimated to be 670 Gt of CO_2 (180 GtC) assuming that the entire volume can be displaced with CO_2 at some time in the future. The distribution between oil and gas is 150 Gt CO_2 (40 GtC), and 520 Gt CO_2 (140 GtC), respectively. This is comparable to the estimates of >40 GtC for exhausted oil wells and >90 GtC for exhausted gas wells in the Second Assessment Report of the Intergovernmental Panel on Climate Change (Watson et al., 1996). One estimate of the prospective sequestering capacity of the oil and gas reservoirs associated with past production plus proven reserves plus estimated undiscovered conventional resources is about 100 GtC for oil fields and 400 GtC for natural gas fields (Hendriks, 1994).

Deep Aquifers: Carbon dioxide disposal into low permeability, deep aquifers in sedimentary basins has been shown to be technically feasible as geologic sinks and offers the largest potential for the landlocked areas of the world. Deep aquifers contain high salinity water and could host large amounts of CO_2 trapped by the formation pressure. The determining factors are the pressure and temperature in the reservoir. At reservoir depths of 800 m and greater, the temperature and pressure of the CO_2 would be above the supercritical condition, which is desirable from a storage perspective. Aquifers suitable for injection of CO_2 must satisfy the following general conditions (Bachu et al., 1994):

- the top of the aquifer must be greater than 800 m below ground level,
- the aquifer should be capped by a regional aquitard (sealing unit),
- the aquifer should have enough porosity and adequate permeability, and
- the injection site should be close to the CO_2 emitting source.

Global estimates of the capacity of this sink vary greatly due to different assumptions with respect to aquifer volumes, percent of the reservoir filled, density of CO_2 under reservoir conditions, and the area suitable for storage. It ranges from 87 GtC to 14,000 GtC if structural traps are not required for secured storage (IEA, 1995). Ribeiro and Henry (1995) estimated the range from 100 to

2400 Gt CO_2 (27-650 GtC). Currently, there is a large-scale project in the Sleipner Vest Field in the North Sea, where 1 million tonnes of CO_2 are injected into the aquifer per year (Baklid et.al, 1996). The other large-scale project which is being developed is in the Natuna Field in Indonesia, where the gas contains up to 71% CO_2 (IEA, 1996). In order to recover the natural gas from the Natuna Field, a way must be found to store the CO_2 in an environmentally acceptable manner.

CO_2 storage in aquifers has the following safety risks and environmental implications: CO_2 escape; dissolution of host rock; devaluation of mineral resources; and effects on groundwater. However, the implications may not be as serious as those for biosphere sinks.

Coal Beds: The use of coal beds as a reservoir rock for storing CO_2 is novel. In coal beds there are significant amounts of methane gas adsorbed in the coal which is called coal bed methane or CBM. By injecting CO_2 into the coal beds, the CO_2 is adsorbed in the coal pore matrix, releasing the methane. Experimental results show that two molecules of CO_2 can be adsorbed in the coal matrix for every molecule of methane it displaces. The use of CO_2 for CBM recovery would have the same effect as enhanced oil recovery and is classified as an enhanced coal bed methane recovery (ECBM) method.

Bachu (2002) defines geological sequestration as "the capture of CO_2 directly from anthropogenic sources and disposing of it deep into the ground for geologically significant periods of time". Sequestration of CO_2 in geological formations is a storage process. Here, coal seam sequestration is defined as the storage of CO_2 from anthropogenic sources into deep, unmineable coal seams for geologically significant times with or without the concomitant recovery of natural gas. According to Byrer and Guthrie (1998), "unmineable coals are too thin, too deep, or too unsafe" to mine. "In recent times, historically mined coals may also be too high in sulfur or mineral matter or too low in BTU value to be economically profitable".

Burlington Resources of the US currently runs the world's first large-scale ECBM pilot utilizing CO_2 injection located in the San Juan Basin, New Mexico. The Alberta Research Council is currently leading a consortium of government and industry partners in a micro-pilot field test to gather reservoir data to determine the feasibility of storing CO_2 while producing methane in the lower permeability CBM reservoirs of Alberta (Gunter et al., 1997). It is too early to determine the value of CO_2 for this application, as it is still in the piloting stage. The attractiveness of disposing of CO_2 in coal beds is that it can be coupled directly with the production of methane. One of the key factors is the value and purity of the CO_2 to be stored. As with other storage options, a key enabling technology is the separation and purification of CO_2.

The global estimates of coal bed methane resources are of the order of 2980-9260 trillion standard cubic feet (84-262 trillion cubic meters) (Kuuskraa et.al, 1992; Rice et al., 1993). Converting these estimates to CO_2 storage capacity (assuming two molecules of CO_2 displacing one molecule of CH_4) yields a potential of 82-263 GtC. The bulk of the world's coalbed methane resource occurs in China, the Asian portion of Russia, Kazakhstan, and India. Australia, portions of Africa, and Central Europe, as well as the United States and Canada also contain varying amounts of this resource (Kelafant et al., 1992).

CHAPTER 3

THEORY

3.1 Introduction

In order to help a better understanding on the gas storage and transport in coal, formation and properties of coal are explained in the following sections. Fundamental information is given for the simulation of CBM and ECBM processes in coal reservoirs. Finally the uncertainty assessment in reserve estimation is explained.

3.2 Coalbed Methane (CBM)

Coal gas is a by-product of the physical and chemical reactions associated with the coalification process (the process by which vegetable matter is converted to coal). Consequently, this makes coal seam reservoirs different than conventional gas reservoirs, in that the coal seam is both the source rock and the reservoir rock for the gas. As much as 46 MSCF of gas can be liberated during the formation of one ton of coal.

The characteristics of CBM reservoirs differ from conventional gas reservoirs in several areas (Table 3.1). Unlike conventional gas reservoirs, coal is both the reservoir rock and the source rock for methane. Coal is a heterogeneous and anisotropic porous media which is characterized by two distinct porosity (dual-porosity) systems: macropores and micropores. The macropores, also known as cleats, constitute the natural fractures common to all coal seams. Micropores, or the matrix, contain the vast majority of the gas. This unique coal characteristic has resulted in classification of CBM as an 'unconventional' gas resource.

Table 3.1. Comparison of CBM and conventional gas reservoir characteristics

Characteristic	Conventional Gas Reservoir	CBM Reservoir
Gas Generation	Gas is generated in the source rock and then migrates into the reservoir.	Gas is generated and trapped within the coal.
Structure	Randomly-spaced Fractures	Uniformly-spaced Cleats
Gas Storage Mechanism	Compression	Adsorption
Transport Mechanism	Pressure Gradient (Darcy's Law)	Concentration Gradient (Fick's Law) and Pressure Gradient (Darcy's Law)
Production Performance	Gas rate starts high then decline. Little or no water initially. GWR decrease with time.	Gas rate increases with time then declines. Initially the production is mainly water. GWR increases with time.
Mechanical Properties	Young Modules $\sim 10^6$. Pore Compressibility $\sim 10^{-6}$	Young Modules $\sim 10^5$ Pore Compressibility $\sim 10^{-4}$

Coal deposits are naturally fractured gas reservoirs. Typically, the natural fractures (cleats) of the coal are initially water saturated, most, if not all, of the gas is adsorbed on the surfaces of the coal, and some gas may be stored as free gas in the cleats and open pores. Figure 3.1 shows the typical production profile of a coal well that differs significantly from the typical decline of a conventional gas well. Wells completed in coalbed formations progress through three distinct stages of production. The inclining gas rate in the early life of a coalbed methane well occurs because water initially occupies the fracture system in the reservoir, which controls flow to the well. Water must be removed from the cleat system before gas can effectively flow to the well. This process is called 'dewatering'. Phase I is characterized by a constant water production rate and declining flowing bottom hole pressure. During this phase the gas rate may be inclining, as shown in Figure 3.1.

Phase II is characterized by 'negative decline' in the gas production rate and a significant decline in the water production rate. Phase III begins well has reached its peak gas rate, and gas production is characterized by a more typical positive decline trend. During this phase, water production is low and/or negligible, and gas and water saturations change very little. The well is considered to be 'dewatered' at the beginning of Phase III. At this point, water production has

reached a low level, and pseudo-steady state flow exists for the remainder of Phase III (Zuber, 1996).
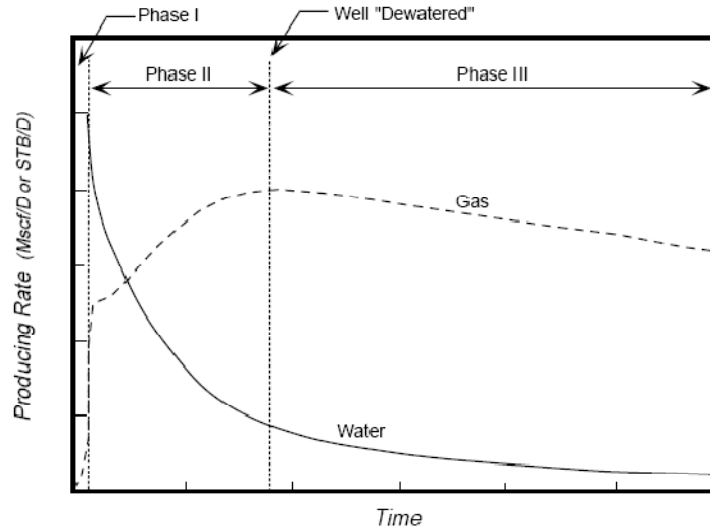
Figure 3.1. Typical coalbed methane production profiles for gas and water rates: three phases of producing life (Zuber, 1996)

To thoroughly evaluate and develop a coalbed methane prospect, the internal structure and character of the coal and the strata surrounding the reservoir must be understood. Since the beginning of the coalbed methane industry, operators have relied greatly on technology from the mining and petroleum industries to evaluate and develop coalbed methane properties. In the following sections, coal characteristics and gas content of coal are described.

3.2.1 Formation of Coal

Coal is not a single material of one chemical composition but a range of natural solids rich in carbon. The complete range is broadly taken to extend from peat – still clearly a breakdown product of vegetable matter – via brown coal, lignite, and bituminuous coal to anthracite.

Coal is the fossilized product of decomposition of abundant tropical forest growths under marshy conditions. Within it is a proportion of material that will

not burn – largely the residue of silt deposited between and on the rotting vegetable matter. It is this incombustible part that yields ash when coal is burnt. In the swamps, plants would grow thickly over long periods of time and their debris would accumulate. Then the area subsided and became flooded, putting an end to growth but also resulting in the vegetable remains being covered with sand and silt. Later the area was lifted by further earth movements and another generation of swamp forest began to grow. The process was repeated many times during periods measured in millions of years.

Over these very long periods the plant components were partly decomposed and compressed. First, micro-organisms needing oxygen from the air ('aerobic'), then others that live without air ('anaerobic') broke down much of the plant protoplasm, cellulose and other parts, though waxes and resins proved more resistant. Further weight of sediments deposited over the tops of these layers increased the pressure and they became slightly warmed. Understandably, the period when plants were being broken down is called the 'biochemical stage'; the later period of compression and mild heating is the 'geochemical stage'.

The name given to the whole sequence of changes is 'coalification' – and how far it has gone is known as the 'rank' of the coal. The whole process is generally more advanced in the older seams, though coals are found of differing rank even at the same geological age since earth movements, pressures and temperatures have all varied enormously. These variations in effects are quite marked, sometimes even within limited areas; consequently a coal seam may change appreciably in thickness and in many cases in rank as it is traced across a coalfield.

The successive layers of decaying plant residues in due course became a series of layers (seams) of coal and the intervening layers, also compressed and hardened, became rock strata such as sandstone – born of sand – and shale, a stone resulting from what had been clay (Berkovitch, 1978).

As organic material is buried, compressed, and dewatered, peat is formed. Peat is a dark brown residuum produced by the partial decomposition and disintegration of plants that grow in marshes and swamps. As peat is buried more deeply, heat and pressure progressively drive off water and volatiles. Peat is then transformed into coal as the carbon content of the fossil organic material increases through devolatilization. In this process called coalification, coals increase in rank from lignite, to sub-bituminous, bituminous, and anthracite, as shown in Figure 3.2. Coal rank is important because it directly influences the gas storage capacity of coal. Several factors influence the rank and type of coal formed: the type of organic material, depositional setting, pH, temperature, reducing potential, depth of burial, and time of burial (Saulsberry et al., 1996).

Coal by definition is not a unique substance, but rather a group of sedimentary rocks comprised primarily of altered vegetal matter. It is a heterogeneous mixture of components. Mineral matter, water and methane are natural components of coal; their relative proportions are important influences on the value of coal. Coal composition has evolved in response to temperature, pressure, and the chemical environment. Though solid in appearance, coal contains gas and oil-like substances, which are formed during coalification. Part of these substances is retained in the coal and part of them is expelled. Coal rank and the relative abundance of various components determine most of the physical and chemical properties of coal (Saulsberry et al., 1996).

Figure content — Coal classification by rank:

Rank German	Rank USA	Refl. Rm$_{oil}$	Vol. M d.a.f. %	Carbon d.a.f. Vitrinite	Bed Moisture	Cal. Value Btu/lb (kcal/kg)	Applicability of Different Rank Parameters
Torf	Peat	0.2	68 / 64	ca. 60	ca. 75		
Weich-	Lignite	0.3	60 / 56		ca. 35	7200 (4000)	
Matt-	Sub- C	0.4	52	ca. 71	ca. 25	9900 (5500)	
Glanz-	Bit. B / C	0.5 / 0.6	48 / 44	ca. 77	ca. 8-10	12600 (7000)	
Flamm-	B	0.7	40				
Gasflamm-	A	0.8	36				
Gas-		1.0	32				
	Medium Volatile Bituminous	1.2	28	ca. 87		15500 (8650)	
Felt-		1.4	24				
	Low Volatile Bituminous	1.6	20				
Ess-		1.8	16				
Mager-	Semi-Anthracite	2.0	12				
Anthrazit	Anthracite	3.0	8	ca. 91		15500 (8650)	
Meta-Anthr.	Meta-Anthr.	4.0	4				

(German rank groups: Braunkohle, Steinkohle; USA High Vol. Bituminous A; additional parameter axes: Bed Moisture (ash-free), Calorific Value (moist, ash-free), Carbon (dry, ash-free), Reflectance of Vitrinite, Volatile Matter (dry, ash-free), Hydrogen (d.a.f.), Moist., X-Ray, Diffr.)

Figure 3.2. Coal classification by rank (Stach et al., 1982)

Through geologic history the major eras of coal formation are the Carboniferous, the Permian, the Mesozoic, and the Cenozoic. For most of the major Carboniferous coal seams, a humid tropical environment was most probable. The regular sequence of sedimentary rocks referred to as a cyclothem includes sandstone, gray shale, limestone, underclay, coal, gray shale, limestone, and black shale (Wanless and Shepard, 1936). The sandstone through coal strata is typically deposited in a land or fresh water environment and the remaining are marine deposits. Cycles usually are not complete and often coals or other units are repeated in a cycle. However, cycles can be useful for mapping coals or coal groups. Over geologic time, a thick (up to several thousand feet) sequence of sediments with a large number of coal seams may accumulate in a basin. Strata, including coal seams, tend to be thickest toward the center of most basins. Basins may be classified as rift, foreland, successor or intermontaine, and cratonic. Rift

37

basins like the may have thick evaporite deposits that accumulated during arid periods while rainfall was restricted by mountains uplifted at the basin margins. Foreland basins form along fold-and-thrust belts and commonly contain significant coalbeds. Successor basins form within orogenic belts in compressional, extensional, and strike-slip settings. Cratonic basins may form by thermal or flexural subsidence. The organic material which accumulated and formed coalbeds was typically deposited in a swamp or water-saturated environment. These might be large marsh areas with fairly uniform sedimentary conditions or small bogs. Many coalbeds were deposited in swamps associated with river deltas, barrier islands, and slowly subsiding areas. Coal formation can vary significantly depending on the environment of deposition. By understanding the depositional environment, some of the variability in coal quality, thickness, and associated factors can be anticipated (Saulsberry et al., 1996).

3.2.2 Properties and Classification of Coal

Coal petrology is the study of the origin, occurrence, and structure of coal. This readily combustible rock contains more than fifty percent by weight and seventy percent by volume carbonaceous material. This material includes inherent moisture formed from compaction, induration, similar to those in peat. Differences in the kinds of plant materials (type), in degree of metamorphism (rank), and in the range of impurity (grade), are characteristic of coal and are used to classify coals. Several significant differences between coal and conventional reservoir rock include: the greater compressibility of coal, the relatively low effective porosity of coal, and the adsorption of gas onto coal's carbon structure.

Physical and chemical properties can vary significantly from seam to seam and over a short distance within a seam. Coal is usually classified by three fundamental characteristics:

- **Grade.** Represents the relative percentage of organic to mineral components.

- **Type.** Represents the various organic constituents.
- **Rank.** Represents the level of maturation reached, ranging from peat through anthracite.

These characteristics are used in classifying coal, as shown in Figure 3.3. The three-axis diagram is a petrographic classification of coal composition in which grade, type, and rank are depicted on three orthogonal axes (Alpern et al., 1989).
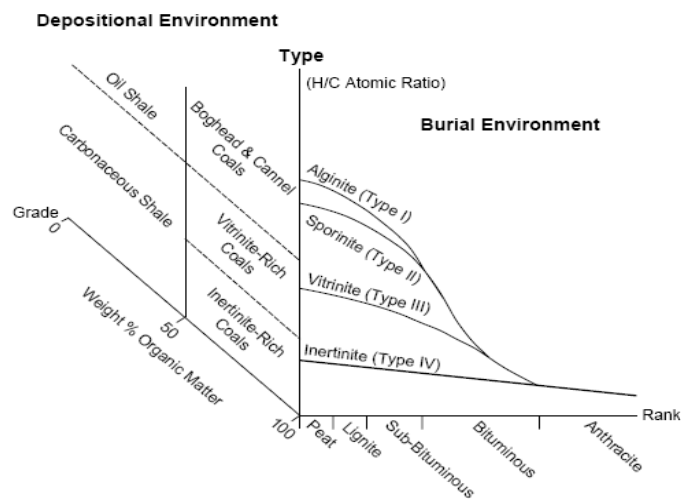
Figure 3.3. Coal classification by grade, type, and rank (Alpern et al., 1989)

Tests for evaluating coal petrology include vitrinite reflectance testing to determine rank and proximate and ultimate analyses to determine grade and to help in evaluating rank. In addition, visual inspection is useful for evaluating cleat development, gross composition of the coal, and other important factors such as mineral filling of fractures and cleats.

The composition of coal often is described by proximate analysis and ultimate analysis. A proximate analysis provides the percentage of fixed carbon (FC), volatile matter (VM), moisture (H_2O), and ash content of the coal, as shown in Figure 3.4.

An ultimate analysis provides the chemical makeup of the coal as percentages of carbon, oxygen, hydrogen, nitrogen, sulfur, and ash. The relative amount of these components can be reported in several ways; the most common include:

- "**As received**" basis includes FC, VM, H_2O, and ash based on moisture in the coal as received for analysis.

- "**Air dried**" basis is the same as "as received" except the moisture content is equilibrated to the lab atmosphere.

- "**Dry**" basis includes only FC, VM, and ash, normalized to 100 percent.

- "**Ash-free**" basis includes only FC, VM, and H_2O normalized to 100 percent.

- "**Dry, ash-free**" basis includes only FC and VM, the organic components, normalized to 100 percent.
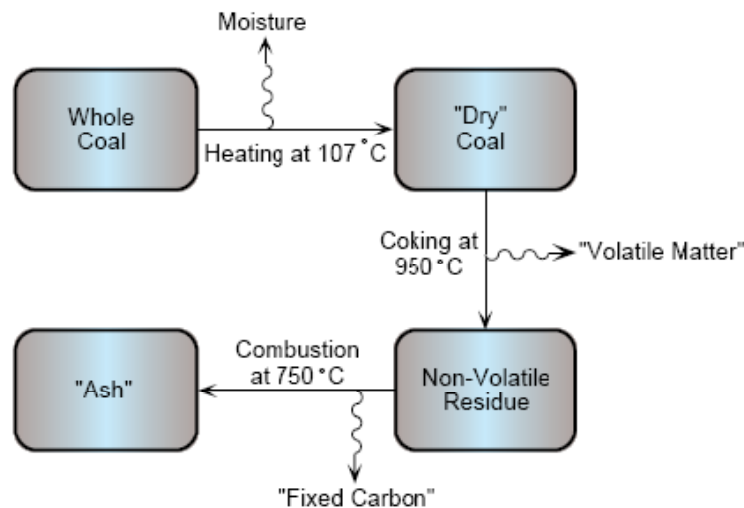
Figure 3.4. The proximate analysis process (Saulsberry et al., 1996)

Coal rank profoundly influences the coalbed reservoir in two ways. First, the processes of coalification (both thermogenic and biogenic) are associated with the generation of oil and gas in the subsurface. Thus, a substantial proportion of the methane, carbon dioxide, and other occluded volatile components of coal may have been generated from the coal itself as by-products of coalification. Second, all of the physical and chemical properties of coal undergo a substantial alteration during coalification. The three levels of coal rank are:

- **Lignite.** A brownish-black coal in which the alteration of vegetal material has proceeded further than in peat, but not so far as sub-bituminous coal, also called brown coal.

- **Bituminous.** Varieties of soft coal which burn freely with a flame and yield volatile matter when heated.

- **Anthracite.** A hard black lustrous coal with 92 percent or more fixed carbon (dry, mineral matter-free), also called hard coal. The permeability of these coals usually is very low.

Most commercial coalbed methane projects are in coals within the rank range of sub-bituminous to low volatile bituminous. Coal of this rank usually provides optimum gas content and natural permeability.

3.2.2.1 As Rank Increases

Vitrinite Reflectance: Though it is not necessary to know the vitrinite reflectance or fixed carbon content of a coal, such rank data often are available and can be valuable for identifying trends in an area. Vitrinite reflectance is determined by average measurements of reflected light usually from the surface of vitrinite in polished coal samples. Vitrinite reflectance increases with rank and is reported as percent reflected light. Typically an oil-immersion medium is used, and the value is reported with a subscript as Ro. Vitrinite reflectances for bituminous coals usually are in the range of 0.5 percent Ro to 1.5 percent Ro. as shown in Figure 3.5 (Van Krevelen, 1961).
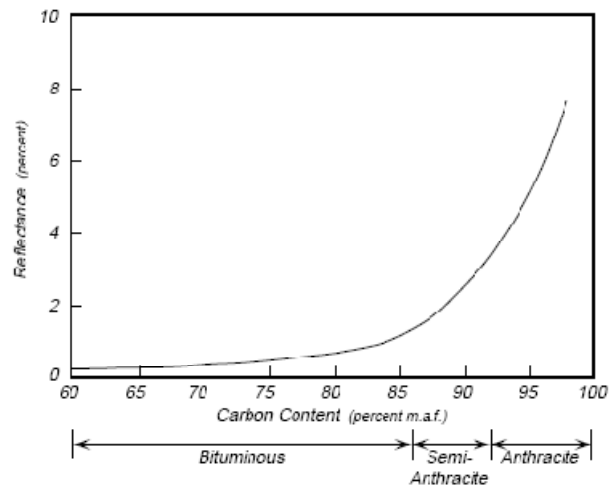
Figure 3.5. Maximum reflectance of vitrinites (Van Krevelen, 1961)

Heating Value: Heating value can be useful in estimating rank, if reflectance or fixed carbon data are not available. Heating value is commonly reported in BTU/lb or calories/gram. The heating value of coal increases with increase in coal rank, as shown in Figure 3.6 (Schmidt, 1979).
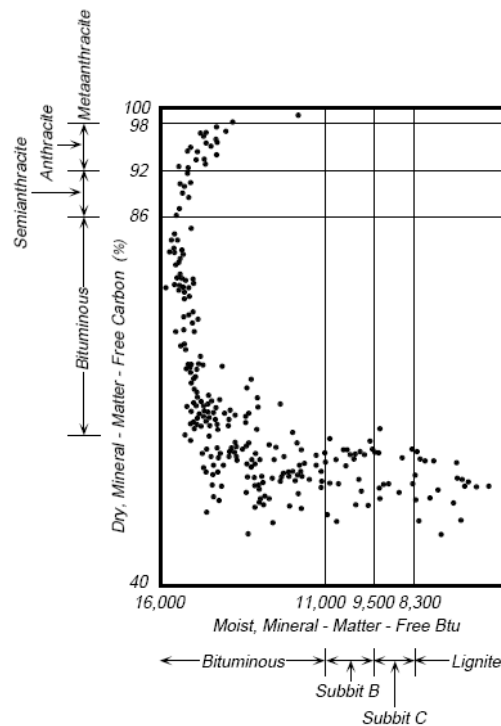
Figure 3.6. Heating values of U.S. coals (Schmidt, 1979)

42

Composition: The percentage of water in coal (inherent moisture) is used to differentiate coals by rank. Low rank coals contain more water than higher rank coals (ASTM, 2000).

The more the original plant remains have been altered by heat and pressure after they have been buried, the higher the rank of the coal. The percentage of carbon in the pure organic matter is taken as the measure of rank but Table 3.2 shows how other properties are also related. There is always moisture associated with coal; as rank increases this moisture falls from the very high proportions in the soggy, partly-decomposed plant debris of peat to the one or two per cent associated with the highest rank coals and anthracites. Across that same range, the hydrogen contents of coals also fall and so does the oxygen, but much more sharply. And rank is reflected too in the values obtained for the volatile matter (Berkovitch, 1978).

Table 3.2. Composition of main types of humic coals (Berkovitch, 1978)

Type of coal	Moisture as found	Carbon, %	Hydrogen, %	Oxygen, %	Nitrogen, %	Volatile Matter, %	Calorific value, Btu/lb
		All on dry, mineral-matter-free basis					
Peat	70-90	45-60	3.5-6.8	20-45	0.75-3	45-75	7,500-9,600
Brown coals and lignites	30-50	60-75	4.5-5.5	17-35	0.75-2	45-60	12,000-13,000
Bituminous coals	1-20	75-92	4.0-5.6	3-20	0.75-2	11-50	12,600-16,000
Anthracites	1.5-3.5	92-95	2.9-4.0	2-3	0.5-2	3.5-10	15,400-16,000

Depth: In most areas, coals increase in rank with increasing depth because rank is most influenced by temperature, pressure, and length of burial. Though rank generally increases with depth, coals at similar depths frequently do not have the same rank because of other variables. For example, igneous intrusives can reverse the rank gradient by contact metamorphism. Lateral variation in rank within a coalbed, is usually related to original depth of burial. However, it also can be caused by proximity to a heat source, such as an igneous intrusive or a hydrothermal source (Saulsberry et al., 1996).

Density: Coal resources can be more accurately estimated if the coal density is known. Because of the porous nature of coal, it can be difficult to accurately determine its volume and thus its density. Usually, apparent density[1] is measured rather than true density[2]. The apparent density of coal reaches a minimum at about 85 percent carbon in the low-volatile bituminous range, as shown in Figure 3.7 (Williamson, 1967).
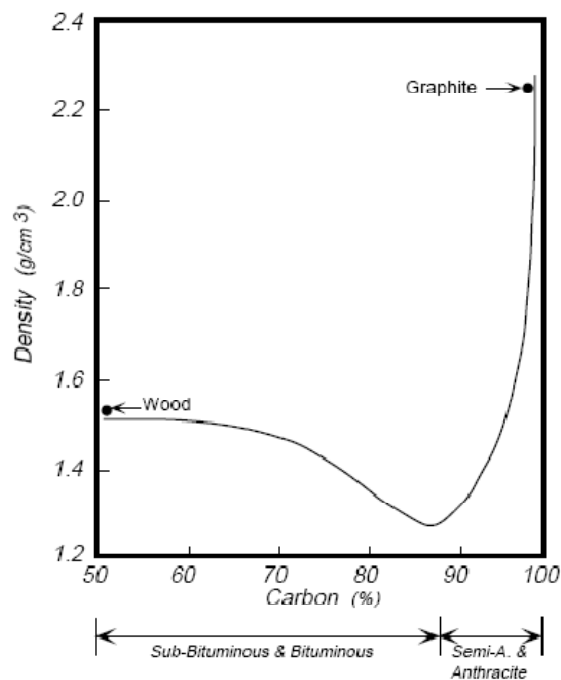
Figure 3.7. Relationship between apparent density and coal rank (Williamson, 1967)

As coal rank increases from lignite to anthracite, the density of the coal initially decreases from lignite to high volatile bituminous coal rank as a result of expulsion of water and compaction and the formation of micropores. In low rank coals which are less than 75 percent C, on a dry, ash-free (daf) basis (lignite and subbituminous ranks), surface areas have been interpreted as primarily contained in macropores >20 nm (Gan et al., 1972; Sharkey and McCartney, 1981). In contrast, density of the high volatile bituminous to anthracite coals increases as a

---

[1] Apparent Density: Density of material including closed and inaccessible pores.
[2] True Density: Density of solid, excluding pores and voids.

result of coalification processes that drives off hydrogen and oxygen. Pores in these higher rank coals are primarily micropores (<2nm) and to a lesser extent transitional pores (2-20 nm). Other work contradicts the interpretation for subbituminous coals. Parkash and Chakrabartty (1986) conclude for a study of subbituminous coals, that micropores rather than macropores are responsible for porosity at this lower rank.

Porosity: Porosity for coals of medium-volatile bituminous through anthracite rank is typically less than five percent (Kidd et al., 1992).

Compressive Strength: Compressive strength of coal reaches a minimum in the low-volatile bituminous range where cleating is most developed, as shown in Figure 3.8 (Jones et al., 1988).
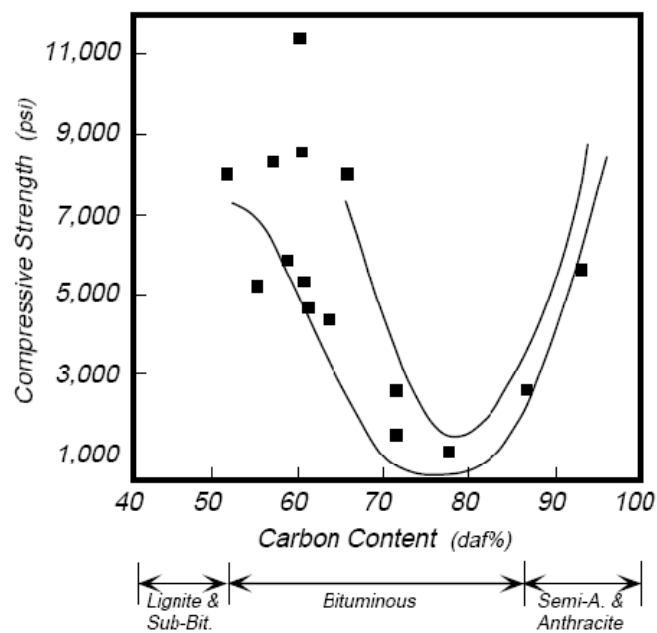
Figure 3.8. Compressive strength of coal (Jones et al., 1988)

Cleats: Cleat formation appears to be influenced by shrinkage, stress release, and extensional strain. Shrinkage during the process of coalification may contribute to cleat formation. Cleat is present in coals with a rank of lignite through anthracite and is commonly best developed in low-volatile bituminous rank coals, as shown

45

in Figure 3.9 (Ammosov and Eremin, 1960). The increased heat and pressure associated with metamorphism causes plastic flow that usually destroys cleat. The effect of rock flowage can be seen by contrasting the highly developed cleat of most seams of bituminous coal which, in general, show few signs of flowage, with the relative absence of cleat in anthracite where such signs are abundant (Kendall and Briggs, 1933). Some flat-lying or gently inclined anthracite coalbeds have well developed cleat systems (Law, 1993).
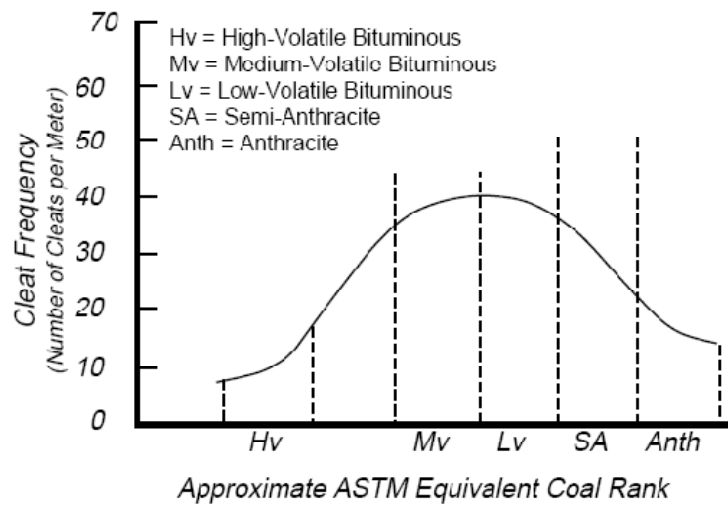
Figure 3.9. Cross-plot of coal rank and cleat frequency (Ammosov and Eremin, 1960)

3.2.2.2 Coal Composition

Coal can be viewed as being composed of water, minerals, and organic components (macerals). Minerals are considered contaminants in most commercial uses of coal. Macerals are the most combustible components of coal and can vary in chemical composition both among maceral varieties within a single coal bed and among coal beds. The general groups of macerals are vitrinite, liptinite, and inertinite. Macerals originate from partially decomposed plant parts that are altered through the coalification process. Their dominant chemical composition is primarily a mixture of carbon, hydrogen, oxygen, nitrogen, and sulfur. Of the major maceral groups, liptinite is richer in hydrogen and inertinite is richer in carbon than vitrinite. All macerals change chemically through the coalification process but at different rates. As a result of differing peat-forming

46

conditions and plant assemblages, organic components are transformed into macerals which arrange structurally into lithotypes that, in turn, comprise facies or the major subunits of a coal bed (Clarkson and Bustin, 1997).

Vitrinite forms from oxygen-rich woody tissues and leaves. Liptinite forms from hydrogen-rich plant oils, resins, cuticles, spores, and algae. Inertinite forms from carbon-rich degraded plant materials, woody tissues altered biochemically or by fire, and other resistant remains. Relatively few gaseous hydrocarbons are derived from inertinite. Sub-bituminous and higher rank coals contain two general subclasses; bright and dull coal. Bright coal is composed of the lithotypes vitrain, clarain, and fusain. The main lithotype in dull coal is durain, which usually has high mineral matter content. Lithotypes, in turn, are composed of various macerals, which are the microscopically recognizable remains of trees and plants. The chemically reactive and inert components as well as the mean reflectance of a coal sample can be determined by using petrographic analysis. Chemically reactive components include vitrinite, exinite, resinite, and semi-fusinite. Inert components include some semifusinite, micrinite, fusinite, and mineral matter.

3.2.2.3 Coal Gas

Because gas generation occurs over millions of years, it cannot be readily investigated. The relative volumes of various gases generated during coalification have been estimated by researchers. However, these numbers tend to vary widely, which attests to the level of uncertainty in coalbed gas generation.

The term 'coalbed methane' is not completely accurate because coalbed gas, though composed primarily of methane, includes other gases. When peat is formed, methane and other gases are produced, first by anaerobic fermentation, bacterial, and fungal alteration, and later in the process of coalification by geomechanical alteration through heat and pressure. The gaseous hydrocarbon generated in greatest quantity is methane. Very small amounts of ethane, propane, and butane are also created during peat formation. Because of the low pressure in the swamp environment, nearly all of these gases escape during peat formation.

The processes of peat formation and coalification increase carbon in the coal because of the loss of hydrogen and oxygen in the expelled moisture and volatiles. Because much of the volatiles that are produced escape, their volumes are uncertain. Volatiles produced include water (H_2O), carbon dioxide (CO_2), methane (CH_4), nitrogen (N_2), and heavier hydrocarbons. More of these volatiles are retained during coalification than during peat formation because of the higher pressures from overlying sediments. Moisture content decreases as coal rank increases. Thus, most of the water produced during coalification (in addition to original moisture) is expelled from the coal. Humic material, which makes up peat, is composed largely of oxygen-rich lignin and cellulose. Because of the chemistry of a humic coal material, its hydrogen loss will be less than that for sapropelic material (Rightmire et al., 1984). Coal more readily adsorbs CO_2 than CH_4, but CO_2 is more soluble in water. Thus, the retained volume of CO_2 tends to decrease and CH_4 increases as water is expelled during coalification.

Coalbed gas is primarily composed of hydrocarbons from C_1 to C_4. The absolute concentration of each hydrocarbon varies from coal to coal. The fraction of gases greater than C_2 can vary from zero to 70% and is referred to as the degree of wetness or the percentage of ethane and higher hydrocarbons (Rice et al., 1993; Clayton, 1998). However, CH_4 is usually the major constituent (88%-98%), with the higher hydrocarbons and CO_2 present in lesser amounts, (Diamond et al., 1998). The CO_2 content of coalbed gas can vary from zero to >99% (Rice et al., 1993; Clayton, 1998). The observation that some coalbed gas can be high in CO_2 content is a particularly pertinent observation, relative to the use of coalbeds as a sequestration sink for CO_2. It clearly shows that, at least in some instances, CO_2 can safely remain in coal for geologically significant time periods. The observation also provides reason to believe that coal can be safely and effectively utilized to both store CO_2 and recover CH_4. Clayton (1998) describes the various origins of CO_2 in coal. Smith et al. (1984) have used stable isotope 13C measurements to show that CO_2 present in the Australian coals they studied was derived from mantle sources during igneous intrusions near the coal seam.

In mean conditions it is assumed that 10 m of coal accumulation (not necessarily one single coal seam) covering 10 km^2 would produce 800×10^6 m^3 of gas during 20 years (Fievez and Mostade, 1998). The volume and the nature of gas generated increase with the rank but the pore storage inversely decreases with coalification, Figure 3.10.
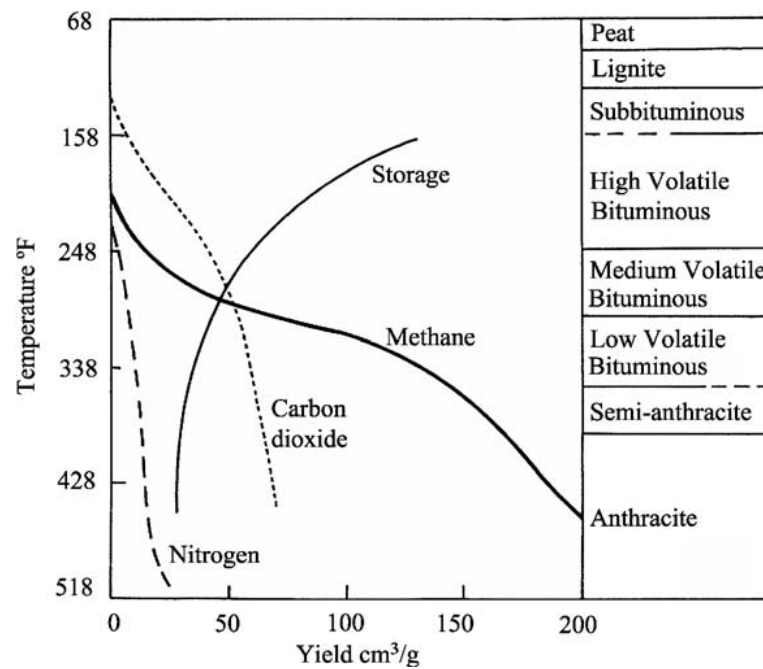
Figure 3.10. Competition between increasing gas production and decreasing storage capacity (Alpern, 2002)

CH$_4$ and other gases are generated during the conversion of plant material to coal. Thermally derived CH$_4$ in coal, as opposed to biogenic CH$_4$, is generated mainly during the bituminous stage of coalification, Figure 3.11. These gases are largely adsorbed onto the coal and small quantities are dispersed in the pore system of the coal (Gentzis, 2000).
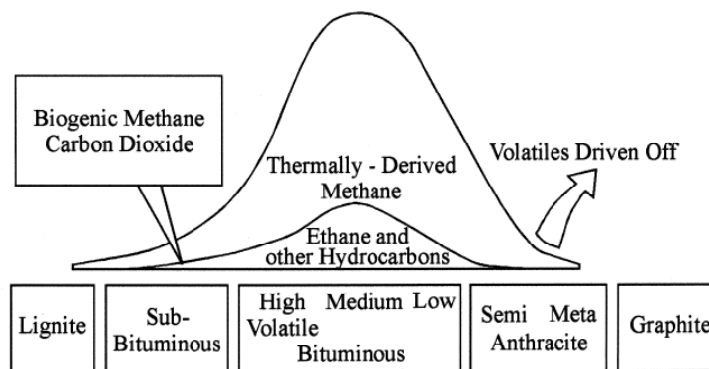
Figure 3.11. Gas generation during coalification (Tissot and Welte, 1984)

3.2.2.4 Mechanical Properties

Several mechanical properties of coal are significantly different from most reservoir rock. Coal is relatively compressible compared to the rock in many conventional reservoirs. Thus, the permeability of coal is more stress-dependent than most reservoir rocks. The orientation and magnitude of stress can strongly influence coalbed methane recovery. Permeability and porosity are functions of the net stress in the system. Because the vertical stress does not change during reservoir production, changes in pore pressure result in changes in effective stress. In the absence of other factors, porosity and permeability will decrease as pore pressure drops. At the same time, gas desorption is thought to cause a reduction of the bulk volume of the coal matrix. When this occurs, the pore volume of the natural fracture system is hypothesized to increase, resulting in an increased fracture system porosity and permeability.

Effective Stress: Geologic forces induce a number of stresses in a coal (or any other) formation. Typically, the stress fields are modeled using a vertical stress and horizontal stresses. The vertical stress usually is caused by the weight of the overlying rock and can be determined by integrating density logs measured from the surface to the depth of the reservoir. If density data are not available, a common assumption is that the vertical stress is equal to one psi per foot times the depth of the reservoir. Permeability and other properties of coal natural fracture system are functions of the net stress applied to the rock. The net stress,

also called the effective stress, is the difference between the stress and the pore pressure of the reservoir. In coalbed methane reservoirs, the pore pressure is the same as the pressure of the fracture system. Prior to production, if the pore pressure of the reservoir is unknown, it may be assumed equivalent to hydrostatic gradient, 0.43 psi per foot.

The fracture system permeability typically is anisotropic, which means that at any given point in the reservoir, permeability varies as a function of the direction of flow. Coal seams are commonly characterized as simple anisotropic reservoirs with two orthogonal horizontal permeability components (k_x and k_y) and a vertical permeability component (k_z). The x and y-directions usually correspond to the directions of the face-cleat and butt-cleat directions. These permeabilities can vary throughout the reservoir.

Homogeneous, unfractured coal is relatively impermeable to gas and water. The permeability of large coal masses, therefore, is predominantly a result of the fracture system. The dependence of the permeability on the cleat leads to the anisotropy exhibited by most coal seams, with the direction of greatest permeability oriented parallel to the continuous face cleat (King and Ertekin, 1988).

The fracture system porosity is the fraction of the bulk volume of the system capable of storing reservoir fluids. Just as in the case of conventional reservoirs, the coalbed methane fracture system pore volume may be occupied by mobile and immobile fluids. Thus, porosity for coalbed methane reservoirs can be reported in two ways. The first is the absolute porosity, which equals the ratio of total pore volume to the bulk volume. Porosity may also be reported as the moveable porosity, which is the ratio the volume of mobile fluid to the bulk volume. The amount of mobile fluid in the system depends strongly on the displacement process used to measure the porosity.

Permeability and porosity are functions of the net stress in the system. Because the vertical stress probably will not change much during reservoir production, changes in effective stress result almost entirely from changes in pore pressure. This means that the reservoir fracture system permeability and porosity depend on the reservoir pressure. In the absence of other factors, porosity and permeability will decrease as pore pressure drops (Saulsberry et al., 1996).

Laboratory testing has shown numerous times that coal permeability decreases as net effective stress increases. Thus, shallow reservoirs with relaxed tectonic forces are more likely to have a high permeability than are deeper reservoirs or reservoirs with strong tectonic forces. Because of the differences in cleat/fracture spacing density, coal permeability can vary considerably for a given stress condition. In general, however, as effective stress increases, permeability decreases (Seidle et al., 1992).

Coal Compressibility: The compressibility of coal is extremely high as compared to conventional gas sand reservoirs. The pore volume compressibility of coal typically is on the order of 400×10^{-6} psi^{-1}. This high degree of compressibility can significantly influence the permeability of coal when reservoir pressure depletes during production. Because coal is a fractured rock, the permeability of coal is dependent upon fracture aperture. In turn, fracture aperture is directly related to the stress condition of the rock at its in-situ condition. The stress condition of the rock is a function of both external stresses and internal stresses (pore pressure).

Shrinkage and Swelling: Coal is a polymer-like network that is often affected by the gas or solvent with which it is in contact. The coal matrix shrinks as water and hydrocarbons are desorbed and swells as certain gases are adsorbed onto its surface.

It is a well-established that as gas is released from a coal reservoir, the coal matrix shrinks, and cleats open, creating a significant improvement in coal (cleat) permeability. There has been considerable speculation and some laboratory

evidence that the process also works in reverse; that is, as gas is adsorbed onto coal, the matrix swells, cleats close, and permeability is reduced. Since CO_2 is much more adsorptive on coal than methane (by 2-3 times), the problem is exacerbated with CO_2 injection (Reeves, 2002).

It is well-known that CO_2 adsorption swells coal, (Toda, 1972; Walker et al., 1988; Dryden, 1963; Briggs and Sinha, 1993). The total uptake of CO_2 on coal includes contributions from physical adsorption on pore walls, pore fillings, and swelling. Surface area measurements of coal conducted at 25°C and at pressures less than 1 atm are largely unaffected by swelling. However, surface area measurements are likely to be affected at higher CO_2 pressures, because coals expand between 1.6% and 3.8% near 50 atm, (Walker et al.,1988). In addition to swelling at high CO_2 pressures, the organic matter in the coal matrix may be extracted by CO_2. Extractions result in higher surface area and pore volume measurements, (Mahajan, 1991)

Gas desorption is thought to cause a reduction of the bulk volume of the coal matrix (Gray, 1987; Harpalani and Chen, 1993). When this occurs, the pore volume of the natural fracture system is hypothesized to increase, resulting in an increased fracture system porosity and permeability. This matrix shrinkage has been observed in limited laboratory experiments, but has not been documented to occur in the field (Saulsberry et al., 1996).

Hydraulic Fracturing: The friable, cleated nature of coal affects the success of hydraulic fracturing treatments, and in certain cases allows for cavitation techniques to dramatically increase production. Strength of the coal reaches a minimum where cleats are more closely spaced. As a result, obtaining competent core samples from coals with well-developed cleat systems is not possible. Therefore, porosity and permeability, and relative permeability of the fracture system, cannot be accurately determined from core analysis. Properties of the fracture system are usually determined from well testing and/or history matching with a reservoir simulator.

3.2.3 Gas Storage in Coals

Coal is a source, reservoir and trap for significant quantities of methane and minor amounts of other gases. This gas, referred to as coalbed methane, is potentially an important economic resource, an explosive and outburst hazard requiring drainage during underground mining, and its leakage to the atmosphere contributes to the greenhouse effect. Coalbed methane, unlike conventional gas resources, is unique in that gas is retained in a number of ways including (Murray, 1991):

- adsorbed molecules within micropores (< 2 nm in diameter);
- trapped gas within matrix porosity;
- free gas (gas in excess of that which can be adsorbed) in cleat and fractures;
- and as a solute in ground water within coal fractures.

Porosity is the portion of the total coal volume that can be occupied by water, helium, or a similar molecule. The size of pore spaces can range from cleat fractures to intramolecular interstices. Coal pores can be classified into three sizes; macropores (>500 Å), mesopores (20 to 500 Å), and micropores (8 to 20 Å). Pore volume and average pore size both decrease with rank through low volatile bituminous (Mahajan, 1978). Porosity tends to decrease with rank into the low volatile bituminous stage, then increases as additional volatiles are lost and pore space is left open. Macroporosity, in general, includes cracks, cleats, fissures, voids in fusinite, etc. Gas in excess of that which can be adsorbed on the coal surfaces can be present as "free gas" within the porosity of the coal, mostly in the fractures. Gas can also be dissolved in water moving through the coalbed. Natural gas is soluble, to a limited degree, in ground water at the pressures and temperatures encountered in most coalbed methane reservoirs.

Coal seams are characterized by dual porosity: they contain a micropore or a primary porosity, and a macropore, or a secondary, fracture porosity system, (Kolesar et al., 1990). Warren and Root (1968) introduced the dual porosity concept when they studied naturally fractured reservoirs. The primary porosity was defined as intergranular and controlled by deposition and lithification. The secondary porosity was considered foramenular, controlled by fractures, fissures, and jointing. They represented the reservoir as a set of building blocks (parallelepiped), where the blocks represented the matrix, and the spacing between fractures. The micropore system in the coal has the same role as the matrix porosity in the conventional dual-porosity reservoir. The micropores have a large storage capacity but contribute little to the long-distance transport of reservoir fluids. The macropore system of a coal seam represents the volume occupied by the natural fracture system (cleats). The primary porosities in coal seams and in conventional reservoirs have similar roles. However, there are differences: due to the size of micropores in coals, the gas exists in the adsorbed state, whereas in conventional dual porosity reservoirs, gas is in the free state. Consequently, the gases stored in these two media obey different laws (Kolesar et al., 1990)

The pore structure of coal is highly heterogeneous, with the pore size varying from a few Angstroms to frequently over a micrometer in size. According to International Union of Pure and Applied Chemistry (IUPAC) classification (1994), pores may be divided into macropores (>50 nm), transient or mesopores (between 2 and 50 nm) and micropores (<2 nm). Gan et al. (1972) studied the structure of a variety eastern US coals using mercury porosimetry and nitrogen adsorption. Their results indicate that many coals exhibit a bidisperse pore structure, with significant fractions of the total pore volume being found in size greater than 30 nm and less than 1.2 nm. Similar bidisperse pore structures are reported by Thimons and Kissell (1973) and Smith and Williams (1984). It has been estimated that micropores account for about 95% of the internal coal surface and thus the potentially available sites for adsorption (Shi and Durucan, 2003b).

3.2.3.1 Structure of Coal

Coal seams may be characterized by two distinctive porosity systems: a well-defined and almost uniformly distributed network of natural fractures (cleats), and matrix blocks containing a highly heterogeneous porous structure between the cleats, Figure 3.12.

Typically, the butt cleat is perpendicular to the face cleat, but the fractures tend to be discontinuous and non-planar. Butt cleats commonly terminate against face cleats.
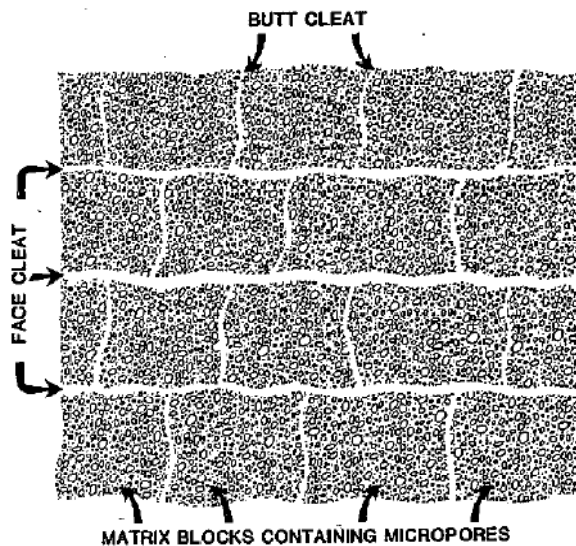
Figure 3.12. Plan view of dual porosity coal seam

Cleat spacing greatly influences coalbed permeability. Cleat spacing is related to rank, petrographic composition, mineral matter content, bed thickness, and tectonic history. In general, at any given rank, closer cleat spacing is associated with brighter coal, less mineral matter, and thinner beds (Levine, 1993). This correlation means that most medium and low-volatile coals will have good permeability if the cleats are open. Permeability can be low to non-existent in semianthracite and anthracite coals because of the destruction of the cleat. Mineral fillings in cleat may also lead to low permeability. If a large proportion of the cleats are filled, absolute permeability may be extremely low, as is the case in parts of the Bowen Basin in Australia and western parts of the Black Warrior

Basin in Alabama (Levine, 1993). Common minerals in cleat are calcite, pyrite, gypsum, kaolinite, and illite. (Penny and Conway, 1993).

"Without a well-developed cleat system, commercial gas production from coalbeds is not possible" (Gamson, 1994). The stored methane is first liberated very slowly from pore matrix by a diffusion process, then progresses more rapidly by a laminar Darcy flux (1-50 md) to the cleat system, where it can be collected more easily when drills for recovery are done perpendicular to the face cleats (pressure oriented).

Aquifers, mineralizations, bituminization, and tectonisation play a negative role because the cleat system must be open for gas circulation and recovery. The cleat system (Figure 3.13) is mainly related to vitrinite, liptinite playing a negative role in low rank coals, the spore exine being more or less elastic till its reflectivity converges with the vitrinite one. Pyrofusinite, when present, may also be positive. In high rank coals, the cleat system is multilayered (trans-microlithotypes), but the cleats can be annihilated by cementation (Alpern and Lemos de Sousa, 2002).
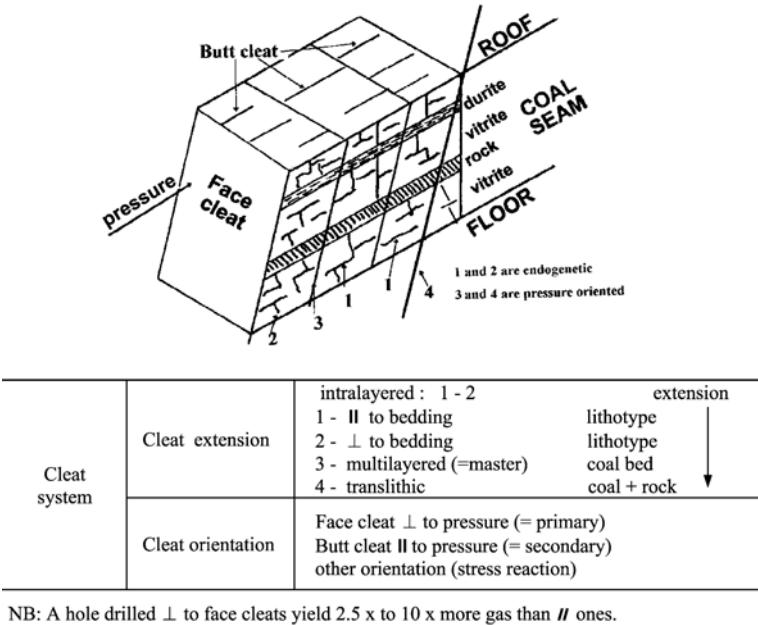
Figure 3.13. The cleat system (Tremain et al., 1991)

A prerequisite for economic gas flow rates is sufficient coal permeability. Most gas and water flows through the coal cleat system and other fractures. Cleat is a miners' term for the natural system of vertical fractures which have formed in most coals usually as a result of the coalification process. Typically, the cleat system in coal comprises two or more sets of subparallel fractures which are oriented nearly perpendicular to bedding. The set of fractures called the face cleat is usually dominant. The spacing of face cleat fractures may range from one tenth of an inch to several inches. The individual face cleats are relatively planar and persistent. Face cleat orientation is related to tectonic forces and is believed to form parallel to the maximum compressive stress (Engelder and Geiser, 1980).

3.2.3.2 Adsorption

Gas is retained in coal mostly by adsorption. Sufficient hydrostatic pressure must be present through geologic history for gas to be retained. If pressure is reduced sufficiently by erosion, uplift, or other means, gas can desorb from the coal leaving little or no gas. Adequate desorption testing should be performed to verify not only the amount, but also the quality of the gas in the coal. The presence of other gases, primarily CO_2, should be determined by analyzing gas samples during desorption tests (Kidd et al, 1992).

During physical sorption, fluid molecules experience a net attraction to a solid surface. Because of the attraction, the density of the fluids near the pore walls is increased, which increases the bulk density of the fluid in the sorbed state. The increased density means that at low pressure, greater volumes of gas can be stored by sorption than by compression.

The surface area of the coal, on which the methane is adsorbed, is very large (20-200 m^2/g) and coalbed methane reservoirs can have as much as five times the amount of gas as that contained in a conventional, sandstone gas reservoir of comparable size (Gale and Freund, 2001).

Definition: The term adsorption is universally understood to mean the enrichment of one or more of the components in the region between two bulk phases (i.e. the interfacial layer). With certain systems, the adsorption process is accompanied by absorption, i.e. the penetration of the fluid into the solid phase. As already indicated, one may then use the term sorption (and the related terms sorbent, sorptive and sorbate) when both the adsorption and absorption exist.

The terms 'adsorption' and 'desorption' are often used to indicate the direction from which the equilibrium states have been approached. Adsorption hysteresis arises when the amount adsorbed is not brought to the same level by the adsorption and desorption approach to a given 'equilibrium' pressure or bulk concentration. The relation, at constant temperature, between the amount adsorbed and the equilibrium pressure, or concentration, is known as the adsorption isotherm.

History: It was not until 1881 that the first attempts were made by Chappuis and Kayser to relate the amount of gas adsorbed to the pressure. In that year, Kayser introduced the term 'adsorption' and over the next few years the terms 'isotherm' and 'isothermal curve' were applied to the results of adsorption measurements made at constant temperature (Forrester and Giles, 1971).

In his 1916 paper, Langmuir had stated that with highly porous adsorbents such as charcoal 'it is impossible to know definitely the area on which the adsorption takes place' and that 'there are some spaces in which a molecule would be closely surrounded by carbon atoms on nearly all sides'. He concluded that equations derived for plane surfaces were not applicable to adsorption by charcoal. Unfortunately, these observations have been overlooked by many investigators, who have applied the simple Langmuir monolayer equation to adsorption data obtained with zeolites and activated carbons.

The significance of Langmuir's comments was appreciated, however, by Dubinin and his co-workers in Moscow, who put forward additional evidence to show that

the mechanism of physisorption in very narrow pores is not the same as that in wider pores: or on the open surface. Dubinin argued that the 'micropores' are filled at low relative pressure by a volume-filling process. By studying a wide range of activated carbons, he identified three groups of pores of different width: micropores, transitional pores (now termed mesopores) and macropores (Rouquerol et al., 1999).

Physisorption and Chemisorption: Adsorption is brought about by the interactions between the solid and the molecules in the fluid phase. Two kinds of forces are involved, which give rise to either physical adsorption (physisorption) or chemisorption. Physisorption forces are the same as those responsible for the condensation of vapors and the deviations from ideal gas behavior, whereas chemisorption interactions are essentially those responsible for the formation of chemical compounds.

The most important distinguishing features may be summarized as follows:

- Physisorption is a general phenomenon with a relatively low degree of specificity, whereas chemisorption is dependent on the reactivity of the adsorbent and adsorptive.

- Chemisorbed molecules are linked to reactive parts of the surface and the adsorption is necessarily confined to a monolayer. At high relative pressures, physisorption generally occurs as a multilayer.

- A physisorbed molecule keeps its identity and on desorption returns to the fluid phase in its original form. If a chemisorbed molecule undergoes reaction or dissociation, it loses its identity and cannot be recovered by desorption

- The energy of chemisorption is the same order of magnitude as the energy change in a comparable chemical reaction. Physisorption is always exothermic, but the energy involved is generally not much larger than the energy of condensation of the adsorptive. However, it is appreciably enhanced when physisorption takes place in very narrow pores.

- Activation energy is often involved in chemisorption and at low temperature the system may not have sufficient thermal energy to attain thermodynamic equilibrium. Physisorption systems generally attain equilibrium fairly rapidly, but equilibration may be slow if the transport process is rate-determining

Physical adsorption is caused by weak attractive forces (Van der Waals forces) that exist between pairs of molecules or atoms. Adsorption of methane to coal is caused by such weak physical forces.

Langmuir Isotherm: Langmuir isotherm relates the capacity for coal to store gas to the external pressure of the gas. As the name implies, an isotherm is evaluated at a constant temperature (reservoir temperature). A sorption isotherm relates the gas storage capacity of a coal to pressure and depends on the rank, temperature, and the moisture content of the coal. The sorption isotherm can be used to predict the volume of gas that will be released from the coal as the reservoir pressure is reduced. A typical sorption isotherm is illustrated in Figure 3.14. A common assumption is that the relationship between gas storage capacity and pressure can be described be an equation originally presented by Langmuir:

$$G_S = \frac{V_L p}{P_L + p}$$

(3.1)

The above equation assumes pure coal and for application in the field, the equation is modified to account for ash and moisture contents of the coal:

$$G_S = (1 - f_a - f_m)\frac{V_L p}{P_L + p}$$

(3.2)

As Figure 3.14 shows, the maximum amount of gas adsorbed is represented by Langmuir volume constant (V_L). Langmuir pressure constant (P_L) represents the pressure at which gas storage capacity equals one half of the maximum storage capacity (V_L). Figures 3.15 (a) and (b) illustrate the impact of P_L and V_L on the

shape of the isotherm curve. The values of P_L and V_L for a particular coal are determined by laboratory isotherm testing.
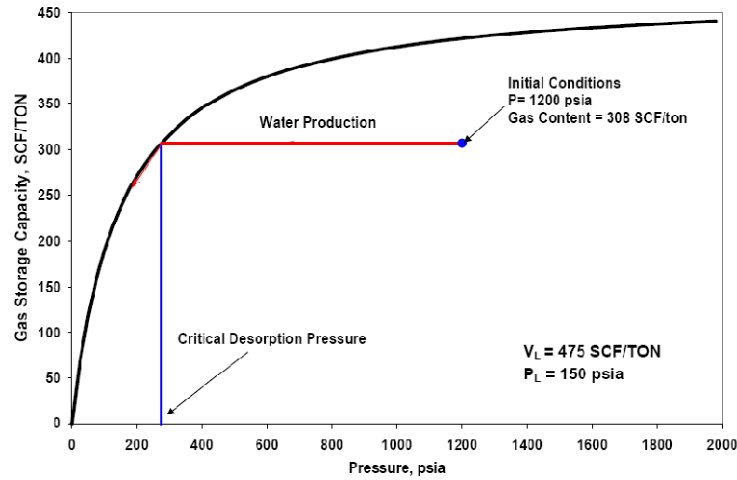
Figure 3.14. A typical Langmuir isotherm
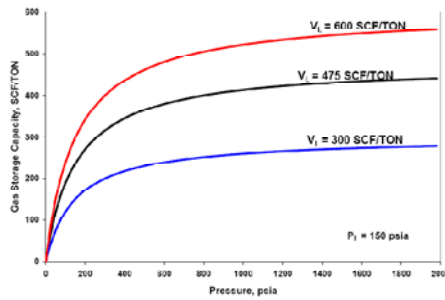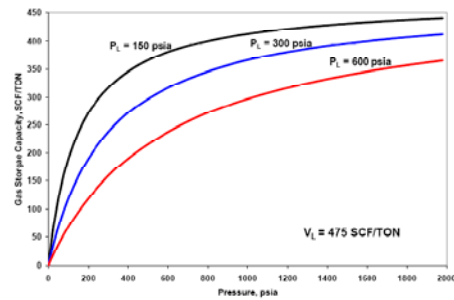
Fig. 3.15 (a)   Fig. 3.15 (b)

Figure 3.15. The impact of Langmuir volume constant (a) and Langmuir pressure constant (b) on the isotherm

It should be noted that most coals are not saturated with gas at initial conditions of the CBM reservoirs. The actual amount of gas in the coal is referred to as the 'gas content'. Gas content is the volume of gas at standard conditions per unit weight (i.e., per ton) of coal or rock. The use of this gas volume per weight rather than gas volume per volume of rock is a convention that originated in the mining industry, which sells coal on the basis of weight. Gas content of the coal is measured by desorption testing, which involves taking coal core, placing it in a container, and measuring the gas that evolves. If initially the gas content of the

coal is below equilibrium with the isotherm, as illustrated in Figure 3.14, no free gas will be present and the cleats will be filled with water.

Anomalously low gas contents can occur near faults if gas has desorbed from the coal and migrated from the strata through a fault or fracture system. Coalbed depth also can be misleading for estimating gas content. For example, some areas contain unconformities created by erosion of the coal and subsequent deposition of additional strata. In such areas, depth of the coals should be measured as the depth below the unconformity. Standard cores usually provide the most reliable gas content estimates. Other types of samples, such as side-wall cores, drill cuttings, and chips from slotting procedures, are sometimes used for desorption tests. However, these types of samples are not as reliable as standard cores.

The traditional method to recover methane depends on pressure reduction. Once the pressure in the coalbed is reduced, coal becomes less capable of retaining methane in an adsorbed form. The gas molecules start detaching themselves from the surface of the pores and micro fractures and the process of desorption are initiated. Desorption is the reverse of adsorption and occurs when the gas pressure within the pores is reduced.

When the in-situ gas content in the coal seam lies directly on the adsorption isotherm, methane is released immediately upon drawdown of water within the wellbore. However in many coalbeds the methane content does not lie on the desorption isotherm, and significant drawdown of pressure at the well bore must occur before methane can be released. After methane is desorbed it must diffuse through the solid matrix. The micropores of coal have a diameter of 0.5 to 1.0 nm and are inaccessible to water (brine).

For a given temperature, the relationship between gas storage capacity of coal and gas pressure is called the adsorption isotherm. Under in-situ conditions, if the gas content is lower than the coal storage capacity, the coalbed is called an undersaturated seam. If the gas content is higher than the coal storage capacity the

coalbed is an oversaturated seam. In this case, not only sorbed gas but also free gas is held in the coal seam.

At low pressures, the relationship between storage capacity and pressure is linear and is referred to as a Henry's Law isotherm. At very high pressures, all of the storage sites will be occupied if sufficient molecules are available, and the storage capacity will reach its maximum value equal to the Langmuir storage capacity. If a sufficient number of molecules are not available, some storage sites will remain unoccupied. When the coal has the capacity to adsorb more gas than is available, the coal is considered to be undersaturated.

Gas content is a measurement of the actual gas contained in a given coal reservoir. A coal reservoir is undersaturated if the actual gas content is less than the isotherm value at reservoir temperature and pressure. Accurate measurements of both gas content and the isotherm are required to estimate the production profile of the well. The ultimate recovery of gas depends on gas content and reservoir pressure. Gas production will not initiate until reservoir pressure falls below the point where the gas content of the coal is in equilibrium with the isotherm. Because most coal reservoirs are aquifers, production of water from the wellbore is the primary mechanism of pressure reduction. If the gas content of the reservoir is below the isotherm, as shown in Figure 3.14, then the reservoir will produce only water initially. After this single phase flow period, bubble flow initiates when reservoir pressure reaches the saturation point on the isotherm. Eventually, two phase flow of gas and water occurs as pressure is further reduced in the reservoir. Because of the relationship between gas desorption and reservoir pressure, it is important to produce coalbed methane wells at the lowest practical pressure.

3.2.3.3 Factors Affecting Adsorption
Many factors affect the sorption isotherm. These factors include ash content, moisture content, temperature, gas and maceral composition, and rank. Each of these factors is discussed below.

Ash Content: Non-coal components act as a diluent and reduce the gas storage capacity of coal. In coal samples that have significant sulfur content, the ash content is not equal to the mineral matter content of the coal. This is because the procedure used to determine the ash content by burning the sample also vaporizes sulfur. In this situation, it may be more accurate to replace the ash content in Equation 3.2 with the mineral matter content computed from the Parr formula, which is shown in Equation 3.3 (Parr, 1928).

$$m_c = 1.08f_a + 0.55s_c \qquad\qquad (3.3)$$

Moisture Content: Water competes for the sorption sites with other molecular species and reduces the storage capacity of non-water molecules. Thus, isotherms should be measured at the in-situ moisture content. Accepted practice is to perform sorption isotherm measurements at the equilibrium moisture content. The equilibrium moisture content, which is defined by ASTM standards, is assumed to be the same as the in-situ moisture content. Moisture content has been shown to decrease methane storage capacity until the critical moisture content is reached (Joubert et al., 1973). Moisture contents above this critical moisture level are generally believed to result in no further decreases in the methane storage capacity. This critical moisture level often is assumed to be the same as the equilibrium moisture content.

Temperature: For a given coal sample, the sorption isotherm is strongly affected by changes in temperature. Theory indicates that the Langmuir storage capacity (V_L) is unaffected by temperature. This implies that the total number of storage sites is insensitive to changes in temperature. However, temperature affects the value of the Langmuir constant ($b = 1/P_L$). As temperature increases, the Langmuir constant will decrease. This means that at a fixed pressure, the amount of gas stored will decrease as temperature increases (Saulsberry et al., 1996).

Reservoir temperature is an important concern in coalbed methane production and enhanced gas recovery because the sorption capacity of coal decreases significantly with increasing temperature (Yang and Saunders, 1985; Scott et al., 1994; Kroos et al., 2001).

Gas Composition: Methane isotherms can result in estimates of pure methane storage capacity that are less than the estimates of the total gas content when the coal contains significant amounts of carbon dioxide, nitrogen or heavier hydrocarbons. For this reason, mixed gas isotherms were computed using extended Langmuir theory (Harpalani and Pariti, 1993).

The extended Langmuir isotherm relationship is shown below:

$$G_{si} = V_{Li}(1 - f_a - f_m)\frac{b_i y_i p}{1 + \sum_{j=1}^{nc} b_j y_j p} \tag{3.4}$$

The gas sorbed on coal is not always pure methane. Coal can also contain appreciable amounts of carbon dioxide, nitrogen, and heavier hydrocarbons. In these cases, a. description of multi component gas sorption is needed in order to predict methane gas-in-place, rates, and reserves. This is true for primary, recovery by pressure depletion and especially true for proposed enhanced recovery processes using carbon dioxide and nitrogen (Arri et al., 1992).

Maceral Composition: Studies on Australian and Canadian coals showed that maceral composition is an important control on CH_4 adsorption, but the degree of influence is rank dependent (Lamberson and Bustin, 1993; Crosdale et al., 1998; Bustin and Clarkson, 1998; Laxminarayana and Crosdale, 1999). Most of these studies concluded that vitrinite is the most important maceral favoring CH_4 sorption on coal compared to similar-rank inertinite. However, investigations on Indian coals showed that the vitrinite content does not influence CH_4 sorption capacities (Laxminarayana and Crosdale, 2002). The affinity of CH_4 for vitrinite might be due to higher specific surface areas and associated with the higher

micropore capacities in vitrinites (e.g. Crosdale et al., 1998; Unsworth et al., 1989). On the other hand, Ettinger et al. (1966) documented for handpicked macerals from the Donezk Basin, Ukraine, that inertinite exhibited higher sorption capacities for CH_4 than vitrinite. Busch et al. (2003) analysed five different Argonne Premium Coals of different rank and similar maceral composition and found that sorption capacities varied strongly for CO_2 and CH_4 within this sample set. They concluded that CH_4 sorption capacity is influenced by rank rather than maceral composition, which is supported by results of Prinz et al. (2001) for coals from the Ruhr Area, Germany (Busch et al., 2006).

The role of coal maceral composition in determining adsorption capacity is clouded. Ettinger et al. (1966) reported that fusinite has a greater sorption than vitrinite, whereas most other studies have found vitrinite to have a greater adsorption capability (Faiz et al., 1992; Lamberson and Bustin, 1993; Crosdale and Beamish, 1993; Faiz and Hutton, 1995).

Rank: Various studies have attempted to establish correlations of CH_4 sorption capacities with rank and poresize distributions (e.g. Nodzenski, 1998; Laxminarayana and Crosdale, 1999; Levy et al., 1997). For the suite of coal samples investigated, results demonstrate a dependency between CH_4 sorption capacity and rank. Levy et al. (1997) found a clear positive relation between CH_4 sorption capacities of moist coals with carbon content (dry ash-free basis), while results for dry samples did not show a clear trend. The behavior for the moist coals was confirmed by Laxminarayana and Crosdale (2002) who reported a linear increase of CH_4 sorption capacities with rank for moist high to low volatile Indian coals. In their study, dry coals showed a decrease in maximum CH_4 sorption capacities with rank. However, in an earlier study on Australian coals, Laxminarayana and Crosdale (1999) demonstrated that CH_4 adsorption capacities on dry coals display a 'U'-shaped trend with rank exhibiting a minimum between 1.5% and 2.0% R_o max. Prinz (2004) also demonstrated for a suite of nine dry Pennsylvanian coals from the Ruhr Basin, Germany, measured at 40°C that dry

coals exhibit a 'U'-shaped trend, as described by Laxminarayana and Crosdale (1999). However, the same samples investigated in the moist state show a linear increase in CH_4 sorption capacity from high volatile bituminous to semi-anthracite rank.

Since Kim's (1977) influential publication and subsequent work by Eddy et al. (1982) and others, it has generally been assumed that total adsorbable methane reservoir capacity increases with coal rank, and rank has been considered the main parameter affecting the methane adsorption capacity of coal (e.g., Ryan, 1992). Other studies however suggest the relationship between methane adsorption, carbon dioxide adsorption and helium density is 'U' shaped with rank with the minimum occurring through the high volatile bituminous coal range (e.g., Moffat and Weale, 1955; Yee et al., 1993; Levy et al., 1997)

Geologic Age: Geologic age may affect the adsorption capacities of coals because coals of different age have different compaction characteristics that can affect the pore size and distribution of pores. Coals of differing age are also composed of plant materials that have different particle dimensions and which, on a bed-scale, can affect the pore size and permeability or interconnectivity of pores. For example, Carboniferous coal beds contain plant remains composed of flattened hollow stems of periderm-rich plants that compact to about less than 0.5 inches in thickness. In contrast, Tertiary age coal beds are composed of the remains of woody plants that can range in thickness from inches to feet. Coal beds of different ages not only differ in lithologic texture but also in the architecture of the facies comprising the bed. The facies architecture of a coal bed will affect its gas-holding capacity. Simply put, coal beds are very heterogeneous in composition both in vertical section and across an area, which may play a major role in the use of a bed as a storage site for CO_2. The stratigraphic and geographic distribution of facies defines subunits of a coal bed that have variable holding capacities for carbon dioxide and methane depending on their continuity and composition. Variations in these properties that define facies are not only observable among beds but within individual bed profiles (McGarry, 2000).

3.2.4 Gas Transport in Coals

The transport of methane through coal matrix is considered a three stage process. With water production and corresponding pressure decline, gas is being produced from the fractures due to pressure gradient. With producing the gas from the fractures, gas starts desorbing from the matrix walls into the fractures. With desorbing the gas from the matrix into the fracture, there will be a concentration gradient inside the matrix which causes the gas diffuse from inside the matrix to the matrix walls. This process is governed by concentration gradient. In the last stage, gas moves through the cleat system to the drainage wells. This process is governed by the pressure gradient. Thus, the cleat acts both as a sink to the micropore system and as a conduit to the wells. Figure 3.16 shows the three-stage process.
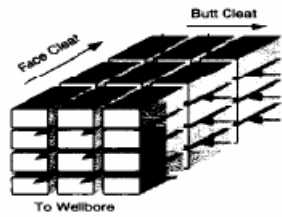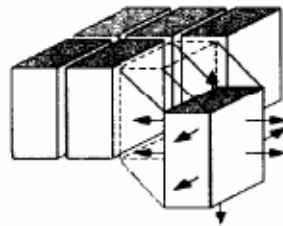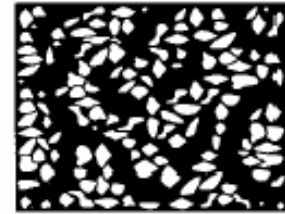
| Fig. 3.16 (a) | Fig. 3.16 (b) | Fig. 3.16 (c) |

Figure 3.16. Three stage gas transport in CBM (a) fluid production from natural fractures, (b) gas desorption from cleat surfaces, (c) molecular diffusion through the coal matrix

If the rate of gas desorption from the coal matrix and subsequent diffusion to the butt cleats to the face cleats is higher than the rate of flow in the face cleats, then CBM production is flow-limited, pressure-driven and can be modeled by Darcy's Law. If the diffusion rate is lower than the flow in the face cleat, then CBM production is diffusion-limited, concentration-driven and can be modeled by Fick's Law. The characteristics of each coalbed determine which model is appropriate (Gentzis, 2000).

For the reservoirs that have been commercially developed to date, diffusion has a minor and usually negligible effect on estimates of gas productivity. Gas production rates are generally limited by permeability rather than by diffusivity. Commercial coalbed methane reservoirs are characterized by a well developed fracture system that results in relatively short diffusion distances and large coal matrix surface area to volume ratios. Because of the presence of natural fractures, it is unlikely that production from a reservoir with commercial levels of permeability will be significantly hindered by low diffusivity.

3.2.4.1 Diffusion through Porous Media

The diffusion process can be defined as "…the process by which matter is transported from one part of a system to another as a result of random molecular motions" (Crank, 1956). The process was quantified by Fick in 1855 with the following relationship.

$$\frac{Q}{A} = -D\frac{dC}{DL} \tag{3.5}$$

Fick's Law states that the mass flux is directly proportional to the applied concentration gradient. The proportionality coefficient, D, is the diffusivity coefficient and is a property of the substance being transported, as well as the medium through which it is being transported. The micropore diffusion coefficient, D, has been experimentally determined to be between 10^{-8} and 10^{-13} cm^2/sec for most coals.

Smith and Williams (1984) presented a detailed review of the mechanisms of gas diffusion through porous media. Their discussion determined that the diffusion of gases through a pore system can be the result of three distinct flow mechanisms that may act individually or simultaneously. The mechanisms are bulk flow, where molecule/molecule interactions dominate (as in the flow through capillary); and two-dimensional (2D) surface flow of adsorbed gas (when an adsorbed gas layer exists).

70

Based on Scott and Dullien (1962) review on the mechanisms of gas transport in porous media, if a pore channel has a diameter which is much greater than the mean free path of the gas molecules, then the gas will flow by Poiseuille flow (forced flow) if it is subjected to a total pressure gradient, by bulk diffusion if it is subjected to a partial pressure (concentration) gradient, or by two dimensional surface diffusion if an adsorbed layer is present.

If the diameter of the pore channel is small compared to the mean free path, then the gas will flow by Knudsen diffusion (molecular streaming) if it is subjected to either a total or partial pressure gradient.

The critical value of pore diameter of the medium in order to have forced flow (due to pressure gradient) is four times larger than the diameter of the micropores in coal. It has been concluded that the first stage of gas transport in coalbed methane, through the micropores is a diffusion process. The diffusion of gas through the micropores can be the result of three distinct mechanisms which may act individually or simultaneously. These mechanisms are:

- Bulk diffusion, where molecule-molecule interactions dominate;
- Knudsen diffusion, where molecule-surface interactions dominate; and
- Two-dimensional surface diffusion of the adsorbed gas layer.

The following rules can be used to determine which mechanism dominates in a particular coal. If the diffusion coefficient is experimentally determined to be inversely proportional to the flowing pressure, then gas transport through the micropores is dominated by bulk diffusion. If the diffusion coefficient is determined to be constant with pressure, then Knudsen diffusion is the dominant mode of transport. Finally, if the mass flux ratio satisfies the following condition:

$$\frac{Q_{free}}{Q_{ads}} < \sqrt{\frac{MW_{ads}}{MW_{free}}} \tag{3.6}$$

The flow of a gas through a capillary, when the mean free path of the gas molecules is small compared to the capillary radius, is governed by the Hagen-Poiseuille law:

$$q = \frac{\pi r_c^4 \bar{p} \Delta p}{8 \mu p L} \qquad (3.7)$$

The criterion of the mean free path being small compared with the capillary radius is met for capillaries with large radii or flow at high pressures.

When the mean free path is large compared to the capillary radius, the flow is governed by the Knudsen (1909) equation:

$$q = \frac{4}{3} \frac{r_c^3}{p} \sqrt{\frac{2\pi RT}{MW}} \frac{\Delta p}{L} \qquad (3.8)$$

The criterion of the mean free path being large compared with the capillary radius is met for capillaries with small radii or flow at low pressures (Ertekin et al., 1986).

Three mechanisms have been identified for diffusion of an adsorbing gas in the macropores. They are molecular diffusion (molecule–molecule collisions dominate), Knudsen diffusion (molecule–wall collisions dominate) and surface diffusion (transport through physically adsorbed layer). The effective macropore diffusivity is thus a complex quantity which often includes contributions from more than one mechanism. As a rule of thumb, molecular diffusion prevails when the pore diameter is greater than ten times the mean free path; Knudsen diffusion may be assumed when the mean free path is greater than ten times the pore diameter. In the intermediate regime both wall collisions and intermolecular collisions contribute to the diffusional resistance and the effective diffusivity depends on both the Knudsen and molecular diffusivities. Because of the dependence of mean free path on pressure, for any given adsorbent and

adsorbate, there will be a transition from Knudsen flow at low pressures to molecular diffusion at high pressures (Shi and Durucan, 2003b).

Fick's Law is used to relate mass transfer to concentration gradients by assuming that the mass flow rate across a surface is proportional to the concentration gradient across the surface, the area of the surface, and the diffusion coefficient of the material through which diffusion occurs. Mass transport is in the direction of decreasing concentration. Theoretically, the diffusion phenomenon is discussed in terms of three components: bulk diffusion, Knudsen diffusion, and surface diffusion. Bulk diffusion is dominated by intermolecular interactions and includes diffusion of one molecular species through a mixture of different molecular species. Knudsen diffusion is dominated by molecule and pore wall interactions. As an example, a molecule in the sorbed state may acquire sufficient energy through collisions with other molecules to escape the sorbed state and move into the free gas state. At some point in time, the molecule will be attracted to the pore walls and return to the sorbed state. The molecule tends to travel in the direction of decreasing concentration during a continued change from the sorbed state to the free gas state. During surface diffusion, mass transfer occurs by movement through the sorbed state fluid without mass transfer into the free gas state. In practice, diffusion includes all three types, and no attempt is made to distinguish between the three processes.

The general solution for the coalbed methane reservoir behavior assumes that gas is transported through the coal primary porosity by diffusion towards the secondary porosity. Upon reaching the secondary porosity, the molecules desorb from the primary porosity surface and enter the free gas state within the secondary porosity. The concentration difference that controls diffusion is the difference between the average gas concentration within a matrix element and the gas concentration at the primary-secondary porosity interface. The sorbed gas molecules at the interface are assumed to be in equilibrium with the free gas molecules within the secondary porosity. The gas concentration at the interface is equal to that computed from the sorption isotherm gas storage capacity at the

pressure of the secondary porosity. Thus, the sorption isotherm relationship functions as the boundary condition at the primary-secondary porosity interface (Saulsberry et al., 1996).

The desorption of gas from coal is not an instantaneous process. Its release can be described qualitatively as 'slow bleeding'. For example, 1 lb of ¼ inch coal and 1 lb of fine coal (275 to 325 meshes) will adsorb the same quantity of methane at 15 psig. However, when pressure is reduced to atmospheric, the fine coal (275 to 325 meshes) desorbs all its gas in about 1 hour; the ¼ inch coal requires about 30 days. For solid coal particles of the order of ½ inch, the desorption process may take 6 months to 1 year. Consequently, the rate of desorption of gas from coal depends upon equilibrated pressure, coal particles size and geometry, and the diffusivity coefficient (Cervik, 1967).

The proportionality constant in Fick's Law is called the diffusion coefficient (D). The diffusion coefficient normally is determined by desorbing methane from a core in a laboratory and measuring the rate of desorption as a function of time. Studies on the Zonguldak coal by Karacan and Okandan (1999) showed that diffusion coefficients vary from location to location and are one of the implications how heterogeneous the coal is interms of gas transport and how difficult to predict the transport functions in such a coal.

Diffusion effects can be quantified by determining a sorption time, τ days, which is related to cleat spacing, s_f ft and the diffusion coefficient, D ft^2/day, as shown in Equation 3.9.

$$\tau = \frac{s_f^2}{8\pi D} \qquad (3.9)$$

This equation includes the proper shape factor for cylindrical matrix elements. Schwerer et al. (1984) have shown that cylindrical matrix elements are adequate

for modeling the diffusion process in coals. The sorption time can be estimated from gas content data.

3.2.4.2 Fluid Flow through Porous Media

In 1856, Darcy presented the results of a series of experiments that became the foundation of the theory of fluid flow through porous media. With water and unconsolidated sandpacks, he arrived at the following empirical relationship:

$$v = \frac{q}{A} = M \frac{\Delta p}{\Delta L} \qquad (3.10)$$

Darcy's law states that the apparent velocity of a flowing fluid in porous media is directly proportional to the applied pressure gradient. His proportionality constant, M, represents the hydraulic conductivity of the medium, which is defined as the permeability of the medium divided by the dynamic viscosity of the fluid. The first explicit separation of the permeability, k_a, which is a macroscopic property of the medium, from the viscosity was given by Wyckoff et al. (1933).

The assumptions inherent to Darcy's law are (1) a single, incompressible fluid is flowing, (2) flow is in the laminar regime, (3) the fluid is immobile at the pore walls, (4) isothermal condition exist, and (5) the fluid and medium are nonreactive (Ertekin et al., 1986).

The application of Darcy's law to gas in low permeability formations requires a correction for the Klinkenberg effect (gas slippage across the capillary walls of the pore channels)

In 1941, Klinkenberg observed that the apparent permeability to a gas was dependent on the reciprocal of the mean flowing pressure. This phenomenon was attributed to the slip velocity (sometimes called Knudsen flow or molecular streaming) across the walls of the internal capillaries. From the molecular theory

of Kundt and Warburg (1875) (which assumes ideal gas behavior), Klinkenberg derived the following expression for apparent permeability:

$$k_a = k_\infty \left(1 + \frac{B}{\bar{p}}\right) \qquad (3.11)$$

He further derived an expression for the slippage factor:

$$B = \frac{4K_l \bar{\lambda}\bar{p}}{r_c} \qquad (3.12)$$

where K_l is a constant and is about equal to unity.

Klinkenberg's experimental data indicated that the slippage factor increased with increasing pressure. Ertekin et al. (1986) developed a dynamic slippage model that is similar to the approach of Adzumi (1937) for slip through capillary tubes. This approach, based on simultaneous flow resulting viscous (Darcian) and diffusion (Fickian) flow processes, yields a pressure, composition, and saturation dependent slippage factor. In this way, it is possible to build the time and space dependent character of the slippage phenomenon into the gas transport equation in porous media.

As pressure is reduced in the cleat system by production of water from wells, gas desorbs into the cleat system. At this point, and for the remainder of the life of the producing wells, two-phase flow occurs in the cleat system. Under two-phase flow conditions, the relative permeability relationships between gas and water control the relative flow of gas and water in the reservoir. Thus, it is important to determine the relative permeability characteristics of the coal being analyzed. The work of Reznik et al. (1974) and Dabbous (1976) in the 1970s suggests that core tests can be used to quantify air water relative permeability characteristics in the coal cleat system. The work of Gash has provided significant improvements in coal relative permeability measurement techniques (Gash, 1991; Gash et al., 1993). Because water and gas flow in coals occurs in the interconnected cleat network,

the relative permeability characteristics of coals are a function of the cleat properties (e.g., spacing width, etc.). Experience has shown that lab-derived relative permeability relationships must be modified to obtain accurate simulation history matches of field data using single-layer reservoir models. (Young and Paul, 1993).

3.3 Enhanced Coalbed Methane (ECBM)

ECBM is defined as the process of injecting a gas or mixture of gases into a coal seam with the purpose of enhancing the desorption of coalbed methane (CBM) and increasing the recovery of CH_4 from the coal.

Coalbed Methane (CBM) is conventionally recovered by means of reservoir pressure depletion, which is simple but inefficient process recovering typically only 50% of the gas in place. Hydraulic pressure is used to assist recovery but, even so, because permeability is normally low; many wells must be drilled to achieve adequate gas flow. However, more efficient recovery, theoretically up to 100% of original gas in place, may be obtained by injecting CO_2, N_2 or other inert gases into the coal reservoir (Puri and Yee, 1990).

3.3.1 Applications of ECBM

The concept of coal seam sequestration was first proposed by Macdonald of Alberta Energy during discussions with Gunter et al., (1997) in 1991. They performed a "proof of concept" study to verify their hypothesis. Even though Macdonald seems to have been the first to have proposed the storage of CO_2 in coal seams for sequestration purposes, the concept of enhanced coalbed methane (ECBM) recovery using CO_2 predates that proposal considerably. In 1972, Every and Dell'osso (1972) found that CH_4 was effectively removed from crushed coal by flowing a stream of CO_2 at ambient temperature through the coal. Figure 3.17 shows a schematic diagram of ECBM.
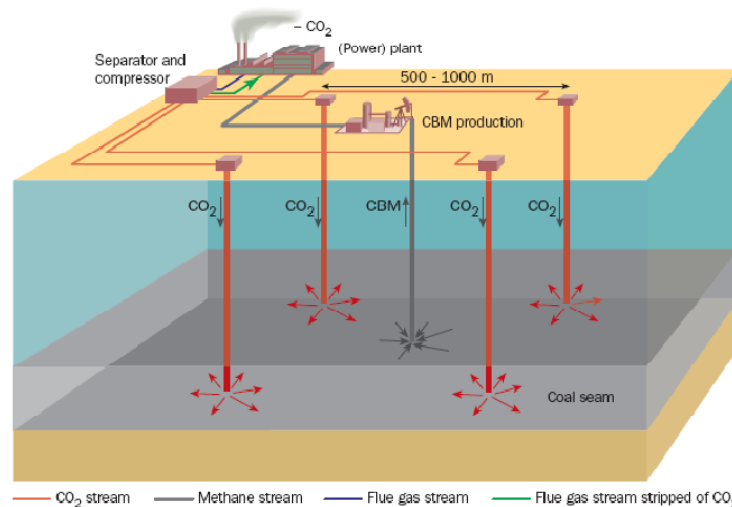
Figure 3.17. Schematic presentation of CO$_2$ storage in coal with simultaneous CBM production

In the late 1980s Amoco Corporation, through a series of patents and numerical simulations, developed the concept for N$_2$-ECBM. In 1993, Amoco successfully demonstrated the process in the field in a small pilot project in the San Juan Basin in Colorado. Amoco also undertook a CO$_2$-ECBM pilot in late 1993, but performance results were not released. For the past 3 years, Burlington Resources along with their partner Amoco have been operating a 13 well CO$_2$-ECBM pilot unit in the San Juan Basin in the southwestern United States. In addition, an economic analysis and 'proof of concept' study of CO$_2$-ECBM is currently taking place in Alberta, Canada. A practical research project has been established under the Implementing Agreement of the IEA Greenhouse Gas R&D Programme to enable international collaboration to support this work. CO$_2$-ECBM is attracting interest in a number of countries and further work has been proposed in the Netherlands and Belgium (Gale and Freund, 2001).

3.3.2 ECBM Processes

The process of gas injection under pressure into coalbeds generally works by having the following effect on the recovery of CBM (Brown et al., 1996; Stevenson, 1997):

78

- Creation of partial pressure gradient for the migration of methane between the coal matrix and the pore space in the coal, thereby enhancing the rate of methane desorption.

- Multi-component adsorption/desorption leading to desorption of CH_4 and adsorption of CO_2.

- Enhancement of coalbed permeability as a result of the gas pressure opening cleats and fractures in the coal that were previously held closed by the stress in the coal, leading to an increased rate of diffusion and flow of gas from the coal after water is removed.

- Increased gas relative permeability due to maintenance of porosity and a decrease in the level of water saturation.

Recently, new technologies have been proposed for enhancing coalbed methane (ECBM) production (Murray, 1994; Wong et al., 1998). The two principal variants are inert gas stripping using nitrogen injection, and displacement desorption employing carbon dioxide (CO_2) injection.

Simulation and early demonstration projects indicate that nitrogen injection ECBM (N_2-ECBM) is capable of recovering 90% or more of gas in place in the coal seam. N_2-ECBM works by lowering the partial pressure of methane to promote desorption. Nitrogen injection rapidly increases methane production rates. The timing and magnitude depends on the distance between the injection and production wells, the natural fracture porosity, and permeability and the sorption properties. N_2 breakthrough at the production well occurs rapidly. The N_2 content of the produced gas continues to increase until it becomes excessive (i.e., 50% or greater) when injection would probably be halted (Figure 3.18).
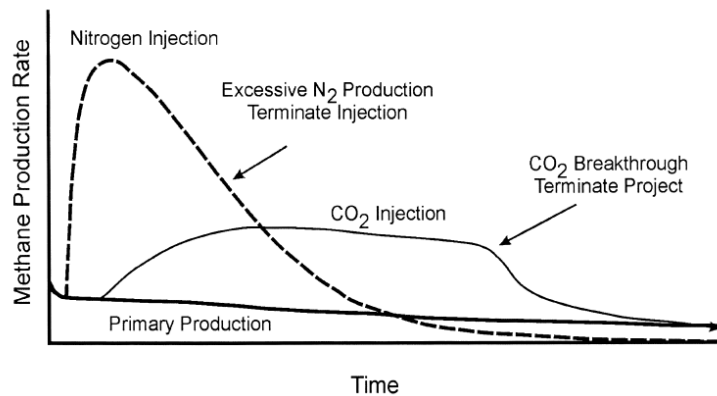
Figure 3.18. Indicative methane production profiles with N_2 and CO_2 injection (Gale and Freund, 2001)

Because the partial pressure of methane is equal to the total pressure multiplied by the mole fraction of methane, nitrogen can be injected to decrease the partial pressure of methane without reducing the total pressure. Lowering the partial pressure of methane by nitrogen injection instead of pressure depletion should increase both the methane production rate and the recovery factor. By maintaining a higher reservoir pressure with the nitrogen, there is a greater driving force throughout the life of the reservoir. This higher reservoir pressure also minimizes the impact of stress dependent permeability effects. Coal permeability has been shown to be highly stress dependent and may decrease substantially as the pore pressure in the reservoir is drawn down.

Carbon dioxide injection is an alternative to nitrogen injection and may provide greater methane recovery than will nitrogen injection. Not only does carbon dioxide reduce the partial pressure to methane, but it also adsorbs in the coal and reduces the capacity of the coal to contain methane (Harpalani and Pariti, 1993).

In the CO_2-ECBM process, injected CO_2 is preferentially adsorbed at the expense of the coalbed methane, which is simultaneously desorbed and can then be recovered as free gas. The CO_2 remains stored within the seam providing the seam is never disturbed. In concept, the process of CO_2-ECBM is quite simple. As CO_2 is injected into a coal reservoir, it is preferentially adsorbed into the coal matrix, displacing the methane that exists in that space. The displaced methane

80

then diffuses into the cleat system, and migrates to and is produced from production wells. As more CO_2 is injected, the radius of displaced methane expands. The process is relatively efficient in theory and, as implied from the isotherms, should require 2-3 volumes of injected CO_2 per volume of incrementally produced methane.

Laboratory isotherm measurements demonstrate that medium to high-rank coal can adsorb approximately twice as much CO_2 by volume as methane, (Puri and Yee, 1990). The common assumption is that, for higher-rank coals, the ECBM process stores 2 moles of CO_2 for every mole of CH_4 desorbed. However, the physical chemistry of this process has not yet been fully defined and there remains the possibility that there are other physical processes active within the reservoir, which could alter this ratio. Early indications from actual applications suggest this ratio might be higher (three or more) depending on channeling of CO_2 through faults and other high permeability pathways. Stanton et al., (2001) determined that some low-rank coals may adsorb as much as 10 moles of CO_2 for every mole of CH_4. Field applications and laboratory experiments showed that this ratio could be even larger at depths greater than ~800 m, where the gaseous CO_2 changes to supercritical CO_2, (Hall et al., 1994). Adsorption isotherms of CO_2, CH_4, and N_2 are illustrated in Figure 3.19. Note that the adsorption capacity of coal is about twice as high for CO_2 as for CH_4 up to a pressure of 6-7 MPa. At higher pressures even more CO_2 can be adsorbed due to a transition of CO_2 from the gas phase to a supercritical phase.

The depth interval for CO_2-ECBM is expected to be the same as that for CBM production (1000-5000 ft (304.8-1524 m)); however, the production increase due to CO_2 injection requires more time to develop than when N_2 injection is used. This is due to the sorption of CO_2 near the well. The sorbed CO_2-CH_4 front is expected to grow elliptically out from the injection wells, because of coal anisotropy. After a sufficient volume of CH_4 has been displaced, the CH_4 productivity increases. When CO_2 breaks through in the production well, the project would then be terminated. Therefore, CO_2-ECBM is potentially capable of

providing storage for anthropogenic CO_2, as well as improving the production of CBM (Gale and Freund, 2000).
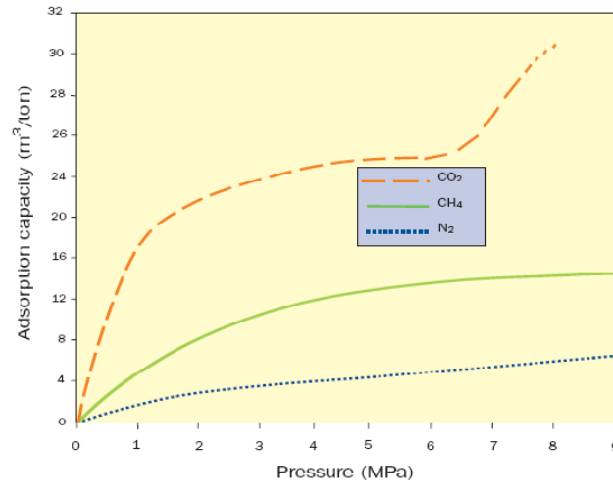
Figure 3.19. Adsorption isotherms of N_2, CH_4 and CO_2 (TNO-NITG, 2003)

There are two areas of reservoir engineering, both dealing with possible permeability reduction mechanisms that are also important to consider: (Reeves and Schoeling, 2000)

3.3.2.1 Shrinkage and Swelling

Matrix shrinkage occurs as methane gas desorbs from coal and is produced during primary production, causing separation of the cleats, a reduction in net stress, and an increase in bulk coal permeability. This permeability increase can be orders of magnitude in some cases, and can substantially improve the long-term performance of CBM wells. When CO_2 is injected into the coal, however, the opposite effect is surmised to occur; the matrix expands, stress increases, and permeability is reduced, exacerbated by high storage capacity of CO_2 on coal. While this effect was originally 'discovered' in the laboratory, proprietary industry studies have revealed that it is strongly affected by scale. Similar to the inability to effectively measure coal relative permeability in the laboratory due to the absence of macro-scale geological anomalies, matrix shrinkage/expansion effects are also affected by macro-scale features. Observing/understanding this phenomenon in the field (as opposed to in the laboratory) is therefore required.

3.3.2.2 Geochemical Reactions

Geochemical reactions may also occur between injected CO_2 and coal formation water and may lead to solids precipitation and permeability reduction. Although the principal reaction pathways between CO_2 and sedimentary formation waters are relatively well understood, most of this work has focused on saline-rich waters that exist in oil and gas fields and storage aquifers. However, since coal formation water is bicarbonate-rich, significant solids precipitation is not expected (the in-situ water is already 'rich' in CO_2; the addition of more CO_2 would therefore have little impact on water geochemistry). Due to the extremely long reaction times associated with the kinetic processes (many years) they cannot be adequately studied in the short term. Geochemical (equilibrium) modeling studies are therefore needed to investigate these issues further.

3.3.3 Reservoir Screening Criteria

Coal exists on all continents but in a wide variety of geologic settings. Some settings may be conducive to geologic sequestration, whereas other settings will be costly and technically difficult. Reservoir screening criteria are essential for locating favorable areas for the successful application of CO_2-ECBM. Gale and Freund (2001) developed a preliminary list of reservoir characteristics that are likely to be important for CO_2-ECBM application. These criteria are:

- Homogeneous reservoir: The coal seam reservoirs(s) should be laterally continuous and vertically isolated from surrounding strata, to prevent escape of CO_2.
- Simple structure: The reservoir should be minimally faulted and folded.
- Adequate permeability: Although a minimum permeability cannot be specified, preliminary simulation indicates that at least moderate permeability is necessary for effective ECBM (1 to 5 mDarcy).
- Optimal depth range: Shallow reservoirs tend to be low in reservoir pressure and gas content, whereas deep reservoirs suffer from diminished

permeability. For deep measures, CO_2 injection may actually improve permeability by maintaining pore pressure. Normally, coal seams at depths of 300-1500 m are considered to be appropriate for CBM.

- Coal geometry: Concentrated coal deposits (few, thick seams) are generally favored over stratigraphically dispersed (multiple, thin seams) measures.

- Gas-saturated conditions: Coal reservoirs that are saturated with respect to methane are preferred from an economic viewpoint. Undersaturated areas can experience a delay in methane production, although CO_2 injection could reduce delays by raising saturation. From a storage viewpoint, undersaturated coal seams are still effective reservoirs.

Other secondary reservoir criteria likely to affect ECBM recovery include coal rank, coal maceral composition (high vitrinite content preferred), low ash content (because ash does not adsorb methane), gas composition, and numerous other factors. These characteristics are shared in common with conventional CBM requirements but, for the most part, they are expected to affect ECBM economics only marginally. Specifically, for effective CO_2 storage, the selected coal seams must not be mined.

3.4 Simulating CBM Reservoirs

Conventional reservoir simulators experience difficulty in properly analyzing production of coalbed methane. To properly account for the adsorption properties of the coal, diffusion in the coal matrix, the effects of pore volume compressibility and the shrinkage of the coal matrix as gas is produced; even two phase, dual porosity finite difference simulators need to be modified. Because over 95% of the gas in place in a coal seam exists initially in an adsorbed state, accurate representation of gas in place needs to incorporate this storage mechanism. Because compressive forces may be very large for coals undergoing pressure drawdown, the model needs to relate changes in permeability and porosity to compressibility. Finally, because the coal matrix changes volume as gas

is produced, coal shrinkage (and thus cleat system expansion) due to gas desorption needs to be considered (Zuber et al., 1987).

Reservoir simulation technology, as a useful tool of reservoir development, has the capability to provide us with an economic means to solve complex reservoir engineering problems with efficiency. Three types of CBM reservoir models are currently used to simulate CBM/ECBM processes based on the evolution of coalbed methane reservoir simulation techniques (Wei et al., 2005):

- **Conventional black oil and compositional model:** The gas diffusion in coal is generally assumed to occur instantaneously, and thus they are actually single porosity models coupled with a gas source function. The source function is assumed as the gas dissolved in oil (Manik, 1999; Manik et al., 2002). This approach is not valuable for description of CBM recovery process due to a lack of supporting theory.

- **Specialized CBM model:** The non-equilibrium diffusion process (pseudo-steady state method) is modeled with a dual porosity system. Additionally, various adsorption models are used to simulate the multicomponent gas adsorption equilibrium. This type of models is now widely used in modeling CBM/ECBM recovery (Law et al., 2002). However, most of such models are still unable to give an acceptable accuracy because of the complicated physical and chemical conditions associated with CBM recovery processes of coal seams.

- **Improved CBM model:** More recently many attempts have been made to improve the CBM/ECBM simulation with alternative models, e.g. unsteady state model, bidisperse pore diffusion model, and triple-porosity simulation model. Additionally, several empirical equations were incorporated in simulator to describe the variation of coal properties due to coal matrix shrinkage. These studies are still at the early stage.

Because of the intricate nature of the flow of methane in coal seams the mathematical description of the phenomena is rather more demanding. Some

researchers proposed the use of empirical models (Airey, 1968; Lidine et al., 1964, McFall et al., 1987) which are based on the simple mathematical descriptions of the physical phenomena observed. These empirical models are relatively practical but they lack the theoretical rigor required for accurate predictions. Single porosity models applied to describe methane flow in coal seams employ partial differential equations valid for conventional reservoirs with some modifications such as inclusion of a pressure dependent source term or the modification of the accumulation term. These single porosity models utilize equilibrium sorption models which do not account for the time dependence of the sorption/diffusion process in the micropore structure of the coal and this results in predictions of higher flow rates and/or higher reservoir pressures (Anbarci and Ertekin, 1991).

The time dependence of transport of methane in the micropores is taken into consideration in non-equilibrium sorption/diffusion models which are essentially obtained by modifications implemented to the conventional dual porosity formulations. In dual porosity approach the mathematical formulation is constructed by a set of coupled equations representing the two-stage flow of methane in the coal seam. While the pseudo steady state non equilibrium models are similar to Warren and Root (1963) model of conventional dual porosity reservoirs, unsteady state sorption models (Sawyer, 1982; Holditch, 1983; Chase, 1980; Chen, 1987; Price and Ancell, 1978; Ancell et al., 1980; Kovalev and Kuznetsov, 1974; Kucuk and Sawer, 1980; Kolesar, 1985; Smith and Williams, 1984; Spencer et al., 1987) are obtained by adaptation of the conventional dual porosity model of De Swaan (1976).

The empirically based models are the simplest models. They are based on simple mathematical descriptions of observable physical phenomena. Airey's first model (1968), decline curves, Lidine's model (1964), and the model of McFall et al. (1987) are some examples of empirically based models. Empirical models are relatively simple, requiring a few input parameters, but they have theoretical difficulties for detailed predictions.

Equilibrium (pressure dependent) sorption models are the models which take the adsorption/desorption process into account. In this approach, the gas adsorbed onto the micropore walls is assumed to be in a continuous state of equilibrium with the free gas pressure in the macropores. In other words, the desorption/diffusion process is sufficiently rapid that the kinetics of the process can be neglected. The validity of the assumption of 'sufficiently rapid' can be determined by comparing the rate of diffusion to the rate of laminar (Darcy) flow. If gas flow is limited by the laminar process, and the diffusion process is significantly faster than the laminar process, then the equilibrium situation can be assumed. Equilibrium models are single-porosity, and partial differential equation models that are modified for coal seams. They can be modified in two ways: (1) including a pressure dependent source term, or (2) the modification of the storage term. These models can be formulated and solved analytically. Airey's second model is an example for equilibrium model. They can also be formulated and solved numerically (e.g., INTERCOMP's first model). The results of equilibrium sorption models are generally optimistic. They give high production rates when the bottom-hole pressure is specified or high average reservoir pressure when production rates are specified. The reason for this is, because of pressure decline, desorbed gas is assumed to enter the macropore system instantaneously. This approach does not take time dependency during transport through the micropore system into account.

Non-equilibrium (pressure and time dependent) models take time dependency into consideration. Non-equilibrium sorption models are modified 'conventional' dual-porosity models. These modifications are necessary because in coal seams (1) methane (reservoir fluid) is highly compressible; (2) gas stored in the primary porosity exists in an adsorbed state, and (3) gas transport through the micropore system is a diffusion process. Two approaches have been used to formulate the 'conventional' dual porosity models for coal seams. Pseudo-steady state formulations use a discretized form of Fick's First Law to describe gas transport through the micropore system, and unsteady state formulations use Fick's Second Law (Jalali, 2004).

3.4.1 Modeling of Important CBM/ECBM Factors

Unique properties of CBM and ECBM reservoirs lead to new attempts for the solution of the drawbacks of modeling techniques applied so far.

3.4.1.1 Multicomponent Gas Sorption

Multicomponent gas adsorption equilibria in coal seams are described using following approaches:

The K-value method is initially modified to describe coal gas sorption equilibria. The modification involves using an immobilized oil phase to simulate the coal matrix, and the solution gas to simulate the adsorbing components (Puri et al., 1991; Arri et al., 1992). Thus this method is not an accurate model with firm theoretical basis.

Extended Langmuir isotherm was suggested to provide a reasonable fit to experimental binary and ternary gas adsorption data using single component sorption isotherms (Arri et al., 1992; Harpalani and Pariti, 1993). However, it is not able to describe the thermodynamics of multicomponent coalbed gas sorption accurately.

Thermodynamic approaches were found to be superior to extended Langmuir equation for total adsorption capacities and equilibrium component predictions. The approaches are typically the idea adsorbed solution (IAS) and real adsorbed solution (RAS) with real gas equation of state (EOS), especially the IAS theory (Stevenson, 1997; Hall et al., 1994, Manik et al., 2002).

Most of current experimental and model studies are limited in the case that the system pressure is below the critical pressure of carbon dioxide. The IAS models are superior to extended Langmuir isotherm for total adsorption capacities and equilibrium component predictions, but it dependent on the pure component

isotherm. Most of IAS models are accurate for binary and ternary gas adsorption at low system pressure, except for high pressure ternary gas adsorption isotherm (Wei et al., 2005).

3.4.1.2 Multicomponent Gas Diffusion

Three types of models are proposed to describe gas diffusion in coal matrix: no diffusion, one-step diffusion and two step diffusion. Figure 3.20 illustrates the framework of current gas diffusion models used in CBM reservoir models.
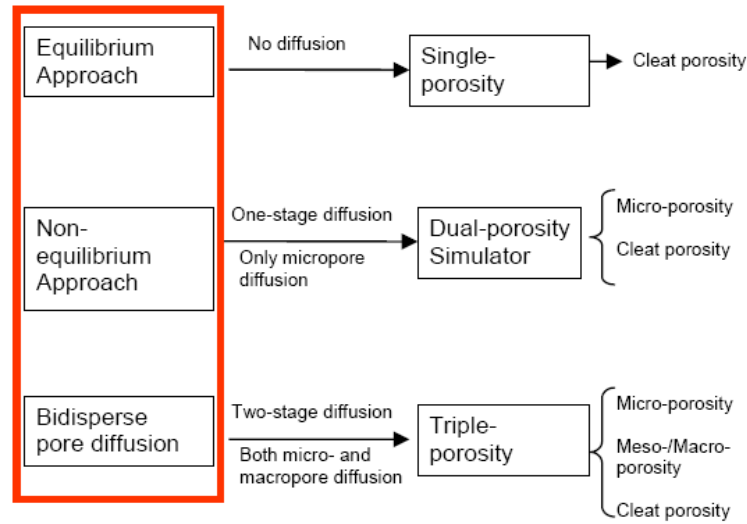
Figure 3.20. Framework of existing gas diffusion models (Wei et al., 2005)

A very good summary of the development of equilibrium and non-equilibrium model (pseudo-steady state and unsteady state formulations) for methane diffusion in coal matrix blocks has been presented by King and Ertekin in 1989. All of the reviewed models basically described gas diffusion process as instantaneous or one-step diffusion process respectively. More recently, researchers have realized that gas adsorption and diffusion in coal matrix with multi-scale pores can be described better by a bidisperse diffusion model (Cui et al., 2004; Shi and Durucan, 2003a; Shi and Durucan, 2003b; Clarkson and Bustin, 1999).

The effective diffusivity is a key parameter in evaluating gas sorption rate in coal matrix. It is generally not constant during production, depending on the gas pressure, concentration, coal wettability and pore structure. Therefore, incorporating these effects in gas diffusion models is crucial to describe CO_2-ECBM processes. From the perspective of numerical simulation, the following issues are of concern:

Pore Structure Dependent Diffusivity: Coals demonstrate very different pore structure, sorption capacity and gas transport behavior due to coal rank, lithology and maceral effects (Unsworth et al., 1989; Laxminarayana and Crosdale, 1999; Smith and Williams, 1984; Gan et al., 1972; Clarkson and Bustin, 1999; Gamson et al., 1993; Crosdale et al., 1998; Gamson et al., 1996). Correspondingly unipore diffusion model and bidisperse model are developed to model different types of gas diffusion processes respectively. So far most of existing diffusion models account for unipore gas diffusion process based on dual-porosity system. Only a few attempts have been made to model gas diffusion in coal matrix using bidisperse models. The bidisperse models generally assume two-step gas diffusion in coal matrix: surface diffusion in microporous system and pore diffusion in meso- and/or macro-pore system. Gas adsorption takes place in the micropores, with the meso-/macro-pores providing storage for free gas, as well as tortuous paths for gas transport between the micropores and cleats.

Pressure and Concentration Dependent Diffusivity: Current studies on this issue are very limited. Two factors are now recognized to induce the pressure-dependence of diffusivity: nonlinear isotherm and matrix swelling and shrinkage due to gas adsorption and desorption. In adsorption system when the equilibrium isotherm is linear, diffusion coefficient is generally independent of concentration. However, when the isotherm is nonlinear the diffusivity is concentration dependent. Adsorption swelling may narrow some micropore entrances (Ceglarska and Zarebska, 2002) and enhance the diffusion energy barrier of adsorbate in micropores, consequently reducing the diffusivities.

90

Multicomponent Gas Counter-Diffusion in Coal Matrix: Modeling multicomponent gas sorption kinetics is now an urgent requirement for ECBM project, especially the counter diffusion process. However, few experimental and theoretical studies have been involved in this issue. Four types of models have proposed to solve this problem: (1) Different adsorbate diffusivity, (2) Analytical solution for ternary gas system, (3) Concentration-dependent micropore diffusivity, and (4) Maxwell-Stefan (MS) equation.

Water Effects on Gas Transport in Coal Matrix: In 2001, Reeves and his colleagues found that to match water production history, the cleat porosity of a dual-porosity model has to be increased to unrealistic values. This indicates that the assumption of water only stored in large fractures (face and butt cleats) may be not necessarily accurate for some water-wet coals. Indeed in water-wet coals the small fracture system remains almost entirely filled with water, and gas sorption kinetics is determined by a slow diffusion process (Mazumder et al., 2003).

3.4.2 Data Needed for Simulation

Three general types of data are needed to use a coalbed methane reservoir simulator:

- **Reservoir description data**, such as absolute cleat permeability and gas content. Generally, these data are entered as arrays because a value must be assigned to every active grid block.
- **Fluid PVT properties**, such as gas viscosity and composition.
- **Recurrent data** or data which may change with time during a simulation run. These data may be entered multiple times in the simulator. They include well productivity indices, rate or bottomhole pressure schedules, and skin factors. Run control parameters such as time step size are recurrent data.

A checklist of data by category is given in Table 3.3. Some data are so important that they should be considered as a minimal data set for simulation. These data, which are all in the Reservoir Description Data category, are:

- **Absolute Cleat Permeability**. Influences the rate of gas recovery.
- **Initial Gas Content**. Influences the gas-in-place and gas recovery.
- **Coal Thickness**. Directly affects gas-in-place and gas and water rates.
- **Adsorption Isotherm**. Influences the timing of initial gas show and ultimate gas recovery.
- **Cleat Porosity**. The place where water is stored in coal. Cleat porosity affects the volume of water produced.

These properties are critical because they determine project economics. Without at least some measurements for them, Considerable guesswork and a corresponding uncertainty in the computed results are required. In this case, a sensitivity analysis should be performed with the simulator to assess the range of probable outcomes as a function of the 'guessed' data (Saulsberry et al., 1996).

Table 3.3. Data needed to use a coalbed methane simulator (Saulsberry et al., 1996)

Table 3.3 (a) Reservoir Description Data

Absolute Cleat Permeability	Reservoir Geometry
Cleat Permeability Orientation	Structural Elevation (dip)
Vertical Permeability	Depth
Porosity	Net Thickness
Initial Gas Content	Stratification (layers)
Adsorption Isotherm	Ash Content
Desorption Pressure	Well Drainage Area
Sorption Time	Initial Reservoir Pressure
Diffusion Coefficient	Initial Water Saturation
Cleat Spacing	Gas-Water Relative Permeability
Pore Volume Compressibility	Gas-Water Capillary Pressure
Matrix Shrinkage Compressibility	Aquifer Rock Properties

Table 3.3 (b) Fluid PVT Data

Gas Formation Volume Factor	Water Formation Volume Factor
Gas Viscosity	Water Viscosity
Gas Gravity	Water Stock Tank Density
Gas Composition	Gas Solubility in Water

Table 3.3 (c) Recurrent Data	
Minimum Timestep Size	Maximum Saturation Change Over Timestep
Maximum Timestep Size	Maximum Pressure Change Over Timestep
Timestep Size Multiplier	Finite Difference Solution Tolerances
Water Production Rate vs. Time	Maximum Allowable Water Production Rate
Gas Production (Injection) Rate vs. Time	Maximum Allowable Gas Production Rate
Bottomhole (Wellhead) Pressure vs. Time	Minimum Allowable Bottomhole Pressure
Well Productivity Index	Wellbore Radius
Skin Factor	Induced Fracture Length

3.5 Estimating Reserve Volumes

Reserves frequently are estimated before drilling or any subsurface development, during the development drilling of the field, after some performance data are available, and after performance trends are well established (Forrest, 1985).

While the ultimate recovery estimates may become accurate at some point in the late life of a reservoir, the reserve estimate at that time still may have a significant risk. Reserve estimating methods usually are categorized into three families: analogy, volumetric, and performance techniques. The performance technique methods usually are subdivided into simulation studies, material-balance calculations, and decline trend analysis (Forrest, 1985). Level of uncertainty in these techniques becomes lesser from analogy to performance techniques, where analogy method is based purely on statistics of a similar field when the prospect in study has none or insufficient wells.

3.5.1 Deterministic and Probabilistic (Statistical) Methods

Reserves of a field can be calculated in two ways as 'deterministic' and 'probabilistic' (statistical) methods. If the value of a variable is known or can be predicted with certainty at the time of decision making, the variable is called a deterministic variable (Newendorp et al., 2000). The deterministic calculation of reserves is where specific values of each input parameter are multiplied together to determine a single estimate of reserves (Ross, 1998). In this case, the

deterministic method has to give the best estimate by highest confidence and this is only possible when enough and quality data are supplied. But, deterministic approach gives only a single number and, therefore, provides no information regarding uncertainty. Arguments presented in favor of the deterministic approach are simple to apply, easy to audit, based on specific criteria, conservative at proved level and, avoids misleading pseudo-accuracy (Ross, 1998).

In the statistical approach, each input parameter is defined by an uncertainty distribution (probability density function). The basis for the distribution is generally three input variables (e.g. low, most likely, high), which may be identical to those values used in the deterministic approach, an estimate of the levels of certainty associated with the low and high values, and an assumption of the type (shape) of the distribution. The distributions are then combined together using statistical methods with some assumptions regarding the level of dependence between parameters (Ross, 1998). Arguments presented in favor of the statistical approach are mathematically correct, documents whole range of uncertainty assigns values to level of uncertainty, leads to greater consistency of results.

As a result, in calculation of reserves by statistical methods, results can be given by cumulative probability levels which mean all the possible reserves add up to 100 %. For providing common understanding reserve estimations are generally summarized by three certainty levels as P10, P50 and P90 reserves. In these terms, P leads to probability and as it gets lesser the level of uncertainty gets higher. By P10 it is meant that there is 90% uncertainty but 10% confidence that the reserves are equal or less than that estimation. Generally, P50 estimates are close to deterministic estimates but it is also possible to see the variation in estimates depending on the variation in the reservoir parameters by probabilistic approach (Schuyler, 1998; Capen 1999; Murtha, 2001). There are principally two methods for statistical calculations, Monte Carlo simulation and decision tree analysis. Monte Carlo technique considers entire ranges of the variables of original gas/oil in place formula rather than deterministic figures (Macary and Hassan, 1999).

94

In reserve calculation of a field there are several uncertain variables. In a traditional oil reservoir with rather homogeneous porosity and structure, uncertain variables that are most affecting the reserves volume can be listed as area, matrix pay thickness, water saturation and original formation volume factor of gas. But in a naturally fractured reservoirs or coal beds which have unique differences from a homogeneous reservoir there are more variables causing uncertainty in reserve estimation which is fracture/cleat parameters.

The degree of uncertainty of reserve estimation variables, range of values they have and probability that they show a value in those ranges must be described in order to see the effects of uncertainty in calculations. Best estimates, by other means, the most probable and certain values can be used resulting to a deterministic calculation of reserves. But, considering that there are limited data in contrast to every possible data point throughout the field, there is always a level of uncertainty which can only be reduced by drilling a new well and collecting more and more data.

It would be meaningful if a whole picture of possible inputs and outcomes are described to see the range of reserves that can exist in the field. This can be performed by using concepts of statistics. The statistical tool, Monte Carlo simulation is relevant in evaluating oil in place calculations based on a statistical approach.

One of the main considerations in calculating the oil in place is that the variables must be independent. But actually petrophysical variables are not independent (Fylling, 2002). High porosity fraction will also be led to high permeability. It is important to determine which factors cause variability or uncertainty in calculations. The dependence can be investigated by sensitivity analysis (Mendenhall and Sincich, 1996).

3.5.2 Probability and Probability Distribution

The classical definition of probability involves a group or a set of equally likely outcomes. A graphical or mathematical representation of the range and likelihoods of possible values that a random variable can have is probability distribution. Probability distributions can be discrete or continuous, depending on the nature of the variable. The horizontal scale of a probability distribution is the measure of the variable, in whatever units or scale are appropriate. The height of a probability distribution above the horizontal axis (amplitude) is proportional to the probability of the values along the horizontal axis (Newendorp et al., 2000).

Figure 3.21 shows an example of a continuous probability distribution. More formally, this is called a probability density function (PDF). It is continuous in the sense that any value of recoverable reserves within the range of x_{min} and x_{max} is possible. That is, there is a continuum of possible values of x between the minimum and maximum values. The curve, f(x), is a mathematical function such that when the area is determined under the distribution by integrating f(x) from x_{min} to x_{max} the resulting area will be 1.0, dimensionless (Newendorp et al., 2000).
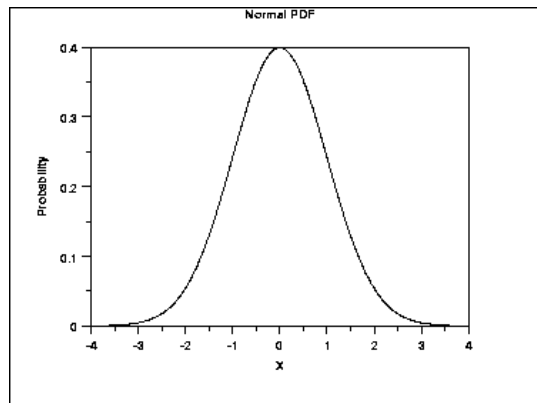
Figure 3.21. Normal probability distribution function

The area under all probability density distributions is, by definition, one. Another characteristic of all probability distributions is that the probabilities are always positive (or zero), but never negative. This means the probability distribution

96

curve, or function, never goes below the horizontal axis. By use of appropriate proportionality constants and/or some integration the vertical scale can be converted to a numerical scale that is proportional to the probability of occurrence of a value or range of values of the random variable. This leads us to the general statement given earlier that the height of the curve above the x-axis is proportional to the probability of occurrence.

Thus, in Figure 3.21, it is concluded that values of x towards the low end of the range and under the high points of the curve are the most probable values. As x gets larger the curve gets lower and lower which implies that the larger ranges of x become decreasingly less probable. The probability of occurrence of a value of x which is less than x_{min} or greater than x_{max} is zero (Newendorp et al., 2000).

3.5.3 Uncertainty Assessment by Monte Carlo Simulation

The most common mathematical basis for the statistical calculation of reserves is the Monte Carlo method. Monte Carlo simulation method used in oil and gas exploration and exploitation investments appeared in petroleum literature in the beginning of 1976 (Briggs, 2001). Monte Carlo simulation takes on special importance in the field of reserve estimation, which introduces significant and vital area of interest to any reservoir engineer. Monte Carlo simulation allows each variable to vary between some minimum and maximum value according to some prescribed distribution, and then solves the problem for a large set of these input variables. The results of Monte Carlo simulation are then presented in graphical form as a probability distribution for the dependent variable. This probability is then interpreted by using statistical methods to determine the likelihood of a particular solution occurring or not occurring (Mendenhall and Sincich, 1996).

In many engineering problems there may be a multitude of input parameters that are not known very accurately and thus have uncertain values. Uncertainty in a variable can occur for a number of reasons. For example, the method of measuring a parameter may have to be predicted into the future, or there may be a

97

limited amount of data for a certain parameter. In any case, the best that can be done for a variable with an uncertain value is to choose a reasonable range over that range. The choice of the particular distribution for a certain variable should be guided by the engineer's knowledge of that variable. Within the Monte Carlo simulation method, the selection of a value for an independent variable is accomplished by using the fact that the integral of the probability distribution will lie between 0 and 1 and will be monotonic in behavior. Thus the selection of a random number between 0 and 1 will yield a distinct random value for the variable between the selected minimum and maximum (NIST, 2007).

Once the independent variables have been determined then the dependent variable, i.e. an evaluation criterion that has been chosen, can be calculated. The process is then repeated a large number of times. The values of the dependent variable are then grouped in class intervals and relative and cumulative probability plots are constructed (NIST, 2007).

The following sequences of steps summarize Monte Carlo simulation method:

1. Establish distributions for each parameter or independent variable.
2. Set up equations which will allow the calculation of the independent variables. This is done by determining expressions for the integrals of probability distributions. It should be recognized that the integral of a probability distribution is the cumulative frequency of the distribution.
3. Generate a random number for each independent variable. A different random number must be determined for each independent variable.
4. Use the random numbers to calculate values for the independent variables.
5. Calculate dependent variable and store the result in a class interval.
6. Return to step 3 and repeat 3 through 5 a large number of times.
7. Construct relative and cumulative frequency diagrams.

A common criticism of the method is that it is not exactly repeatable; however, it is simply a matter of running enough passes to ensure an acceptable level of repeatability. The key advantages of the method over other statistical approaches are no constraints on input and output distributions; and, can accommodate dependencies (Ross, 1998).

CHAPTER 4

STATEMENT OF THE PROBLEM

The increased level of greenhouse gases due to human activity is the main factor for climate change. CO_2 is the main constitute among these gases. Subsurface storage of CO_2 in geological systems such as coal reservoirs is considered as one of the safe and promising perspectives. By injecting CO_2 into the coal beds, methane is released with CO_2 adsorption in the coal matrix and this process is known as an enhanced coal bed methane recovery (ECBM). Gas production from coalbed methane reservoirs (CBM) became an important part of natural gas production from unconventional resources. Turkey needs energy and obeys the international environmental regulations. Since the coal seams in Amasra field are found relatively deeper and not studied detailed enough yet, it can be considered both for CBM and ECBM recovery processes among the coal reservoirs of Zonguldak basin. Carbon dioxide emitted from Zonguldak Çatalağzı Power Plant or Ereğli Iron and Steel Factory can be used as a source for CO_2 to enhance methane production.

From this point of view, gas reserve estimation in coal seams of Amasra district resource area-A will be done using stochastic approach with the use of uncertainty in rock and fluid data. In order to determine the continuity of coal seams, the correlation study will be conducted with the available well data. The transport and storage of CH_4 and CO_2 in coal seams can be influenced by several coal properties such as permeability, porosity, coal density, cleat spacings, adsorption isotherm, compressibility, water saturation, permeability anisotropy and shrinkage and swelling. Therefore the effect of aforementioned properties on the efficiency of CBM and ECBM recovery processes will be investigated in one of the most prospective coal seam with a compositional reservoir simulator.

CHAPTER 5

FIELD DESCRIPTION

5.1 General Description of Zonguldak Coal Basin

Zonguldak coal basin contains the only major bituminous coal deposits of Turkey where Carboniferous coal-bearing strata have been mined for more than a century (Yalcin et al., 2002).

The hard-coal reserves of Zonguldak Coal Basin are estimated to be 1.5×10^9 tonnes and are spread over an area of about 13,000 km^2. This estimate includes the seams down to -1200 m below the sea level (M.T.A., 1992a; 1992b; 1994). There known to be thin coal seams below -1200 m that, technically and economically, cannot be mined and, thus, practically no data are available for them. Presently, only the seams down to -425 m are being mined. No gallery has dipped down below -560 m in the basin. There are around 40 coal seams of which 25 are being mined. The seam thicknesses vary from 1 m to 10 m. The average total coal thickness is approximately 40 m. The dip angles of the seams display a wide range, changing from horizontal to nearly vertical. The geological structure of the basin is highly faulted and fractured. The coal seams of the basin have been known to be extremely gassy. Geographically, the basin is located in the humid, Northwestern part of Turkey, on the Black Sea coast (Serpen and Alpkaya, 1998).

The Carboniferous coal-bearing sequence represents the uppermost part of a thick Paleozoic (Cambrian-Ordovician to Carboniferous) section that lies on a Precambrian basement consisting of granites and amphibolites (Figure 5.1). This sequence contains the Namurian Alacaagzi Formation, the Westphalian A Kozlu Formation, and the Westphalian B-D Karadon Formation. The Westphalian A

deltaic unit (Kozlu Formation) is mainly composed of sandy lithology and bears most of the coal seams. The Westphalian B-D unit (Karadon Formation) consists of coarser clastics and fewer coal seams, which were deposited in a flood plain environment (Yalcin et al., 2002).
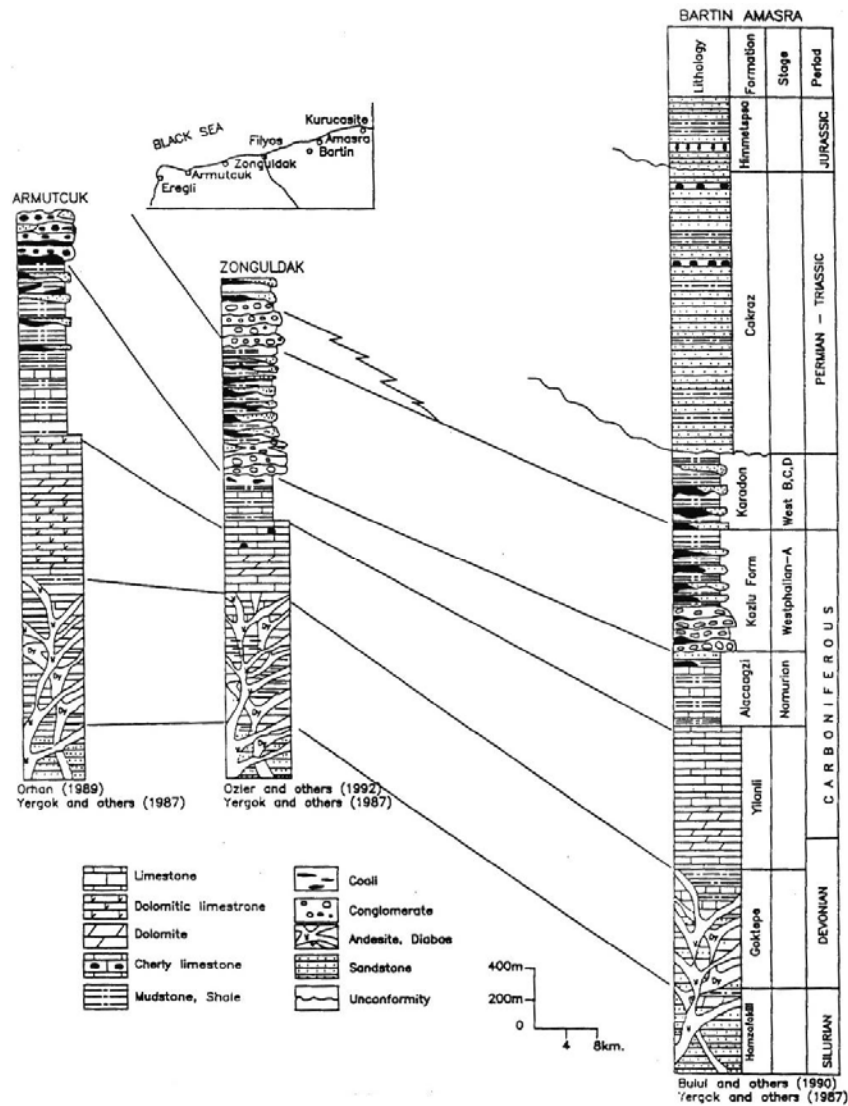
Figure 5.1. Idealized stratigraphic column of Zonguldak coal basin (Orhan, 1995)

The region is rainy year around and has a large network of rivers and creeks that usually disappear in karsts before reaching the sea. Although there has not been reported a significant water problem in the mines, the existence of an aquifer above the carboniferous (above -360 m) is known. The hydrostatic pressure

measured above the carboniferous changes from 5 atm in relatively dry to 50 atm in rainy seasons (Serpen and Alpkaya, 1998).

The Zonguldak Basin is divided into 5 main coal production sections (Table 5.1). Each section is further divided into subsections.

Table 5.1. Organization of Zonguldak Basin mines and mining districts

Coalfield Lease I	*Coalfield Lease II* *Zonguldak*			*Coalfield Lease III*
Armutcuk	*Kozlu*	*Uzulmez*	*Karadon*	*Amasra*
Alacaagzi Mine Kandilli Mine	Incir Harman Mine Ihsaniye Mine	Caydamar Dilaver Mine Asma Mine	Gelik Mine Karadon Mine Kilimli Mine	Amasra Mine

Brief information about these sections is provided below (Serpen and Alpkaya, 1998):

- **Kozlu:** This is the most important section for coal production. It includes 23 coal seams with dip angles ranging from 45° to 90°. The region has been tectonically very active with a tectonic line at every 50 to 100 m. Mining continues in the entire section. The coal seams of the Kozlu formation are known to be extremely gassy. The records of the gas measurements in the mines indicate a gas existence of 5 to 25 m^3/ton.

- **Karadon:** This formation consists of 23 seams, the dip angles are between 15° and 60°. The section has a large areal spread. Some small private companies continue surface mining in the region in addition to the underground mining by Turkish Hard-Coal Enterprise.

- **Üzülmez:** The 23 coal seams in the Üzülmez Formation have dip angles varying from 40° to 90°.

- **Armutçuk:** This is a small coal production area. It includes 4 economically mineable seams. Near vertical orientation (80° - 90° dip angles) of the seams has a negative impact on coal mining.

- **Amasra:** This section consists of 25 seams with dip angles in the range of 15° to 40°, The 300 to 700 m thick calcareous rock at the top of the

carboniferous causes mining problems. The most distinguishing feature of this section is its having been subject to less tectonic activities.

The thermal maturity level (coalification stage) of the Carboniferous coals varies both laterally and vertically and ranges, basin wide, from subbituminous to low volatile bituminous rank; in terms of vitrinite reflectance this variation ranges from 0.45% to 1.70% R_o (mean random vitrinite reflectance) respectively. As shown in Table 5.2, the maturity of coals, as far as available from boreholes and mines, shows distinct variations among the three areas of the basin (Yalcin et al., 2002).

Table 5.2. Rank variations of coals in Zonguldak Basin (Yalcin et al., 2002, modified)

Armutcuk Area	*Zonguldak Area*	*Amasra Area*
0.72-0.87% R_o	0.82-1.7% R_o	0.45-0.98% R_o
High volatile-B bituminous to high volatile-A bituminous	High volatile-A bituminous to low volatile-A bituminous	Subbituminous to high volatile-A bituminous

5.2 Previous Studies on the Estimation of Coal and CBM Reserves of Zonguldak Coal Basin

Over the years, several studies on the geology (Kerey, 1982 and 1985), tectonics (Okay, 1989), palynology (Agrali, 1964; Akyol, 1974; Akgun and Akyol, 1992), and mining engineering aspects (Bilgin et al., 1988) have been conducted. Studies on the coal properties were limited to a few organic petrographical investigations until 1992 (Okay, 1939; Artuz, 1971; Buzkan, 1987; Karayigit, 1989). Despite many coalbed gas outbursts and explosions that resulted in casualties and economic loss, the basin was not considered from the standpoint of CBM potential, with the exception of very limited in-situ gas content measurements (Masszi and Kahil, 1988, unpublished data). A multidisciplinary project was initiated in 1991 to study different CBM related aspects of the basin and the coals. Since then, some results have been published (Yalcin, 1991; 1995a; 1995b, 1997; Yalcin et al., 1994; Gurdal, 1998; Hosgormez et al., 1998). Karacan (1998) and Karacan and Okandan (1999) investigated the effect of different heterogeneities

on gas flow and storage in coal beds. They emphasized that each coal seam may differ both compositionally and structurally and this may totally alter the storage and production behavior of coal-gas system. This brings the necessity that almost each target coal seam should be treated individually to understand the storage and production mechanisms of the coal contained in that seam. In their study, the structural properties of the two coals (Acılık K-6 and Çay K-3) in relation to coalbed methane recovery were investigated by X-Ray Computerized Tomography (CT), and scanning electron microscopy (SEM).

Previous studies for the determination of coalbed methane content of the Zonguldak Basin depend on the coal reserves and the methane contents of the coals found in the basin. Serpen and Alpkaya (1998) estimated the coal reserves that can be used for methane production, the data from various sources have been evaluated but mostly the records of M.T.A., 1992b and 1994 have been honored. Only the seams of appropriate thickness above the depth of -1200 m have been considered in reserve estimates. The thickness criteria given in Lama and Bartosiewicz (1982) have been used in screening. According to these criteria, it has been assumed that a total effective coal thickness of 5 to 10 m would be sufficient for multiple-seam well completion. For shallow coal seams, 1.5 to 3 m of thickness has been assumed satisfactory for single-seam well completion. In the beginning of that study, the information available in various sources (mostly the records of the state agencies) about the coal reserves of the Zonguldak Basin was gathered. The data were, then, screened for the use in the evaluation of the coalbed methane potential of the basin. Meticulous examination, however, revealed that a significant proportion of the available data could not be used for the purposes of that study. The principal reasons were the inconsistencies and incompatibilities of the data acquired by different sources, ambiguities in the methods used to obtain the data, and the discontinuities of the data in time and space. Moreover, because the purpose of the data collection in the basin had been to help coal mining, some crucial information needed to evaluate the methane production potential had never been collected. As an example, there exist coal seams in the basin of which the thicknesses, depths, and the geographic locations

are not convenient for coal mining but may be effectively used for methane production. These types of seams have never been the subject of a detailed study. About 300 wells drilled in various locations (mostly in the Kozlu Section) provide valuable information but are far from covering the entire basin. Although the depths of -1200 m have been covered in some investigations, the information about the seams deeper than the current coal production depths of -500 m are usually speculative (even for the seams above -500 m, no satisfactory information is available if they are not mined). In the world practice, the methane producing seams extend to the depths of -1500 m and even deeper coal seams are now considered to be economic for methane production (Byrer et al., 1982). Therefore, the lack of satisfactory information about the coal seams deeper than -500 m makes the coalbed methane potential estimates of the Zonguldak Basin very speculative. Another difficulty encountered in that study relates to the tectonic structure of the basin. Because of very active tectonic background of the basin, significant changes in the thicknesses and continuities of the seams are observed. This causes two problems: First, the estimate of the total coal reserves becomes more approximate. Second, because of the various thickness and continuity criteria used in the selection of the potential methane production seams, the estimate of the coalbed methane reserves becomes subjective. In addition, small-scale discontinuities that cannot affect coal mining have never been reported. This information, however, is crucial for methane flow and therefore to determine the number of methane production wells. A limited number of measurements of the methane contents are available in a limited number of coal seams. The pressure and permeability information that is very important for methane production is practically nonexistent. In light of the above evaluation, Monte Carlo simulation was chosen to estimate the methane production potential of the Zonguldak Basin. Their study consists of three phases. In the first phase, the hard-coal reserves of the basin that can be used in methane production were determined.

The computations were based on the proven, probable and possible coal reserves of the basin. This approach provides definite advantages over the deterministic

106

definition of the reserves in cases where the data are accompanied by uncertainties. The numerical measure of the uncertainty associated with each reserve definition can conveniently be used in the statistical evaluation of the data. In that study, consistent with the standard definitions used in the oil industry, proven, probable and possible reserves are associated with a likelihood of higher than 90%, 50%, and 10%, respectively. In the second phase, the methane content distributions of the coal seams were computed based on the data obtained by several methods at different locations in the basin. The third phase of their study was the estimation of the total and the recoverable gas reserves of the basin. The results were obtained for the sections (Armutcuk, Kozlu, Uzulmez, Karadon and Amasra) as well as the entire basin. For completeness, an economic evaluation of a development project was also carried out. Because of similar problems to those for the technical evaluation, they favored the stochastic approach also to evaluate the project economics.

Table 5.3 shows the hard-coal reserves as given in Serpen and Alpkaya (1998) of the Zonguldak Basin estimated from geological data that can be used in methane production. The distribution of the reserves to the five coal production sections, Armutcuk, Kozlu, Uzulmez, Karadon, and Amasra, are indicated. The reserves are designated as proven, probable, possible, and total. For the entire Basin, the proven (135,505,844 tonnes), probable (426,202,993 tonnes), possible (764,912,742 tonnes), and the total reserves (1,343,113,808 tonnes) are estimated. As discussed before, it is possible to obtain different reserve estimates by using the information from different sources.

Table 5.3. Coal reserves based on geological data of Zonguldak coal basin to be used in methane production (tonnes) (Serpen and Alpkaya, 1998)

Section / Subsections	Proven	Probable	Possible	Total
Armutcuk				
Kandilli *Alacaagzi* *Kireclik*	20,171,259	12,532,100	54,079,294	89,155,466
Kozlu				
Ihsaniye *Incirharmani*	12,100,300	23,651,082	225,000,000	264,835,575
Uzulmez				
Asma *Dilaver* *Caydamar*	47,280,602	101,754,000	79,300,000	233,114,075
Karadon				
Gelik *Karadon* *Kilimli*	26,597,022	93,540,366	344,571,002	469,631,390
Amasra				
Amasra A *Amasra B*	29,356,661	194,725,445	61,962,446	286,377,302
Zonguldak Basin Total	135,505,844	426,202,993	764,912,742	1,343,113,808

Table 5.4 shows the proven, probable, possible, and the total coal reserves estimated from the wells drilled at various locations in the basin. The estimates in Table 5.4 are considerably different from those given in Table 5.3. Although the information obtained from the wells can be considered to be more reliable, due to the insufficient number of wells drilled in the basin, it could not be used to represent the average properties of the basin. Furthermore, even for the Kozlu-section where a fairly large number of wells have been drilled, the coal reserve estimates by the well data appear to be extremely conservative. Therefore, the well data have been used qualitatively, mainly for the consistency check of the geological information.

Table 5.4. Coal reserves based on well data in Zonguldak coal basin (tonnes) (Serpen and Alpkaya, 1998)

Section or subsection	Proven	Probable	Possible	Total
Kozlu	1,383,155	4,057,789	21,157,749	26,598,693
Amasra	28,136,985	37,777,260	425,690,476	491,604,721
Gelik	3,340,343	10,021,033	36,605,698	49,967,074
Baglik	3,208,482	9,625,627	33,385,930	46,220,039
Karadon	1,403,019	2,272,483	9,089,932	12,765,434
Zonguldak Basin	37,471,984	63,754,192	525,929,785	627,155,961

To demonstrate the sensitivity of the methane reserve estimates to the estimates of the coal reserves, however, they computed the methane reserves of the Kozlu section by using the coal reserves from both geological and well information.

The methane contents of the Zonguldak coal seams have been measured or estimated by various sources, (Canteck, 1988; Yalcin and Durucan, 1991a and 1991b). Some direct and indirect standard methods have been used in the measurements and estimations, such as 'United States Bureau of Mines (USBM)' direct method or 'Kim', 'Volatile Matter', 'Rank', 'Adsorption Isotherms' and 'Sampling of Exhaust Mine Air' indirect methods. The comparison of the results from Canteck (1988) with the adsorption/desorption studies of Yalcin and Durucan (1991a and 1991b) showed that they are consistent. It must be noted, however, that the methane content estimates of Canteck (1988) were based on coal samples taken from the galleries that had been being mined for some time. Therefore, the methane contents given in Canteck (1988) should represent the conservative estimates. Serpen and Alpkaya (1998) tabulated the methane contents of the coal seams in the Zonguldak Basin obtained by various procedures by Canteck (1988). The methane contents are indicated as the minimum, most likely, and the maximum values (Table 5.5). The methane contents for the Uzulmez and Amasra sections have been obtained by analogy to the seams of similar composition and depth in the other three production sections.

Serpen and Alpkaya (1998) have used the Monte Carlo simulation to determine the coalbed methane reserves of the Zonguldak Basin. They have obtained the results in terms of distributions. In the simulations, the coal reserves shown in Tables 5.3 and 5.4 and the methane contents shown in Table 5.5 were used. The coal reserves and the methane contents were input as the minimum, most likely, and the maximum reserves. The proven reserves in Tables 5.3 and 5.4 were taken as the minimum reserves, the sum of the proven and the probable reserves as the most likely, and the total reserves (the sum of the proven, probable, and possible reserves) as the maximum reserves. As expected, the accuracy of the results was strongly dependent on the accuracy of the estimates of the in-situ coal reserves (Tables 5.3 and 5.4) and the methane contents (Table 5.5) of the seams.

As a result, Serpen and Alpkaya (1998) estimated 1.5×10^9 m^3 proven (90% probability), 4.8×10^9 m^3 possible (50% probability), and 7×10^9 m^3 probable (50% probability) methane reserves in the Zonguldak Basin. For the economic evaluation of the coalbed methane potential of the region, the recoverable methane reserves must be known. Unfortunately, the available data do not permit the computation of the recovery factors. In their study, they have chosen the minimum, most likely, and the maximum values of the recovery factor as 0.1, 0.4, and 0.65, respectively. Based on these recovery factors, they estimated 1.03×10^9 m^3 proven, 1.9×10^9 m^3 possible, and 2.9×10^9 m^3 probable recoverable methane reserves in the Zonguldak Basin.

Table 5.5. Methane contents in Zonguldak coal basin (Serpen and Alpkaya, 1998)

| Section | Method | Methane Content (m^3/ton) | | |
		Minimum	Most Likely	Maximum
Armutcuk	USBM	1.13	6.54	11.75
	KIM	6.6	8.74	10.95
	Volatile Matter	6	6.9	7
	Rank	5	5	5
Kozlu	USBM	0.7	1.9	3.9
	KIM	7.1	13.5	16.1
	Volatile Matter	7	10	12
	Rank	5	5.9	6
Uzulmez	By Analogy	5	7.7	10
Karadon	USBM	0.4	1.16	1.8
	KIM	6	10.1	12.3
	Volatile Matter	8	8.5	9
	Rank	5	6.7	8
Amasra	By Analogy	5	7.7	10

Amasra mining district was divided into two resource areas; A and B as shown in Figure 5.2.
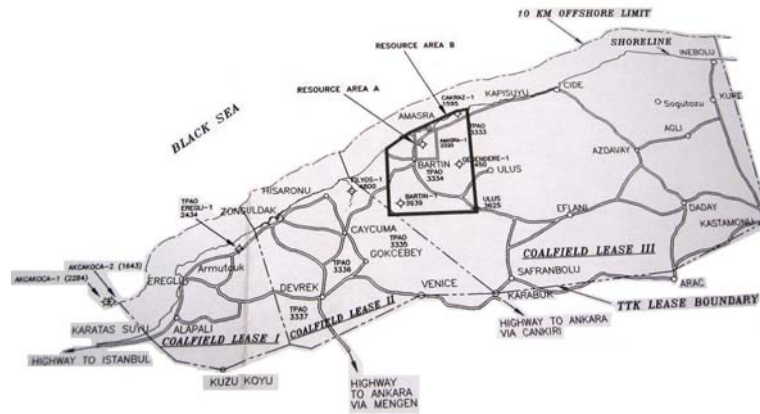
Figure 5.2. Zonguldak basin areal map

In this thesis, Resource Area A of the Amasra District was chosen for gas in place estimation and simulation studies because of the availability of lithologic data from the wells drilled in the region. Also the depths of the seams found in the area are convenient for an enhanced coalbed methane study.

111

CHAPTER 6

METHODOLOGY

6.1 Gas in Place Estimation with Risk Analysis

Traditional reserve definition suggests that reserves can be classified in three groups such as 'proved', 'possible' and 'probable'. All of these three terms lead to some level of uncertainty. It depends on the engineer's point of view to classify reserve estimation as proved or possible considering the percent of uncertainty, for example it can be accepted that if there is 10% uncertainty in estimation the reserves can be named as proved.

One of the main considerations in calculating the gas in place is that the variables must be independent. But actually petrophysical variables are not independent (Fylling, 2002). High porosity fraction will also led to high permeability. It is important to determine which factors cause variability or uncertainty in calculations. The dependence can be investigated by sensitivity analysis (Macary and Hassan, 1999).

A key step in analyzing a coalbed methane reservoir is to estimate the gas-in-place. Coals are dual gas storage reservoirs: gas is stored in the coal matrix micropore system via adsorption and in the coal fracture network system as free gas. Thus, calculating gas-in-place for coal reservoirs involves estimating the volume of free gas in the fracture network and the volume of adsorbed gas in the matrix system. The data used for estimating gas-in-place for coalbed methane reservoirs are obtained from a variety of sources. These include well logs, core testing and well transient and/or production testing (McLennan et al., 1995).

Equation 6.1 is the volumetric gas-in-place equation for coalbed methane reservoirs. This equation includes the appropriate terms for estimating the free gas in the coal interconnected fracture system and the adsorbed gas in the coal matrix. Gas dissolved in the water is almost always negligible and has not been included in Equation 6.1.

$$G_i = A_c h \left[\frac{43560 \phi_f (1 - S_{wfi})}{B_{gi}} + 1.359 C_{gi} \rho_c (1 - f_a - f_m) \right] \qquad (6.1)$$

Where G_i, A, h, ϕ_f, S_{wfi}, B_{gi}, C_{gi}, ρ_c, f_a and f_a are gas in place at initial reservoir conditions (Mscf), area (acre), coal thickness (ft), effective porosity (fraction), interconnected fracture water saturation (fraction), gas formation volume factor at initial pressure (Mscf/rcf), initial sorbed gas concentration (scf/tonne), pure coal density (g/cc), average weight fraction of ash (fraction) and average weight fraction of moisture (fraction) respectively. 43,560=Conversion Factor, ft^2/ac and 1.359=Conversion Factor, $[(Mscf)(tonne)(cm^3)]/[(ac\text{-}ft)(scf)(g)]$.

In Equation 6.1 the first part of the parenthesis give the free gas found in the cleats of the coal and the second part is the adsorbed gas in the micropores. The units of terms in Equation 6.1 are those that are typically reported in core test reports and/or well logs. The initial adsorbed gas concentration is reported in scf/tonne of dry, ash-free coal, which are the units that are normally obtained when canister desorption and proximate analysis tests are conducted on coal samples.

6.1.1 Use of @Risk™ in Monte Carlo Simulation

The variables given in Equation 6.1 have some uncertainties. A simulation study is required to obtain a single value from the values of ranges. Palisade's risk analysis tool @Risk™ uses Monte Carlo Simulation to show the possible outcomes and how likely they are to occur. @Risk™ is an add-in product that can be used with Microsoft Excel Spreadsheet program. Uncertain values are replaced with

probability distribution functions, such as; normal, uniform or triangular distributions. Example @Risk™ commands to be entered into cells for probability distribution functions are; RiskNormal (100, 10), RiskUniform (20, 30), RiskExpon (A1+A2), RiskTriang (10, 20, 30).

Before starting modeling, dependent and independent variables must be decided. Independent variables' distribution functions are given by the user where the dependent variables' probability function is obtained by simulation of the independent variables. Dependent variables in this study were the free gas in cleats, adsorbed gas in the coal matrix and the sum of them. The equations were formulated using the independent variables for the free gas, adsorbed gas and for the total gas in place. Cells for dependent variables are selected and the 'Add to Output' button is used to define them as the dependent variables. Field area, coal thickness, cleat porosity, initial water saturation, gas formation volume factor, initial sorbed gas concentration, coal density, ash and moisture contents were the independent variables. Before starting to the simulation, number of simulations were set using 'Simulation Settings' window.

The number of simulations should be selected carefully. Indeed the more the number of simulations, the more outcomes can be covered, but the more time required for the simulation runs. However, after a value, the fluctuations of the results stop. Therefore a simulation size test was conducted by selecting 10, 25, 50, 100, 250, 500, 1,000, 2,500, 5,000, 10,000, 25,000, 50,000 and 100,000 as number of simulations. As seen from the Figure 5.1 the fluctuations of the total gas in place value stabilize after 5000 simulations. In this test Area #1 was selected and the P50 values were used.
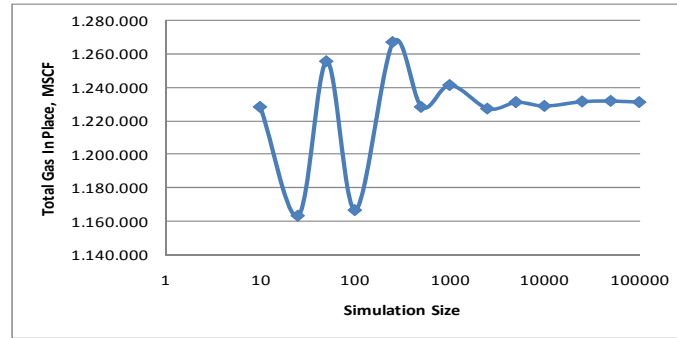
Figure 6.1. Effect of simulation size on IGIP

In this study these simple and practical features of @Risk™ are used to simulate the uncertainty in gas in place amount of Resource Area A of Amasra mining district. Simulation settings are set to Monte Carlo simulation and 5000 iterations. Procedure in simulating the original gas in place by @Risk™ is follows:

1. Independent variables that are influencing the dependent variable (original gas in place) are determined. These variables are area, cleat porosity, cleat water saturation, net thickness, initial sorbed gas concentration, gas formation volume factor, coal density, weight fractions of ash and moisture.

2. Data sets for each independent variable are prepared and distribution functions for them are defined.

3. Dependent variable is built by the volumetric method and then the cell is selected as output.

4. Simulation settings are chosen and simulation is run.

5. Results of the simulation showing probability distribution functions of independent and dependent variables and their detailed statistical information are taken and evaluated.

In following sections determination of the ranges of the values for each of the independent variables were given.

6.1.2 Area

One of the screening criteria for the convenient enhanced coalbed methane reservoir is the continuity of the coal layer. Although, some small interruptions in the continuity of the seam are not so important for mining purposes, they can be barriers for the flow of coalbed methane. Therefore it is very important to make a good correlation between coal seams.

6.1.2.1 Correlation Study

Lithologic information with elevation and coordinate data for 115 wells found in the Resource Area A were taken from the Turkish Coal Enterprise (TTK) Zonguldak. Since these wells were drilled by General Directorate of Mineral Research and Exploration (MTA), main aim was to locate the coal seams and to determine depths of them. Coordinates and the names of the wells are given in Tables 6.1 (a) and (b).

Table 6.1. Coordinates of the wells (TTK, 2003)

Table 6.1 (a) Coordinates of the wells (AK1 to K10)							
Well	*East, m*	*North, m*	*Elevation, m*	*Well*	*East, m*	*North, m*	*Elevation, m*
AK1	99094	98175	396	Bostanlar-37	100910	98105	255
AK2	99645	99232	193	Bostanlar-38	100315	97785	258
AK3	99658	99422	162	Bostanlar-K17	99324	97155	242
AK4	98510	97390	338	Çamlık-16A	99550	94933	83
AK5	97820	98320	144	Çamlık-56	98956	94234	171
AK6	97670	97920	143	Çamlık-77	98766	93585	184
AK7	97365	98040	85	Çömlekkıran-65	96708	97020	354
AK8	98060	96690	291	Çömlekkıran-66	96472	96288	409
AK9	99982	98258	397	Dökük-23	99290	100360	126
AK10	99922	97966	357	Fermitkadı-55	96888	91975	191
AK11	99565	98327	416	Gömü-27	97680	98855	121
AK12	99154	97996	422	Gömü-28	97050	98990	89
AK13	98843	97148	327	Gömü-29	98130	98900	175
AK14	99826	97024	234	Gömü-80	97574	98281	134
AK15	99533	97913	288	Gömü-81	96837	98269	96
AK16	99037	98386	429	Gömü-84	96817	99124	68
Amasra-43	99950	100270	16	Gömü-85	97029	99293	28
Amasra-50	97750	97013	371	Gömü-86	98057	99091	111
Askersuyu-31	98540	98400	296	Gömü-K24	97162	98710	128
Bedesten-21	99425	99685	31	Gömü-K27	97517	98360	112
Bedesten-45	100260	100035	23	Gömü-K32	97089	97988	128
Bedesten-83	100259	99725	21	Gömü-K37	97843	97807	169
Bostanlar-36	99440	98095	336	K10	99559	96752	228

Table 6.1 (b) Coordinates of the wells (K11 to Uzunöz-82)							
Well	East, m	North, m	Elevation, m	Well	East, m	North, m	Elevation, m
K11	98701	96608	219	Kazpınar-K6	97922	95534	174
K13	99040	96972	292	Kazpınar-K12	98928	96670	244
K14	99332	96371	245	Kazpınar-K19	99420	95400	179
K15	99002	96345	243	Kazpınar-K22	98923	95283	168
K16	99749	96599	230	Kazpınar-K23	98707	94814	187
K18	98784	95855	219	Kazpınar-K25	98298	94869	154
K20	99702	96245	202	Kazpınar-K28	99310	95721	215
K21	98464	95736	226	Kazpınar-K31	98413	95304	191
K30	99426	97523	322	Kazpınar-K33	98275	96450	281
K34	99058	98786	308	Kuşkayası-32	98425	97455	355
Kaman-10	97782	94179	77	S6	98424	95948	114
Kaman-14	96300	94240	147	S12	99274	93505	55
Kaman-39	96976	93515	150	S33	98735	96470	212
Kaman-53	96450	93290	75	S34	98970	97540	302
Kaman-58	97974	93631	58	S35	99655	97280	253
Kaman-60	97368	93908	132	S40	99405	98845	264
Kaman-61	98362	94160	119	S41	99950	99465	90
Kaman-75	98027	93178	54	S47	98945	99065	254
Karaçay-9	97640	91000	13	S71	99853	96779	232
Karaçay-11	97823	91899	20	S74	99204	96770	301
Karaçay-K29	98152	92373	25	S89	100042	97413	251
Kazpınar-7	98554	94985	162	Sondaj-13	97195	95301	130
Kazpınar-18	96817	95834	316	Şah-Mah-42	100855	99710	127
Kazpınar-20	98187	94598	140	Şıbben-48	98700	92208	168
Kazpınar-51	98331	96586	299	Tarlaağzı-22	96910	97985	125
Kazpınar-62	98057	95785	210	Tarlaağzı-26	97475	97980	120
Kazpınar-63	97531	95789	137	Uğurlar-1	99639	94345	67
Kazpınar-64	97716	96415	261	Uğurlar-2	98508	92803	100
Kazpınar-69	97696	94903	100	Uğurlar-3	97751	95283	125
Kazpınar-78	98125	95125	191	Uğurlar-4	100912	94822	114
Kazpınar-K1	97832	94422	81	Uğurlar-73	100263	95496	139
Kazpınar-K2	97878	95055	119	Uğurlar-K26	98753	93104	42
Kazpınar-K3	97659	95529	121	Uzunöz-15	97180	96950	346
Kazpınar-K4	97983	94300	108	Uzunöz-82	97201	90928	39
Kazpınar-K5	98042	94446	129				

The surface map of the field can be seen in Figure 6.2. The north part of the field is bounded with Black Sea.

117
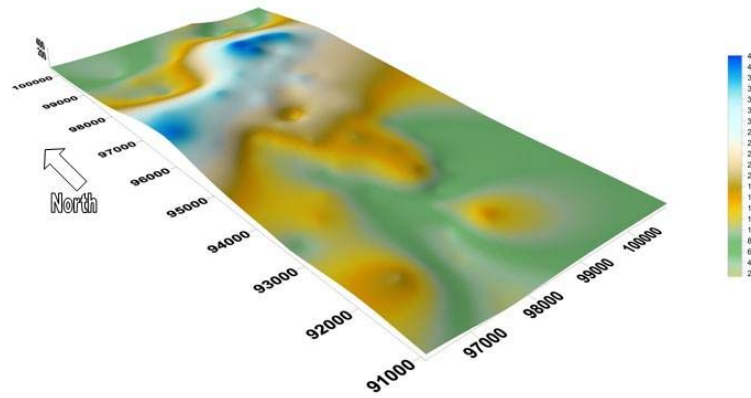
Figure 6.2. Surface map of the resource area-A of Amasra district, unit is meter

An example for the lithologic information is given in Table 6.2. Except a few wells, the age or maturity information for the coals do not exist.

Table 6.2. Lithologic information for Uğurlar-1 well

Depth from the Surface, m		Lithology
Start	End	
0	150	Agglomerate
150	188	Andesite-tuff
188	240	Limestone
240	537	Clayey sandstone
537	538	Coal
538	744	Clayey sandstone
744	745	Coal
745	965	Clayey sandstone
965	966	Coal
966	970	Clayey sandstone
970	972	Coal
972	1060	Clayey sandstone

From Figure 6.3, it can be seen that there are four coal layers which were cut during drilling. In Appendix A, all of the lithologic information is tabulated. It is very difficult to correlate the coals using the existing written data. Therefore, Macromedia Flash program was used to visualize the written data. In order to make a true scaled visualization, each pixel denoted one meter of length. Types of the formations were written on the appropriate places. Depths of lithologic changes were shown with horizontal red lines. Sea level was shown with a black horizontal line. Coals were shown with a letter 'K' on the left and a horizontal red line. If the thickness of the coal layer was more than one meter, then the thickness

118

value was written to the right hand side of the red line. The thickness of the red line was also proportional to the thickness of the coal layer. A sample of the visualized well lithologic information is shown in Figure 6.3. Other figures for the visualization of the wells were given in Appendix B.

The wells are found on the field in a dispersed fashion. Several trials were performed in order to make the correlations of the coal seams using the prepared visualizations. These trials include the matching of the seams by comparing two neighbor wells with each other, grouping them in a small section, or grouping them all together. However, all of these trials were unsatisfactory. The data of these studies were not given in this thesis.

In geologic studies, generally the formations are shown by the cross sections. These cross sections are drawn on a line. Similarly in this study the field was divided into nine horizontal and five vertical areas. Area instead of line was used because of the need for including all the data found in the wells. In Figure 6.4, the locations of the wells can be seen.
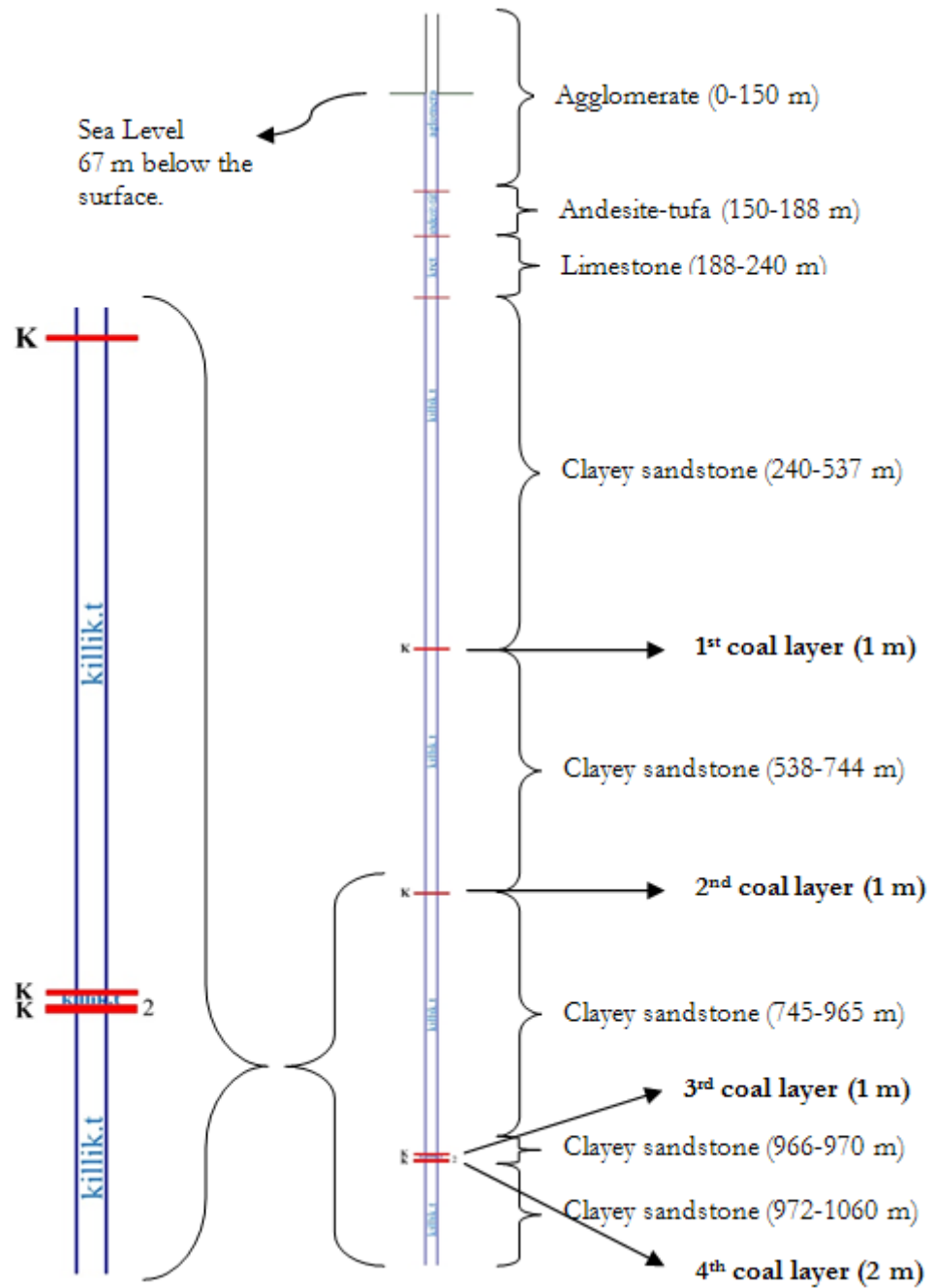
Figure 6.3. Visualization of Uğurlar-1 well

120

Figure 6.4. Locations of the wells on the resource area-A of Amasra district

The area is approximately 4600 m wide in East to West direction and 9400 m length in South to North directions. As mentioned before the field was divided into nine horizontal (east to west) and five vertical (south to north) areas (Figure 6.5).
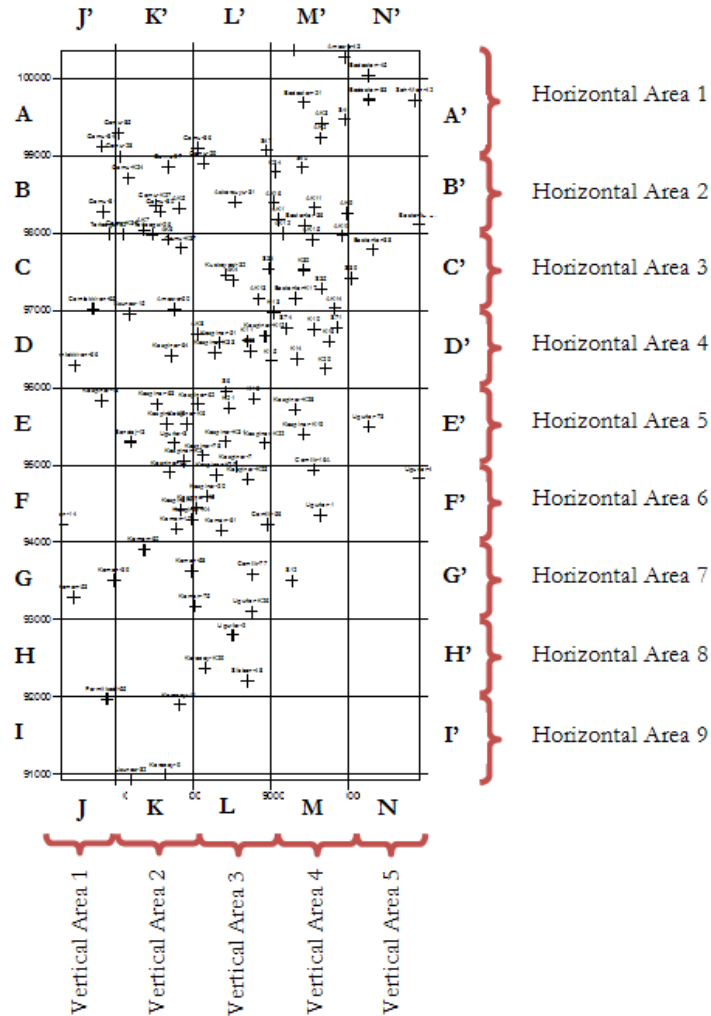
Figure 6.5. Horizontal and vertical cross-sections

The visualized wells that are found on these areas were placed on a plane by using Macromedia Flash program in order to obtain a cross sectional view. Some of the wells were placed both on horizontal and vertical areas whenever possible. These wells were used for the cross checking of the connections. In the correlation study, thicknesses and depths of the seams, lithologic information, dip angles of the seams were all taken into consideration. Because there were too few deep

122

wells, number of the points (wells) defining the seams at deeper parts of the reservoir was not so much. Figure 6.6 shows the visualization of the Horizontal Area 1 and the correlations of the coals as an example. Other figures showing the correlations of the seams are given in Appendix C.
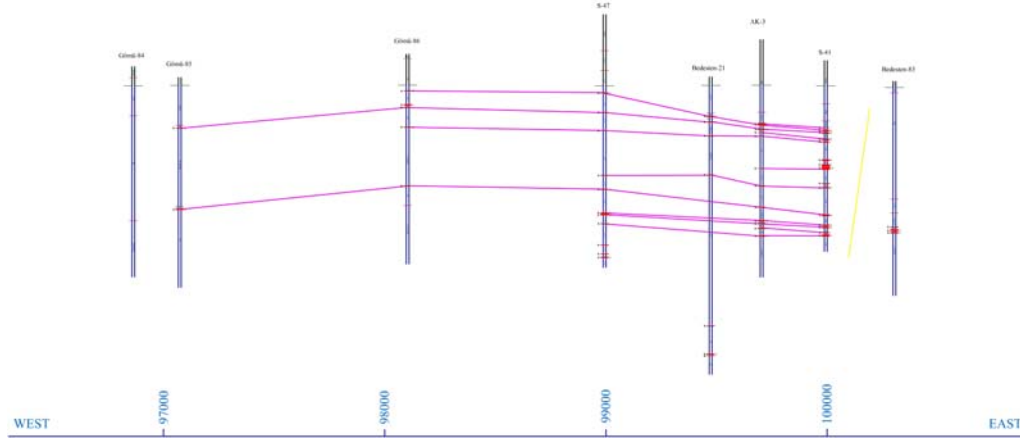
Figure 6.6. Correlation of the seams found on the Horizontal Area-1

At the end of the correlation study 63 coal layers were determined. Locations of the faults were cross checked with the information taken from Turkish Hard Coal Enterprise. Also the locations of the guide layer 'Şiferton Layer' were used to check the correctness of the correlations. These coal layers were defined with the well ID and the number of the coal seam starting from top. As an example, Table 6.3 shows the Coal Layer#1 defined with the wells. Coal Layer#1 can be seen on the Figure 6.6 as the upper most coal seam starting from the Gömü-85 well. Results of the correlation studies are given in Appendix D.

Table 6.3. Coal Layer#1

Hor. Area 1	Hor. Area 2	Ver. Area 3	Ver. Area 4
Gömü-85 – I	Gömü-80 – I	Askersuyu-31 – V	AK2 – III
Gömü-86 – III	Gömü-27 – II	Gömü-29 – II	AK3 – III
S47 – II	AK5 – III	Gömü-86 – III	S41 – III
Bedesten-21 – II	Gömü-29 – II		Bedesten-21 – II
AK3 – III	Askersuyu-31 – V		K34 – IV
S41 - III	AK16 – II		AK16 – II
	S40 – I		AK11 – V
	AK11 – V		AK9 – IV
	AK9 – IV		

6.1.2.2 Determination of the Area

The coal layers were drawn on millimetric papers and the areas of the coal layers were measured using a planimeter. The planimeter is a drafting instrument used to measure the area of a graphically represented planar region. The region being measured may have any irregular shape, as the coal layers have. The planimeter consists of a brass cylinder, two arms connected with an elbow, a wheel and a scale on the wheel. The brass cylinder is anchored to the table with a point, like a compass point. It pivots, but does not slide. The elbow joint bents and slides freely. The pointer on the other end is used to trace the perimeter of the region. Near the elbow is a wheel, which simply rolls and slides along the tabletop. The scale is on the wheel itself, so it tells how far the wheel has turned. Sure enough, that number is proportional to the area of the region. The conversion factor depends on the scale of the drawing. Therefore a known area was used to find the conversion factors.

Figure 6.7 shows the drawing of the Coal Layer#1. The blue area is the area bounded with the outermost wells. This area was assumed to be the minimum area. The green area is the area that surrounds the blue area with a rectangle. This green area was assumed to be the maximum area. The average of the two values was taken as the most likely value.
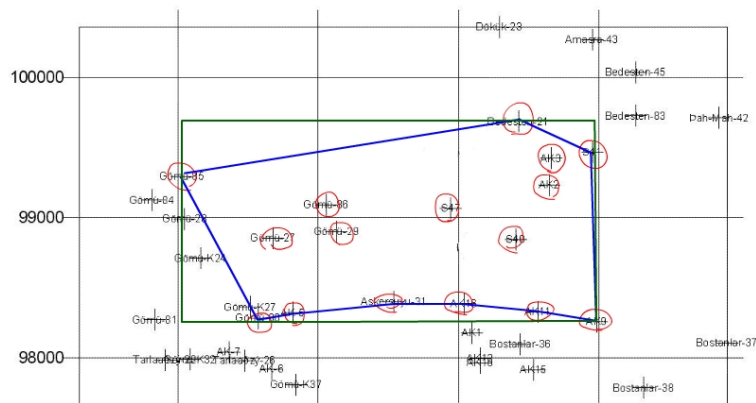
Figure 6.7. Area of Coal Layer#1

The minimum, most likely and maximum values of the all 63 coal layers can be seen on Tables 6.4 (a) and (b).

Table 6.4. Area values of the coal layers

Table 6.4 (a) Area values of the coal layers (1 to 44)

Coal Layer	Area, m²			Area, acre		
	Minimum	Most Likely	Maximum	Minimum	Most Likely	Maximum
1	3,394,027	3,798,614	4,203,200	839	939	1,039
2	1,876,182	2,370,291	2,864,400	464	586	708
3	1,885,033	3,059,317	4,233,600	466	756	1,046
4	2,908,940	3,820,870	4,732,800	719	944	1,169
5	2,465,129	2,926,165	3,387,200	609	723	837
6	220,482	436,641	652,800	54	108	161
7	42,840	235,620	428,400	11	58	106
8	42,840	235,620	428,400	11	58	106
9	42,840	235,620	428,400	11	58	106
10	26,699	54,950	83,200	7	14	21
11	196,892	276,646	356,400	49	68	88
12	83,706	164,253	244,800	21	41	60
13	1,898,000	3,036,800	4,175,600	469	750	1,032
14	1,011,500	1,576,750	2,142,000	250	390	529
15	689,939	1,119,970	1,550,000	170	277	383
16	991,669	1,149,435	1,307,200	245	284	323
17	575,168	941,184	1,307,200	142	233	323
18	497,622	799,211	1,100,800	123	197	272
19	497,622	799,211	1,100,800	123	197	272
20	652,803	1,041,802	1,430,800	161	257	354
21	652,803	1,041,802	1,430,800	161	257	354
22	497,622	799,211	1,100,800	123	197	272
23	4,192,324	6,410,762	8,629,200	1,036	1,584	2,132
24	3,138,817	4,111,409	5,084,000	776	1,016	1,256
25	39,750	72,875	106,000	10	18	26
26	12,970,983	16,587,892	20,204,800	3,205	4,099	4,993
27	88,525	194,263	300,000	22	48	74
28	765,934	1,232,967	1,700,000	189	305	420
29	308,224	520,712	733,200	76	129	181
30	290,275	673,138	1,056,000	72	166	261
31	5,490,720	7,767,360	10,044,000	1,357	1,919	2,482
32	1,415,861	2,219,931	3,024,000	350	549	747
33	245,316	510,258	775,200	61	126	192
34	400,879	671,240	941,600	99	166	233
35	1,037,486	1,408,743	1,780,000	256	348	440
36	547,032	811,116	1,075,200	135	200	266
37	454,296	655,948	857,600	112	162	212
38	368,508	589,054	809,600	91	146	200
39	601,892	880,546	1,159,200	149	218	286
40	1,105,187	1,251,794	1,398,400	273	309	346
41	239,350	579,675	920,000	59	143	227
42	450,514	678,857	907,200	111	168	224
43	450,514	678,857	907,200	111	168	224
44	589,382	920,091	1,250,800	146	227	309

Table 6.4 (b) Area values of the coal layers (45 to 63)

Coal Layer	Area, m^2			Area, acre		
	Minimum	Most Likely	Maximum	Minimum	Most Likely	Maximum
45	589,382	920,091	1,250,800	146	227	309
46	1,902,982	2,446,691	2,990,400	470	605	739
47	5,911,111	7,330,556	8,750,000	1,461	1,811	2,162
48	324,715	403,158	481,600	80	100	119
49	280,800	345,600	410,400	69	85	101
50	9,138	24,369	39,600	2	6	10
51	9,138	24,369	39,600	2	6	10
52	905,143	1,316,572	1,728,000	224	325	427
53	544,548	1,019,874	1,495,200	135	252	369
54	1,557,287	2,057,844	2,558,400	385	508	632
55	11,615	95,408	179,200	3	24	44
56	210,000	305,000	400,000	52	75	99
57	368,333	581,967	795,600	91	144	197
58	368,333	581,967	795,600	91	144	197
59	414,391	1,322,396	2,230,400	102	327	551
60	1,932,089	2,638,045	3,344,000	477	652	826
61	1,406,636	2,490,918	3,575,200	348	616	883
62	150,378	254,989	359,600	37	63	89
63	700,541	868,671	1,036,800	173	215	256
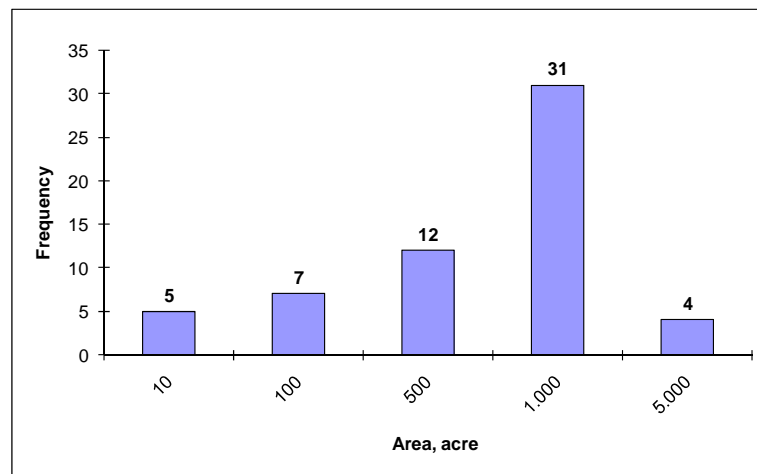
Figure 6.8. Histogram of the area values

As can be seen from Figure 6.8 most of the coal layers have at least 1000 acres of area. Total sum of the average areas was found as 25,791 acres.

126

6.1.3 Coal Thickness

The thicknesses of the coal seams vary in the study area. The minimum and maximum thicknesses were estimated using the thickness data from the wells found in the layer. In Table 6.5 the coal thickness values of the Coal Layer#1 wells are given. The minimum thickness is 1 m (3.28 ft), and maximum thickness is 6 m (19.7 ft). The average thickness value which was found as 2.56 m (8.4 ft) was used as the most likely value in Monte Carlo simulation.

Table 6.5. Coal thickness values of Coal Layer#1 (TTK, 2003)

Well ID	Coal Thickness, m
Gömü-85	2
Gömü-86	1
S47	1
Bedesten-21	2
AK3	2
S41	2
Askersuyu-31	6
Gömü-29	2
AK2	2
Gömü-80	1
Gömü-27	3
AK5	3
AK16	4
S40	1
AK11	6
AK9	3

Coal thicknesses range from 3.28 ft to 26.24 ft in the reservoir. For some of the coal layers the same thickness values were used (i.e. constant thickness) due to their values that do not vary.

Table 6.6. Thickness values of the coal layers

Coal Layer	Thickness, ft			Coal Layer	Thickness, ft		
	Minimum	Most Likely	Maximum		Minimum	Most Likely	Maximum
1	3.28	8.4	19.7	33	3.28	5.25	9.84
2	3.28	13.68	26.24	34	6.56	9.38	16.4
3	3.28	5.18	13.12	35	3.28	6.1	9.84
4	3.28	5.87	9.84	36	3.28	3.28	3.28
5	3.28	6.33	16.4	37	3.28	3.71	6.56
6	3.28	4.1	6.56	38	3.28	3.28	3.28
7	6.56	7.64	9.84	39	3.28	5.74	9.84
8	6.56	8.76	9.84	40	3.28	3.84	6.56
9	3.28	9.84	16.4	41	3.28	4.36	6.56
10	3.28	13.12	32.8	42	3.28	3.28	3.28
11	3.28	4.1	6.56	43	3.28	3.28	3.28
12	3.28	6.56	9.84	44	3.28	3.28	3.28
13	9.84	14.76	19.68	45	3.28	4.36	6.56
14	6.56	8.76	9.84	46	3.28	7.15	13.12
15	6.56	7.87	9.84	47	3.28	6.72	19.68
16	3.28	5.25	6.56	48	3.28	3.74	6.56
17	6.56	9.02	16.4	49	3.28	4.92	6.56
18	3.28	3.28	3.28	50	3.28	3.28	3.28
19	3.28	3.28	3.28	51	3.28	3.28	3.28
20	3.28	7.54	9.84	52	3.28	3.28	3.28
21	3.28	3.28	3.28	53	6.56	9.18	13.12
22	3.28	8.76	19.68	54	3.28	4.23	6.56
23	3.28	4.99	13.12	55	3.28	5.48	6.56
24	3.28	6.04	9.84	56	3.28	5.25	9.84
25	3.28	3.28	3.28	57	3.28	3.28	3.28
26	3.28	6.23	16.4	58	3.28	5.48	9.84
27	3.28	4.26	6.56	59	6.56	6.56	6.56
28	3.28	4.23	6.56	60	3.28	6.56	9.84
29	3.28	3.28	3.28	61	3.28	9.45	16.4
30	3.28	6.56	9.84	62	3.28	3.28	3.28
31	3.28	5.08	13.12	63	3.28	6.56	9.84
32	3.28	5.84	9.84				

6.1.4 Cleat Porosity

Cleat or fracture porosities of the coal reservoirs are lower than the conventional gas reservoirs. The cleats are not the storage area for the gas both a pathway from the matrices to the wells. Most of the gas in the coal reservoirs exists in the adsorbed phase in the micropores of the coals. However some of the gas exists as free gas in the cleats. Especially for the Amasra region where the cleat water saturation is very low (TTK, 2003). Porosity is estimated 1% (King et al., 1986; Remner et al., 1986; Anbarci and Ertekin, 1990), 2% (Kolesar and Ertekin, 1986; Ertekin and Sung, 1986; Zuber et al., 1987; Sung and Ertekin, 1987; Paul et al.,

1990) and 6% (Mohaghegh and Ertekin, 1991) for minimum, most likely and maximum cases respectively according to the literature survey.

6.1.5 Water Saturation

Although in general the coal reservoirs are water saturated, coal seams are dry in Amasra District. Therefore a constant water saturation of 0.01 is taken.

6.1.6. Formation Volume Factor

The formation volume factor is a function of specific gravity of the gas, reservoir temperature and the pressure as given in Table 6.7.

Table 6.7. Gas formation volume factor as a function of gas gravity and temperature (Zuber, 1996)

	Gas Formation Volume Factor, MSCF/RCF			
	Gravity = 0.6		*Gravity = 0.7*	
Pressure, psi	*80 °F*	*120 °F*	*80 °F*	*120 °F*
15	0.00099	0.00092	0.00099	0.00092
50	0.00331	0.00307	0.00331	0.00308
100	0.00665	0.00618	0.00668	0.00620
200	0.01347	0.01248	0.01360	0.01257
300	0.02046	0.01890	0.02075	0.01910
400	0.02763	0.02543	0.02815	0.02581
600	0.04247	0.03886	0.04375	0.03975
800	0.05800	0.05272	0.06045	0.05439
1,000	0.07417	0.06699	0.07826	0.06969
1,200	0.09092	0.08160	0.09707	0.08557
1,400	0.10812	0.09646	0.11667	0.10189
1,600	0.12560	0.11146	0.13669	0.11846
1,800	0.14315	0.12650	0.15666	0.13507
2,000	0.16055	0.14144	0.17611	0.15146
2,200	0.17760	0.15617	0.19467	0.16743
2,400	0.19411	0.17058	0.21207	0.18278
2,600	0.20992	0.18456	0.22821	0.19742
2,800	0.22499	0.19808	0.24306	0.21124
3,000	0.23923	0.21106	0.25667	0.22424
3,200	0.25266	0.22347	0.26912	0.23640
3,400	0.26529	0.23532	0.28050	0.24776
3,600	0.27711	0.24661	0.29093	0.25840
3,800	0.28821	0.25733	0.30050	0.26830
4,000	0.29861	0.26752	0.30931	0.27754

The specific gravity of the gas can be calculated from the apparent molecular weight by using the composition by the ideal gas assumption using Equation 6.2.

$$\gamma = \frac{\rho_{gas}}{\rho_{air}} = \frac{MW_{gas}}{MW_{air}} = \frac{MW_{gas}}{29} \qquad (6.2)$$

Gas molecular weight can be calculated from the composition of the gas. Results of the three gas analysis tests are given in Table 6.8.

Table 6.8 Gas analysis for Amasra coals (TTK, 2003)

Canister #	Methane, vol%	iso-Pentanes, vol%	n-Pentanes, vol%	CO_2, vol%	O_2, vol%	N_2, vol%	MW	Sp. Grav.
162	93.29	Trace	Trace	1.01	2.85	2.83	17.09	0.59
243	88.07	0	0	0.74	5.58	5.61	17.77	0.61
132	65.09	0.079	0	2.36	16.18	16.29	21.25	0.73

The results for Canister #132 show unusually high nitrogen and oxygen content which is thought as because of a contact of the gas with air. Therefore it was neglected for the calculation of the specific gravity which was determined as 0.6. Although it is known that the temperature of each coal layer varies with depth, the reservoir temperature is assumed to be constant as measured 94°F (TTK, 2003). Gas specific gravity is taken as 0.6, then the gas formation volume factor becomes only a function of pressure.
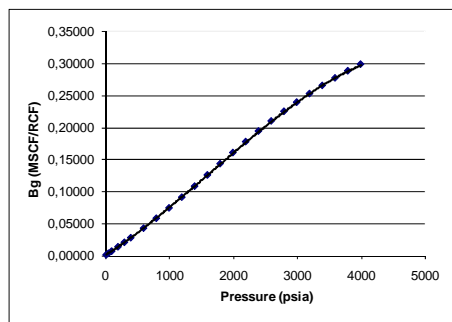
Figure 6.9 (a) FVF 0.6 gravity and 80°F
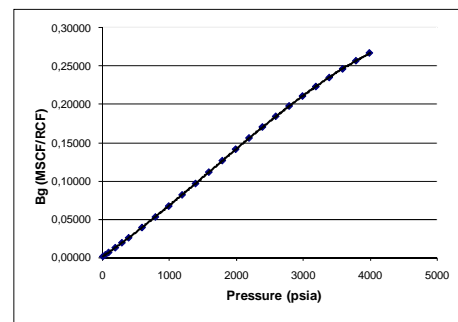
Figure 6.9 (b) FVF 0.6 gravity and 120°F

Figure 6.9. Gas formation volume factor for 0.6 gravity at 80°F and 120°F (using data from Zuber, 1996)

Third order polynomial equations of the trend lines for the gas formation volume factors were obtained as shown in Figure 6.9. Equation 6.3 is for 80°F and Equation 6.4 is for 120°F. The formation volume factor can be easily determined for 94°F.

$$B_g\big|_{80°F} = -3 \times 10^{-12}p^3 + 1 \times 10^{-8}p^2 + 6 \times 10^{-5}p - 4 \times 10^{-5} \qquad (6.3)$$

$$B_g\big|_{120°F} = -2 \times 10^{-12}p^3 + 9 \times 10^{-9}p^2 + 6 \times 10^{-5}p - 3 \times 10^{-5} \qquad (6.4)$$

The pressure gradient for the coal reservoirs are changing from 0.1 psi/ft to 0.9 psi/ft. However, in general the reservoir pressures are calculated by using water pressure gradient, 0.43 psi/ft whenever the reservoir is water saturated. However, Hoch (2005) pointed out that in Horseshoe Canyon reservoir the water gradient is less than 30% of the water saturation gradient and named this as the dry coal anomaly. Similarly, in Amasra, 30% of the water pressure gradient (0.129 psi/ft) was used to determine the initial reservoir pressure.

Coal layers were found at different depths depending on the surface shapes and coal seam dip angle. Tables 6.9 (a) and (b) tabulate the depth and calculated pressure values for all of the coal layers.

Table 6.9 Depth and pressure values of the coal layers

Table 6.9 (a) Depth and pressure values of the coal layers (1 to 12)

Coal Layer	Depth, ft			Coal Layer	Pressure, psia		
	Minimum	*Average*	*Maximum*		*Minimum*	*Average*	*Maximum*
1	262.5	929.5	2660.9	1	33.9	119.9	343.3
2	2099.8	2351.4	2490.3	2	270.9	303.3	321.2
3	971.2	1763.5	2047.3	3	125.3	227.5	264.1
4	65.6	683.5	1893.1	4	8.5	88.2	244.2
5	311.7	1161.4	2706.8	5	40.2	149.8	349.2
6	1148.4	1582.0	1883.3	6	148.1	204.1	242.9
7	1925.9	2159.2	2322.9	7	248.4	278.5	299.7
8	1952.2	2184.9	2339.4	8	251.8	281.9	301.8
9	2044.1	2308.2	2450.9	9	263.7	297.8	316.2
10	1243.5	1419.2	1604.4	10	160.4	183.1	207.0
11	895.7	1183.4	1633.9	11	115.5	152.7	210.8
12	1430.5	1546.9	1601.1	12	184.5	199.6	206.5

Table 6.9 (b) Depth and pressure values of the coal layers (13 to 63)

Coal Layer	Depth, ft			Coal Layer	Pressure, psia		
	Minimum	Average	Maximum		Minimum	Average	Maximum
13	2723.2	3728.4	5600.7	13	351.3	481.0	722.5
14	4721.4	4993.0	5298.8	14	609.1	644.1	683.5
15	1962.0	3317.9	4157.0	15	253.1	428.0	536.3
16	3707.5	4066.5	4399.8	16	478.3	524.6	567.6
17	4137.3	4396.9	4652.5	17	533.7	567.2	600.2
18	4472.0	4576.6	4754.2	18	576.9	590.4	613.3
19	4642.6	4793.1	5000.2	19	598.9	618.3	645.0
20	2920.1	4011.2	5262.7	20	376.7	517.4	678.9
21	3271.2	4412.9	5682.7	21	422.0	569.3	733.1
22	5088.8	5480.2	5807.4	22	656.5	706.9	749.2
23	1761.9	2373.9	3051.3	23	227.3	306.2	393.6
24	1965.3	2211.8	2444.3	24	253.5	285.3	315.3
25	623.4	728.2	892.4	25	80.4	93.9	115.1
26	1223.8	1835.6	2936.5	26	157.9	236.8	378.8
27	1551.9	2048.5	2477.2	27	200.2	264.3	319.6
28	433.1	908.1	1355.1	28	55.9	117.1	174.8
29	685.7	1033.1	1542.1	29	88.5	133.3	198.9
30	856.3	1085.4	1463.3	30	110.5	140.0	188.8
31	1988.3	2327.6	2788.9	31	256.5	300.3	359.8
32	2739.6	2988.4	3340.1	32	353.4	385.5	430.9
33	984.3	1258.6	1515.8	33	127.0	162.4	195.5
34	2208.1	2363.0	2618.2	34	284.8	304.8	337.7
35	2293.4	2729.4	3202.3	35	295.8	352.1	413.1
36	2342.6	2505.7	2683.9	36	302.2	323.2	346.2
37	2355.8	2595.5	2788.9	37	303.9	334.8	359.8
38	3523.8	3564.6	3655.0	38	454.6	459.8	471.5
39	3418.8	3700.0	3865.0	39	441.0	477.3	498.6
40	3425.4	3800.3	4101.3	40	441.9	490.2	529.1
41	3737.1	3957.7	4147.2	41	482.1	510.5	535.0
42	3828.9	4064.7	4232.5	42	493.9	524.3	546.0
43	3917.5	4131.9	4308.0	43	505.4	533.0	555.7
44	2437.8	2587.3	2870.9	44	314.5	333.8	370.3
45	2126.1	2210.4	2332.8	45	274.3	285.1	300.9
46	1761.9	2212.2	2782.3	46	227.3	285.4	358.9
47	1998.1	2737.2	3766.6	47	257.8	353.1	485.9
48	2044.1	2167.0	2309.8	48	263.7	279.5	298.0
49	2283.6	2356.4	2385.3	49	294.6	304.0	307.7
50	2696.9	2733.7	2818.4	50	347.9	352.6	363.6
51	2788.9	2833.0	2936.5	51	359.8	365.5	378.8
52	2368.9	2702.4	3559.9	52	305.6	348.6	459.2
53	2103.1	2429.8	2880.7	53	271.3	313.4	371.6
54	2132.7	2947.2	3527.0	54	275.1	380.2	455.0
55	1460.1	1660.9	1788.1	55	188.4	214.3	230.7
56	1394.4	1646.0	1771.7	56	179.9	212.3	228.5
57	2979.1	3318.4	3550.0	57	384.3	428.1	458.0
58	3005.4	3354.1	3602.5	58	387.7	432.7	464.7
59	3182.6	3408.8	3596.0	59	410.6	439.7	463.9
60	3182.6	3301.3	3477.9	60	410.6	425.9	448.6
61	1761.9	2751.8	3215.4	61	227.3	355.0	414.8
62	2414.8	2523.0	2690.4	62	311.5	325.5	347.1
63	2962.7	3175.2	3412.2	63	382.2	409.6	440.2

Calculated gas formation volume factors are given in Table 6.10.

Table 6.10. Gas formation volume factors

Coal Layer	Gas FVF, Mscf/rcf			Coal Layer	Gas FVF, Mscf/rcf		
	Minimum	Most Likely	Maximum		Minimum	Most Likely	Maximum
1	0.002009	0.007291	0.021568	33	0.007731	0.009944	0.012039
2	0.016858	0.018961	0.020128	34	0.017762	0.019058	0.021207
3	0.007626	0.014072	0.016421	35	0.018475	0.022149	0.026182
4	0.000475	0.005328	0.015142	36	0.018887	0.020258	0.021763
5	0.002394	0.009158	0.021957	37	0.018998	0.021016	0.022653
6	0.009053	0.012581	0.015061	38	0.028952	0.029305	0.030088
7	0.015414	0.017353	0.018722	39	0.028045	0.030479	0.031915
8	0.015632	0.017568	0.018860	40	0.028102	0.031351	0.033980
9	0.016395	0.018599	0.019797	41	0.030801	0.032723	0.034382
10	0.009822	0.011250	0.012764	42	0.031600	0.033659	0.035131
11	0.007020	0.009336	0.013006	43	0.032373	0.034248	0.035795
12	0.011342	0.012293	0.012737	44	0.019687	0.020946	0.023350
13	0.022096	0.030726	0.047310	45	0.017077	0.017781	0.018805
14	0.039448	0.041863	0.044597	46	0.014059	0.017796	0.022597
15	0.015713	0.027176	0.034468	47	0.016013	0.022215	0.031058
16	0.030544	0.033675	0.036603	48	0.016395	0.017418	0.018612
17	0.034295	0.036578	0.038837	49	0.018393	0.019003	0.019246
18	0.037240	0.038165	0.039739	50	0.021873	0.022185	0.022904
19	0.038749	0.040084	0.041928	51	0.022653	0.023028	0.023909
20	0.023769	0.033191	0.044274	52	0.019108	0.021920	0.029264
21	0.026774	0.036719	0.048049	53	0.016886	0.019619	0.023434
22	0.042718	0.046226	0.049175	54	0.017132	0.024000	0.028980
23	0.014059	0.019150	0.024889	55	0.011584	0.013228	0.014275
24	0.015741	0.017792	0.019741	56	0.011048	0.013106	0.014140
25	0.004851	0.005683	0.006994	57	0.024272	0.027180	0.029179
26	0.009662	0.014667	0.023909	58	0.024497	0.027487	0.029633
27	0.012334	0.016431	0.020018	59	0.026013	0.027959	0.029577
28	0.003347	0.007120	0.010728	60	0.026013	0.027033	0.028555
29	0.005345	0.008123	0.012254	61	0.014059	0.022339	0.026295
30	0.006705	0.008544	0.011610	62	0.019493	0.020404	0.021818
31	0.015931	0.018761	0.022653	63	0.024132	0.025950	0.027988
32	0.022235	0.024352	0.027367				

6.1.7 Initial Sorbed Gas Concentration

Methane adsorption characteristics of coal reservoirs are determined by adsorption tests. The Langmuir Isotherms can be drawn by using the data of adsorption tests. The maximum amount of gas can be adsorbed is called as the Langmuir volume and the pressure at the half of the Langmuir volume is called as Langmuir pressure.

There exist two adsorption tests done for the coal samples taken at different depths from a well found in Amasra. The Langmuir Volume and Langmuir Pressure values determined from these tests are 10.30 scm/tonne, 2.227 MPa and 14.06 scm/tonne, 9.904 MPa respectively. The differences between these values show that the adsorption characteristics change from coal to coal.

The following Langmuir equation is used to estimate the minimum, most likely and maximum adsorbed gas content at the pressures calculated from the average coal layer depth:

$$G_s = \frac{V_L p}{P_L + p} \tag{6.5}$$

Average coal layer depths are given in Table 6.9. Both of the adsorption isotherms were used and the average of them was used as the most likely value in the simulation. Tables 6.11 (a) and (b) show the values that were used as the initial sorbed gas concentrations at the Monte Carlo simulations.

Table 6.11. Initial sorbed gas concentrations

Table 6.11 (a). Initial sorbed gas concentrations (1-40)						
Coal	Adsorbed Gas, scf/tonne			Coal	Adsorbed Gas, scf/tonne		
Layer	Minimum	Most Likely	Maximum	Layer	Minimum	Most Likely	Maximum
1	38.3	68.4	98.5	21	140.9	186.5	232.1
2	86.6	131.4	176.2	22	163.8	206.7	249.7
3	67.9	109.1	150.3	23	87.3	132.1	177.0
4	28.7	53.4	78.0	24	82.3	126.4	170.6
5	46.9	81.1	115.3	25	30.5	56.2	82.0
6	61.8	101.3	140.8	26	70.3	112.1	153.9
7	80.6	124.5	168.4	27	77.1	120.4	163.7
8	81.4	125.5	169.5	28	37.4	67.1	96.8
9	85.3	129.9	174.5	29	42.2	74.2	106.2
10	56.1	93.9	131.6	30	44.1	77.0	110.0
11	47.7	82.2	116.7	31	85.8	130.5	175.2
12	60.6	99.7	138.9	32	105.1	151.5	197.9
13	124.5	171.1	217.6	33	50.4	86.0	121.7
14	153.7	198.0	242.3	34	86.9	131.8	176.6
15	114.0	160.6	207.3	35	97.7	143.7	189.7
16	132.8	179.0	225.1	36	91.2	136.6	181.9
17	140.6	186.2	231.8	37	93.9	139.5	185.1
18	144.6	189.9	235.1	38	120.4	167.0	213.7
19	149.4	194.2	238.9	39	123.8	170.4	216.9
20	131.5	177.7	223.9	40	126.3	172.8	219.3

	Table 6.11 (b). Initial sorbed gas concentrations (41-63)						
Coal Layer	Adsorbed Gas, scf/tonne			Coal Layer	Adsorbed Gas, scf/tonne		
	Minimum	Most Likely	Maximum		Minimum	Most Likely	Maximum
41	130.2	176.5	222.8	53	88.9	134.0	179.1
42	132.8	178.9	225.1	54	103.9	150.3	196.7
43	134.4	180.4	226.5	55	64.4	104.8	145.1
44	93.6	139.2	184.9	56	63.9	104.1	144.3
45	82.2	126.4	170.5	57	114.0	160.7	207.3
46	82.3	126.5	170.6	58	114.9	161.6	208.3
47	98.0	144.0	190.0	59	116.4	163.0	209.7
48	80.9	124.8	168.8	60	113.5	160.2	206.9
49	86.7	131.5	176.4	61	98.4	144.4	190.5
50	97.9	143.9	189.9	62	91.7	137.1	182.6
51	100.7	146.9	193.1	63	110.2	156.8	203.4
52	97.0	142.9	188.8				

6.1.8 Coal Density

The density of the Amasra coal is around 1.54 g/cc (TTK, 2003). However, from the literature it was seen that it has a range of 1.29 g/cc to 1.83 g/cc (Nugroho and Arsegianto, 1993; Nelson, 1999). A triangular distribution was used as the 1.54 g/cc as the most likely value for coal density.

6.1.9 Ash and Moisture Content

The ash and moisture contents of a coal can be found by a proximate analysis. The results of the proximate analysis of the Amasra coals are shown in Table 6.12. Normal distribution was used for the estimation of ash and moisture content values.

Table 6.12. Ash and moisture contents of Amasra coals (TTK, 2003)

Ash, weight %	Moisture, weight %
23.92	6.20
17.71	8.50
8.20	6.25
9.08	5.86
8.87	4.79
12.00	4.75
5.98	5.51
11.71	6.64
2.42	5.85

135

The mean and standard deviation are calculated as 0.1110, 0.0641 respectively for ash content and 0.0604, 0.0112 for moisture content in units of weight fraction.

6.2 Simulation of CO_2 Sequestration in Coal Layer #26

Among coal layers, Coal Layer #26 was selected as an example for the simulation study. The selection was based on the reservoir size and the number of the wells. The main goal of the simulation study is to analyze the effect of various coal parameters on the performance of CH_4 production and CO_2 injection. Therefore optimizing the number and the location of production and injection wells was thought to be the subject of another study. Another gain from this study is the development of data preparation procedure for a CO_2 sequestration simulation study in a coalbed.

Preparation of the input data file, gridding method and the locations of the wells are given in the following sections. Effects of the changes in several parameters were studied case by case. A base case which includes the most likely data was used as a reference case and the other parameters were changed by leaving other base case parameters constant. Although a porosity change was expected due to the change in overburden stress a feature of the simulator for the shrinkage and swelling effects were tested in another case. The increase in the production was observed when the carbon dioxide injection initiated. The effect of the starting time for the injection was a subject of another case. Production of the injected carbon dioxide together with methane or ceasing the production at breakthrough to sequester the carbon dioxide was examined. Since the primary aim was sequestration of the carbon dioxide, the production wells were shut in when the breakthrough occurred in all other cases. Change in cleat permeability, cleat porosity, coal density and coal compressibility were studied. Adsorption parameters have a great effect on the amount and production history of the reservoir as seen in another case. It was estimated that Amasra coal is dry.

However, the case for a wet reservoir was also studied. The anisotropy due to face and butt cleat permeabilities affected the production profile in a case studied.

Computer Modeling Group's (CMG) general equation-of-state based compositional reservoir simulator, GEM was used to achieve the aforementioned goals. GEM is used for modeling the flow of three-phase, multi-component fluids. GEM is a robust, fully compositional simulator used to model any type of reservoir where the importance of the fluid composition and their interactions are essential to the understanding of the recovery process. GEM simulates a variety of structurally complex and varying fluid combinations beyond the conventional black oil simulators as well as K-value compositional simulators. It can be used to model following cases:

- Single and multi-component CBM recovery
- gas condensate recovery,
- volatile oil reservoirs,
- CO_2 and hydrocarbon injection,
- gas cycling and re-cycling,
- water-alternating gas (WAG) processes.

6.2.1 Reservoir Gridding

There were 40 wells used in correlation of Coal Layer #26 in the reservoir. The coordinates of the wells are listed in Table 6.13. In order to simplify the use of given coordinate data, the origin was generated by subtracting the lowest values of both east and north directions from the entire coordinate values (Table 6.13). They increase along the south-north, and west-east directions. However, in GEM the coordinate system is different; i.e., the values should increase along the north-south and west-east directions. To convert the data, the highest Y-axis value (20,004 ft) was subtracted from the all Y-axis values and the negative values were converted to positive multiplying with -1. The surface map of the Coal Layer #26

was drawn with Golden Software Surfer™ Version 8 (Figure 6.10) using the simplified data.

Table 6.13. Coordinates of the wells in Coal Layer #26

Well Name	Original Data		Simplified Data		Converted Data	
	X, ft (West to East)	Y, ft (South to North)	X, ft (West to East)	Y, ft (South to North)	X, ft (West to East)	Y, ft (North to South)
AK12 - I	325,324	321,525	9,364	20,004	9,364	0
AK15 - I	326,568	321,253	10,607	19,732	10,607	272
AK4 - IV	323,211	319,537	7,251	18,016	7,251	1,988
AK6 - VI	320,455	321,276	4,495	19,755	4,495	249
Amasra-50 - VII	320,718	318,300	4,757	16,779	4,757	3,225
Çömlekkıran-65 - II	317,299	318,323	1,339	16,802	1,339	3,202
Çömlekkıran-66 - I	316,525	315,921	564	14,400	564	5,604
Fermitkadı-55 - I	317,890	301,770	1,929	249	1,929	19,755
Gömü-K37 - VII	321,023	320,905	5,063	19,384	5,063	620
K11 – I	323,838	316,971	7,878	15,450	7,878	4,554
K21 – I	323,060	314,110	7,100	12,589	7,100	7,415
Kaman-10 - I	320,823	309,001	4,862	7,481	4,862	12,524
Kaman-14 - I	315,960	309,201	0	7,681	0	12,323
Kaman-39 - I	318,178	306,823	2,218	5,302	2,218	14,702
Kaman-58 - I	321,453	307,203	5,492	5,683	5,492	14,322
Kaman-60 - I	319,464	308,112	3,504	6,592	3,504	13,413
Kaman-61 - I	322,726	308,939	6,765	7,418	6,765	12,586
Karacay-11 - I	320,957	301,521	4,997	0	4,997	20,004
Kazpınar-18 - I	317,657	314,431	1,696	12,911	1,696	7,094
Kazpınar-20 - I	322,152	310,376	6,191	8,855	6,191	11,149
Kazpınar-51 - I	322,624	316,899	6,664	15,378	6,664	4,626
Kazpınar-62 - I	321,725	314,271	5,765	12,750	5,765	7,254
Kazpınar-63 - I	319,999	314,284	4,039	12,763	4,039	7,241
Kazpınar-64 - I	320,606	316,338	4,646	14,817	4,646	5,187
Kazpınar-69 - I	320,541	311,377	4,580	9,856	4,580	10,148
Kazpınar-78 - I	321,948	312,105	5,988	10,585	5,988	9,420
Kazpınar-K1 - I	320,987	309,799	5,026	8,278	5,026	11,726
Kazpınar-K12 - I	324,583	317,174	8,622	15,654	8,622	4,351
Kazpınar-K2 - I	321,138	311,875	5,177	10,355	5,177	9,649
Kazpınar-K25 - I	322,516	311,265	6,555	9,745	6,555	10,260
Kazpınar-K3 -III	320,419	313,431	4,459	11,910	4,459	8,094
Kazpınar-K4 - I	321,482	309,398	5,522	7,878	5,522	12,127
Kazpınar-K5 - I	321,676	309,877	5,716	8,357	5,716	11,648
Kazpınar-K6 - II	321,282	313,447	5,322	11,926	5,322	8,078
Kuşkayası-32 - V	322,932	319,750	6,972	18,229	6,972	1,775
S34 –III	324,721	320,029	8,760	18,508	8,760	1,496
Sondaj-13 - II	318,897	312,683	2,936	11,162	2,936	8,842
Tarlaağzı-22 - I	317,962	321,489	2,001	19,968	2,001	36
Tarlaağzı-26 - I	319,815	321,472	3,855	19,952	3,855	52
Uzunöz-15 - IV	318,848	318,093	2,887	16,572	2,887	3,432

138
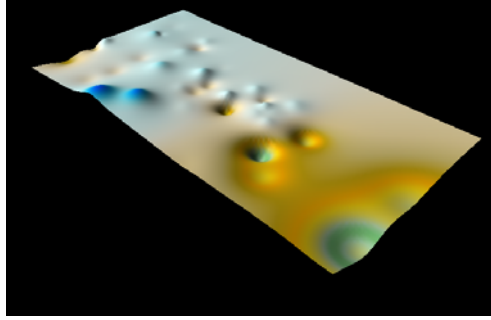
Figure 6.10 (a) Inverse Distance to a Power   Figure 6.10 (b) Kriging
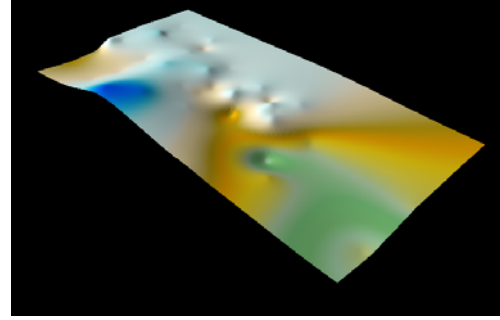
Figure 6.10. Formation top map of the Coal Layer #26 before correction

As can be seen from Figure 6.10, few formation tops were too high or too deep that was unusual distribution and should be taken into consideration. This might be due to the erroneous correlation of the coal seams or most probably the type of selected gridding method. The kriging method was used in this study. This method generates the unknown data by smoothing the known data points (Figure 6.10 b). In order to have more realistic distribution, such data points belong to six wells (Kaman-60–I, Kazpınar-69–I, Kazpınar-20–I, Kuşkayası-32–V, K11–I and AK6–VI) were excluded from the data file and the formation tops were regenerated and shown in Figure 6.11 for the Coal Layer #26.
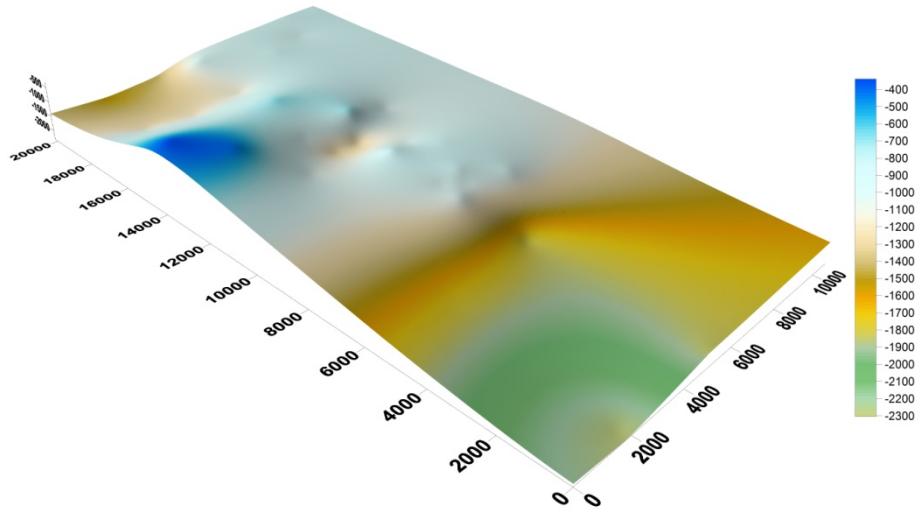
Figure 6.11. Formation top map of the Coal Layer #26 after correction (ft)

Gridding of the data was accomplished by the following procedure:

- Grid Data menu of the Surfer™ was selected,

139

- The file and the worksheet were opened,
- Data columns and the gridding method were specified,
- 160 ft of spacing was selected.

The reservoir was divided into a total of 8636 grids with 127 rows and 68 columns when the length and width of the grids set as 160 ft. The file with 'grd' extension created by the Surfer™ includes formation top depths of all of the grids required by the GEM.

The distribution of the thickness values for the entire reservoir was done similarly using Surfer™.

6.2.2 Input Data Preparation

Input data files were prepared for all of the cases which include the required information. The data file should include input/output control data, reservoir description, component properties, rock-fluid data, initial conditions, numerical methods control and well and recurrent data. The data that were entered in each of these parts were explained in the following sections using an example data file.

6.2.2.1 Input/Output Control

This section defines the project title, type and frequency of the output data.

TITLE1 'Layer 26'
The project is identified as 'Layer 26'.

MAXERROR 20
Maximum number of error messages before the simulation terminates is 20.

INUNIT FIELD
Field units are specified for input data.

INTERRUPT INTERACTIVE

Indicates that user will be prompted interactively for further action to be taken when the user interrupts the simulation run by CTRL-C.

WPRN WELL TIME, WPRN GRID TIME, WPRN ITER BRIEF

WPRN is used to control the frequency of writing data to the output print files. Well and grid results are written to the output file at every time specified by subsequent recurrent 'DATE' keyword in the input file. A summary of time step convergence behavior is also written to the output file.

WSRF WELL 1, WSRF GRID TIME

WSRF is used to control the frequency of writing well and/or grid information to the output simulation results file. Well results are written at each time step and grid results are written at every time specified in the input file.

DIARY CHANGES

After each time step, a line specifying the size and location of the maximum changes in pressure, saturation and composition during the time step is printed to the terminal screen.

RANGECHECK ON

A control of the input data to determine if it is within an expected range of numbers feature is turned on.

OUTPRN WELL BRIEF, OUTPRN GRID NONE, OUTPRN RES NONE

OUTPRN identifies what information is written to the output print file. Only a summary of the well information is written.

OUTSRF WELL PAVG FGIP MGIP MWIP TGIP TWIP RECG
OUTSRF GRID ADS 'CH4' ADS 'CO2' PRES SG SW Z 'CH4' Z 'CO2'
OUTSRF RES ALL

OUTSRF identifies what information is written to the simulation results file. Well or special variables: average reservoir pressure, gas in place in the fracture, gas in

place in the matrix, water in place in the matrix, total gas in place in the reservoir, total water in place in the reservoir, total gas recovery. Grid results: adsorbed mass fraction of methane, adsorbed mass fraction of carbon dioxide, rservoir pressure, gas saturation, water saturation, flobal mole fraction of methane, global mole fraction of carbon dioxide.

6.2.2.2 Reservoir Description

The coordinate system, number of the grids, porosity system, matrix to fracture flow calculation methods, porosity and permeability data and matrix shrinkage/swelling parameters were given in this part.

GRID VARI 68 127 1

A rectangular grid system composing of 68 grids in I direction, 127 grids in J direction and 1 grid in K direction allowing layers of variable thickness located at different depths is specified. That is, there are 68 rows, 127 columns and 1 coal layer. The largest values in west-east direction 10607 ft enlarged to 10720 ft (3267 m) and in south-north direction 20004 ft enlarged to 20160 ft (6144 m) in order to convert them to a fold of 160 ft (49 m) which is the size of a grid block.

KDIR DOWN

Indicates the K index increases downward, so larger layer numbers K mean deeper blocks.

DI IVAR 68*160
DJ JVAR 127*160

DI and DJ signals input of an array of grid block lengths (160 ft) for the I and J directions.

DK ALL 15*7 8 2*9 2*10 2*11 2*12 13 12 11 10 9 8 7 2*6 22*5 3*4 10*3 15*7…

DK signals input of an array of grid block thicknesses measured in the K direction. Thickness values were estimated and entered for each of the grid block (Figure 6.12)
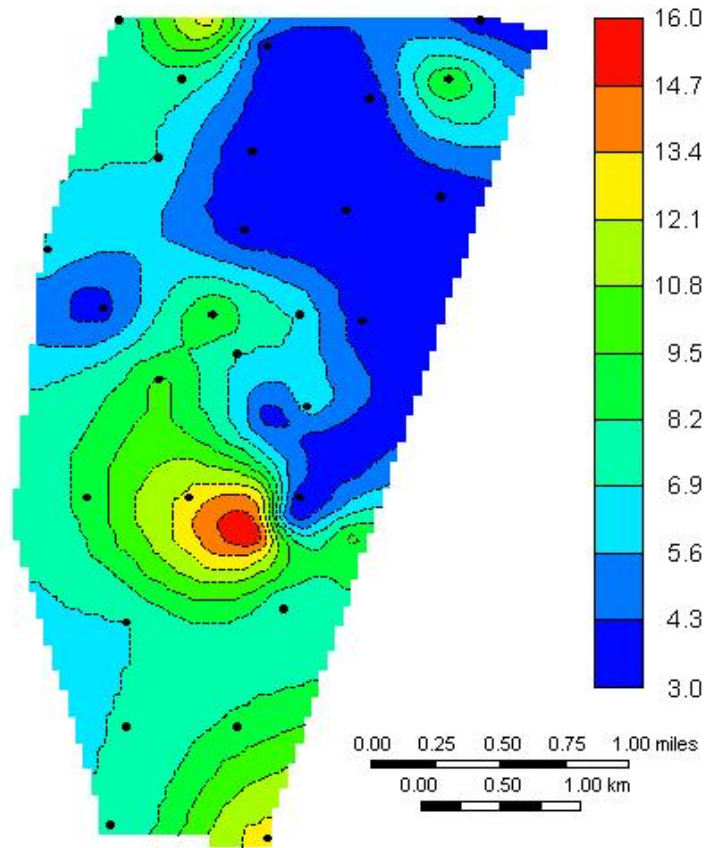
Figure 6.12. Isopach map of coal thickness (ft)

DTOP 1392 1402 1413 1424 1435 1446 1457 1468 1479 1490 1501 1511 1521 1522…

The depths of the grid blocks were defined with DTOP keyword. Depths were measured downwards from a horizontal reference surface; sea level in our case.

DUALPOR

Indicates that a dual porosity option is to be used in the simulator. This option allows each simulator block to have up to two porosity systems, one called its matrix porosity and the other called its fracture porosity. This keyword is required for the simulation of coalbed reservoirs.

SHAPE GK

Indicates the use of Gilman and Kazemi (1983) style formulation for the shape factor. This method is to be used in calculating matrix to fracture flows within blocks for dual porosity models. Shape factor reflects the geometry of the matrix

143

elements and it controls the flow between the two porous regions. Gilman and Kazemi (1983) formulation uses:

$$Transmissibility = 4k \left(\frac{1}{L_x^2} + \frac{1}{L_y^2} + \frac{1}{L_z^2} \right) V_m \qquad (6.6)$$

Where; L_x, L_y and L_z are fracture spacings which were set using DIFRAC, DJFRAC and DKFRAC keywords, k is the permeability and V_m is the total matrix volume.

TRANSFER 3

Indicates the type of matrix-fracture model for treating different phases in dual-porosity reservoirs. Pseudo-capillary pressure model with corrections to contact areas between phases is the default and used model in this study.

NULL FRACTURE IJK 1:13 1:2 1:1 0 1:12 3:6 1:1 0 1:11 7:10 1:1 0 1:10 11:14 1:1 0…
NULL MATRIX IJK 1:13 1:2 1:1 0 1:12 3:6 1:1 0 1:11 7:10 1:1 0 1:10 11:14 1:1 0…

All blocks are considered active unless a block is specifically designated as being null. Null blocks do not participate in any of the simulators calculations. Moreover, they are a barrier to any flow. Null blocks were determined by using millimetric paper.

POR FRACTURE CON 0.02, POR MATRIX CON 0.04

POR keyword was used to specify the porosities of the grid blocks. In this study porosity values were defined same for each grid blocks. Because of the lack of porosity information for the Amasra basin, the literature data were used. Experiments on the Acılık K-6 coal done by Karacan and Okandan (1999) showed that the matrix porosity was in the range of 4.0% and 5.1%. Matrix porosity of 4.0% was taken constant for each cases. Methane is also can be found as free gas in cleat system. The change in cleat porosity was studied. The range of the cleat porosity was used as minimum 0.01 (King et al., 1986; Remner et al., 1986; Anbarci and Ertekin, 1990), most likely 0.02 (Kolesar and Ertekin, 1986; Ertekin and Sung, 1986; Zuber et al., 1987; Sung and Ertekin, 1987; Paul et al.,

1990) and maximum 0.1 (Reeves and Pekot, 2001). The histogram of the literature cleat porosity values are given in Figure 6.13. The porosity value below 0.01 causes the simulator to abnormally terminate.
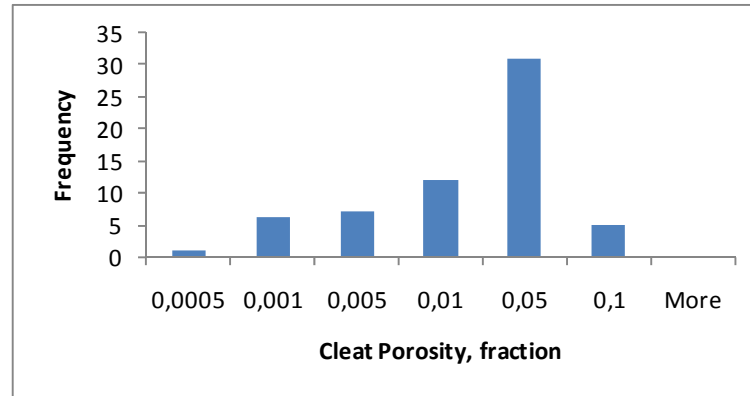
Figure 6.13. Histogram of literature cleat porosity values

PERMI FRACTURE CON 8.0, PERMI MATRIX CON 0.01
PERMJ MATRIX CON 0.01, PERMJ FRACTURE CON 8.0
PERMK MATRIX CON 0.001, PERMK FRACTURE CON 1.0

Matrix and fracture (cleats) permeabilities were specified for each direction. Fracture permeabilities were higher than matrix permeabilities. Matrix permeabilities should be the values measured from a piece of unfractured coal, while fracture permeabilities should be entered as effective fracture permeabilities: that is, the permeability of the fracture system with respect to a volume of reservoir rock. The direction of the face cleat and butt cleat was not known. Therefore in both directions cleat permeabilities were taken equal. And anisotropy of the face and butt cleat permeabilities was studied as an example case. Matrix permeability was assumed to be low (0.01 md) in lateral directions and very low (0.001 md) in vertical direction. Change in cleat permeability was studied as a case. The range was determined from the literature survey. 0.01 md (Roadifer et al., 2003), 8 md (Jikich et al., 2004) and 100 md (Hoch, 2005) were used as minimum, most likely and maximum values. Figure 6.14 shows the histogram of cleat permeability values. Although in some papers permeability as high as 300 md was reported (Onsager and Cox, 2000), the range was limited to 100 md in this study.
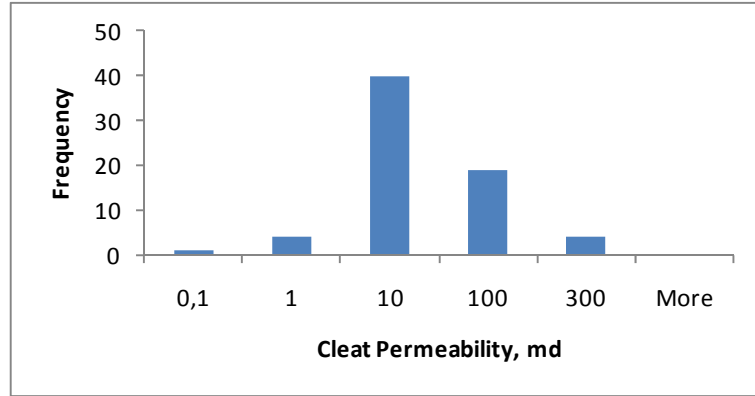
Figure 6.14. Histogram of literature cleat permeability values

DIFRAC CON 6., DJFRAC CON 6., DKFRAC CON 6.

Fracture spacings are used to calculate matrix to fracture transfer coefficient. Fracture spacings should be measured from centre line to centre line in the appropriate direction. 1 ft, 6 ft and 17 ft of cleat spacing were used as minimum, most likely and maximum cases.

PINCHOUTARRAY CON 1

Blocks that are designated as pinched out allow fluid to pass through them vertically, but not laterally. There were no pinched out blocks in the reservoir.

PRPOR FRACTURE 237, PRPOR MATRIX 237
CPOR FRACTURE 0.0002, CPOR MATRIX 0.0002

PRPOR keyword is used to input the reference pressure for the rock compressibility determination. CPOR signals the input of rock compressibility. The functional form used in the calculation of porosity in a formation containing fluid at pressure p is:

$$\emptyset(p) = \emptyset\left[1 + c_f\left(p - p_{ref}\right)\right] \tag{6.7}$$

Where c_f is the rock compressibility and ϕ is the initial porosity.

146

Average reservoir pressure was used as the reference pressure. A very wide range of rock compressibility values were studied by using 0.000001 psi^{-1}, 0.0002 psi^{-1} and 0.01 psi^{-1}.

CROCKTYPE 1
This option allows the user to define different rock compressibility options in various parts of the reservoir. When the CROCKTYPE keyword used, settings for CPOR and PRPOR will be mostly ignored.

CPRPOR MATRIX 237, CPRPOR FRACTURE 237
CCPOR MATRIX 0.0002, CCPOR FRACTURE 0.0002
CPRPOR keyword signals the input of reference pressure for calculating the effect of rock compressibility. CCPOR is the pressure dependence of formation porosity; that is, rock compressibility.

POISSR 0.2, YOUNGM 521000, STRINF 0.0101, PRESLN 1436.5, EXPPM 3.0
These keywords are used to enter the Palmer and Pansoori (1996) model parameters. This model accounts for change in fracture porosity and absolute permeability due to change in net overburden stress and matrix shrinkage/swelling. Matrix shrinkage or swelling occurs as a result of desorption or adsorption of gaseous species. POISSR is a value for the (dimensionless) poisson ratio used in calculating the ratio of bulk to axial modulus required for the P&M model. YOUNGM is a value for the Young's modulus used in calculating the pore compressibility. STRINF is a value for the strain at infinite pressure required in the P&M equation. PRESLN is a value for the Langmuir pressure. EXPPM is a dimensionless exponent used in calculating the change in fracture permeability as a function of the change in fracture porosity.

Flow in the fracture system in coal is described by Darcy flow. The absolute permeability appearing in Darcy's Law is not constant but varies in situ with the change in the net overburden stress (overburden pressure-pore pressure) and with effects associated desorption/adsorption of gas in the matrix. As the gas is desorbed matrix volume shrinks which in turn allows for fracture apertures to

open. As the pressure is reduced therefore there are two competing effects, pore closure due to compressibility effects and pore enlargement due to matrix shrinkage. The Palmer and Mansoori model accounts for both effects and allows for changes in porosity and absolute permeability to be calculated as a function of changes fracture pressure and matrix shrinkage/swelling. Equation 6.8 reproduces the Palmer and Mansoori (1996) relationship.

$$\frac{\emptyset}{\emptyset_i} = 1 + c_f(p - p_i) + \varepsilon_L \left(1 - \frac{K}{M}\right) \left(\frac{p_i}{p_i + P_L} - \frac{p}{p + P_L}\right) \tag{6.8}$$

Where $\emptyset_i$ is initial natural fracture porosity, $\emptyset$ is fracture porosity at pressure p, c_f is pore volume compressibility (1/psia), p_i is initial pressure (psia), p is pressure (psia), ε_L is strain at infinite pressure, K is bulk modulus (psia), M is axial modulus (psia) and P_L is Langmuir pressure (psia).

This relationship shows that the porosity divided by the initial porosity decreases as a result of pore compression caused by pressure drawdown plus the increase caused by matrix shrinkage. The ratio of bulk to axial modulus is related to the Poisson's ratio as indicated by Equation 6.9.

$$\frac{K}{M} = \frac{1}{3} \left(\frac{1 + \vartheta}{1 - \vartheta}\right) \tag{6.9}$$

Where ν is the Poisson's ratio (dimensionless).

The P&M theory relates the absolute permeability ratio to the porosity ratio in the following manner:

$$\frac{k}{k_i} = \left(\frac{\emptyset}{\emptyset_i}\right)^\alpha \tag{6.10}$$

Where α is typically equal to 3.

6.2.2.3 Component Properties

Number of the components and the equation of state model were given in this section.

MODEL PR

Peng-Robinson equation of state is used to model the fluid properties.

NC 2 0

There were two primary components excluding water.

COMPNAME 'CO2' 'CH4'

These components were carbon dioxide and methane.

TRES 94

Reservoir temperature was assumed to be constant and equal all over the reservoir. Reservoir temperature was given as 94 °F by TTK (2003).

6.2.2.4 Rock-Fluid Data

Relative permeability data and the coalbed methane feature properties were given in this section.

ROCKFLUID

This keyword indicates the beginning of rock-fluid data.

RPT 1 DRAINAGE SCALING-NEW

RPT indicates that relative permeability curves will be defined by table entries.

The relative permeability curve of Law et al. (2002) was used in this study (Figure 6.15)
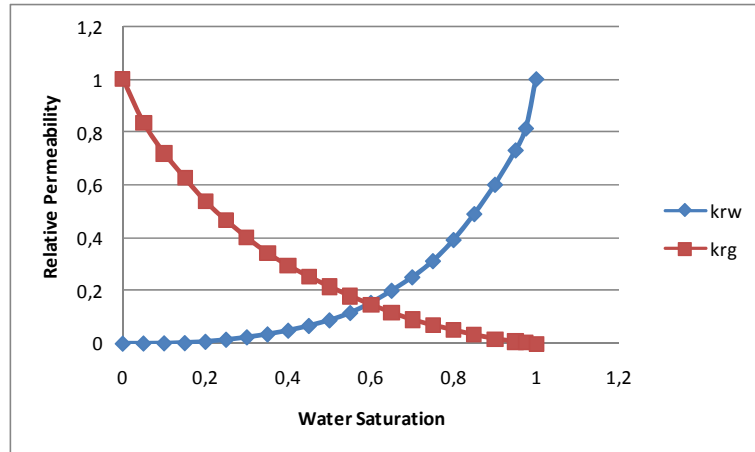
Figure 6.15. Relative permeability curve (Law et al., 2002)

SWT

0.000000 0.000000 0.0000060 0.000000

0.050000 0.000600 0.0000050 0.000000…

SWT indicates the start of the water oil relative permeability table. The numbers in each line represent water saturation, relative permeability to water at the given water saturation, relative permeability to oil in the presence of the given water saturation and water-oil capillary pressure respectively.

SLT

0.000000 1.000000 0.000000 0.000000

0.050000 0.835000 0.00000006 0.000000…

SLT indicates the start of the liquid-gas relative permeability table. The numbers in each line represent total liquid saturation, relative permeability to gas for the given saturation, relative permeability to oil in the presence of gas and connate water for the given water saturation and gas-oil capillary pressure respectively.

ADGMAXC 'CO2' MATRIX CON 0.540527, ADGMAXC 'CO2' FRACTURE CON 0

ADGMAXC 'CH4' MATRIX CON 0.270263, ADGMAXC 'CH4' FRACTURE CON 0

ADGMAXC specifies the maximum moles of adsorbed component per unit mass of rock. It was entered for both components separately.

ADGCSTC 'CO2' MATRIX CON 0.001392, ADGCSTC 'CO2' FRACTURE CON 0

ADGCSTC 'CH4' MATRIX CON 0.000696, ADGCSTC 'CH4' FRACTURE CON 0

ADGCSTC introduces the inverse pressure parameter for the Langmuir isotherm model. The extended Langmuir isotherm is used for multicomponent adsorption.

There were two adsorption test results available for Amasra coal. One of the tests was done on a coal sample of Karadon formation and other one was a sample of Kozlu formation. The average depth of the Coal Layer #26 was 1788 ft (545 m) and it was found in Karadon formation. Therefore, the Langmuir pressure and Langmuir volume values of the adsorption test belongs to Karadon formation coal was used for the base case. These values were 1436.4 psi and 496.5 scf/tonne. The effects of change of adsorption parameters were also studied and the results of the Kozlu formation sample were used as 323.0 psi and 363.7 scf/tonne. However these tests were performed using methane and there were no data available for carbon dioxide. In the literature it is seen that the coal has a nearly two folds bigger Langmuir volume and half a value of Langmuir pressure. Analogously, adsorption parameters for carbon dioxide were estimated 718.2 psi and 993.1 scf/tonne for the base case and 161.5 psi and 727.5 scf/tonne when the adsorption parameters were changed.

ROCKDEN MATRIX CON 96.13807, ROCKDEN FRACTURE CON 96.13807

Coal mass density in units of lb/ft^3. This is the actual rock density, not including its pore space. Coal densities ranging from 1.289 g/cm^3 to 1.83 g/cm^3 were reported. 1.54 g/cm^3 of coal density value was given by the Turkish Hard Coal Enterprise, Zonguldak (TTK, 2003).

COAL-DIF-COMP 'CO2' MATRIX CON 0.003855
COAL-DIF-COMP 'CH4' MATRIX CON 0.001928

This keyword activates the multi-component coalbed features in GEM, and also specifies the matrix (coal) to fracture (cleat) diffusion process in a coalbed. COAL-DIF-COMP keyword indicates gas phase diffusion values for a specified component in cm^2/sec that describes matrix (coal) to fracture (cleat) mass transfer.

6.2.2.5 Initial Conditions

The reservoir initialized with the data entered in this section.

INITIAL

INITIAL indicates the beginning of initial condition values.

USER_INPUT

This keyword specifies that pressure, composition and saturation of each grid block will be entered.

PRES FRACTURE ALL 263 263 262 262 261 260 259 258 257 255 254…
PRES MATRIX ALL 263 263 262 262 261 260 259 258 257 255 254…

Initial pressures for fracture and matrix porosities and for each grid block were entered. The pressure values were estimated using a pressure gradient of 0.129 psi/ft which was 30% of water pressure gradient of 0.43 psi/ft. Hoch (2005) remarked that for the Horseshoe Canyon Formation which is dry similar to Amasra Coal, the pressure gradient was less than 30% of water hydrostatic pressure.

SW MATRIX CON 0.00, SW FRACTURE CON 0.01

No water saturation in the matrix and 1% water saturation in the fracture were specified initially.

ZGLOBALC 'CO2' MATRIX CON 0.0, ZGLOBALC 'CO2' FRACTURE CON 0.0
ZGLOBALC 'CH4' MATRIX CON 1.0, ZGLOBALC 'CH4' FRACTURE CON 1.0

ZGLOBALC indicates input of initial grid block global composition on a component-by-component basis. There were initially no carbon dioxide and the only component beside water was methane.

6.2.2.6 Numerical Methods Control

NUMERICAL

NUMERICAL identifies the beginning of all numerical methods control keywords.

NORM PRESS 100, NORM SATUR 0.1

NORM specifies the typical changes in the basic variables during a time step. The time step size is adjusted internally such that the average change in pressure and saturation during a time step equals 100 psia and 0.1 respectively.

DTMIN 1.E-06

DTMIN identifies the minimum time step size was 1E-6 days.

6.2.2.7 Well and Recurrent Data

RUN

Identifies the beginning of all well and recurrent data keywords.

DATE 2007 01 01

Indicates that the well change will occur at a specified date.

DTWELL 0.1

Identifies the first time step size as 0.1 days to be used immediately after the current well change.

AIMSET MATRIX CON 3., AIMSET FRACTURE CON 3.

Implicit formulations were assigned for all grid blocks.

AIMWELL WELLNN

This keyword sets the neighbors of active well blocks and the neighbors of the neighbors to implicit.

WELL 'UZUNOZ-15' or WELL 'TAGZI-22INJ'

Well name is identified. For each well a different name was used.

PRODUCER 'UZUNOZ-15' or INJECTOR 'TAGZI-22INJ'

Well type definitions were entered.

OPERATE MIN BHP 50. CONT or

OPERATE MAX STG 30000 CONT, OPERATE MAX BHP 1161.6 CONT

Well operating constraints were given by this keyword. Producer wells operate until they reached to minimum 50 psia and the simulation continues. There were two constraints defined for the injector wells. They are limited with maximum 30,000 scf/day surface gas rate and given bottom hole pressure.

GEOMETRY K 0.5 0.37 1. 0.

GEOMETRY specifies the well geometric characteristics to be used by the simulator to calculate the well index internally. K sub keyword identifies that the well is parallel to K axis; that is vertical. The numbers specifies the well bore radius, geometric factor for the well element, fraction of a circle that the well models and well skin factor respectively.

PERF GEO 'UZUNOZ-15' 19 22 1 1. OPEN FLOW-TO 'SURFACE' or

PERF GEO 'TAGZI-22INJ' 14 1 1 1. OPEN FLOW-FROM 'SURFACE'

PERF specifies the location of the well completion grid blocks. The location of the well defined with the grid block indexes of I, J and K directions.

OPEN 'UZUNOZ-15' or OPEN 'TAGZI-22INJ'

Well status identified.

IWELLBORE MODEL 1936. 1936. 0.000742 77. 94. 0.5

IWELLBORE specifies that the well bore pressure drops will be computed for this injector. Tubing data are required for the pressure drop computation. Well depth (ft), well length (ft), relative well roughness, well head temperature (°F), reservoir temperature (°F) and well tubing radius (ft) should be entered.

INCOMP SOLVENT 1. 0.

Indicates the composition of injected fluid as 100% carbon dioxide according to the order of the entered component names.

STOP

STOP causes simulation to terminate.

6.2.3 Well Locations and Shut-in Times

The formation top map of the Coal Layer #26 is given in Figure 6.11. As can be seen from the figure south and north parts of the reservoir are deeper comparing to the middle sections. There are several production well patterns used for gas injection such as 5 spot or 9 spot patterns.

In this study however using the density difference between methane and carbon dioxide, carbon dioxide was injected from the deeper parts and methane was produced from the middle of the reservoir (Figure 6.16).

Figure 6.16. 3D visualization of formation top with well locations (ft)

The production and injection well names are given in Table 6.14. There were 19 production wells and 9 injection wells. Two of the production wells and three of the injection wells do not exist originally in the reservoir. They were placed in appropriate grids according to the well pattern and named with a NK prefix.

Table 6.14. Locations of production and injection wells

Production Wells			Injection Wells		
Well Name	Grid Index		Well Name	Grid Index	
	I	J		I	J
UZUNOZ-15	19	22	TAGZI-22INJ	14	1
AMASRA-50	31	21	AK-12INJ	60	1
KPINAR-51	43	30	FKADI-55INJ	13	124
KPINAR-K12	55	28	KARACAY-11INJ	33	126
SONDAJ-13	19	56	NK-3INJ	29	109
KPINAR-K21	45	47	NK-4INJ	15	109
KAMAN-39	15	93	NK-5INJ	22	10
KAMAN-58	35	91	AK-4INJ	46	13
NK-1	23	74	S-34INJ	56	10
NK-2	10	74			
KPINAR-K5	37	74			
KPINAR-78	38	60			
KPINAR-18	12	45			
KPINAR-63	26	46			
KPINAR-62	37	46			
KPINAR-64	30	33			
CKIRAN-66	5	36			
GOMU-K37	33	5			
KPINAR-K3	29	52			

Injection of the carbon dioxide caused a breakthrough after a while. The production wells should be shut in to cease the carbon dioxide production. Shut-in times were determined by checking the amount of surface carbon dioxide production rates of each production well after a simulation. When the CO_2 production rate exceeded 100 scf/day the date noted and entered for the next run as an input (Figure 6.17 and Table 6.15). However, the change in shut-in times affected the next run and another check for the surface carbon dioxide rates required. The simulation was done afterwards with new shut-in times (Figure 6.18 and Table 6.16).
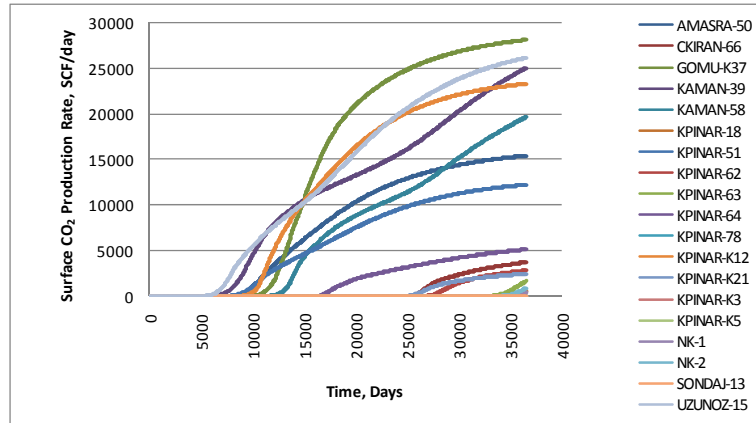
Figure 6.17. Production rates of carbon dioxide if the wells were not shut-in

Table 6.15. First shut-in dates

Well Name	First Shut-in Time	
	Date	Days
UZUNOZ-15	01.03.2022	5538
AMASRA-50	01.11.2029	8340
KPINAR-51	01.07.2028	7852
KPINAR-K12	01.09.2031	9009
SONDAJ-13	-	-
KPINAR-K21	01.01.2076	25202
KAMAN-39	01.01.2024	6209
KAMAN-58	01.03.2059	19052
NK-1	01.11.2103	35367
NK-2	01.11.2100	34272
KPINAR-K5	-	-
KPINAR-78	-	-
KPINAR-18	01.05.2101	34453
KPINAR-63	01.03.2098	33297
KPINAR-62	01.11.2080	26968
KPINAR-64	01.03.2052	16496
CKIRAN-66	01.05.2076	25323
GOMU-K37	01.07.2034	10043
KPINAR-K3	-	-

After nearly 5500 days of production the carbon dioxide production rates started to increase. The dates when they exceeded 100 scf/day were taken as first shut-in dates. Right after the dates obtained SHUTIN keywords were entered for each production well except the wells where the limit was not reached.
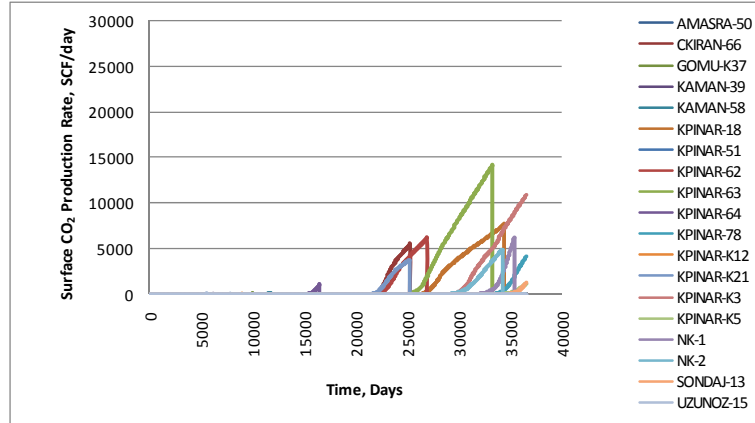
Figure 6.18. Production rates of carbon dioxide after first shut-in

Addition of shut-in dates was changed for the production history of the reservoir. Therefore a second check was required for the determination of accurate shut-in dates. The sudden decrease in the production rates shows the first shut-in dates. New or corrected shut-in dates are given in Table 6.16.

Table 6.16. Corrected shut-in dates

| Well Name | Corrected Shut-in Time | |
	Date	Days
UZUNOZ-15	01.03.2022	5538
AMASRA-50	01.11.2029	8340
KPINAR-51	01.07.2028	7852
KPINAR-K12	01.09.2031	9009
SONDAJ-13	01.11.2102	35002
KPINAR-K21	01.05.2066	21670
KAMAN-39	01.01.2024	6209
KAMAN-58	01.05.2038	11443
NK-1	01.09.2094	32020
NK-2	01.03.2087	29279
KPINAR-K5	01.07.2101	34514
KPINAR-78	01.01.2099	33603
KPINAR-18	01.07.2079	26479
KPINAR-63	01.01.2076	25202
KPINAR-62	01.09.2067	22158
KPINAR-64	01.05.2049	15461
CKIRAN-66	01.11.2066	21854
GOMU-K37	01.03.2034	9921
KPINAR-K3	01.11.2087	29524

158
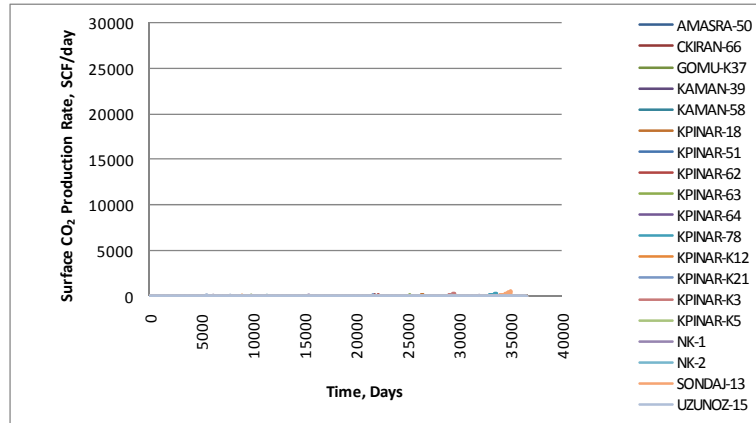
Figure 6.19. Production rates of carbon dioxide after corrected shut-in

Figure 6.19 shows that after entering of corrected shut-in dates the carbon dioxide production was totally ceased as well as methane production for that well. The scale of the figure is not reduced to show the decrease in the CO_2 production comparing to Figures 6.17 and 6.18.

CHAPTER 7

RESULTS AND DISCUSSION

7.1 Gas in Place Estimation with Risk Analysis

63 coal layers having different properties such as depth, thickness and area were determined by correlating the coal seams in Amasra Resource Area A. Methane is found in a coal reservoir as an adsorbed and a free gas states. The initial gas in place amounts both free and adsorbed states were estimated by Monte Carlo simulation for each coal layer.
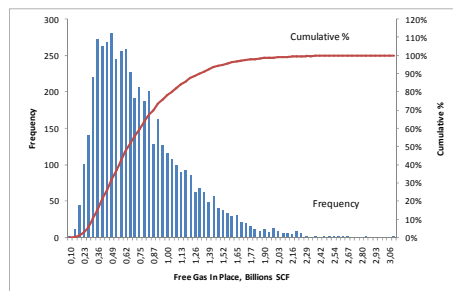
Figure 7.1 (a) Free Gas
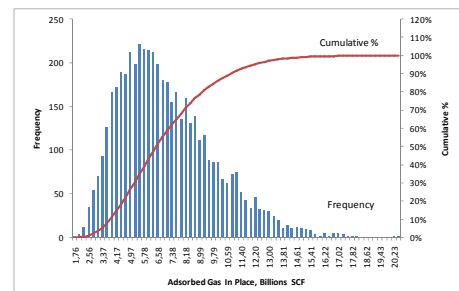
Figure 7.1 (b) Adsorbed Gas
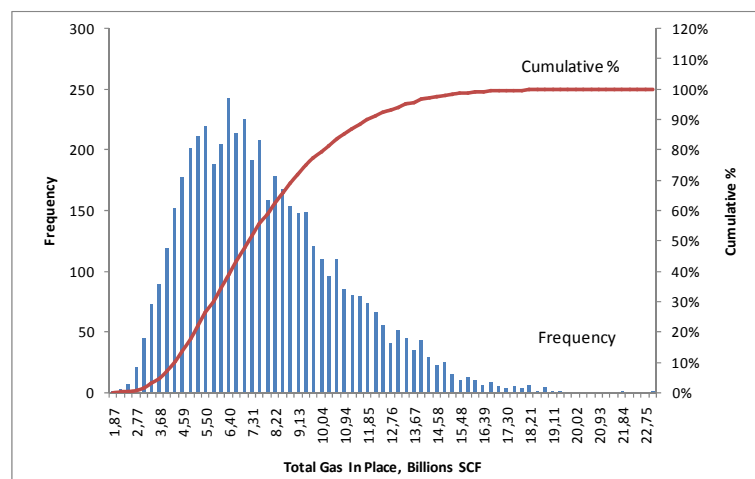
Figure 7.1 (c) Total Gas

Figure 7.1. Histogram and cumulative distribution of gas in place estimate for Coal Layer #26

Figures 7.1 (a), (b) and (c) show the histogram and cumulative distribution function of free gas, adsorbed gas and total gas in place estimates as an example for Coal Layer #26. Histogram plots showed that the distributions of gas in place amounts were skewed to the left side, which meant that the estimations were more conservative. This was mainly due to the asymmetric distribution of coal thickness and porosity values. Coal thicknesses were generally low and therefore the most likely values for thicknesses lay on the left side. Besides, 1%, 2% and 6% of porosity values were used as minimum, most likely and maximum values. One can never be sure exactly how much gas in place actually in the coal reserves but it can be estimated. Consequently the amount thought to be in the reserves was estimated as three figures:

- **Proven (P90)** The lowest figure, the amount that we are 90% sure.
- **Probable (P50)** The average figure, the amount that is expected to be closest to the true reserves.
- **Possible (P10)** The highest figure, the amount that we are 10% sure.

Tables 7.1 (a) and (b) show the results of the Monte Carlo simulation for each layer giving P10, P50 and P90 estimates for free, adsorbed and total gas in place.

Table 7.1. Probabilistic estimation of initial free gas in place for coal layers

Table 7.1 (a) Free gas in place estimates for coal layers (1 to 45)											
No	*Free Gas, MMscf*			*No*	*Free Gas, MMscf*			*No*	*Free Gas, MMscf*		
	P10	*P50*	*P90*		*P10*	*P50*	*P90*		*P10*	*P50*	*P90*
1	246.9	107.9	44.9	16	95.9	57.8	33.5	31	577.1	304.7	155.7
2	345.7	183.2	89.8	17	190.7	107.3	58.5	32	181.7	101.1	54.4
3	150.5	79.1	39.9	18	50.4	29.9	17.3	33	16.7	8.9	4.6
4	103.4	45.4	18.4	19	53.0	31.4	18.3	34	72.3	40.9	22.4
5	168.6	75.0	33.0	20	128.2	70.2	37.3	35	103.6	59.2	32.2
6	12.9	7.2	3.9	21	63.9	37.7	21.2	36	26.9	16.1	9.5
7	18.1	9.3	4.4	22	212.4	109.8	54.3	37	31.6	18.2	10.3
8	18.7	9.9	4.8	23	485.8	250.8	124.8	38	28.3	17.0	9.9
9	24.5	11.8	5.2	24	240.1	137.4	75.8	39	87.1	48.7	26.8
10	6.0	2.9	1.3	25	0.7	0.4	0.2	40	88.9	53.0	30.4
11	6.5	3.7	2.1	26	1,294.3	644.7	314.1	41	47.6	26.1	13.6
12	6.9	3.8	2.0	27	7.8	4.3	2.3	42	37.1	22.3	12.9
13	768.0	437.4	239.4	28	21.6	11.8	6.1	43	37.9	22.6	13.2
14	278.0	165.0	94.9	29	7.6	4.3	2.4	44	32.2	19.3	11.2
15	118.7	69.0	38.4	30	21.3	11.4	5.8	45	39.8	23.1	12.9

Table 7.1 (b) Free gas in place estimates for coal layers (46 to 63)

No	Free Gas, MMscf			No	Free Gas, MMscf			No	Free Gas, MMscf		
	P10	P50	P90		P10	P50	P90		P10	P50	P90
46	185.3	100.7	53.3	52	85.4	32.4	8.3	58	51.7	28.6	15.6
47	928.4	471.4	226.3	53	201.1	62.7	12.5	59	126.8	70.7	36.3
48	16.1	9.5	5.4	54	222.9	72.1	15.8	60	240.4	138.2	76.9
49	16.0	9.5	5.5	55	7.6	2.0	0.2	61	279.9	143.5	70.7
50	0.9	0.5	0.3	56	27.7	7.6	1.6	62	8.7	5.2	2.9
51	1.0	0.5	0.3	57	42.4	16.4	4.1	63	75.8	43.7	24.1

Table 7.2. Probabilistic estimation of initial adsorbed gas in place for coal layers

No	Adsorbed Gas, MMscf			No	Adsorbed Gas, MMscf			No	Adsorbed Gas, MMscf		
	P10	P50	P90		P10	P50	P90		P10	P50	P90
1	1,826.1	1,094.5	630.6	22	1,153.0	712.3	403.8	43	221.7	170.8	129.8
2	2,938.1	1,863.7	1,036.1	23	4,027.2	2,437.0	1,463.9	44	236.1	178.4	131.4
3	1,611.4	965.3	579.5	24	2,012.4	1,386.3	923.9	45	324.6	230.6	160.6
4	801.2	537.8	341.2	25	8.1	5.6	3.8	46	1,524.0	1,007.5	639.9
5	1,383.8	833.4	479.5	26	10,784.6	6,472.1	3,801.2	47	7,116.3	4,171.7	2,386.7
6	126.9	85.3	54.9	27	68.9	45.6	29.2	48	133.5	95.6	68.1
7	154.3	98.3	53.0	28	236.0	161.4	107.2	49	126.3	94.1	68.5
8	164.0	103.3	55.8	29	74.7	53.5	37.1	50	7.1	4.8	2.9
9	217.3	120.9	57.4	30	222.8	138.9	82.3	51	7.2	4.9	3.0
10	61.6	34.7	17.2	31	4,735.9	2,932.4	1,807.7	52	343.2	262.0	196.9
11	62.8	44.3	30.1	32	1,314.0	884.6	576.4	53	794.1	548.6	364.9
12	68.4	44.6	27.4	33	176.8	109.8	66.1	54	831.8	610.0	440.7
13	4,450.6	3,227.3	2,279.0	34	587.5	392.4	263.8	55	35.1	21.1	10.4
14	1,459.7	1,108.6	827.5	35	783.6	540.9	362.1	56	120.7	80.1	51.8
15	832.4	615.7	444.8	36	203.2	154.0	115.0	57	171.9	130.5	97.2
16	570.8	440.7	331.0	37	246.1	172.2	122.2	58	359.9	241.2	158.8
17	1,123.1	776.7	527.5	38	180.8	137.5	101.4	59	873.4	599.1	357.1
18	275.9	211.5	158.2	39	570.3	390.0	265.9	60	1,647.1	1,164.9	787.2
19	280.7	216.0	163.5	40	557.3	415.5	313.3	61	2,304.8	1,442.9	834.3
20	778.3	535.6	349.4	41	297.6	200.2	130.2	62	65.7	48.6	34.7
21	354.3	272.0	202.0	42	218.5	169.0	129.4	63	526.2	377.3	254.8

Table 7.3. Probabilistic estimation of initial gas in place for coal layers

Table 7.3 (a) Initial gas in place estimates for coal layers (1 to 45)

No	IGIP, MMscf			No	IGIP, MMscf			No	IGIP, MMscf		
	P10	P50	P90		P10	P50	P90		P10	P50	P90
1	2,015.5	1,225.3	712.7	16	644.4	501.7	382.8	31	5,210.4	3,257.7	2,033.1
2	3,228.1	2,076.7	1,155.0	17	1,280.3	895.5	607.1	32	1,462.9	993.8	654.0
3	1,733.3	1,051.4	637.8	18	314.8	243.4	183.6	33	190.0	119.6	72.8
4	873.5	590.0	379.5	19	323.0	249.1	190.1	34	643.0	437.0	296.3
5	1,519.5	918.2	537.1	20	879.1	611.9	404.6	35	868.4	605.1	408.3
6	137.3	93.3	60.4	21	404.3	312.4	233.3	36	222.8	171.7	129.7
7	170.1	108.5	58.4	22	1,333.9	831.3	472.1	37	271.5	191.5	137.1
8	179.6	114.1	62.5	23	4,416.9	2,718.8	1,656.1	38	202.0	155.3	116.0
9	238.1	132.9	64.0	24	2,201.9	1,536.3	1,030.4	39	641.4	442.7	300.5
10	66.9	37.9	18.9	25	8.6	6.1	4.2	40	622.1	471.5	358.7
11	67.7	48.2	33.3	26	11,870.2	7,159.9	4,270.8	41	337.4	229.3	148.9
12	73.7	48.8	30.1	27	75.2	50.3	32.5	42	246.5	193.4	148.7
13	5,079.1	3,714.5	2,625.7	28	251.7	174.6	117.6	43	250.4	195.2	149.2
14	1,685.3	1,284.6	962.1	29	80.2	58.2	40.7	44	260.2	199.2	148.5
15	922.4	689.7	504.2	30	240.2	151.2	90.7	45	355.4	254.6	179.2

Table 7.3 (b) Initial gas in place estimates for coal layers (46 to 63)

No	IGIP, MMscf			No	IGIP, MMscf			No	IGIP, MMscf		
	P10	P50	P90		P10	P50	P90		P10	P50	P90
46	1,673.4	1,117.2	712.4	52	380.1	293.7	224.1	58	402.6	272.2	180.6
47	7,937.9	4,673.2	2,702.8	53	878.7	609.1	410.0	59	977.2	678.3	405.0
48	146.1	105.5	76.2	54	918.1	679.7	498.9	60	1,842.0	1,314.4	895.3
49	138.4	104.6	76.6	55	38.0	23.1	11.3	61	2,538.3	1,598.2	926.5
50	7.9	5.4	3.3	56	131.0	87.1	57.2	62	72.3	54.1	39.1
51	8.0	5.5	3.4	57	191.2	146.8	110.7	63	590.0	423.8	289.0

In the tables it was conspicuous that sum of free gas and adsorbed gas was not equal to the total gas in place value. The reason for that is the calculation of P10, P50 and P90 values for free gas and adsorbed gas separately. One should look at the specific probability value which was aimed to estimate.

In the estimation of the gas in place, a range rather than constant values was used. Tables 7.4 (a) and (b) show the estimated gas in place determined from the lowest, average and highest values of Monte Carlo simulation results.

Table 7.4. Estimated initial free gas in place determined from Monte Carlo simulation results for coal layers

No	Free Gas, MMscf			No	Free Gas, MMscf			No	Free Gas, MMscf		
	Max.	Mean	Min.		Max.	Mean	Min.		Max.	Mean	Min.
1	717.3	131.3	9.0	22	500.2	124.1	15.7	43	57.7	24.3	6.6
2	761.6	203.1	29.0	23	1,151.9	283.7	45.2	44	50.7	20.6	5.3
3	378.4	89.0	10.2	24	460.2	149.2	30.0	45	76.8	24.9	5.2
4	257.7	54.2	2.4	25	1.3	0.4	0.1	46	379.8	111.4	21.5
5	440.8	90.4	7.1	26	3,101.5	737.2	104.0	47	2,276.6	534.1	63.1
6	26.6	7.9	1.6	27	15.1	4.7	1.0	48	31.3	10.2	2.8
7	38.6	10.4	0.9	28	51.5	13.0	1.8	49	26.2	10.2	2.9
8	37.1	11.0	1.4	29	14.8	4.7	1.0	50	1.6	0.6	0.1
9	57.4	13.5	1.3	30	43.8	12.7	1.8	51	1.8	0.6	0.1
10	15.1	3.3	0.2	31	1,330.3	340.1	51.6	52	85.4	32.4	8.3
11	12.2	4.0	0.9	32	358.2	110.6	18.8	53	201.1	62.7	12.5
12	14.6	4.2	0.7	33	33.9	9.9	1.9	54	222.9	72.1	15.8
13	1,504.6	477.4	106.7	34	136.9	44.8	8.6	55	7.6	2.0	0.2
14	447.6	177.4	47.8	35	216.9	64.2	12.3	56	27.7	7.6	1.6
15	240.1	74.6	15.0	36	43.5	17.3	4.9	57	42.4	16.4	4.1
16	159.4	62.1	15.9	37	58.7	19.8	4.6	58	111.6	31.4	5.6
17	400.1	117.4	25.0	38	44.3	18.2	4.8	59	236.3	77.2	12.9
18	81.6	32.1	8.3	39	161.0	53.4	10.6	60	472.7	150.3	28.6
19	89.3	33.7	8.6	40	144.7	56.8	16.1	61	621.6	162.1	20.7
20	300.0	77.5	13.4	41	94.6	28.6	5.7	62	14.4	5.5	1.3
21	111.7	40.6	9.5	42	59.2	23.8	5.4	63	138.1	47.4	9.8

Table 7.5. Estimated initial adsorbed gas in place determined from Monte Carlo simulation results for coal layers

No	Adsorbed Gas, MMscf			No	Adsorbed Gas, MMscf			No	Adsorbed Gas, MMscf		
	Max.	Mean	Min.		Max.	Mean	Min.		Max.	Mean	Min.
1	3,466.8	1,174.4	278.1	22	2,115.2	754.3	141.6	43	338.9	173.6	79.2
2	4,857.9	1,935.6	370.6	23	8,122.3	2,615.8	715.7	44	373.7	181.5	77.3
3	3,456.5	1,039.0	248.5	24	4,190.1	1,435.5	443.1	45	570.5	237.8	72.8
4	1,393.5	557.9	157.5	25	13.3	5.8	1.9	46	2,673.7	1,049.6	333.4
5	2,440.8	890.7	211.0	26	20,498.4	6,947.5	1,760.3	47	12,881.7	4,514.7	1,181.4
6	231.3	88.6	26.7	27	134.8	47.5	11.2	48	219.2	98.6	38.1
7	276.1	101.7	19.0	28	414.8	167.6	54.8	49	197.3	96.2	38.5
8	296.5	107.3	14.5	29	109.1	54.8	20.7	50	12.2	5.0	1.3
9	462.4	130.5	11.5	30	427.2	146.9	36.5	51	12.2	5.1	1.3
10	122.9	37.6	4.1	31	8,539.8	3,137.3	927.7	52	533.8	266.6	118.1
11	104.7	45.7	16.8	32	2,283.4	919.6	265.8	53	1,491.5	568.3	194.1
12	134.0	46.6	12.7	33	331.3	116.6	28.6	54	1,370.6	626.8	258.1
13	7,803.0	3,312.5	1,269.7	34	1,222.0	412.4	134.6	55	61.0	22.2	2.4
14	2,233.5	1,131.5	508.3	35	1,287.3	560.3	179.8	56	209.6	84.1	30.5
15	1,240.7	628.8	260.5	36	301.6	156.9	67.1	57	258.4	132.6	61.4
16	817.9	447.1	198.0	37	476.5	178.6	70.3	58	642.9	252.4	74.8
17	2,201.9	807.1	282.1	38	265.8	139.6	59.3	59	1,372.5	611.2	153.6
18	401.4	214.9	102.7	39	985.7	407.6	140.7	60	2,927.3	1,197.0	382.5
19	408.3	219.7	90.3	40	859.4	426.1	214.1	61	4,757.9	1,511.2	362.2
20	1,298.6	551.2	170.4	41	534.3	208.7	56.1	62	99.0	49.6	20.2
21	547.9	275.4	128.9	42	321.6	172.1	84.7	63	875.2	386.3	150.2

Table 7.6. Estimated initial gas in place determined from Monte Carlo simulation results for coal layers

No	IGIP, MMscf			No	IGIP, MMscf			No	IGIP, MMscf		
	Max.	Mean	Min.		Max.	Mean	Min.		Max.	Mean	Min.
1	3,560.6	1,305.7	316.6	22	2,545.6	878.3	157.3	43	369.4	197.9	95.5
2	5,260.7	2,138.8	465.3	23	8,626.0	2,899.5	799.7	44	385.1	202.0	94.7
3	3,668.1	1,128.0	290.2	24	4,409.2	1,584.7	502.5	45	625.2	262.8	90.0
4	1,574.7	612.1	164.8	25	13.9	6.3	2.1	46	2,833.9	1,161.0	380.2
5	2,634.6	981.1	238.8	26	23,048.7	7,684.7	1,865.1	47	15,061.1	5,048.9	1,373.6
6	251.9	96.5	30.2	27	144.0	52.3	15.0	48	230.3	108.8	46.7
7	307.8	112.1	21.5	28	429.7	180.6	61.3	49	211.0	106.4	44.9
8	321.4	118.3	17.0	29	116.5	59.5	23.2	50	12.7	5.5	1.5
9	507.9	144.1	13.4	30	468.9	159.6	40.9	51	13.5	5.6	1.5
10	132.0	41.0	4.4	31	8,930.2	3,477.3	1,000.0	52	576.2	299.0	136.4
11	112.6	49.7	19.5	32	2,412.2	1,030.2	290.7	53	1,638.5	631.0	229.8
12	141.9	50.7	13.6	33	352.8	126.5	30.8	54	1,463.2	698.9	306.7
13	9,088.9	3,789.9	1,492.7	34	1,347.0	457.2	166.3	55	65.1	24.2	2.6
14	2,602.8	1,308.9	587.7	35	1,369.4	624.5	206.4	56	237.3	91.7	32.4
15	1,408.7	703.4	283.1	36	329.9	174.2	75.3	57	279.2	149.1	66.5
16	971.2	509.2	248.6	37	527.6	198.4	80.8	58	691.1	283.8	85.5
17	2,395.7	924.5	344.4	38	301.1	157.8	71.1	59	1,524.3	688.4	182.1
18	442.7	247.1	119.8	39	1,116.6	461.0	158.1	60	3,200.9	1,347.3	440.9
19	456.5	253.4	117.1	40	953.5	482.9	243.7	61	5,261.8	1,673.2	388.6
20	1,440.1	628.6	200.2	41	606.2	237.3	70.5	62	108.7	55.1	22.3
21	580.1	316.0	151.1	42	353.8	195.9	95.5	63	955.0	433.7	166.4

P10, P50 and P90 estimations for gas in place of each coal layer were summed up to obtain possible, probable and proven values for Amasra Basin resource area-A (Tables 7.7, 7.8 and 7.9).

Table 7.7. Probabilistic estimation of initial free gas in place for Amasra resource area A

Free Gas, Billions SCF		
P10	P50	P90
8.80	4.70	2.43

Table 7.8. Probabilistic estimation of initial adsorbed gas in place for Amasra resource area A

Adsorbed Gas, Billions SCF		
P10	P50	P90
65.77	42.63	26.93

Table 7.9. Probabilistic estimation of initial gas in place for Amasra resource area A

Total Gas, Billions SCF		
P10	P50	P90
72.97	47.74	30.46

Similarly, minimum, average and maximum estimations of each layer were summed up and given in Tables 7.10, 7.11 and 7.12.

Table 7.10. Estimated initial free gas in place determined from Monte Carlo simulation results for Amasra resource area A

Free Gas, Billions SCF		
Max.	Mean	Min.
19.20	5.24	0.89

Table 7.11. Estimated initial adsorbed gas in place determined from Monte Carlo simulation results for Amasra resource area A

Adsorbed Gas, Billions SCF		
Max.	Mean	Min.
119.51	44.83	13.43

Table 7.12. Estimated initial gas in place determined from Monte Carlo simulation results for Amasra resource area A

Total Gas, Billions SCF		
Max.	Mean	Min.
132.01	50.06	15.29

7.2 Simulation of Coal Layer #26

Coal Layer #26 having more initial gas in place was selected to study the effects of several factors for the sequestration of carbon dioxide and production of methane. These factors were the coal properties (i.e. permeability, porosity, cleat spacing, coal compressibility, coal density, permeability anisotropy and Langmuir parameters) or injection of carbon dioxide, water saturation, and time.

7.2.1 Coal Bed Methane (CBM) Production

Coalbed Methane (CBM) production and effects of shrinkage and swelling were studied and the values of the parameters are given in Table 7.13.

Table 7.13. Parameter values considered for runs 1 and 2

Run		1	2
Case		Basecase	Effect of Shrinkage and Swelling
Shrinkage & Swelling Effects		Included	**Ignored**
CH₄ Production	*Start, Date*	Jan. 2007	Jan. 2007
	End, Date	Jan. 2107	Jan. 2107
CO₂ Injection	*Start, Date*	-	-
	End, Date	-	-
Permeability, md	*Face Cleat*	8	8
	Butt Cleat	8	8
Porosity, fraction	*Matrix*	0.04	0.04
	Cleats	0.02	0.02
Cleat Spacing, ft		6	6
Coal Compressibility, 1/psi		2×10^{-4}	2×10^{-4}
Coal Density, lb/ft³		96.14	96.14
Pressure Gradient, psi/ft		0.129	0.129
Langmuir Volume, scf/ton	CO_2	993.05	993.05
	CH_4	496.52	496.52
Langmuir Pressure, psi	CO_2	718.2	718.2
	CH_4	1436.5	1436.5
Water Saturation, fraction		0.01	0.01

Table 7.14. Simulation results for runs 1 and 2

Run			1	2
Cum. CH₄ Prod., Billions scf			2.63	2.64
Cum. CO₂ Inj., Millions tonne			-	-
CH₄ Recovered, % of IGIP			72.92	73.15
Gas in Place, Billions SCF	Adsorbed (Matrix)		2.73	2.73
	Free	Matrix	0.59	0.59
		Cleats	0.29	0.29
	Total		3.61	3.61

7.2.1.1 Base Case

The most probable properties were used to define the base case to simulate the methane production from Coal Layer #26. Methodology used for the preparation of input data for the base case and estimation of the ranges are given in Chapter 6. Base case data was prepared according to dry reservoir conditions that were explained in Chapter 6. In this case carbon dioxide was not injected into the coal layer. Shrinkage and swelling of the coal affected the coal permeability and porosity according to Palmer and Mansoori (1996) (See Equation 6.8).
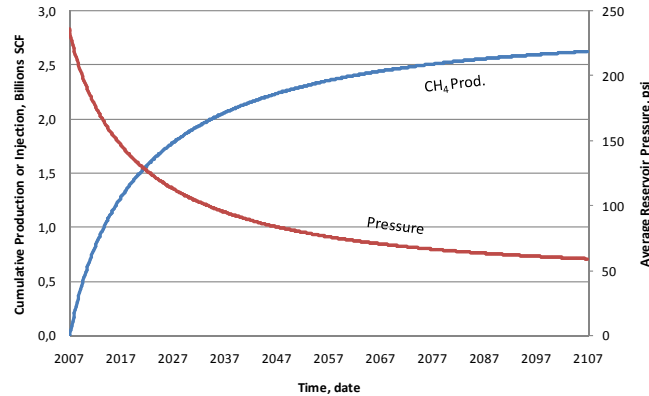
Figure 7.2. Run 1: base case

7.2.1.2 Effect of Shrinkage and Swelling (CBM)

In this case, the base case data are used to describe the Coal Layer #26. Although the feature for the shrinkage and swelling effects due to adsorption or desorption of the methane was not used in this case, effects of the change in overburden stress due to pore pressure reduction was included. Carbon dioxide was not injected into the coal. The porosity of the matrix and fracture system at pressure p is calculated using the following equation:

$$\emptyset(p) = \emptyset_i \left[1 + c_f \left(p - p_{ref} \right) \right] \tag{7.1}$$

Where $\emptyset_i$ is the initial porosity (0.02) and c_f is the coal compressibility (2×10^{-4} 1/psi) at reference pressure p_{ref} (237 psi).
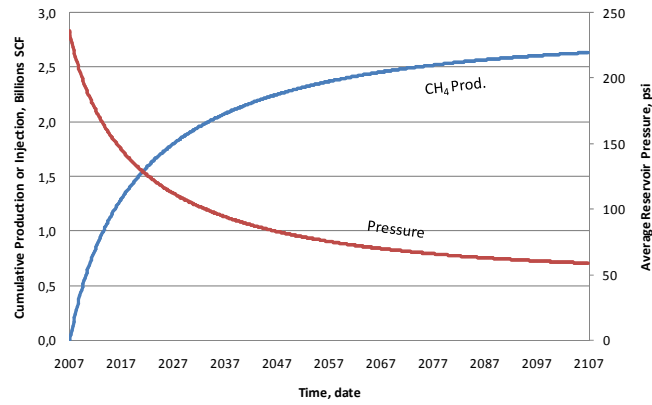
Figure 7.3. Run 2: effect of shrinkage and swelling
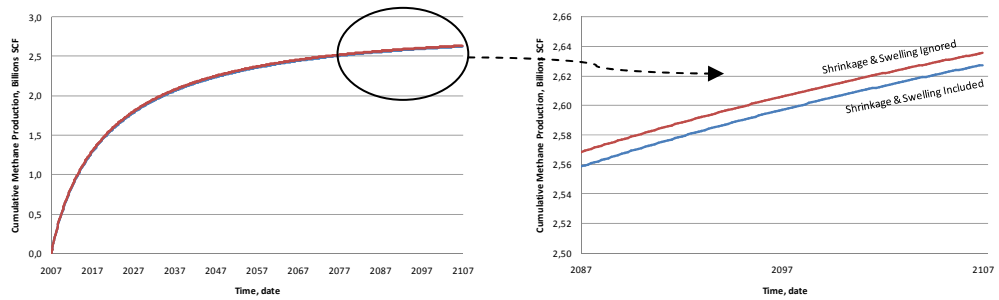
Fig. 7.4 (a)   Fig. 7.4 (b) Zoomed Part

Figure 7.4. Runs 1 and 2: effect of shrinkage and swelling on CH₄ production
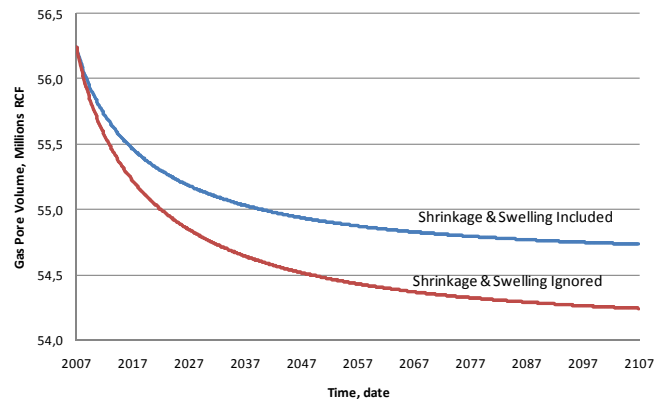
Figure 7.5. Runs 1 and 2: effect of shrinkage and swelling on gas pore volume

Figure 7.5 shows that in both cases whether shrinkage included or not, the porosity decreased. This decrease was more when shrinkage effects ignored as expected. According to this difference in between both cases it can be thought that there is a confusion in Figure 7.4. Because, it is expected that the cumulative production should be more when the shrinkage effects included. However as given by Equation 6.10 the cleat permeability is a function of cleat porosity when the shrinkage and swelling feature included. The decrease in pressure also caused the reduction in cumulative production.

7.2.2 Enhanced CBM Production with CO_2 Injection (ECBM)

The total amount of methane production from the coal layer reaches a plateau after a while because of the pressure decrease in the coal reservoir. In order to produce the adsorbed methane from the coal by the means of enhanced production methods, carbon dioxide can be injected into the reservoir. There are mainly two advantages of CO_2 injection: (1) the enhancement of coal bed methane production, (2) the sequestration of CO_2.

Carbon dioxide emitted from Zonguldak Çatalağzı Power Plant can be used in Amasra district resource area A for sequestering CO_2 and/or enhancing the methane production.

169

The values of the parameters for the enhanced coalbed methane production with and without ceasing the production at CO_2 breakthrough and starting CO_2 injection after 20 years of production are given in Table 7.15. Simulation results and gas in place values are given in Table 7.16.

Table 7.15. Parameter values considered for runs 3, 4 and 5

Run		3	4	5
Case		Enhanced Coal Bed Methane Production with Injection of CO_2	ECBM Production with Inj. of CO_2 (Prod. Wells Shut In at CO_2 Breakthrough)	ECBM Production with Injection of CO_2 after 20 years of CH_4 Production
Shrinkage & Swelling Effects		Included	Included	Included
CH_4 Production	*Start, Date*	Jan. 2007	Jan. 2007	Jan. 2007
	End, Date	Jan. 2107	**Nov 2102**	Jan. 2107
CO_2 Injection	*Start, Date*	**Jan. 2007**	Jan. 2007	**Jan. 2027**
	End, Date	**Jan. 2107**	Jan. 2107	Jan. 2107
Permeability, md	*Face Cleat*	8	8	8
	Butt Cleat	8	8	8
Porosity, fraction	*Matrix*	0.04	0.04	0.04
	Cleats	0.02	0.02	0.02
Cleat Spacing, ft		6	6	6
Coal Compressibility, 1/psi		2×10^{-4}	2×10^{-4}	2×10^{-4}
Coal Density, lb/ft³		96.14	96.14	96.14
Pressure Gradient, psi/ft		0.129	0.129	0.129
Langmuir Volume, scf/ton	*CO_2*	993.05	993.05	993.05
	CH_4	496.52	496.52	496.52
Langmuir Pressure, psi	*CO_2*	718.2	718.2	718.2
	CH_4	1436.5	1436.5	1436.5
Water Saturation, fraction		0.01	0.01	0.01

Table 7.16. Simulation results for runs 3, 4 and 5

Run			3	4	5
Cum. CH_4 Prod., Billions scf			3.27	3.23	3.14
Cum. CO_2 Inj., Millions tonne			0.52	0.52	0.42
CH_4 Recovered, % of IGIP			90.68	89.55	87.18
Gas in Place, Billions SCF	*Adsorbed (Matrix)*		2.73	2.73	2.73
	Free	*Matrix*	0.59	0.59	0.59
		Cleats	0.29	0.29	0.29
	Total		3.61	3.61	3.61

7.2.2.1 Production Wells Remain Open at CO_2 Breakthrough

Carbon dioxide was injected into the system as soon as production wells were opened. This caused an early breakthrough of carbon dioxide from the production wells and it was produced with methane. Although the cumulative methane production was increased, more than one third of the injected carbon dioxide was also produced.
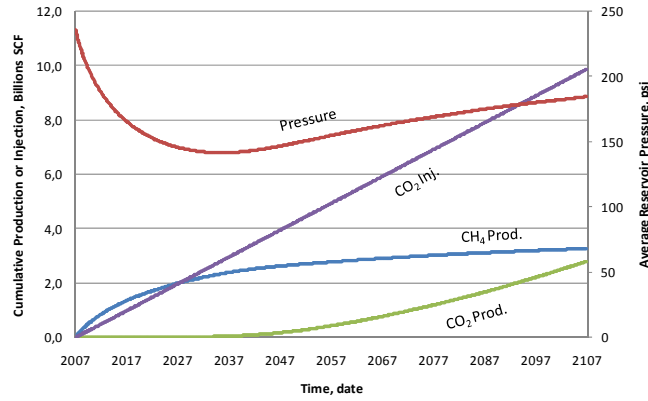
Figure 7.6. Run 3: ECBM production with CO_2 injection

7.2.2.2 Production Wells Shut in at CO_2 Breakthrough

Injected carbon dioxide was started to be produced from the production wells when it reached them. Reproducing CO_2 is an unwanted case when the aim is to sequester CO_2. Therefore it was assumed when the daily production rate of carbon dioxide exceeded 100 scf/day, the production wells were shut in. Table 7.16 shows the fluid in place for run #4.

A total injected CO_2 amount of 9.87×10^9 SCF was injected with a constant rate of 30,000 SCF/day in 100 years. Since the sequestered CO_2 is expressed in mass units of tonnes, the injected CO_2 amount was converted by using the gas density by Equation 7.2.

$$\rho = \frac{pMW}{zRT} \tag{7.2}$$

Where p is 1 atm, CO_2 molecular weight (MW) is 44.01 g/gmole, z is the compressibility factor and is assumed to be 1, R is 82.06 atm·cm^3/mole·K and T is 15.6 °C. The density of CO_2 was calculated as 0.00186 g/cm^3 (5.3×10^{-5} tonne/scf). Using 9.87×10^9 scf, the injected mass of CO_2 was found as 519,151 tonnes in 100 years or 5192 tonnes/year.

171

The average CO_2 emission of a coal consuming power plant is 1 tonne for each MWh energy produced (Nguyen and Allinson, 2002). Zonguldak Çatalağzı Power Plant's theoretical production capacity is 1,933,200 MWh/year (EÜAŞ, 2007). The amount of carbon dioxide emitted from this plant was then estimated as 1,933,200 tonnes/year. In order to sequester CO_2 and/or enhance the methane production, CO_2 emission coming from this source can be used in Amasra district resource area A. Only 0.3% of the CO_2 emission can be injected into the Coal Layer #26.
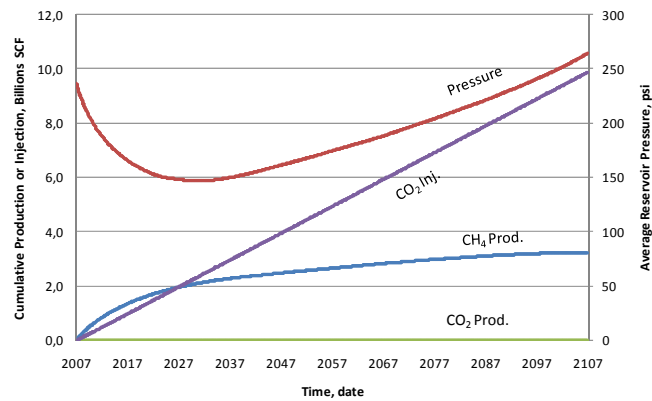
Figure 7.7. Run 4: ECBM production (production wells shut in at CO_2 breakthrough)
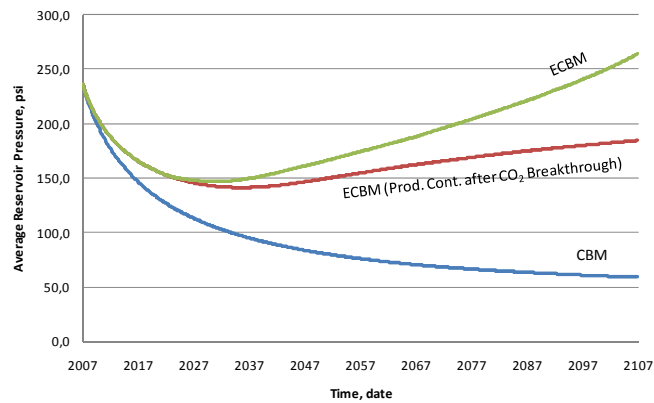
Figure 7.8. Runs 1, 3 and 4: effect of ceasing production on reservoir pressure
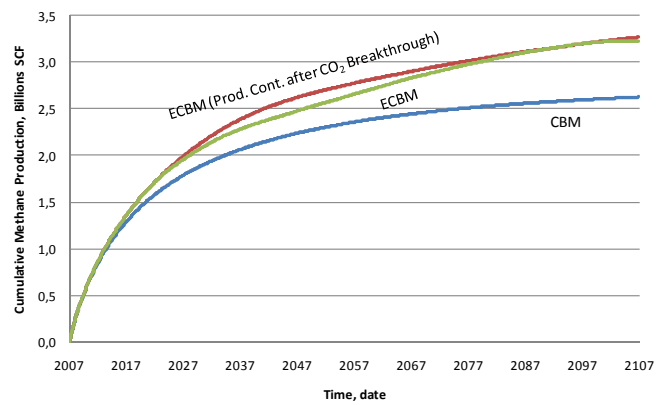
Figure 7.9. Runs 1, 3 and 4: effect of ceasing production on CH$_4$ production
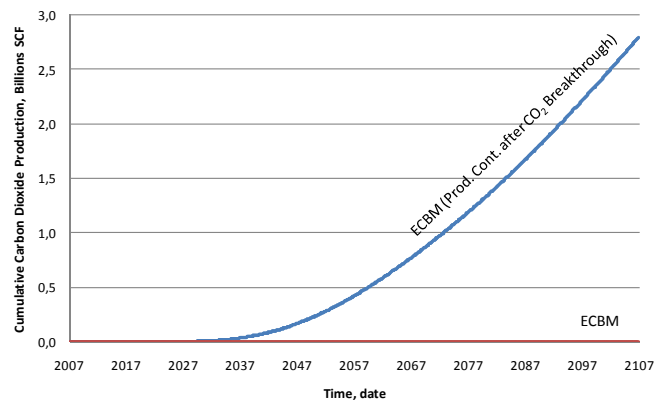
Figure 7.10. Runs 3 and 4: effect of ceasing production on CO$_2$ production
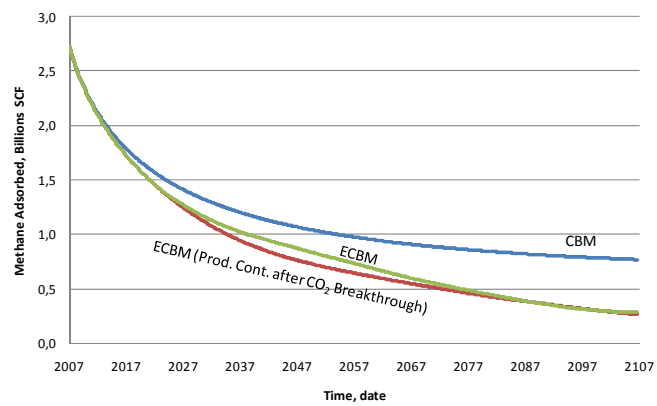
Figure 7.11. Runs 1, 3 and 4: effect of ceasing production on CH$_4$ desorption

173
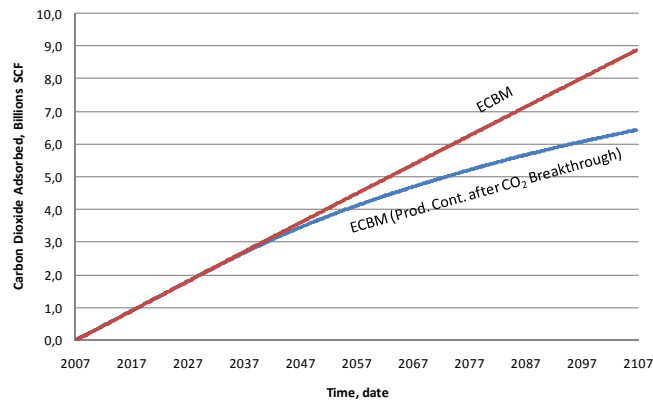
Figure 7.12. Runs 3 and 4: effect of ceasing production on CO₂ adsorption

Ending the production of CO_2 by shutting in the production wells at breakthrough of CO_2 affected also the methane production. However the differences between methane productions were not that big. Shutting in the production wells caused the gradual increase in reservoir pressure, because of the continuing CO_2 injection.

7.2.3 CO₂ Injection after 20 years of CH₄ Production

Production of methane reduced the reservoir pressure. When the pressure declined the methane production rate also dropped. Injection of CO_2 enhanced the methane production. In this run, CO_2 was injected into the coal after 20 years of CH_4 production and the production wells were shut-in after CO_2 breakthrough.
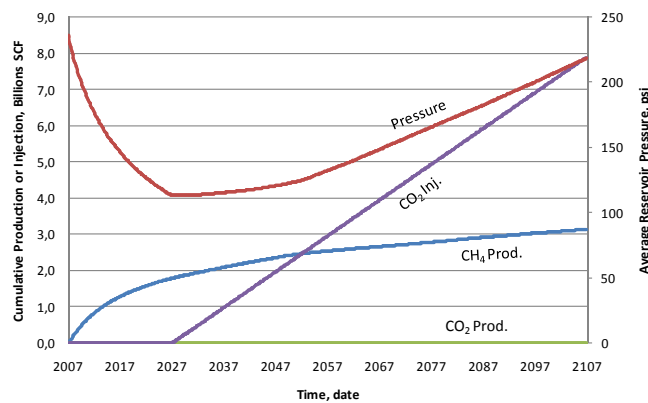
Figure 7.13. Run 5: ECBM production with CO₂ injection after 20 years of CH₄ production

174
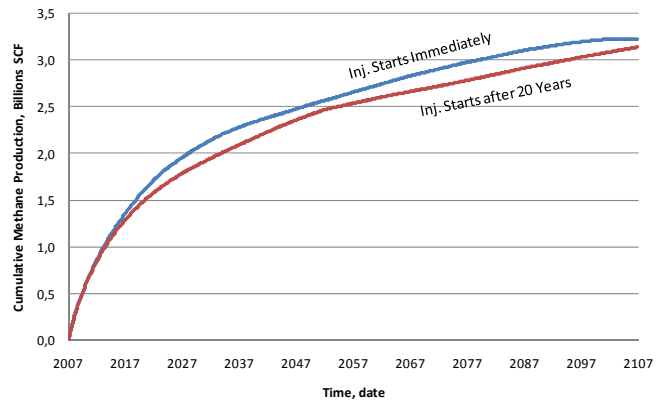
Figure 7.14. Runs 4 and 5: effect of CO$_2$ injection time on CH$_4$ production
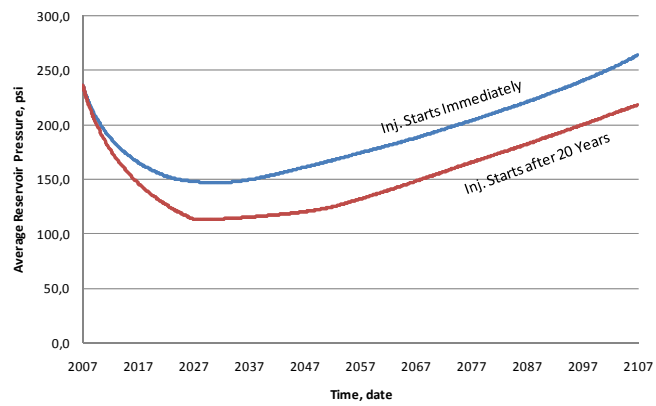
Figure 7.15. Runs 4 and 5: effect of CO$_2$ injection time on reservoir pressure
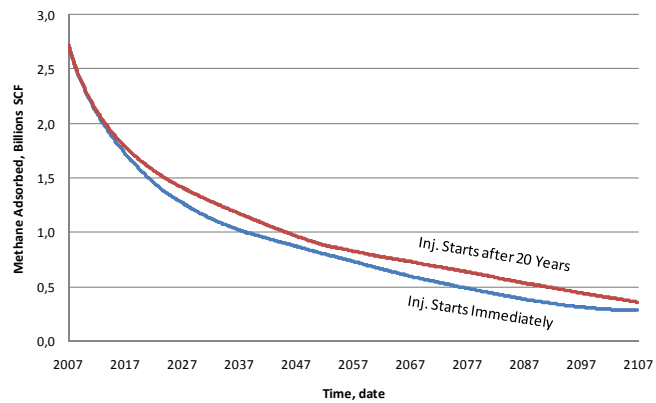
Figure 7.16. Runs 4 and 5: effect of CO$_2$ injection time on CH$_4$ desorption

When the coal reservoir is dry, injection of carbon dioxide as soon as production starts is more logical. The most important parameter in that case is the increase in the reservoir pressure.

7.2.4 Cleat Permeability

As expected, production rate of methane was dependent on cleat permeability. The values of the parameters for the enhanced coalbed methane production when the cleat permeability reduced and increased are given in Table 7.17. Simulation results and gas in place values are given in Table 7.18.

Table 7.17. Parameter values considered for runs 6, 7, 8 and 9

Run		6	7	8	9
Case		Effect of Cleat Permeability Reduction	Effect of Cleat Permeability Reduction (CO$_2$ Injection Started after 20 years of CH$_4$ Production)	Effect of Cleat Permeability Increase	Effect of Cleat Permeability Increase (CO$_2$ Injection Started after 20 years of CH$_4$ Production)
Shrinkage & Swelling Effects		Included	Included	Included	Included
CH$_4$ Production	Start, Date	Jan. 2007	Jan. 2007	Jan. 2007	Jan. 2007
	End, Date	Jan. 2107	Jan. 2107	Mar. 2049	Mar. 2069
CO$_2$ Injection	Start, Date	Jan. 2007	**Jan. 2027**	Jan. 2007	**Jan. 2027**
	End, Date	Jan. 2107	Jan. 2107	Jan. 2107	Jan. 2107
Permeability, md	Face Cleat	**0.1**	**0.1**	**100**	**100**
	Butt Cleat	**0.1**	**0.1**	**100**	**100**
Porosity, fraction	Matrix	0.04	0.04	0.04	0.04
	Cleats	0.02	0.02	0.02	0.02
Cleat Spacing, ft		6	6	6	6
Coal Compressibility, 1/psi		2×10^{-4}	2×10^{-4}	2×10^{-4}	2×10^{-4}
Coal Density, lb/ft^3		96.14	96.14	96.14	96.14
Pressure Gradient, psi/ft		0.129	0.129	0.129	0.129
Langmuir Volume, scf/ton	CO$_2$	993.05	993.05	993.05	993.05
	CH$_4$	496.52	496.52	496.52	496.52
Langmuir Pressure, psi	CO$_2$	718.2	718.2	718.2	718.2
	CH$_4$	1436.5	1436.5	1436.5	1436.5
Water Saturation, fraction		0.01	0.01	0.01	0.01

Table 7.18. Simulation results for runs 6, 7, 8 and 9

Run			6	7	8	9
Cum. CH$_4$ Prod., Billions scf			0.34	0.32	3.39	3.39
Cum. CO$_2$ Inj., Millions tonne			0.22	0.18	0.52	0.42
CH$_4$ Recovered, % of IGIP			9.35	8.77	94.09	94.10
Gas in Place, Billions SCF	Adsorbed (Matrix)		2.73	2.73	2.73	2.73
	Free	Matrix	0.59	0.59	0.59	0.59
		Cleats	0.29	0.29	0.29	0.29
	Total		3.61	3.61	3.61	3.61

7.2.4.1 Cleat Permeability Reduced

When the cleat permeability reduced to 0.1 md from 8 md, severe reduction in methane recovery was observed. Only 10% of the initial gas in place was produced from the reservoir after 100 years of operation.

Figure 7.17. Run 6: effect of cleat permeability reduction
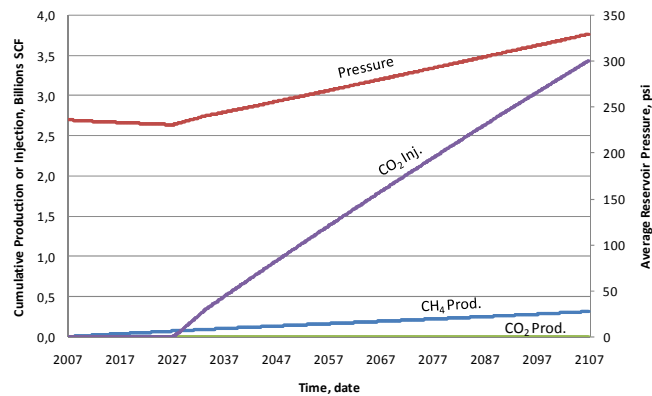
Figure 7.18. Run 7: effect of cleat permeability reduction (CO_2 injection started after 20 years of CH_4 production)

Figure 7.19. Runs 6 and 7: effect of CO$_2$ injection time on CH$_4$ production when cleat permeability reduced
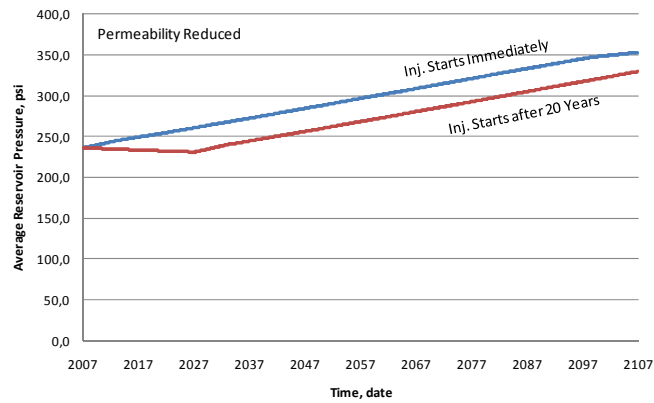
Figure 7.20. Runs 6 and 7: effect of CO$_2$ injection time on reservoir pressure when cleat permeability reduced
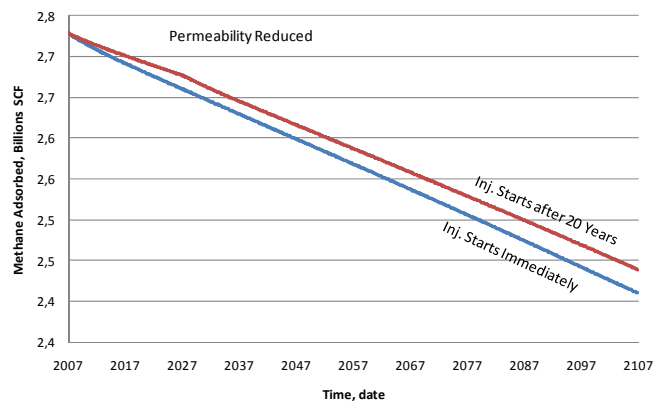
Figure 7.21. Runs 6 and 7: effect of CO$_2$ injection time on CH$_4$ desorption when cleat permeability reduced

178

7.2.4.2 Cleat Permeability Increased

If the permeability of cleats was increased to 100 md, gas in place was recovered faster and more. Production wells, however, needed to be all closed in 40 years because of the carbon dioxide breakthrough.

Figure 7.22. Run 8: effect of cleat permeability increase
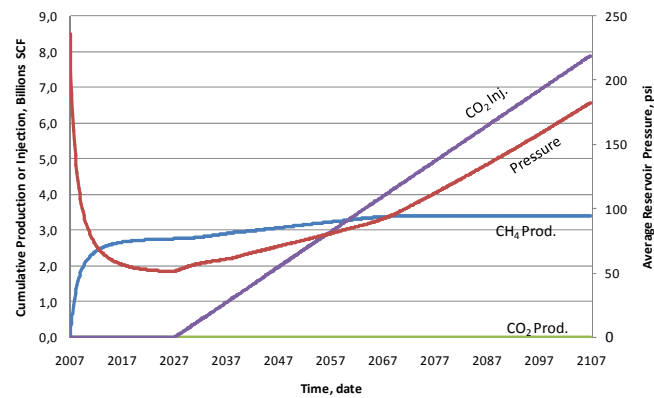
Figure 7.23. Run 7: effect of cleat permeability increase (CO_2 injection started after 20 years of CH_4 production)

179
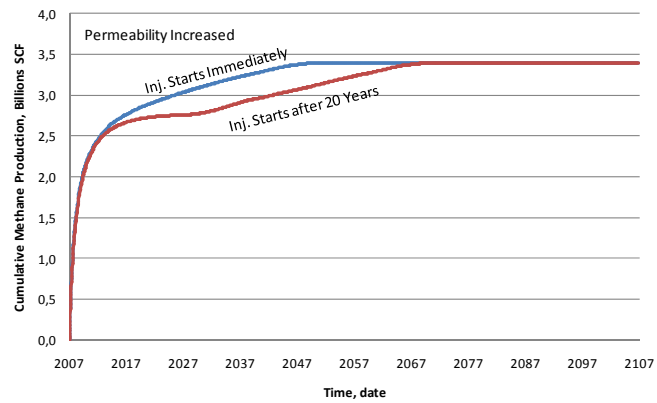
Figure 7.24. Runs 8 and 9: effect of CO₂ injection time on CH₄ production when cleat permeability increased
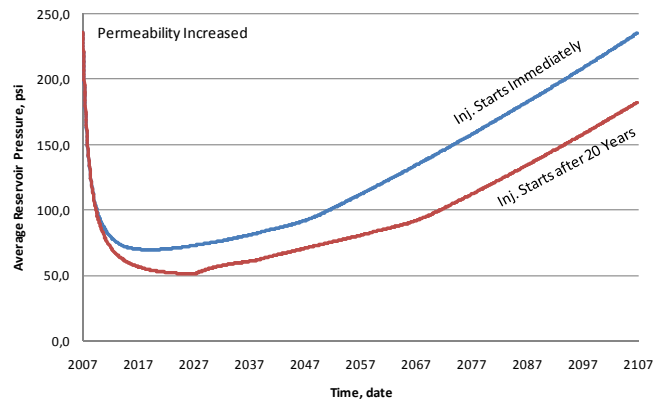
Figure 7.25. Runs 8 and 9: effect of CO₂ injection time on reservoir pressure when cleat permeability increased
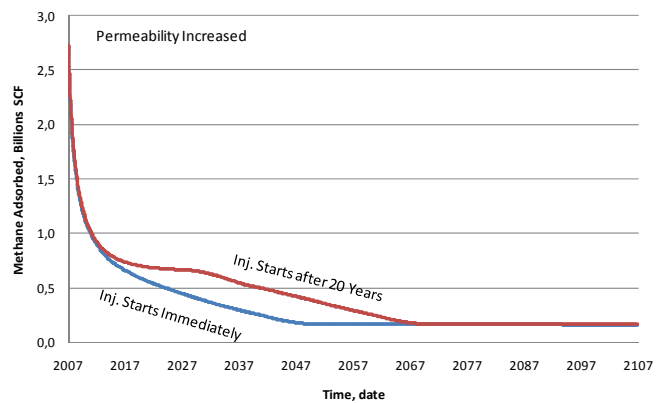
Figure 7.26. Runs 8 and 9: effect of CO₂ injection time on CH₄ desorption when cleat permeability increased

180

Although starting CO_2 injection after 20 years provided the same ultimate CH_4 recovery with the immediate CO_2 injection, as can be seen from Figure 7.24 approximately 20 more years required to reach at this value.

7.2.4.3 Effects of Cleat Permeability

Cleat permeability is one of the most important parameters required for the accurate simulation of CBM or ECBM recovery processes. Figure 7.27 shows that the estimation of the cleat permeability must be done as accurate as possible. The increase in cleat permeability accelerated the CH_4 production and the cumulative production was also obtained at higher values.

Figure 7.28 shows that the decrease in cleat permeability resulted in increase in pressure. Because of the less displacement efficiency of injected CO_2 for the low permeability cases, the pressure was buildup within the system. As a result more CH_4 was remained at adsorbed state (Figure 7.29).
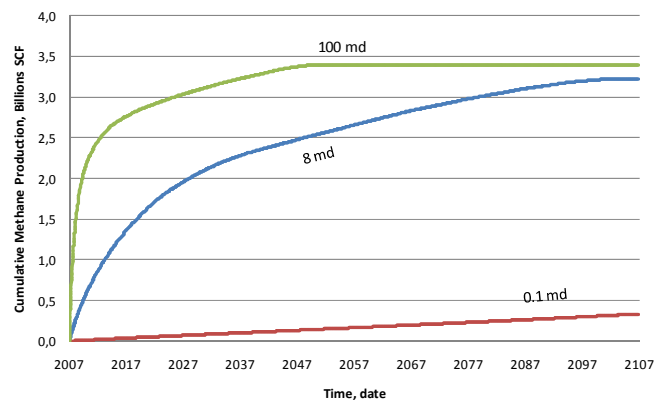
Figure 7.27. Effect of cleat permeability on CH_4 production (CO_2 inj. started at 2007)
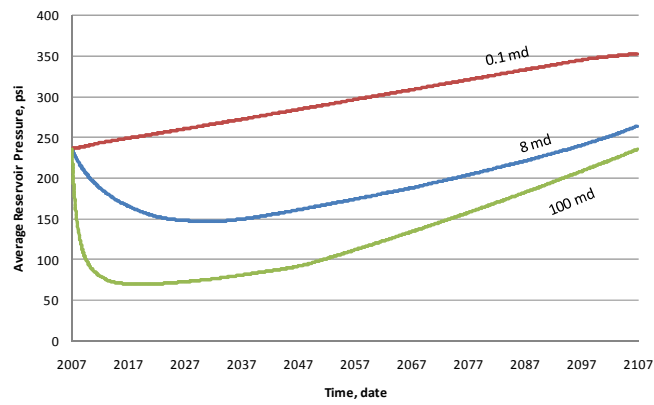
Figure 7.28. Effect of cleat permeability on reservoir pressure (CO₂ inj. started at 2007)
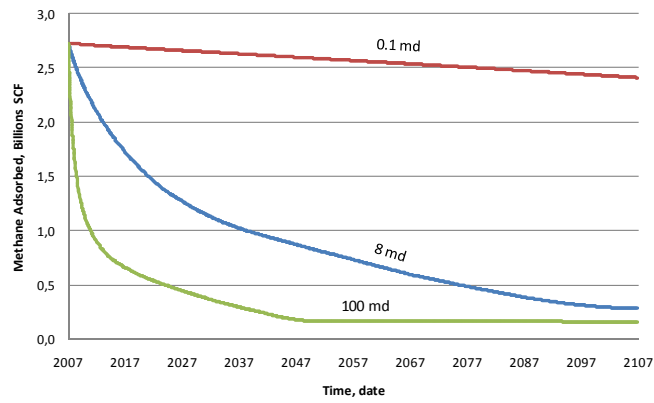
Figure 7.29. Effect of cleat permeability on CH₄ desorption (CO₂ inj. started at 2007)

7.2.5 Cleat Porosity

The values of the parameters for the enhanced coalbed methane production when the cleat porosity reduced and increased are given in Table 7.19. Simulation results and gas in place values are given in Table 7.20.

Table 7.19. Parameter values considered for runs 10, 11, 12 and 13

Run		10	11	12	13
Case		Effect of Cleat Porosity Reduction	Effect of Cleat Porosity Reduction (CO_2 Injection Started after 20 years of CH_4 Production)	Effect of Cleat Porosity Increase	Effect of Cleat Porosity Increase (CO_2 Injection Started after 20 years of CH_4 Production)
Shrinkage & Swelling Effects		Included	Included	Included	Included
CH_4 Production	Start, Date	Jan. 2007	Jan. 2007	Jan. 2007	Jan. 2007
	End, Date	Sep. 2085	Jan. 2107	Jan. 2107	Jan. 2107
CO_2 Injection	Start, Date	Jan. 2007	**Jan. 2027**	Jan. 2007	**Jan. 2027**
	End, Date	Jan. 2107	Jan. 2107	Jan. 2107	Jan. 2107
Permeability, md	Face Cleat	8	8	8	8
	Butt Cleat	8	8	8	8
Porosity, fraction	Matrix	0.04	0.04	0.04	0.04
	Cleats	**0.01**	**0.01**	**0.10**	**0.10**
Cleat Spacing, ft		6	6	6	6
Coal Compressibility, 1/psi		2×10^{-4}	2×10^{-4}	2×10^{-4}	2×10^{-4}
Coal Density, lb/ft³		96.14	96.14	96.14	96.14
Pressure Gradient, psi/ft		0.129	0.129	0.129	0.129
Langmuir Volume, scf/ton	CO_2	993.05	993.05	993.05	993.05
	CH_4	496.52	496.52	496.52	496.52
Langmuir Pressure, psi	CO_2	718.2	718.2	718.2	718.2
	CH_4	1436.5	1436.5	1436.5	1436.5
Water Saturation, fraction		0.01	0.01	0.01	0.01

Table 7.20. Simulation results for runs 10, 11, 12 and 13

Run			10	11	12	13
Cum. CH_4 Prod., Billions scf			3.14	3.07	3.58	3.46
Cum. CO_2 Inj., Millions tonne			0.52	0.42	0.52	0.42
CH_4 Recovered, % of IGIP			89.99	88.02	88.23	85.36
Gas in Place, Billions SCF	Adsorbed (Matrix)		2.76	2.76	2.62	2.62
	Free	Matrix	0.59	0.59	0.56	0.56
		Cleats	0.15	0.15	0.88	0.88
	Total		3.50	3.50	4.06	4.06

7.2.5.1 Cleat Porosity Reduced

Porosity of cleats was dropped to 0.01. Low cleat porosity caused a decrease in the amount of the free gas in place found in the cleat system. The cumulative amount of CH_4 production also decreased; however, methane recovery remained almost same.
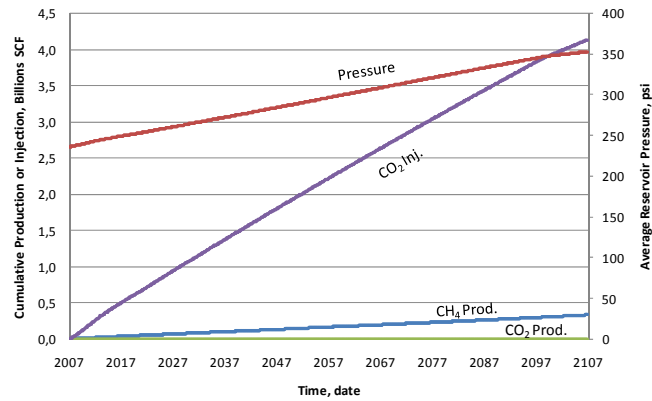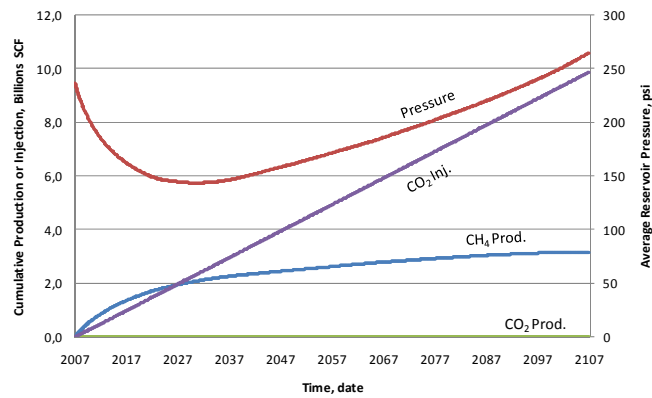
Figure 7.30. Run 10: effect of cleat porosity reduction
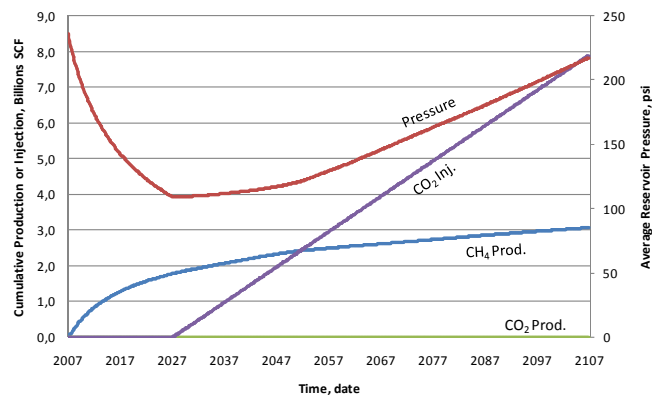
Figure 7.31. Run 11: effect of cleat porosity reduction (CO_2 injection started after 20 years of CH_4 production)
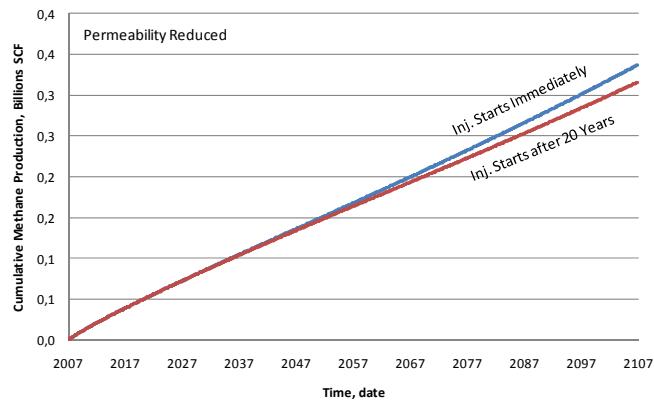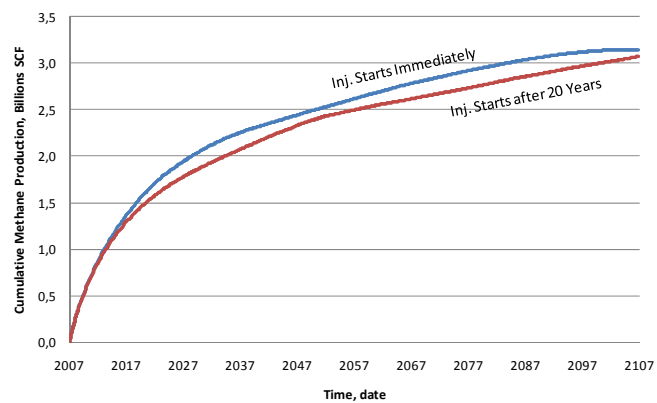

Figure 7.32. Runs 10 and 11: effect of CO_2 injection time on CH_4 production when cleat porosity reduced

184
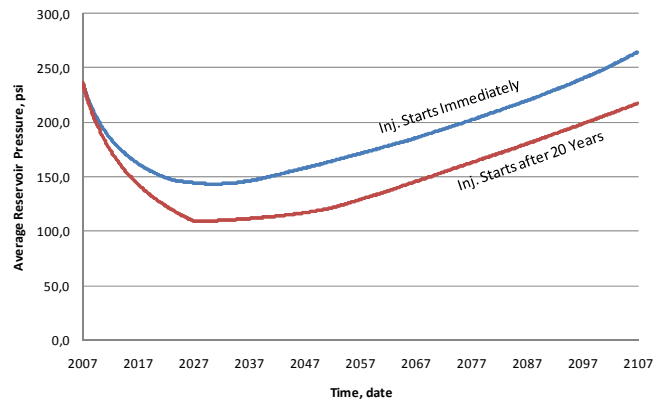
Figure 7.33. Runs 10 and 11: effect of CO$_2$ injection time on reservoir pressure when cleat porosity reduced
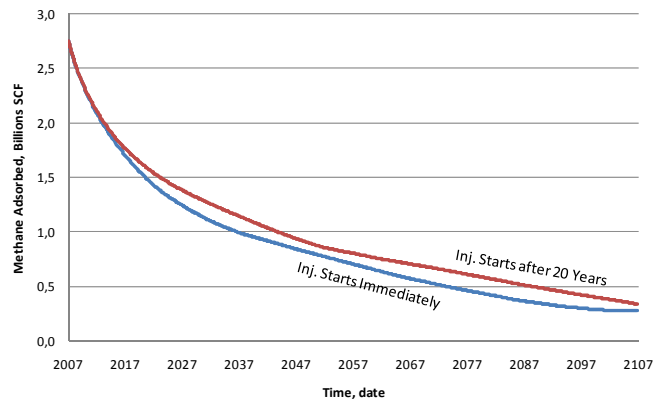
Figure 7.34. Runs 10 and 11: effect of CO$_2$ injection time on CH$_4$ desorption when cleat porosity reduced

7.2.5.2 Cleat Porosity Increased

If the cleat porosity was raised to 6%, free gas existed in cleats increased too. However, the gas in place in the matrix decreased. Increase in cleat porosity caused a reduction in matrix volume. Therefore, a reduction in the adsorbed gas was observed.
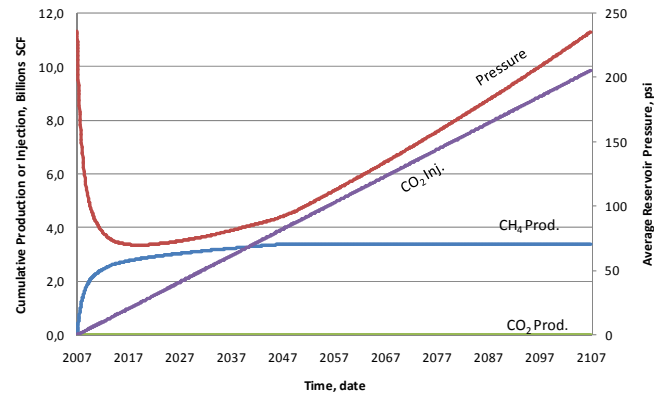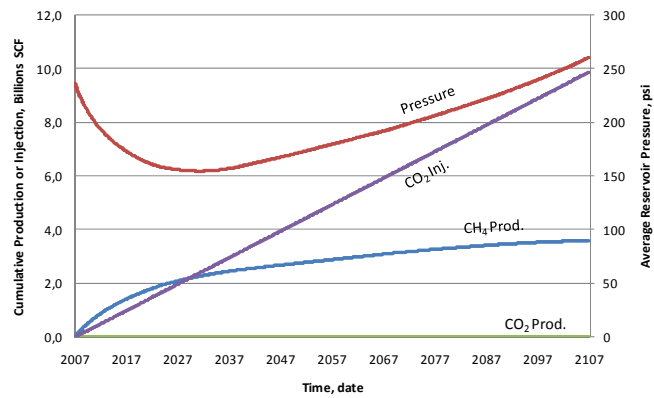
Figure 7.35. Run 12: effect of cleat porosity increase
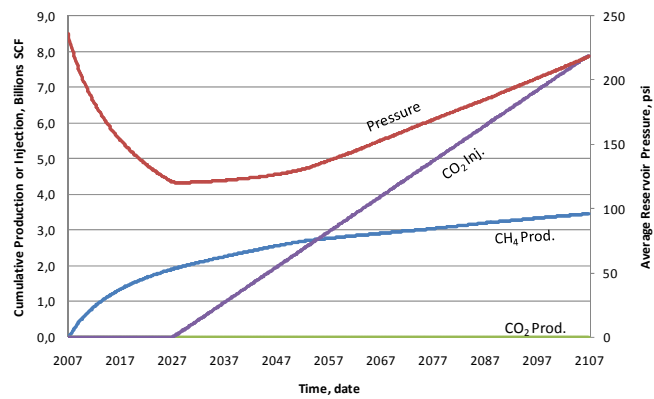
Figure 7.36. Run 13: effect of cleat porosity increase (CO_2 injection started after 20 years of CH_4 production)
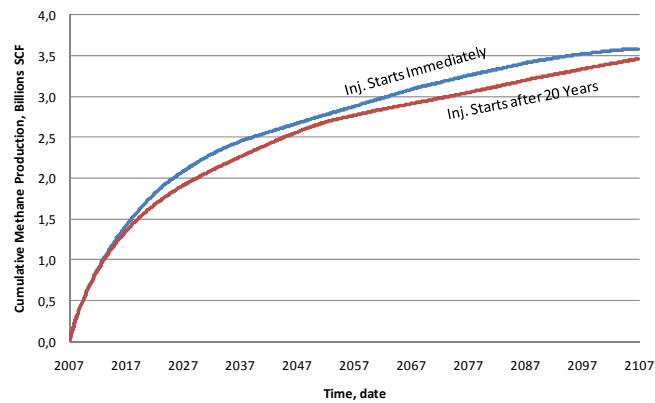
Figure 7.37. Runs 12 and 13: effect of CO_2 injection time on CH_4 production when cleat porosity increased
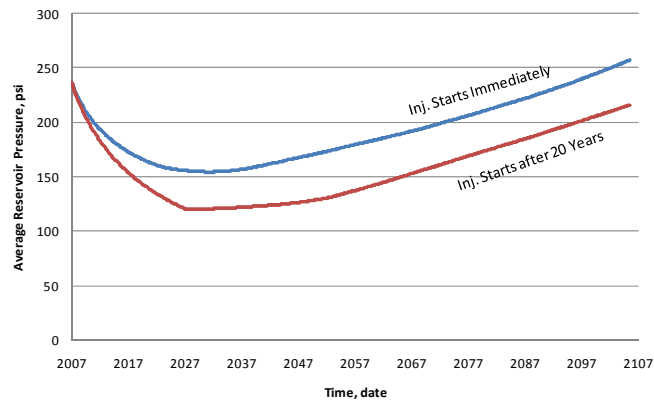
Figure 7.38. Runs 12 and 13: effect of CO$_2$ injection time on CH$_4$ production when cleat porosity increased
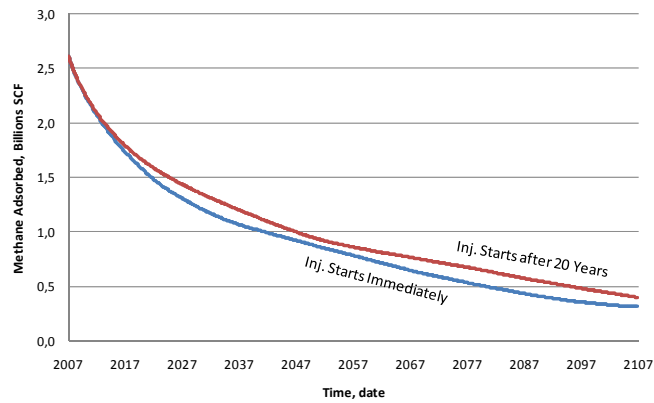
Figure 7.39. Run 12 and 13: effect of CO$_2$ injection time on CH$_4$ desorption when cleat porosity increased

7.2.5.3 Effect of Cleat Porosity

Although the cumulative methane production was increased when the cleat porosity was high because of the increase in the total gas in place (Figure 7.40). Methane recovery percents were remained almost constant. Cleat porosity did not affect the production, but the storage capacity.
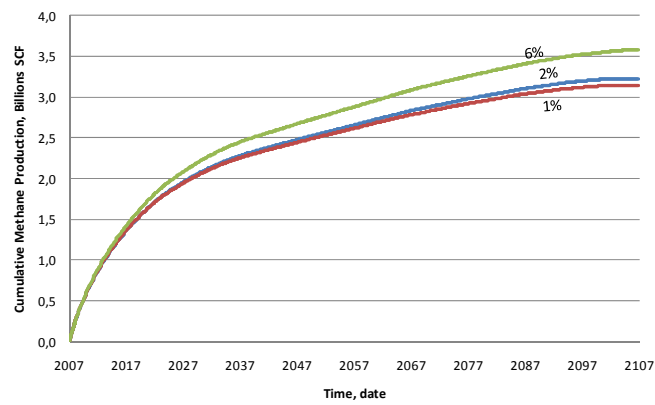
Figure 7.40. Effect of cleat porosity on CH$_4$ production (CO$_2$ inj. started at 2007)
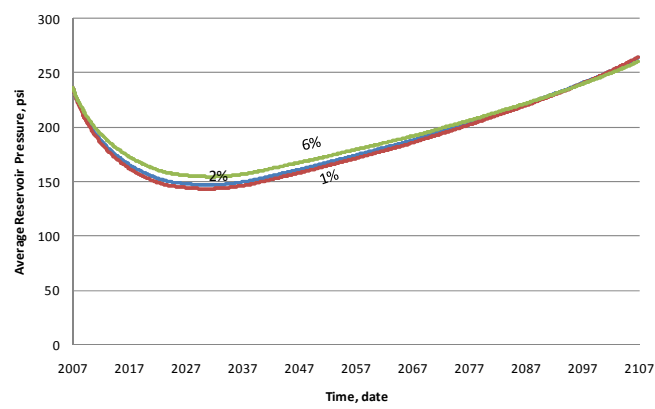
Figure 7.41. Effect of cleat porosity on reservoir pressure (CO$_2$ injection started at 2007)
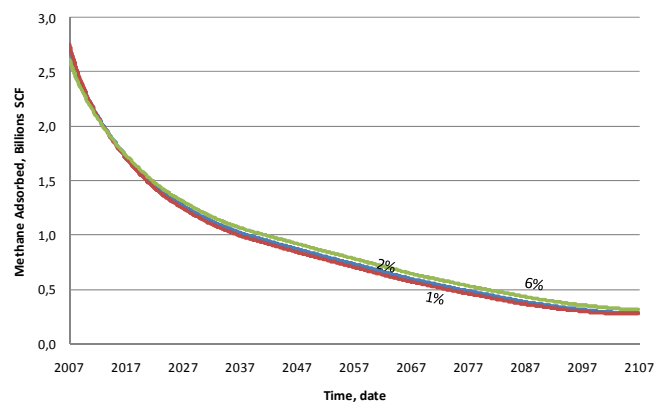
Figure 7.42. Effect of cleat porosity on CH$_4$ desorption (CO$_2$ injection started at 2007)

188

7.2.6 Cleat Spacing

The values of the parameters for the enhanced coalbed methane production when the cleat spacing reduced and increased are given in Table 7.21. Simulation results and gas in place values are given in Table 7.22.

Table 7.21. Parameter values considered for runs 14, 15, 16 and 17

Run		14	15	16	17
Case		Effect of Cleat Spacing Reduction	Effect of Cleat Spacing Reduction (CO_2 Injection Started after 20 years of CH_4 Production)	Effect of Cleat Spacing Increase	Effect of Cleat Spacing Increase (CO_2 Injection Started after 20 years of CH_4 Production)
Shrinkage & Swelling Effects		Included	Included	Included	Included
CH_4 Production	Start, Date	Jan. 2007	Jan. 2007	Jan. 2007	Jan. 2007
	End, Date	Jan. 2103	Jan. 2107	Nov. 2101	Jan. 2107
CO_2 Injection	Start, Date	Jan. 2007	**Jan. 2027**	Jan. 2007	**Jan. 2027**
	End, Date	Jan. 2107	Jan. 2107	Jan. 2107	Jan. 2107
Permeability, md	Face Cleat	8	8	8	8
	Butt Cleat	8	8	8	8
Porosity, fraction	Matrix	0.04	0.04	0.04	0.04
	Cleats	0.02	0.02	0.02	0.02
Cleat Spacing, ft		**1.018234**	**1.018234**	**17.63633**	**17.63633**
Coal Compressibility, 1/psi		2×10^{-4}	2×10^{-4}	2×10^{-4}	2×10^{-4}
Coal Density, lb/ft³		96.14	96.14	96.14	96.14
Pressure Gradient, psi/ft		0.129	0.129	0.129	0.129
Langmuir Volume, scf/ton	CO_2	993.05	993.05	993.05	993.05
	CH_4	496.52	496.52	496.52	496.52
Langmuir Pressure, psi	CO_2	718.2	718.2	718.2	718.2
	CH_4	1436.5	1436.5	1436.5	1436.5
Water Saturation, fraction		0.01	0.01	0.01	0.01

Table 7.22. Simulation results for runs 14, 15, 16 and 17

Run			14	15	16	17
Cum. CH_4 Prod., Billions scf			3.23	3.14	3.20	3.13
Cum. CO_2 Inj., Millions tonne			0.52	0.42	0.52	0.42
CH_4 Recovered, % of IGIP			89.65	87.22	88.87	86.88
Gas in Place, Billions SCF	Adsorbed (Matrix)		2.73	2.73	2.73	2.73
	Free	Matrix	0.59	0.59	0.59	0.59
		Cleats	0.29	0.29	0.29	0.29
	Total		3.61	3.61	3.61	3.61

7.2.6.1 Cleat Spacing Reduced

Cleat spacing is the distance between the center lines of the fractures. The higher the cleat spacing the higher the matrix volume. Cleat spacing was decreased to 1.0 ft.
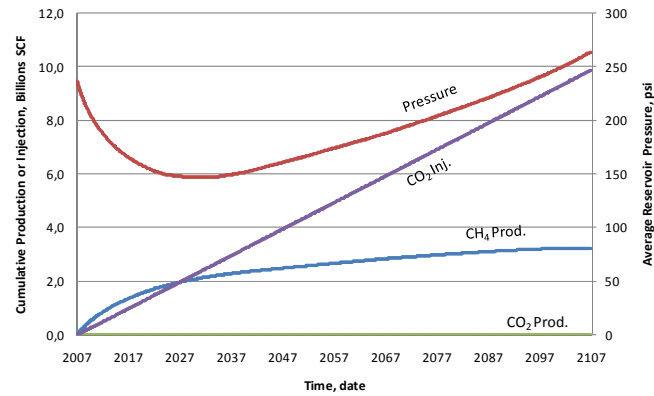
Figure 7.43. Run 14: effect of cleat spacing reduction
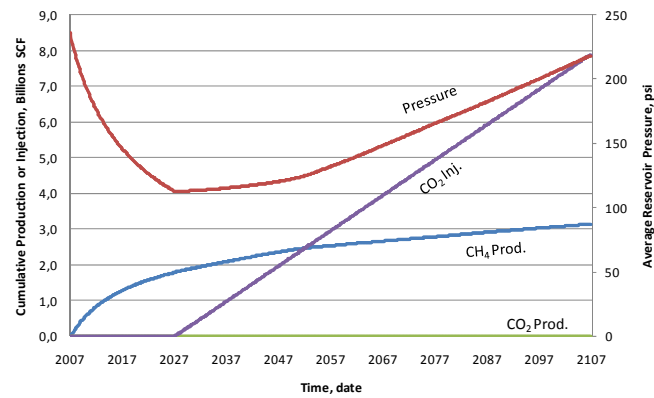
Figure 7.44. Run 15: effect of cleat spacing reduction (CO_2 injection started after 20 years of CH_4 production)
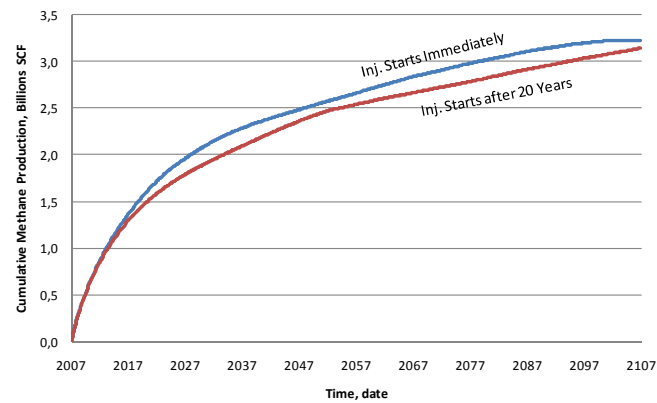
**Figure 7.45. Runs 14 and 15: effect of CO_2 injection time on CH_4 production when cleat spacing reduced**

190
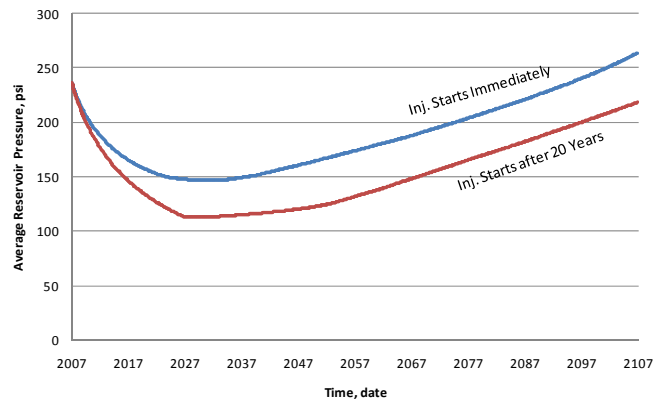
Figure 7.46. Runs 14 and 15: effect of CO$_2$ injection time on CH$_4$ production when cleat spacing reduced
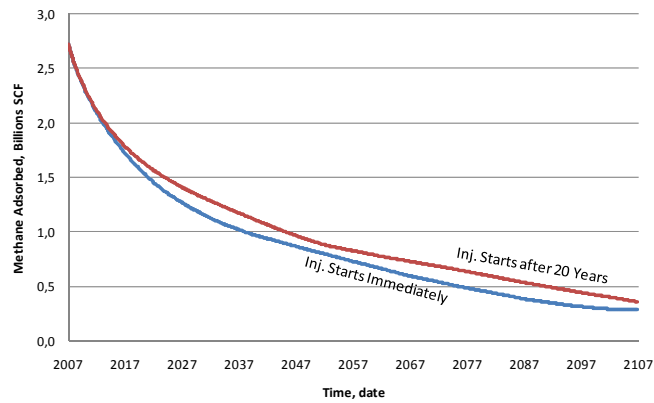
Figure 7.47. Runs 14 and 15: effect of CO$_2$ injection time on CH$_4$ desorption when cleat spacing reduced

7.2.6.2 Cleat Spacing Increased

Cleat spacing was raised to 17.6 ft.
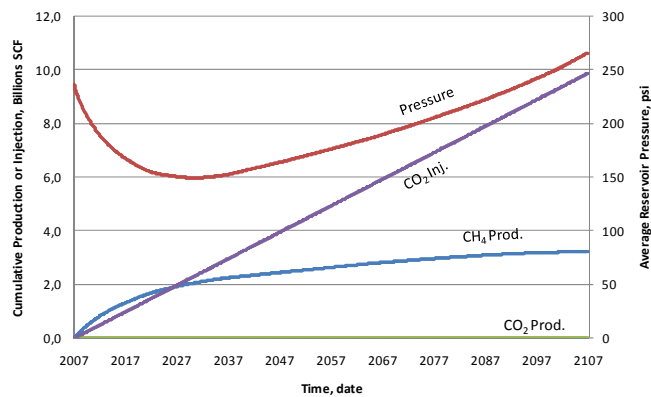
Figure 7.48. Run 16: effect of cleat spacing increase
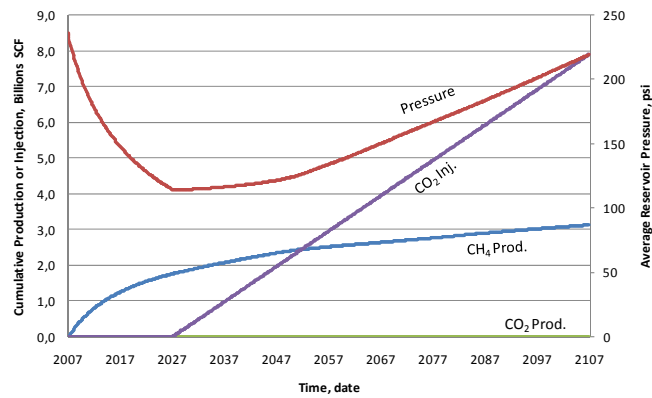
Figure 7.49. Run 17: effect of cleat spacing increase (CO$_2$ injection started after 20 years of CH$_4$ production)
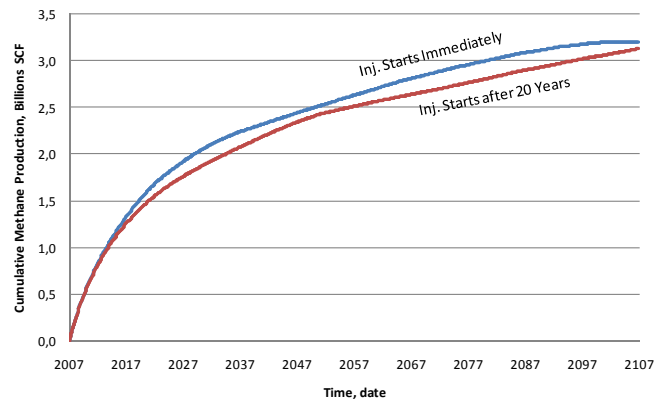
Figure 7.50. Runs 16 and 17: effect of CO$_2$ injection time on CH$_4$ production when cleat spacing increased
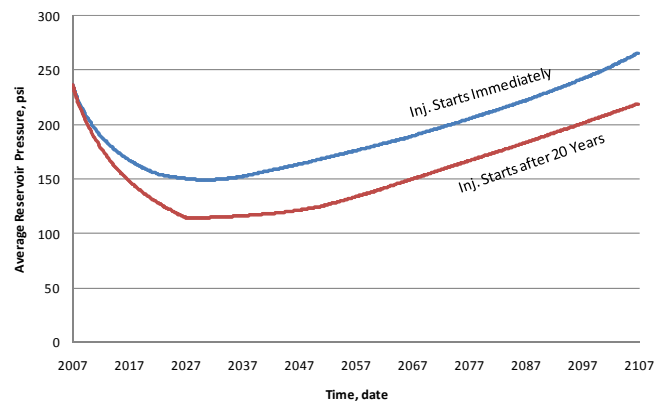
Figure 7.51. Runs 16 and 17: effect of CO$_2$ injection time on CH$_4$ production when cleat spacing increased

192
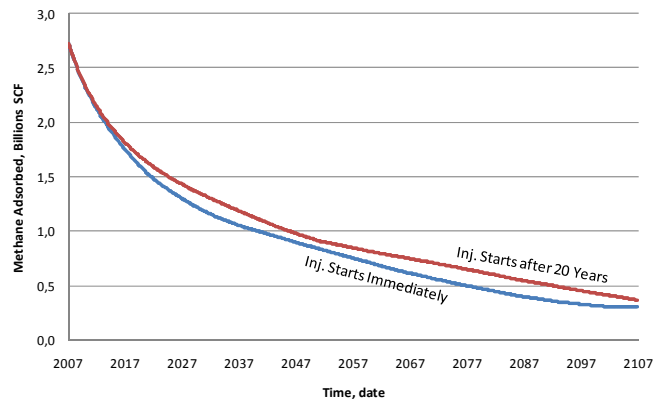
Figure 7.52. Runs 16 and 17: effect of CO_2 injection time on CH_4 desorption when cleat spacing increased

7.2.6.3 Effect of Cleat Spacing

Cleat spacing affected the matrix to fracture flow by the shape factor given in the transmissibility equations used in the simulation. Transmissibility and cleat spacing are inversely proportional. However, the following figures show almost identical production profiles. A slight increase in the cumulative methane production when the cleat spacing was low can be seen in Figure 7.53. Decrease in the cleat spacing causes an increase in the surface area where the matrix to fracture flow occurs, since cleat spacing affects the size of the matrix blocks.
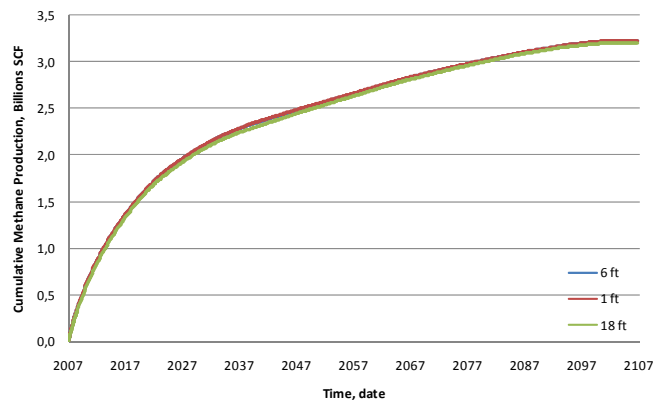
Figure 7.53. Effect of cleat spacing on CH_4 production (CO_2 injection started at 2007)
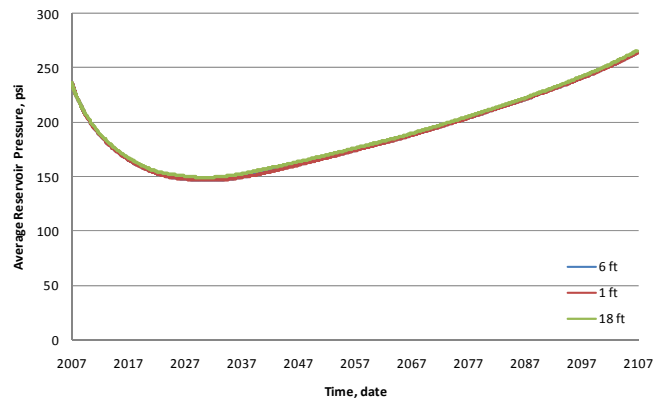
Figure 7.54. Effect of cleat spacing on reservoir pressure (CO_2 injection started at 2007)
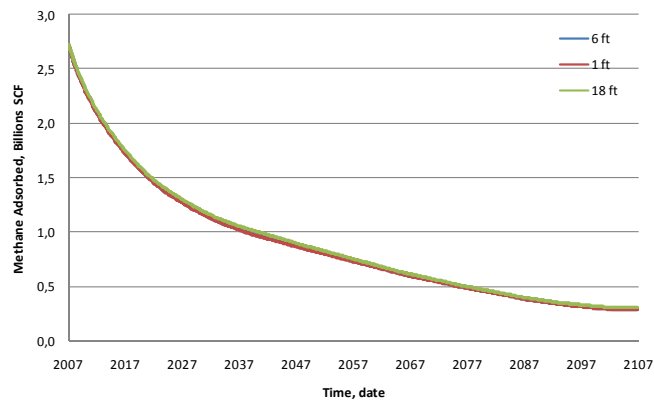
Figure 7.55. Effect of cleat spacing on CH_4 desorption (CO_2 injection started at 2007)

7.2.7 Coal Density

Coal density is important property for the gas in place estimation, since the adsorption parameters are related with the mass of the coal.

The values of the parameters for the enhanced coalbed methane production when the coal density reduced and increased are given in Table 7.23. Simulation results and gas in place values are given in Table 7.24.

Table 7.23. Parameter values considered for runs 18, 19, 20 and 21

Run		18	19	20	21
Case		Effect of Coal Density Reduction	Effect of Coal Density Reduction (CO_2 Injection Started after 20 years of CH_4 Production)	Effect of Coal Density Increase	Effect of Coal Density Increase (CO_2 Injection Started after 20 years of CH_4 Production)
Shrinkage & Swelling Effects		Included	Included	Included	Included
CH_4 Production	Start, Date	Jan. 2007	Jan. 2007	Jan. 2007	Jan. 2007
	End, Date	Sep. 2088	Jan. 2107	Jan. 2107	Jan. 2107
CO_2 Injection	Start, Date	Jan. 2007	**Jan. 2027**	Jan. 2007	**Jan. 2027**
	End, Date	Jan. 2107	Jan. 2107	Jan. 2107	Jan. 2107
Permeability, md	Face Cleat	8	8	8	8
	Butt Cleat	8	8	8	8
Porosity, fraction	Matrix	0.04	0.04	0.04	0.04
	Cleats	0.02	0.02	0.02	0.02
Cleat Spacing, ft		6	6	6	6
Coal Compressibility, 1/psi		2×10^{-4}	2×10^{-4}	2×10^{-4}	2×10^{-4}
Coal Density, lb/ft³		**80.46882**	**80.46882**	**114.242**	**114.242**
Pressure Gradient, psi/ft		0.129	0.129	0.129	0.129
Langmuir Volume, scf/ton	CO_2	993.05	993.05	993.05	993.05
	CH_4	496.52	496.52	496.52	496.52
Langmuir Pressure, psi	CO_2	718.2	718.2	718.2	718.2
	CH_4	1436.5	1436.5	1436.5	1436.5
Water Saturation, fraction		0.01	0.01	0.01	0.01

Table 7.24. Simulation results for runs 18, 19, 20 and 21

Run			18	19	20	21
Cum. CH_4 Prod., Billions scf			2.82	2.83	3.62	3.44
Cum. CO_2 Inj., Millions tonne			0.52	0.42	0.52	0.42
CH_4 Recovered, % of IGIP			89.21	89.75	87.90	83.65
Gas in Place, Billions SCF	Adsorbed (Matrix)		2.29	2.29	3.25	3.25
	Free	Matrix	0.58	0.58	0.58	0.58
		Cleats	0.29	0.29	0.29	0.29
	Total		3.16	3.16	4.12	4.12

7.2.7.1 Coal Density Reduced

Coal density was decreased to 80.5 lb/ft³ (1.29 g/cm³) from 96.14 lb/ft³ (1.54 g/cm³).
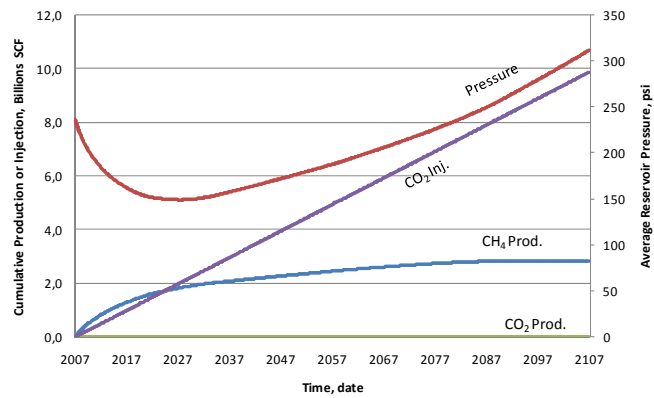
Figure 7.56. Run 18: effect of coal density reduction
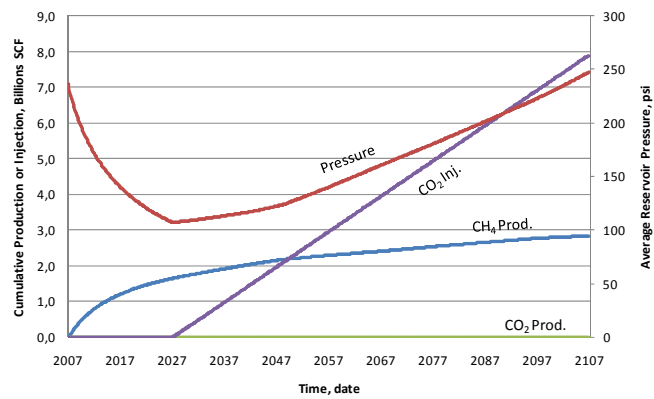
Figure 7.57. Run 19: effect of coal density reduction (CO_2 injection started after 20 years of CH_4 production)
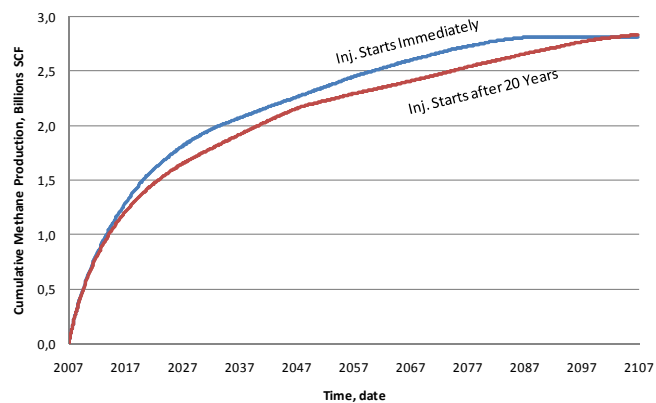
Figure 7.58. Runs 18 and 19: effect of CO_2 injection time on CH_4 production when coal density reduced
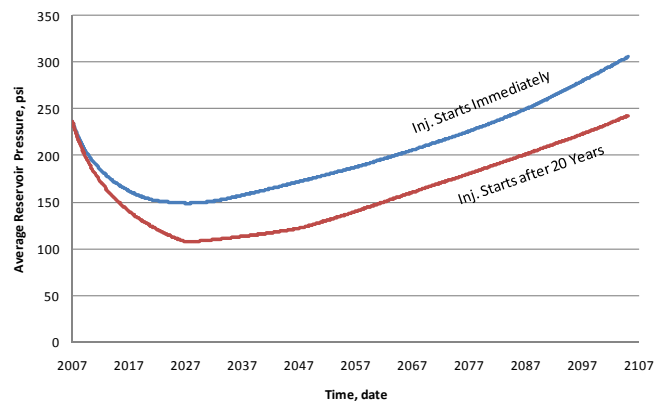
Figure 7.59. Runs 18 and 19: effect of CO$_2$ injection time on CH$_4$ production when coal density reduced
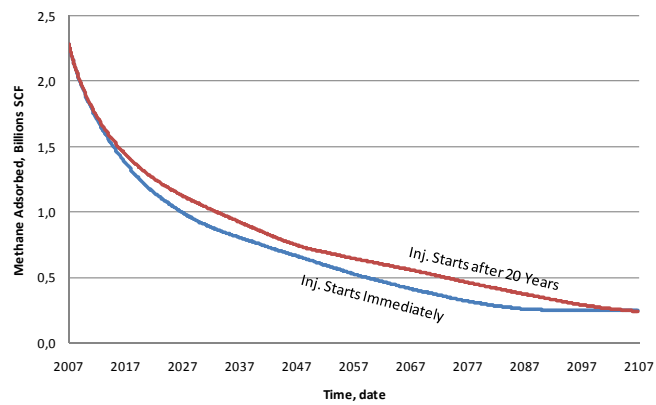
Figure 7.60. Runs 18 and 19: effect of CO$_2$ injection time on CH$_4$ desorption when coal density reduced

7.2.7.2 Coal Density Increased

Coal density was raised to 114.2 lb/ft^3 (1.83 g/cm^3).
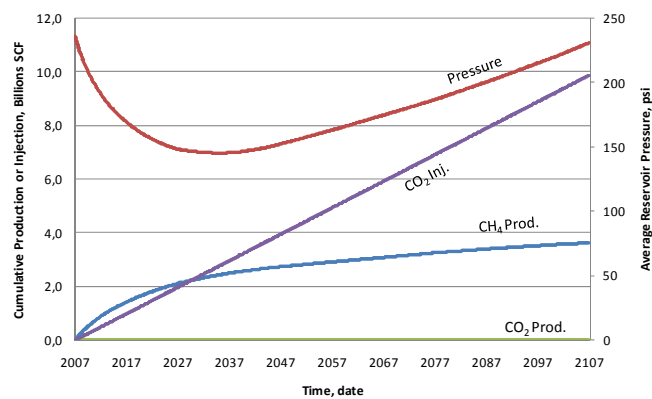
Figure 7.61. Run 20: effect of coal density increase

197
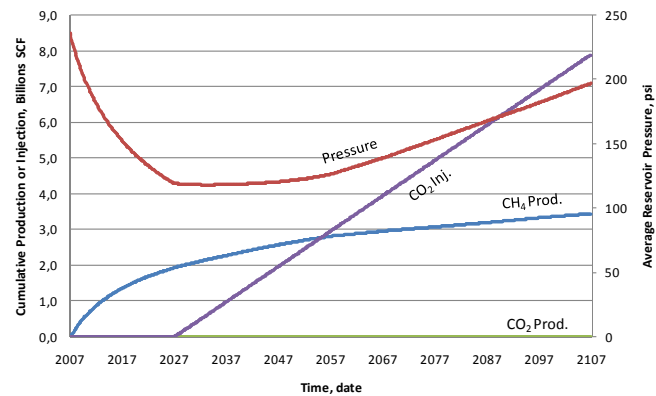
Figure 7.62. Run 21: effect of coal density increase (CO_2 injection started after 20 years of CH_4 production)
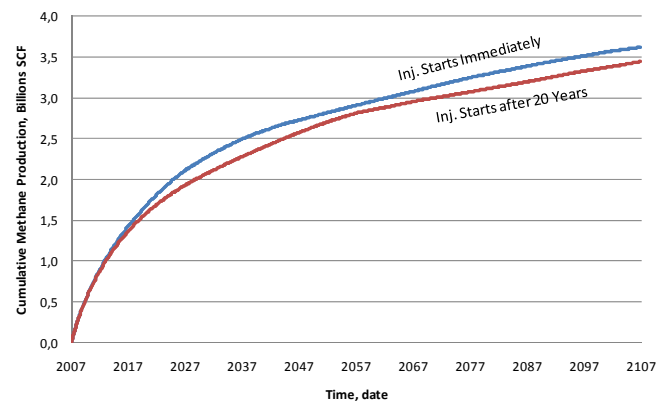
Figure 7.63. Runs 20 and 21: effect of CO_2 injection time on CH_4 production when coal density increased

Figure 7.64. Runs 20 and 21: effect of CO_2 injection time on CH_4 production when coal density increased

198
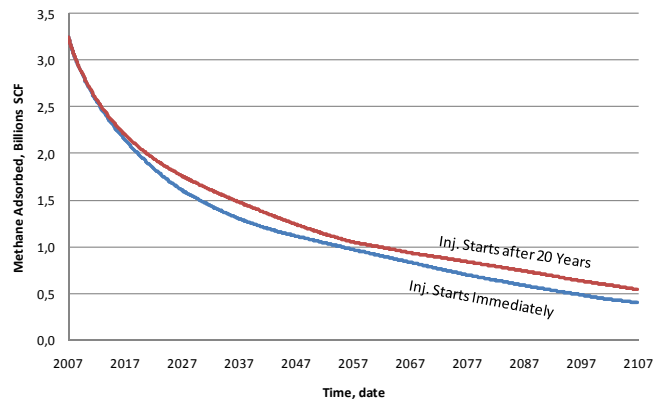
Figure 7.65. Runs 20 and 21: effect of CO_2 injection time on CH_4 desorption when coal density increased

7.2.7.3 Effect of Coal Density

Coal density is directly related to the adsorbed amount of gas in the matrices of coal reservoir. Therefore cumulative methane production was higher when the coal density was also high. Figure 7.67 shows that the increase in the pressure was low for the denser coal. The reason for that can be explained in the same logic. Denser coal has also more capacity for adsorbing carbon dioxide which in turn caused a lower increase in the pressure.
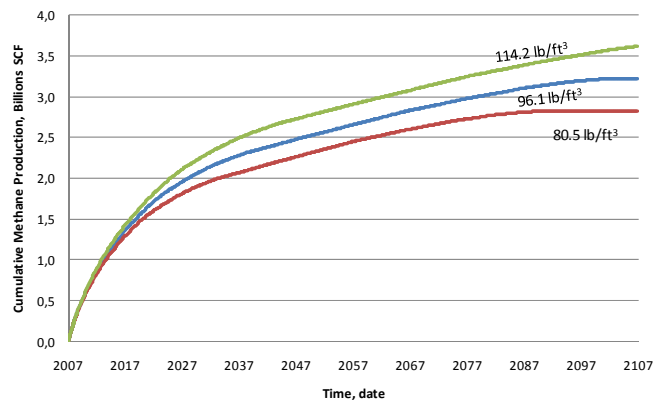
Figure 7.66. Effect of coal density on CH_4 production (CO_2 injection started at 2007)
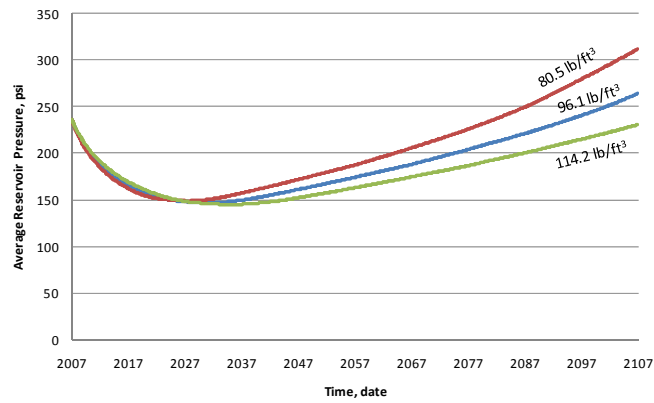
Figure 7.67. Effect of coal density on reservoir pressure (CO_2 injection started at 2007)
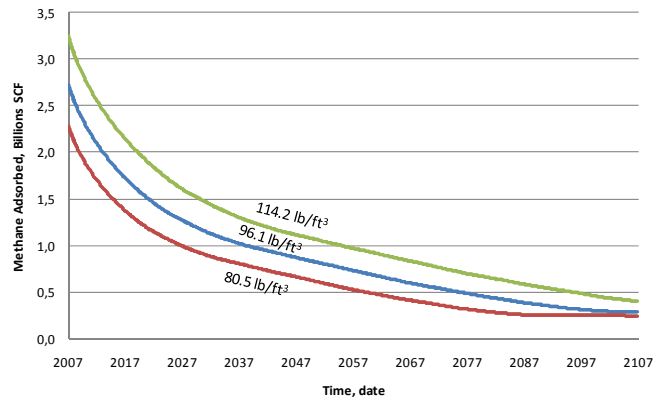
Figure 7.68. Effect of coal density on CH_4 desorption (CO_2 injection started at 2007)

7.2.8 Coal Compressibility

The values of the parameters for the enhanced coalbed methane production when the coal compressibility reduced and increased are given in Table 7.25. Simulation results and gas in place values are given in Table 7.26.

Table 7.25. Parameter values considered for runs 22, 23, 24 and 25

Run		22	23	24	25
Case		Effect of Compressibility Reduction	Effect of Compressibility Reduction (CO$_2$ Injection Started after 20 years of CH$_4$ Production)	Effect of Compressibility Increase	Effect of Compressibility Increase (CO$_2$ Injection Started after 20 years of CH$_4$ Production)
Shrinkage & Swelling Effects		Included	Included	Included	Included
CH$_4$ Production	*Start, Date*	Jan. 2007	Jan. 2007	Jan. 2007	Jan. 2007
	End, Date	Jul. 2101	Jan. 2107	May. 2104	Jan. 2107
CO$_2$ Injection	*Start, Date*	Jan. 2007	**Jan. 2027**	Jan. 2007	**Jan. 2027**
	End, Date	Jan. 2107	Jan. 2107	Jan. 2107	Jan. 2107
Permeability, md	*Face Cleat*	8	8	8	8
	Butt Cleat	8	8	8	8
Porosity, fraction	*Matrix*	0.04	0.04	0.04	0.04
	Cleats	0.02	0.02	0.02	0.02
Cleat Spacing, ft		6	6	6	6
Coal Compressibility, 1/psi		**1×10⁻⁶**	**1×10⁻⁶**	**4×10⁻⁴**	**4×10⁻⁴**
Coal Density, lb/ft³		96.14	96.14	96.14	96.14
Pressure Gradient, psi/ft		0.129	0.129	0.129	0.129
Langmuir Volume, scf/ton	*CO$_2$*	993.05	993.05	993.05	993.05
	CH$_4$	496.52	496.52	496.52	496.52
Langmuir Pressure, psi	*CO$_2$*	718.2	718.2	718.2	718.2
	CH$_4$	1436.5	1436.5	1436.5	1436.5
Water Saturation, fraction		0.01	0.01	0.01	0.01

Table 7.26. Simulation results for runs 22, 23, 24 and 25

Run			22	23	24	25
Cum. CH$_4$ Prod., Billions scf			3.23	3.16	3.22	3.11
Cum. CO$_2$ Inj., Millions tonne			0.52	0.42	0.52	0.42
CH$_4$ Recovered, % of IGIP			89.78	87.91	89.33	86.41
Gas in Place, Billions SCF	*Adsorbed (Matrix)*		2.73	2.73	2.73	2.73
	Free	*Matrix*	0.59	0.59	0.59	0.59
		Cleats	0.29	0.29	0.29	0.29
	Total		3.61	3.61	3.61	3.61

7.2.8.1 Coal Compressibility Reduced

Coal compressibility was decreased to 1x10⁻⁶ psi⁻¹.
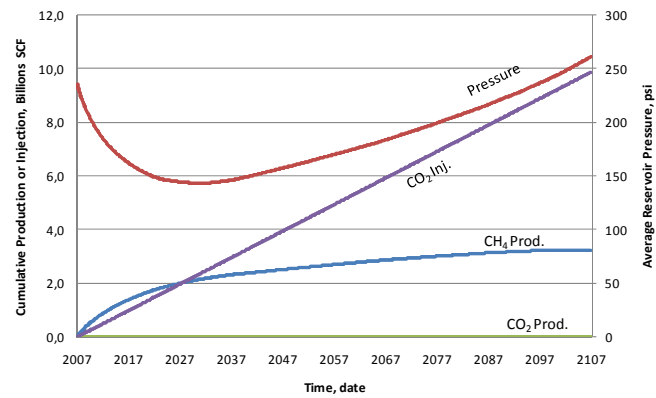
Figure 7.69. Run 22: effect of coal compressibility reduction
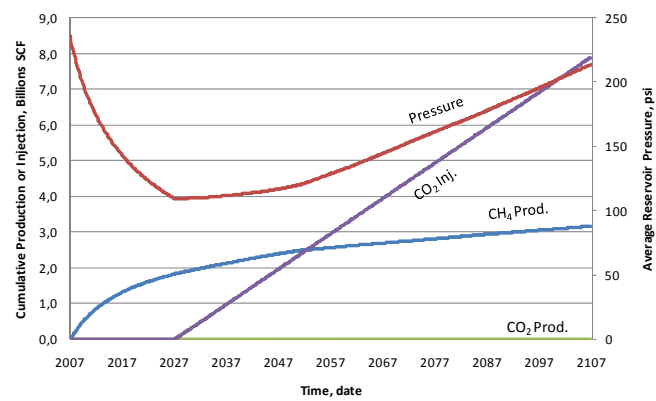
Figure 7.70. Run 23: effect of coal compressibility reduction (CO_2 injection started after 20 years of CH_4 production)
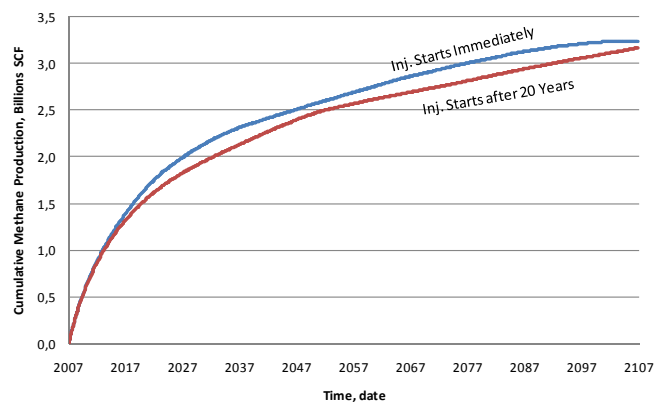
Figure 7.71. Runs 22 and 23: effect of CO_2 injection time on CH_4 production when coal compressibility reduced
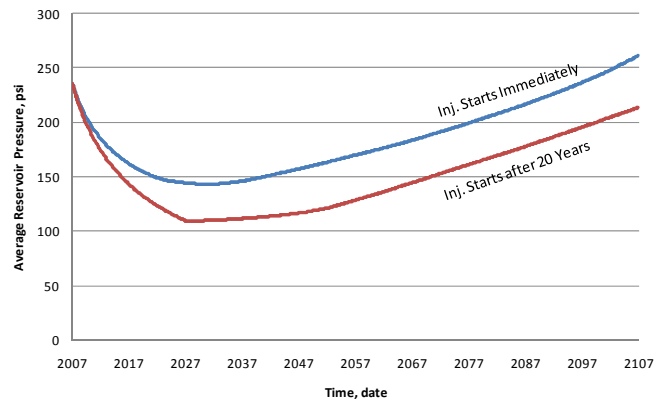
Figure 7.72. Runs 22 and 23: effect of CO_2 injection time on CH_4 production when coal compressibility reduced
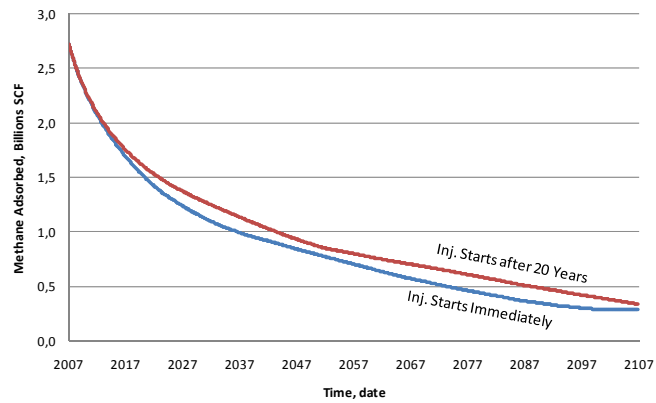
Figure 7.73. Runs 22 and 23: effect of CO_2 injection time on CH_4 desorption when coal compressibility reduced

7.2.8.2 Coal Compressibility Increased

Coal compressibility was raised to 4×10^{-4} psi^{-1}.
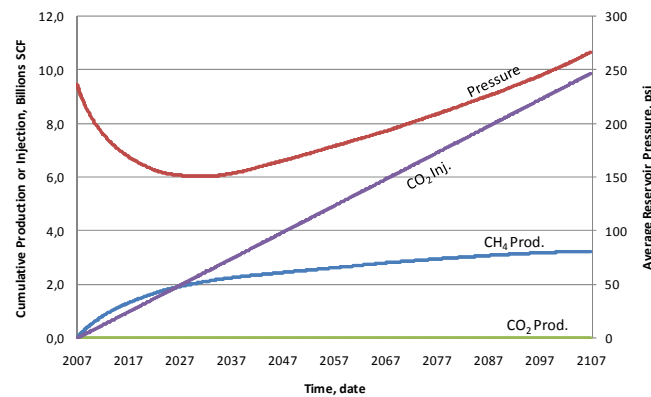
Figure 7.74. Run 24: effect of coal compressibility increase

203
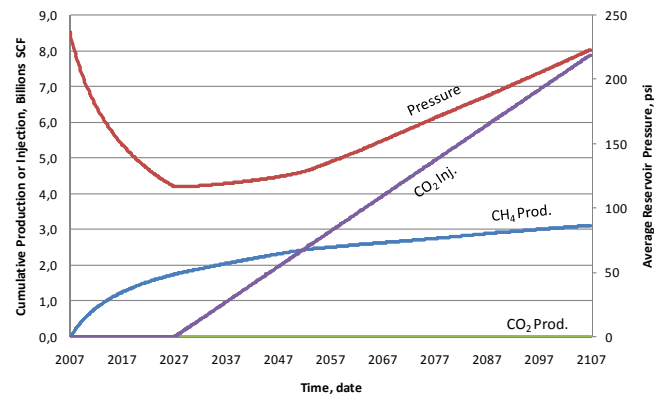
Figure 7.75. Run 25: effect of coal compressibility increase (CO_2 injection started after 20 years of CH_4 production)
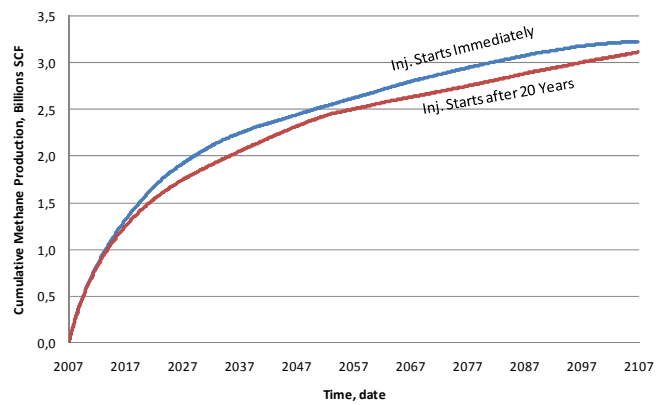
Figure 7.76. Runs 24 and 25: effect of CO_2 injection time on CH_4 production when coal compressibility increased
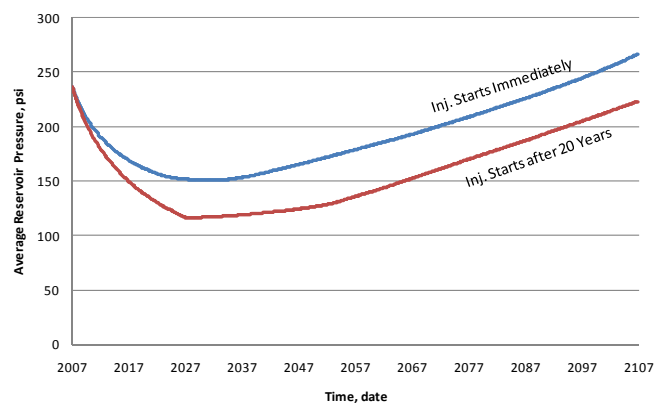
Figure 7.77. Runs 24 and 25: effect of CO_2 injection time on CH_4 production when coal compressibility increased
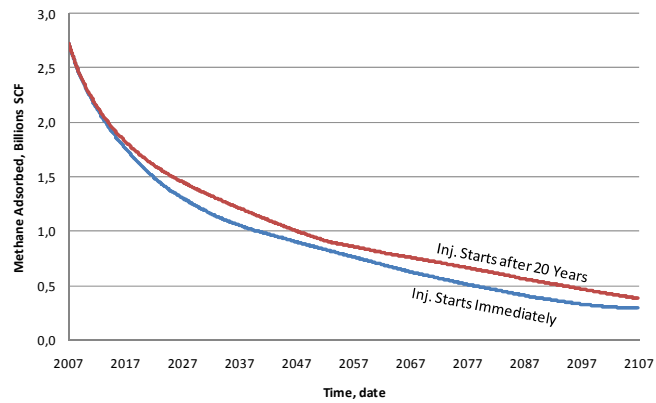
Figure 7.78. Runs 24 and 25: effect of CO$_2$ injection time on CH$_4$ desorption when coal compressibility increased

7.2.8.3 Effect of Coal Compressibility

The change in coal compressibility affected slightly the cleat porosity and therefore the cleat permeability due to the change in reservoir pressure. The effect of coal compressibility on methane production was insignificant. A 400 fold increase in coal compressibility reduced 0.3% in ultimate methane production.
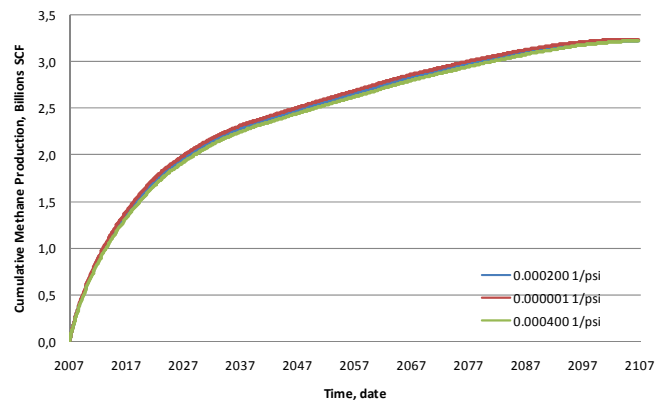
Figure 7.79. Effect of coal compressibility on CH$_4$ production (CO$_2$ inj. started at 2007)
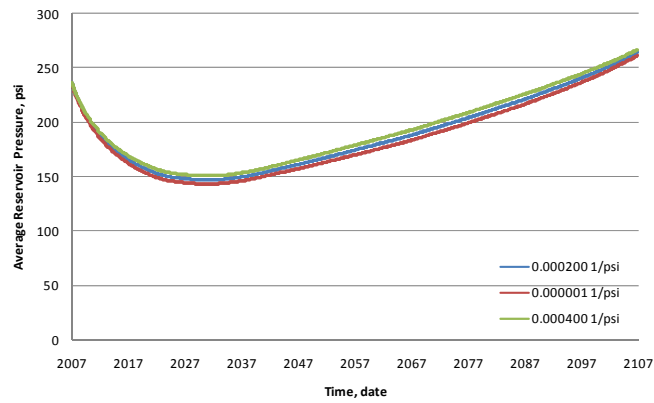
Figure 7.80. Effect of coal compressibility on reservoir pressure (CO_2 inj. started at 2007)
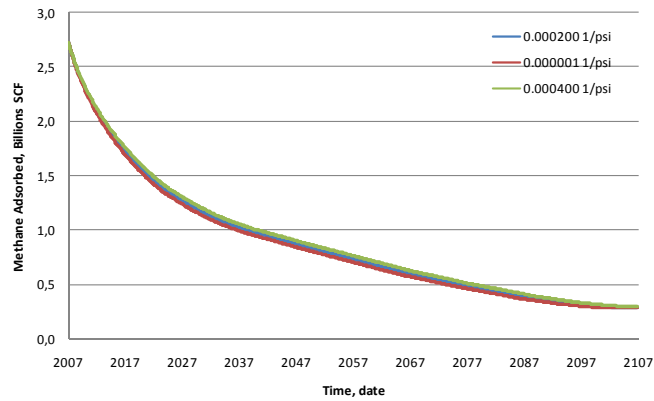
Figure 7.81. Effect of coal compressibility on CH_4 desorption (CO_2 inj. started at 2007)

7.2.9 Coal Adsorption Parameters

The amount of adsorbed gas in place is directly related with adsorption parameters. Maximum amount of gas adsorbed in unit mass and inverse of Langmuir pressure were input to the simulator.

The values of the parameters for the enhanced coalbed methane production when the adsorption parameters were changed are given in Table 7.27. Simulation results and gas in place values are given in Table 7.28.

Table 7.27. Parameter values considered for runs 26 and 27

Run		26	27
Case		Effect of Change in Adsorption Parameters	Effect of Change in Adsorption Parameters (CO_2 Injection Started after 20 years of CH_4 Production)
Shrinkage & Swelling Effects		Included	Included
CH₄ Production	Start, Date	Jan. 2007	Jan. 2007
	End, Date	Jan. 2107	Jan. 2107
CO₂ Injection	Start, Date	Jan. 2007	**Jan. 2027**
	End, Date	Jan. 2107	Jan. 2107
Permeability, md	Face Cleat	8	8
	Butt Cleat	8	8
Porosity, fraction	Matrix	0.04	0.04
	Cleats	0.02	0.02
Cleat Spacing, ft		6	6
Coal Compressibility, 1/psi		2×10^{-4}	2×10^{-4}
Coal Density, lb/ft³		96.14	96.14
Pressure Gradient, psi/ft		0.129	0.129
Langmuir Volume, scf/ton	CO₂	**727.48**	**727.48**
	CH₄	**363.74**	**363.74**
Langmuir Pressure, psi	CO₂	**161.5**	**161.5**
	CH₄	**323.0**	**323.0**
Water Saturation, fraction		0.01	0.01

Table 7.28. Simulation results for runs 26 and 27

Run			26	27
Cum. CH₄ Prod., Billions scf			5.00	4.71
Cum. CO₂ Inj., Millions tonne			0.52	0.42
CH₄ Recovered, % of IGIP			73.29	68.99
Gas in Place, Billions SCF	Adsorbed (Matrix)		5.97	5.97
	Free	Matrix	0.58	0.58
		Cleats	0.29	0.29
	Total		6.84	6.84

7.2.9.1 Coal Adsorption Parameters Changed

Coal adsorption parameters; Langmuir volume and Langmuir pressure were changed for methane and carbon dioxide as shown in Table 7.27.
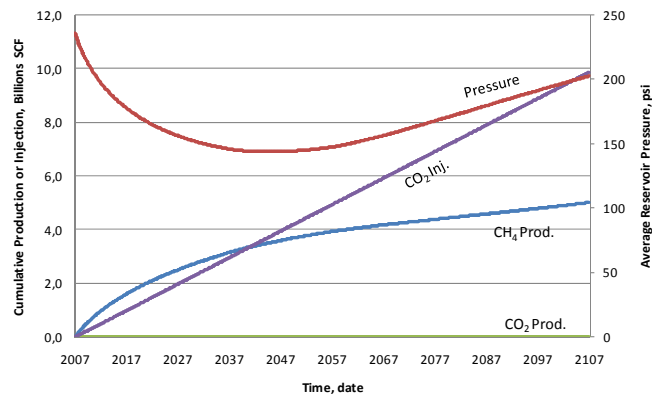
Figure 7.82. Run 26: effect of change in coal adsorption parameters
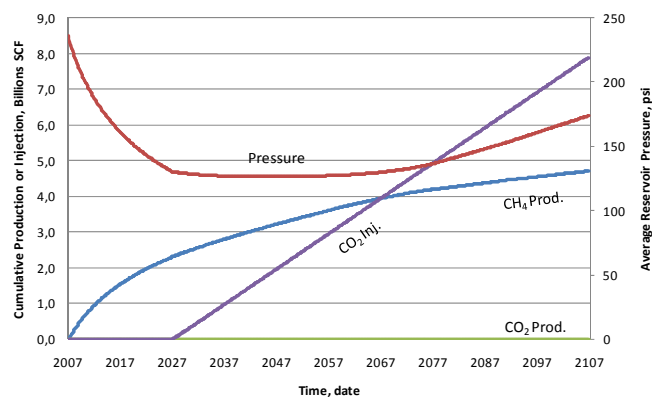
Figure 7.83. Run 27: effect of change in coal adsorption parameters (CO_2 injection started after 20 years of CH_4 production)
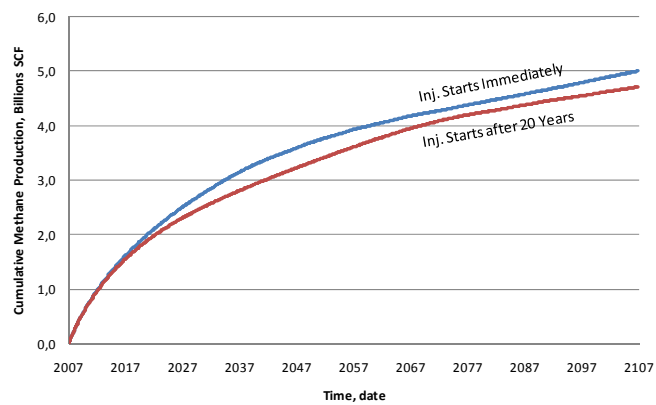
Figure 7.84. Runs 26 and 27: effect of CO_2 injection time on CH_4 production when coal adsorption parameters changed
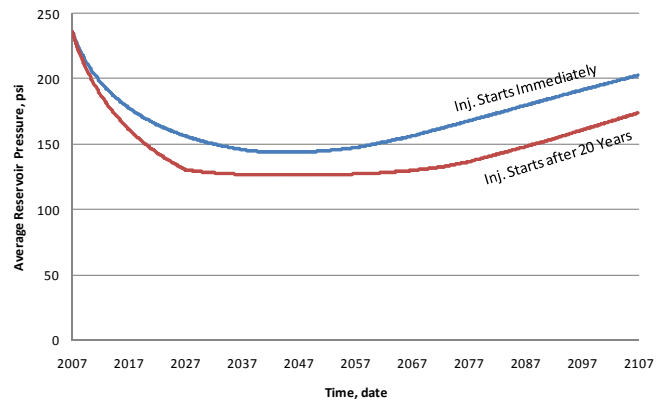
Figure 7.85. Runs 26 and 27: effect of CO$_2$ injection time on CH$_4$ production when coal adsorption parameters changed
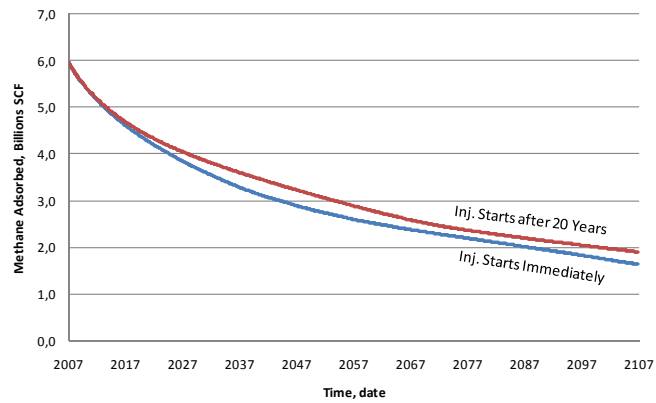
Figure 7.86. Runs 26 and 27: effect of CO$_2$ injection time on CH$_4$ desorption when coal adsorption parameters changed

7.2.9.2 Effect of Adsorption Parameters

Adsorption isotherms of coal samples taken from Karadon and Kozlu formation are given in Figure 7.87. Kozlu formation (deeper than Karadon formation) having lower Langmuir volume (363.74 scf/tonne) resulted in higher ultimate recovery because of lower Langmuir pressure (323 psi) than that of Karadon formation (1436.5 psi). In base case (Karadon formation), although the higher Langmuir volume (496.52) was used, less methane production was observed.
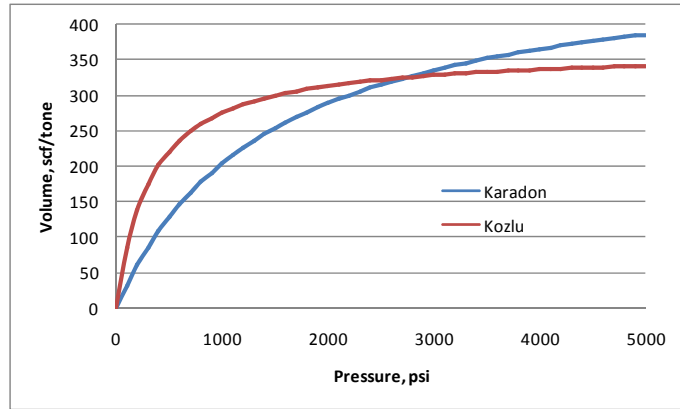
Figure 7.87. Adsorption isotherms of Karadon and Kozlu formations for methane (TTK, 2003)
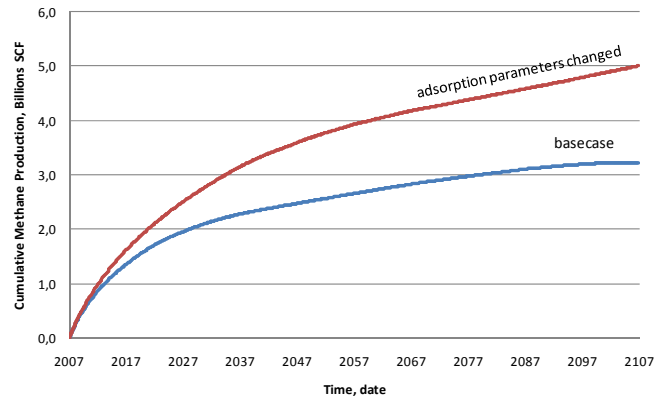
Figure 7.88. Effect of adsorption parameters on CH₄ production (CO₂ inj. started at 2007)
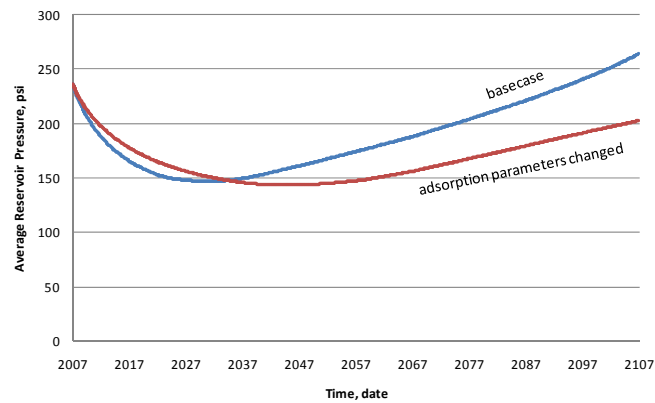
Figure 7.89. Effect of adsorption parameters on reservoir pressure (CO₂ inj. started at 2007)

210
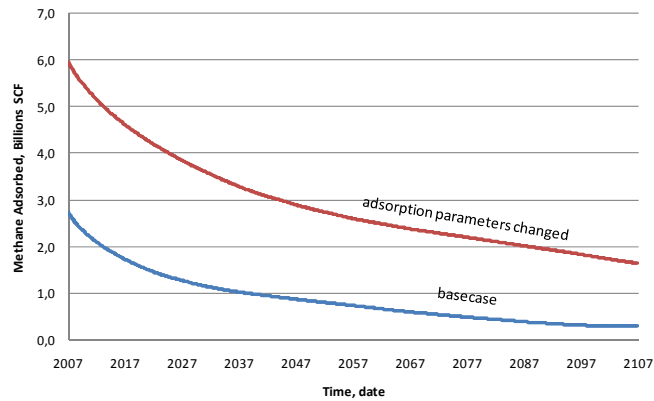
Figure 7.90. Effect of adsorption parameters on CH$_4$ desorption (CO$_2$ inj. started at 2007)

7.2.10 Water Saturation

When the reservoir is water saturated, hydrostatic pressure gradient of 0.43 psi/ft was used to estimate the reservoir pressure. This increase in the pressure resulted in more adsorbed gas found in the coal matrix, but almost no free gas in the cleats. The values of the parameters when the reservoir is water saturated are given in Table 7.29.

Table 7.29. Parameter values considered for runs 28, 29, and 30

Run		28	29	30
Case		Effect of Water Saturation	Effect of Water Saturation (CO$_2$ Injection Started after 20 years of CH$_4$ Production)	Effect of Water Saturation (CO$_2$ Injection Started after 40 years of CH$_4$ Production)
Shrinkage & Swelling Effects		Included	Included	Included
CH$_4$ Production	*Start, Date*	Jan. 2007	Jan. 2007	Jan. 2007
	End, Date	Sep. 2015	Jan. 2107	Jan. 2107
CO$_2$ Injection	*Start, Date*	Jan. 2007	**Jan. 2027**	**Jan. 2047**
	End, Date	Sep. 2015	Jan. 2107	Jan. 2107
Permeability, md	*Face Cleat*	8	8	8
	Butt Cleat	8	8	8
Porosity, fraction	*Matrix*	0.04	0.04	0.04
	Cleats	0.02	0.02	0.02
Cleat Spacing, ft		6	6	6
Coal Compressibility, 1/psi		2×10^{-4}	2×10^{-4}	2×10^{-4}
Coal Density, lb/ft³		96.14	96.14	96.14
Pressure Gradient, psi/ft		**0.433**	**0.433**	**0.433**
Langmuir Volume, scf/ton	*CO$_2$*	993.05	993.05	993.05
	CH$_4$	496.52	496.52	496.52
Langmuir Pressure, psi	*CO$_2$*	718.2	718.2	718.2
	CH$_4$	1436.5	1436.5	1436.5
Water Saturation, fraction		**0.99**	**0.99**	**0.99**

Simulation results and gas/water in place values are given in Table 7.30.

Table 7.30. Simulation results for runs 28, 29 and 30

Run			28	29	30
Cum. CH₄ Prod., Billions scf			-	6.62	6.60
Cum. CO₂ Inj., Millions tonne			-	0.42	0.52
CH₄ Recovered, % of IGIP			-	73.99	73.79
Gas in Place, Billions SCF	*Adsorbed (Matrix)*		6.84	6.84	6.84
	Free	*Matrix*	2.11	2.11	2.11
		Cleats	0.01	0.01	0.01
	Total		8.96	8.96	8.96
Water in place, STB			3.37×10⁶	3.37×10⁶	3.37×10⁶

In order to see the reaction of the simulator, an unrealistic scenario of CO_2 injection before water production was applied. The simulation of this case was terminated at September 2015 after nearly 8 years from the start of production. The simulator repeated the time steps several times because of the gas and water composition variations were too large. Although the time step size decreased below 0.1×10^{-5} days, the composition variation could not be prevented and the simulation stopped. This behavior of the simulator showed that, the injection of carbon dioxide before producing water from the coal caused problems. These problems were mainly because of the water preventing desorption of methane from the coal matrix. The following figure shows the pressure at the grid block found in 13th column and 123rd row. The unreasonable drop in pressure in one month caused termination of the simulation later.
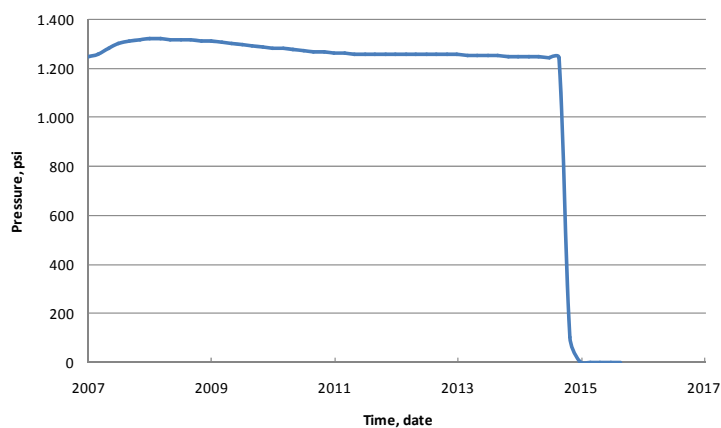
Figure 7.91. Unreasonable pressure drop at grid block: (13,123)
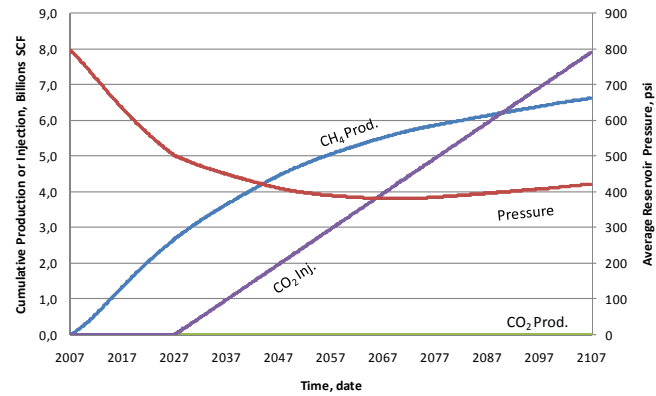
Figure 7.92 (a)
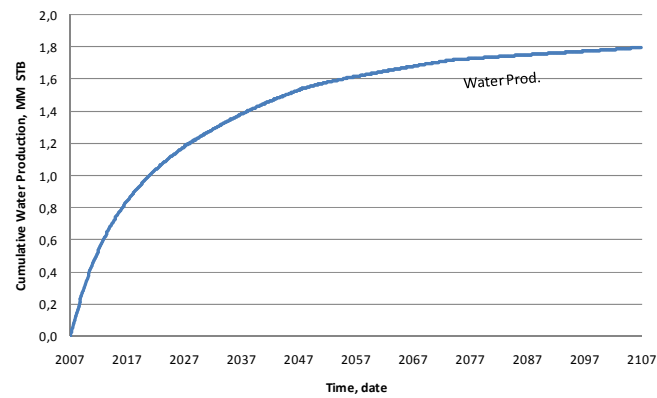
Figure 7.92 (b)
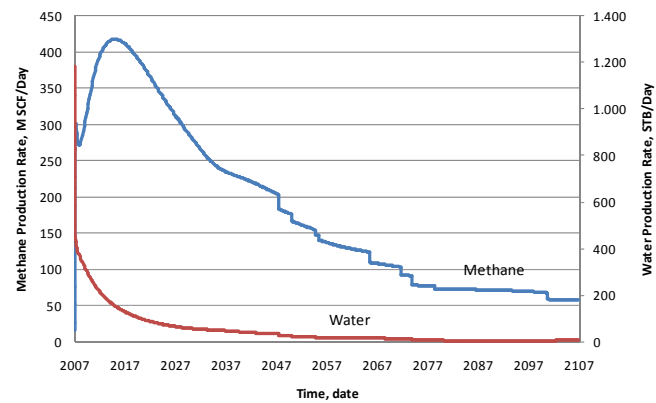
Figure 7.92 (c)

Figure 7.92. Run 29: effect of water saturation (CO_2 injection started after 20 years of CH_4 production)

213
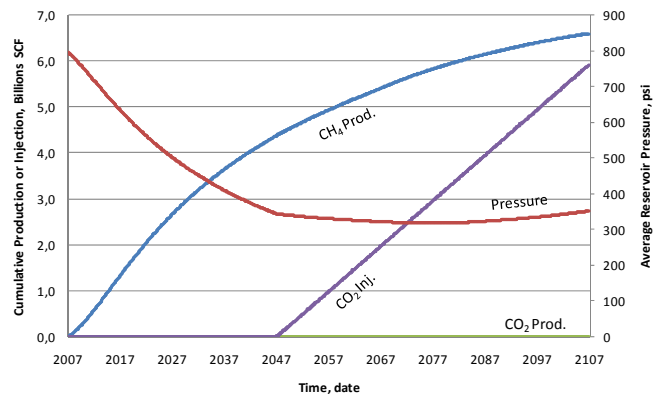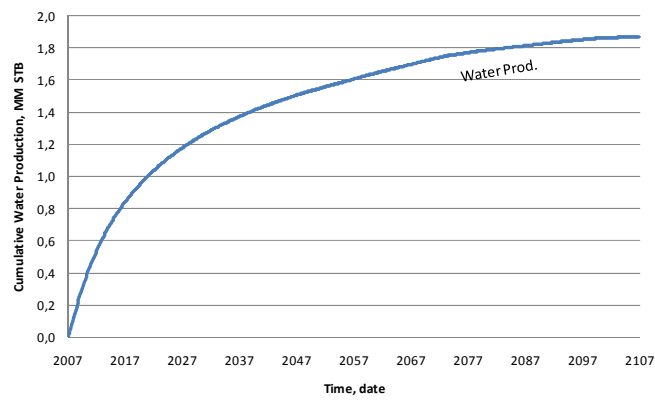
Figure 7.93 (a)

Figure 7.93 (b)
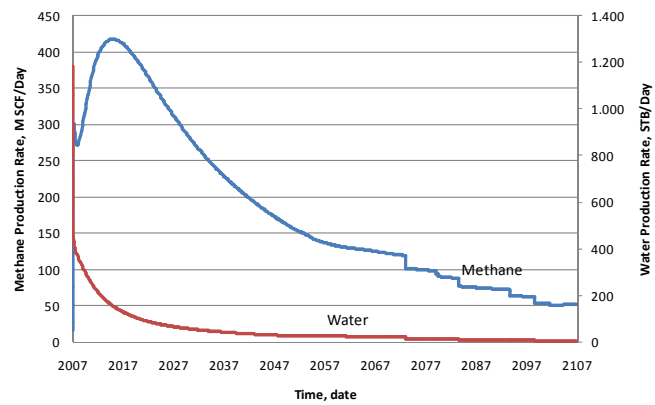
Figure 7.93 (c)

Figure 7.93. Run 30: effect of water saturation (CO_2 injection started after 40 years of CH_4 production)
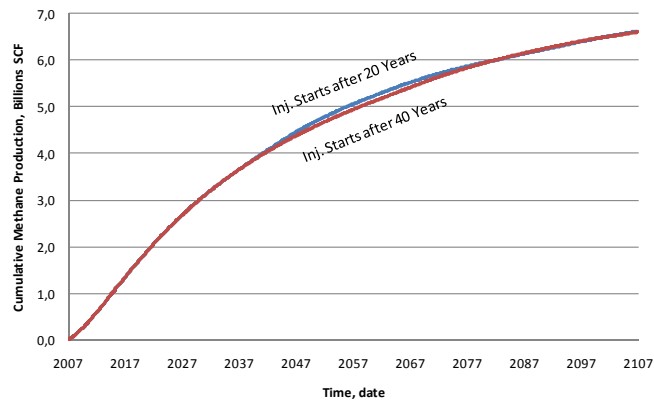
Figure 7.94. Runs 29 and 30: effect of CO_2 injection time on CH_4 production when coal is water saturated
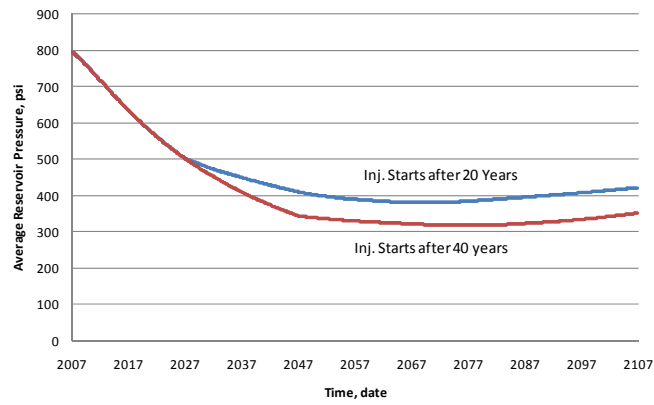
Figure 7.95. Runs 29 and 30: effect of CO_2 injection time on CH_4 production when coal is water saturated
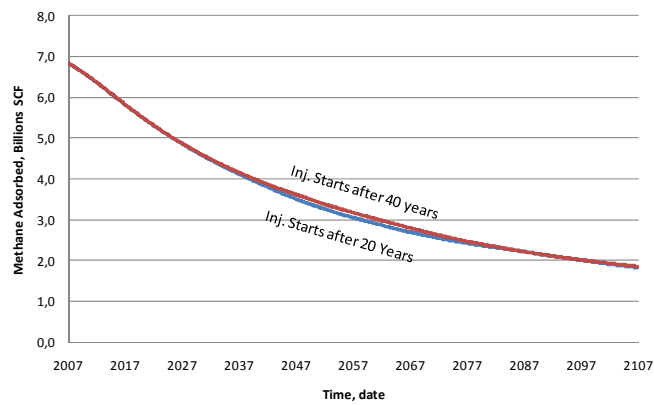
Figure 7.96. Runs 29 and 30: effect of CO_2 injection time on CH_4 desorption when coal is water saturated

7.2.11 Coal Anisotropy

Coal has an anisotropic structure. Flow in coal follows the continuous face cleats rather than the butt cleats which are orthogonal to face cleats in general. However the permeability ratio between face and butt cleats is not known for Zonguldak basin, neither the direction of the face cleat. Therefore base case was prepared assuming equal permeabilities in each direction. Anisotropy was studied as another case and the permeability ratio of 1:8 was used.

The values of the parameters for the enhanced coalbed methane production when the adsorption parameters were changed are given in Table 7.31. Simulation results and gas in place values are given in Table 7.32.

Table 7.31. Parameter values considered for runs 31 and 32

Run		31	32
Case		Effect of Coal Anisotropy	Effect of Coal Anisotropy (CO_2 Injection Started after 20 years of CH_4 Production)
Shrinkage & Swelling Effects		Included	Included
CH_4 Production	Start, Date	Jan. 2007	Jan. 2007
	End, Date	Jan. 2107	Jan. 2107
CO_2 Injection	Start, Date	Jan. 2007	**Jan. 2027**
	End, Date	Jan. 2107	Jan. 2107
Permeability, md	Face Cleat	8	8
	Butt Cleat	**1**	**1**
Porosity, fraction	Matrix	0.04	0.04
	Cleats	0.02	0.02
Cleat Spacing, ft		6	6
Coal Compressibility, 1/psi		2×10^{-4}	2×10^{-4}
Coal Density, lb/ft³		96.14	96.14
Pressure Gradient, psi/ft		0.129	0.129
Langmuir Volume, scf/ton	CO_2	993.05	993.05
	CH_4	496.52	496.52
Langmuir Pressure, psi	CO_2	718.2	718.2
	CH_4	1436.5	1436.5
Water Saturation, fraction		0.01	0.01

216

Table 7.32. Simulation results for runs 31 and 32

Run			31	32
Cum. CH$_4$ Prod., Billions scf			2.85	2.71
Cum. CO$_2$ Inj., Millions tonne			0.52	0.42
CH$_4$ Recovered, % of IGIP			79.19	75.26
	Adsorbed (Matrix)		2.73	2.73
Gas in Place,	Free	Matrix	0.59	0.59
Billions SCF		Cleats	0.29	0.29
	Total		3.61	3.61
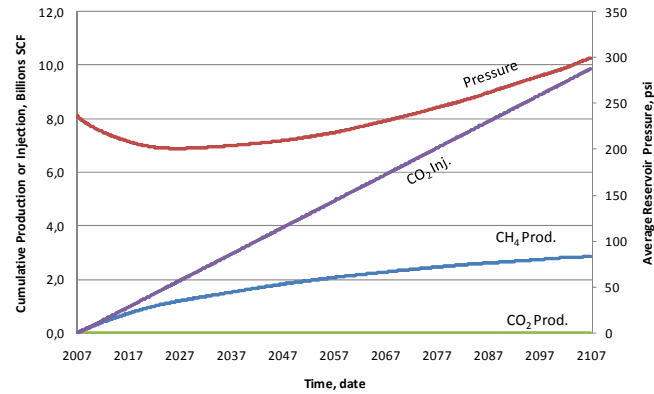
Figure 7.97. Run 31: effect of coal anisotropy
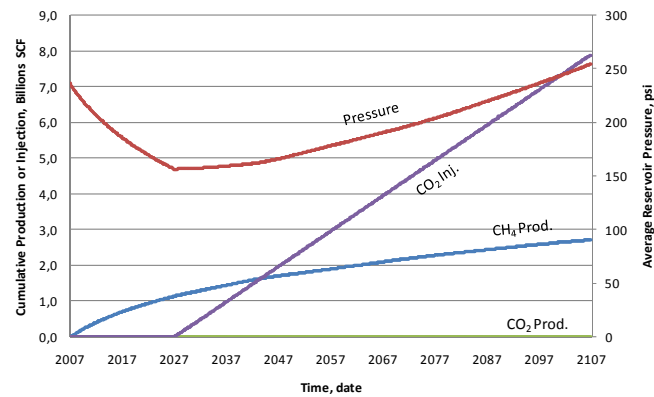
Figure 7.98. Run 32: effect of coal anisotropy (CO$_2$ injection started after 20 years of CH$_4$ production)

217
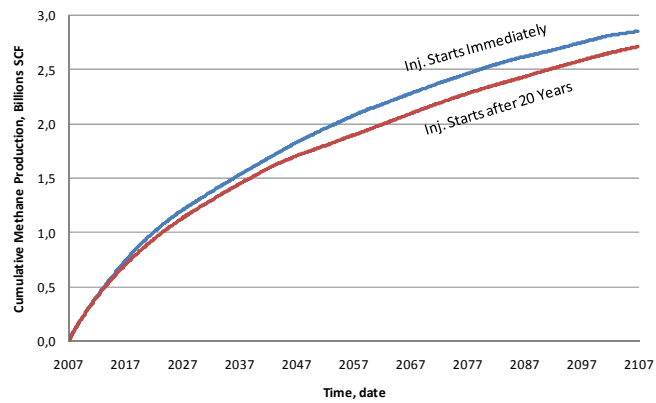
Figure 7.99. Runs 31 and 32: effect of CO_2 injection time on CH_4 production when coal was anisotropic
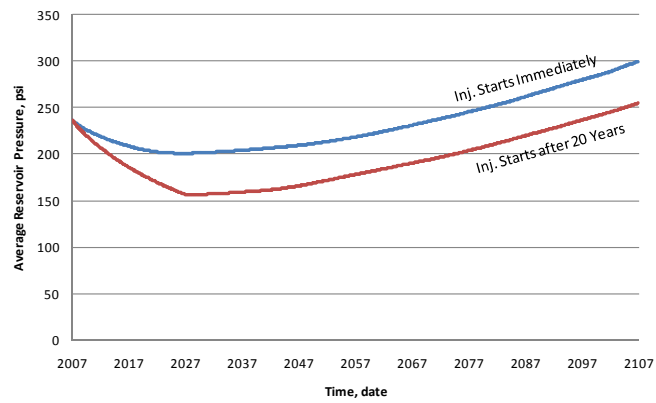
Figure 7.100. Runs 31 and 32: effect of CO_2 injection time on reservoir pressure when coal was anisotropic
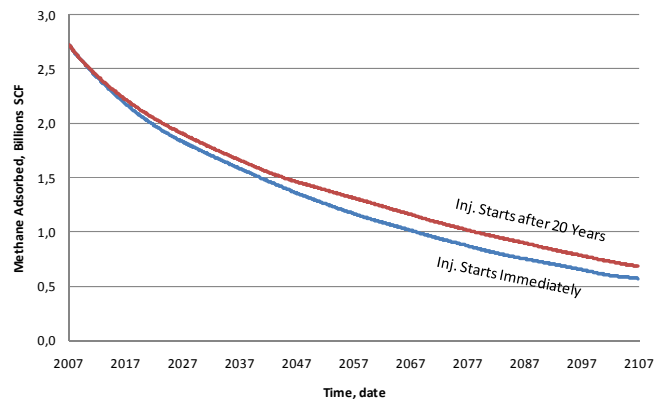
Figure 7.101. Runs 31 and 32: effect of CO_2 injection time on CH_4 desorption when coal was anisotropic
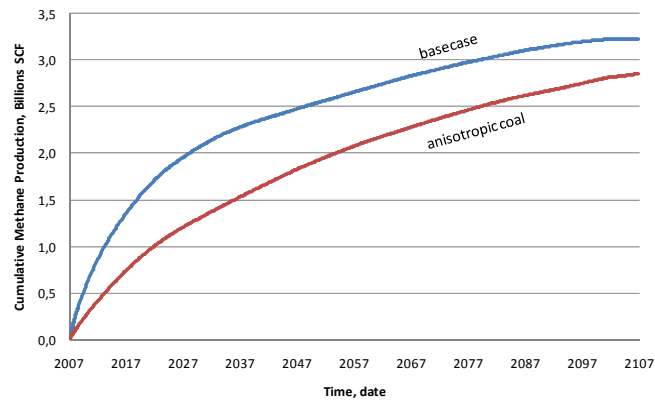
Figure 7.102. Effect of coal anisotropy on CH$_4$ production (CO$_2$ injection started at 2007)
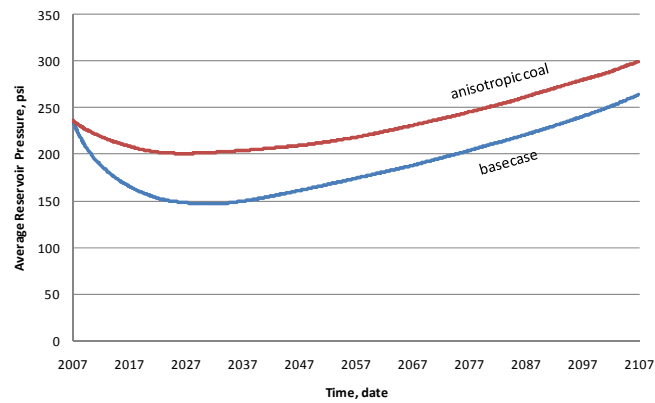
Figure 7.103. Effect of coal anisotropy on reservoir pressure (CO$_2$ injection started at 2007)
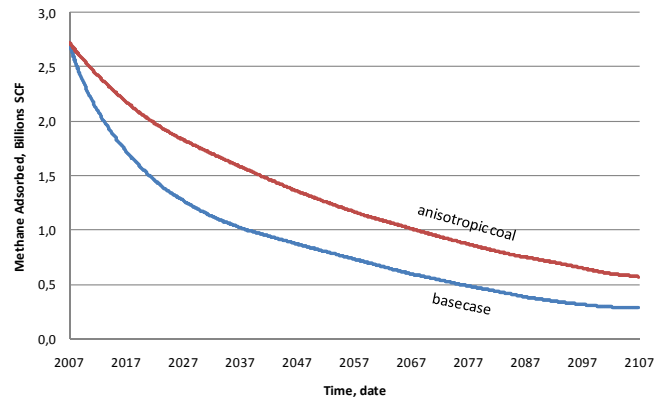
Figure 7.104. Effect of coal anisotropy on CH$_4$ desorption (CO$_2$ injection started at 2007)

When the coal cleat permeability was anisotropic, CO$_2$-CH$_4$ front propagated elliptically out from the injection wells (Figure 7.106). However, a circular shape formed when the face and butt cleat permeability values were taken equal (Figure

219

7.105). Meanwhile the amount of methane production decreased for the anisotropic coal in spite of the same CO_2 injection.

| 01.01.2027 | 01.01.2047 | 01.01.2067 | 01.01.2087 | 01.01.2107 | Legend |
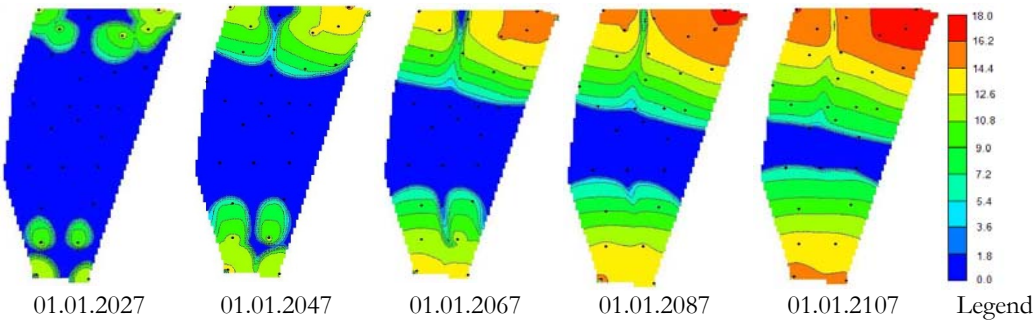
Figure 7.105. Run 4: Base Case ECBM - CO_2 Adsorption (scf/ft³ of coal)
(CO2 injection started at 2007)

| 01.01.2027 | 01.01.2047 | 01.01.2067 | 01.01.2087 | 01.01.2107 | Legend |
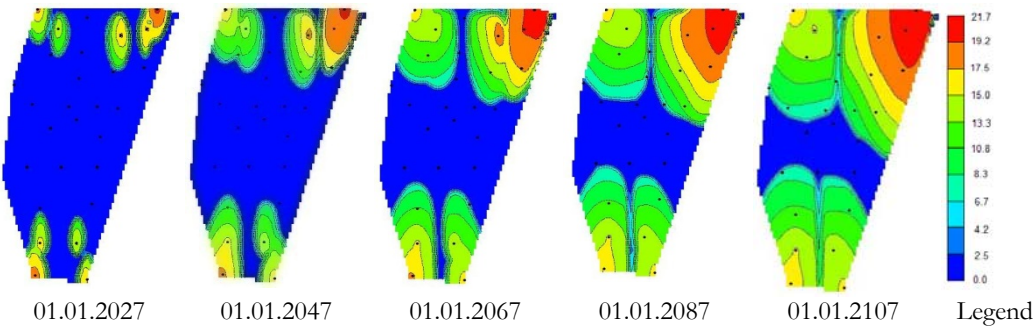
Figure 7.106. Run 31: Anisotropic Coal - CO_2 Adsorption (scf/ft³ of coal)
(CO2 injection started at 2007)

CHAPTER 8

CONCLUSIONS

The coalbed methane capacity of Amasra resource area-A coal seams having heterogeneous structure was estimated by performing the continuity based correlation study and probabilistic calculations with limited data. 63 coal layers with varying properties of depth, thickness and area were defined. Probabilistic calculations give the chance to be informed about better or worse cases that may occur since the data used in calculations have uncertainty. From the results and discussions presented in this thesis, the following conclusions can be drawn.

1. The initial methane in place found in all these seams both in free and adsorbed states were estimated using probabilistic calculations resulted in possible reserve (P10) of 72.97 billions scf, probable reserve (P50) of 47.74 billions scf and proven reserves (P90) of 30.46 billions scf.
2. Since Amasra coal reservoir is not saturated with water, almost 10% of the total gas in place was found to be in the cleats as free gas.
3. Coal layer #26 which was selected to use in the simulation studies has an area of 4099 acres, average thickness of 6.23 ft and depth of 1788 ft (545 m). P50 reserve estimation is 6.47 billions scf in matrix and 0.645 billions scf in fracture.

A number of simulation runs were designed to foster a better understanding of the response of the Coal Layer #26 (Karadon formation) having more initial gas in place to different parameters during methane production and carbon dioxide storage for CBM and ECBM recovery processes.

4. Inclusion of shrinkage and swelling feature on the simulator affected the pore volume decrease which was due to change in overburden stress with the reduction of pressure. Although decrease in the cleat porosity was less when shrinkage and swelling effects included, the decrease in the cleat permeability as a function of porosity diminished the methane production.

5. Cumulative methane production was enhanced with the injection of carbon dioxide (ECBM) approximately 23% (3.23 billions scf) than that of CBM recovery (2.63 billions scf).

6. Although closing the wells to production because of CO_2 breakthrough had a negative effect on methane production initially, there was no difference between ultimate methane productions whether the wells remained open or closed, but more carbon dioxide was sequestered when the production ceased at the wells.

7. Injected carbon dioxide amount of 5192 tones/year in base case was only capable to sequester only 0.3% of the yearly carbon dioxide emission of Zonguldak Çatalağzı Power Plant nearby. Considering the gas in place capacity of the coal layer #26 as 15% of the resource area-A, it can be said that the project aiming ECBM recovery rather than carbon sequestration would be successful.

8. In spite of water saturated coal reservoirs where the water production is required initially, it can be possible to start immediately the injection of CO_2 with methane production for a dry coal reservoir. However, the dryness of the coal reservoir decreased the pressure required for the adsorption of methane which in turn decreased the amount of gas in place.

9. Cleat permeability being one of the most crucial parameter in the coal reservoir affected the rate of methane production. A decrease in permeability reduced the injectivity of CO_2. As a result, the pressure was buildup within the system.

10. The more free gas was found in higher porosity cleat systems. Although the cumulative methane production was increased when the cleat porosity rose, methane recovery percents were remained almost constant.

11. The lower the cleat spacing the higher the rate of transfer between fracture and matrix was observed. The rate of gas desorption from the coal matrix and subsequent diffusion to both butt and face cleats was higher than the rate of flow in the face cleats, then production was flow-limited, pressure-driven and was defined by Darcy's Law. Therefore, the change in the cumulative production was very low.

12. The cumulative methane production was higher when the coal was denser, since coal density was directly related to the adsorbed amount of gas in the matrices of coal reservoir. Denser coal has also more capacity for adsorbing carbon dioxide which in turn caused a steady increase in the pressure.

13. The change in coal compressibility affected slightly the cleat porosity and therefore the cleat permeability due to the change in reservoir pressure. The effect of coal compressibility on methane production was insignificant. A 400 fold increase in coal compressibility reduced 0.3% in ultimate methane production.

14. Langmuir volume defined as maximum adsorption capacity. Kozlu formation (deeper than Karadon formation) having lower Langmuir volume resulted in higher ultimate recovery because of lower Langmuir pressure than that of Karadon formation. In base case (Karadon formation), although the higher Langmuir volume was used, less methane production was observed.

15. Permeability anisotropy generated the CO_2-CH_4 front in elliptic shape. However, a circular shape formed when the face to butt cleat permeability ratio was one (isotropic permeability).

CHAPTER 9

FURTHER STUDIES

In this study gas in place estimation and effects of several coal characteristics were examined with a limited data in hand. As the accuracy of the information increases, the uncertainty as wells as the range of minimum and maximum gas in place values decreases. One of the coal layers was simulated to see the sensitivity of the parameters, such as cleat permeability, cleat porosity, coal density, cleat spacing, permeability anisotropy, compressibility. However, well pattern, number of the production and injection wells, gas rate, multi-seam completion, hydraulic fracturing and similar parameters were not studied to find an optimum solution for methane production.

Hydraulic fracturing plays a critical role in the exploitation of coalbed methane because of the unique nature of coalbed methane, and because coal seams tend to have lower permeability. Hydraulic fracturing attempts to achieve four primary goals in coal completions: 1) bypass near wellbore damage; 2) stimulate production and accelerate dewatering; 3) distribute the pressure drawdown to reduce fines production; and 4) effectively connect the wellbore to the reservoir (Jeu et al., 1988). A hydraulic fracturing study should be done in order to optimize the production of methane.

Reservoir pressure is one of the most important parameters of a coal reservoir. The initial pressure usually is determined from well tests performed very early in the producing life of a reservoir. These tests usually consist of a short production period measured in hours followed by a shut-in period. In Amasra basin, a study for the determination of a reservoir pressure should be done in order to make a good estimate of gas in place.

224

It is simply not possible to accurately measure permeability of fracture systems in laboratory samples. Cores taken in a virgin coalbed have been broken by the drilling process, and confining stresses have been relieved. To date, the best estimates of permeability have been made by 'history matching' observed production data. Therefore permeability, direction of the face cleats and the permeability anisotropy ratio should be determined.

REFERENCES

AAPG Position: Climate Change (accessed 2007)
http://dpa.aapg.org/gac/papers/climate_change.cfm

Adzumi, H. (1937) Studies on the Flow of Gaseous Mixtures through Capillaries – II: The Molecular Flow of Gaseous Mixtures. *Bull., Chem. Soc. Japan,* Vol. 12, pp. 285-291.

Airey, E.M. (1968) Gas Emission from Broken Coal. An Experimental and Theoretical Investigation. *International Journal of Rock Mechanics and Mining Sciences,* Vol. 5, pp. 475-494.

Agrali, B. (1964) Palinological correlation of the Lower Carboniferous in the Amasra and Zonguldak basins (in Turkish). *Bulletin of the Turkish Geological Society,* Vol. 12, pp. 95-112.

Akgun, F., Akyol, E. (1992) Palynology and paleoecology of the coals of the Amasra-Bartin Carboniferous basin (in Turkish). *Turkish Journal of Earth Sciences,* Vol. 1, pp. 49-56.

Akyol, E. (1974) Palynological investigation of the Namurian and Westphalian A coal seams at -50 m Asma gallery in the Zonguldak-Uzulmez region (in Turkish). *Journal of the General Directorate of the Mineral Research and Exploration of Turkey,* Vol. 83, pp. 47-108.

Alpern, B., Lemos de Sousa M.J., Flores, D. (1989) A Progress Report on the Alpern Coal Classification. *International Journal of Coal Geology*, Vol. 13, pp. 1-19.

Alpern, B., Lemos de Sousa, M.J. (2002) Documented international enquiry on solid sedimentary fossil fuels; coal: definitions, classifications, reserves-resources,and energy potential. *Inter. J. of Caol Geology,* Vol. 50, pp. 3-41.

Ammosov, I.I., Eremin, I.V. (1960) Fracturing in Coal, *Academy of Sciences of the U.S.S.R.,* Institute of Geology and Exploitation of Natural Fuels, Moscow, U.S.S.R..

Anbarci, K., Ertekin, T. (1990) A Comprehensive Study of Pressure Transient Analysis With Sorption Phenomena for Single-Phase Gas Flow in Coal Seams. *SPE 20568, Ann. Tech.Conf. and Exhibitin,* New Orlans, LA, 23-26 September.

Anbarci, K., Ertekin, T. (1991) A Simplified Approach for In-Situ Characterization of Desorption Properties of Coal Seams. *SPE 21808*, *Rocky Mountain Regional Meeting and Low-Permeability Reservoirs Symposium*, Denver, Colorado, 15-17 April.

Ancell, K.L., Lambert, S., Johnson, F.S. (1980) Analysis of the Coalbed Degasification Process at a Seventeen Well Pattern in the Warrior Basin of Alabama. *SPE 8971*, *presented at the SPE/DOE Symposium on Unconventional Gas Recovery*, Pittsburgh, Pennsylvania, 18-21 May.

Arri, L.E., Yee, D., Morgan, W.D., Jeansonne, M.W. (1992) Modeling Coalbed Methane Production with Binary Gas Sorption. *SPE 24363*, *presented at the Rocky Mountain Regional Meeting*, Casper, Wyoming, 18-21 May.

Artuz, S. (1971) Petrographic investigations of the Westphalian A, Haci Memis coal seams in theAsma and Dilaver regions of the Zonguldak area (in Turkish). *Istanbul University, College of Natural Sciences Monographs,* Vol. 21.

Australian Greenhouse Office (2002) Living with Climate Change – An Overview of Potential Climate Change Impacts on Australia. Summary and Outlook.

Bachu, S., Gunter, W.D., Perkins, E.H. (1994) Aquifer disposal of CO_2: hydrodynamic and mineral trapping. *Energy Convers Mgmt.* Vol. 35, pp. 269-279.

Bachu, S. (2002) Sequestration of CO_2 in geological media in response to climate change: road map for site selection using the transform of the geological space into the CO_2 phase space. *Energy Convers. Manage.*, Vol. 43, pp. 87-102.

Baklid, A., Korbol, R., Owren, G., Sleipner, V. (1996) CO_2 Disposal, CO_2 Injection into a shallow underground aquifer. *SPE 36600*, *presented at the Ann. Tech. Conf. and Exhibition*, Denver, Colorado, 6-9 October.

Berkovitch, I. (1978) Coal: Energy and Chemical Storehouse. *Portcullis Press.* Norwich, Great Britain.

Bilgin, N, Akgun, I.S., Shahriar, K. (1988) The classification of coal seams in Amasra coalfield according to their mechanical strength (in Turkish). *Proceedings of the 6th Coal Congress of Turkey,* pp. 411-425.

Brighton Webs Ltd. (accessed 2007) *http://www.brighton-webs.co.uk/*.

Brohan, P., Kennedy, J.J., Haris, I., Tett, S.F.B., Jones, P.D. (2006) Uncertainty estimates in regional and global observed temperature changes: a new dataset from 1850. *J. Geophysical Research*, Vol. 111.

Briggs, H., Sinha, R.P. (1933) Expansion and contraction of coal caused respectively by the sorption and discharge of gas. *Proc. Royal Soc. Edinburgh*, Vol. 53, pp. 48-53.

Briggs, A.R. (2001) Reserve Estimates for Naturally Fractured Reservoirs. *SPE 71037*, Rocky Mountain Petroleum Technology Conference held in Keystone, Colorado, 21-23 May.

Brown, K., Casey, D.A., Enever, J.R., Facer, R.A., Wright K. (1996) New South Wales Coal Seam Methane Potential, *Facer and Wright*, U.S.A.

Busch, A., Gensterblum, Y., Krooss, B.M. (2003) Methane and CO2 sorption and desorption measurements on dry Argonne Premium Coals: pure components and mixtures. *International Journal of Coal Geology*, Vol. 55, pp. 205-224.

Busch, A., Gensterblum, Y., Krooss, B.M., Siemons, N. (2006) Investigation of high-pressure selective adsorption/desorption behaviour of CO_2 and CH_4 on coals: An experimental study. *International Journal of Coal Geology*, Vol. 66, pp. 53-68.

Bustin, R.M., Clarkson, C.R. (1998) Geological controls on coalbed methane reservoir capacity and gas content. *International Journal of Coal Geology*. Vol. 38, pp. 3-26.

Buzkan, I. (1987) Petrological evaluation of the coals of the Kozlu Formation in the Karadon region of Zonguldak area (in Turkish). *Ph.D. Thesis,* Istanbul Technical University, Turkey, 115 p.

Byer, C.W., Malone, R.D., Hunt, A.E. (1982) Preliminary Resource Assessment of Coalbed Methane in the U.S. *SPE/DOE 10799, presented at the Unconventional Gas Recovery Symposium*, Pittsburgh, Pennsylvania, 16-18 May.

Byrer, C.W., Guthrie, H.D. (1998) Carbon Dioxide Storage Potential in Coalbeds: A Near-Term Consideration for the Fossil Energy Industry. *In Proceedings of the 23rd International Conference on Coal Utilization & Fuel Systems*, Clearwater, FL, pp. 593-600.

Canteck (1988) Measurements of Methane Conditions in the Coal Mines of Kozlu, Armutcuk, and Karadon Areas of the Zonguldak Coalfield, Turkey. *Canteck Consulting Limited*, Calgary, Alberta, Canada.

Capen, E.C. (1999) Probabilistic Reserves! Here at Last? *SPE 73828*, *Reservoir Evaluation & Engineering*, Vol. 4, No. 5, pp. 387-394.

Ceglarska, S.G., Zarebska, K. (2002) The competitive sorption of CO2 and CH4 with regard to the release of methane from coal. *Fuel Process Technology*, Vol. 72-78, pp. 423-429.

Cervik, J. (1967) Behavior of Coal-Gas Reservoirs, *SPE 1973*, *Annual Eastern Regional Meeting*, Pittsburgh, Pennsylvania, 2-3 November.

Chaback, J.J., Morgan, D., Yee, D. (1996) Sorption Irreversibilities and Mixture Compositional Behavior during Enhanced Coal Bed Methane Recovery Processes. *SPE 35622*, *presented at the Gas Technology Conference*, Calgary, Alberta, Canada, 28 April – 1 May.

Chase, R.W. (1980) Degasification of Coal Seams via Vertical Boreholes: A Field and Computer Simulation Study. *Ph.D. Dissertation*, Pennsylvania State University, PA.

Chen, J.C. (1987) A Two-Dimensional, Two-Phase Simulation Model for Coalbed Methane Recovery. *M.Sc. Thesis*, University of Alabama.

Clarkson, C.R., Bustin, R.M. (1997) The effect of methane gas concentration, coal composition and pore structure upon gas transport in Canadian coals: implications for reservoir characterization. *International Coalbed Methane Symposium*, University of Alabama, Tuscaloosa, Al, USA, May 12-16.

Clarkson, C.R., Bustin, R.M. (1999) The effect of pore structure and gas pressure upon the transport properties of coal: a laboratory an modeling study. 2.Adsorption rate modeling. *Fuel*, Vol. 78, pp. 1345-1362.

Clayton, J.L. (1998) Geochemistry of Coalbed Gas - A Review. *Int. Journal of Coal Geology,* Vol. 35, pp. 159-173.

Crank, J. (1956) Mathematics of Diffusion. *Clarendon Press.*, Oxford.

Croiset, E, Thambimuthu, K.V. (1998) Coal combustion with flue gas recirculation for CO_2 recovery. *Fourth International Conference on Greenhouse gas Control Technologies*, Interlaken, Switzerland.

Crosdale, P., Beamish, B. (1993) Maceral effects on methane sorption by coal. In: Beston, J.W. (Ed.), New Developments in Coal Geology, *Symposium*, Brisbane, pp. 95-98.

Crosdale, P.J., Beamish, B.B., Valix, M. (1998) Coalbed methane sorption related to coal composition. *International Journal of Coal Geology*. Vol. 35, pp. 147-158.

Cui, X., Bustin, R.M., Dipple, G. (2004) Selective transport of CO_2, CH_4, and N_2 in coals: Insights from modeling of experimental gas adsorption data. *Fuel,* Vol. 83, pp. 293-303.

Dabbous, M.K. et al. (1976) Gas-Water Capillary Pressure in Coal at Various Overburden Pressures. *Society of Petroleum Engineers Journal,* pp. 261-268.

Darcy, H. (1856) Les Fontaines Publiques de la Ville de Dijon. Dalmont, Paris.

DeSwaan, A.O. (1976) Analytical Solutions for Determining Naturally Fractured Reservoir Properties by Well Testing. *SPE 5346*, *SPE Journal*, Vol. 16, No. 3, pp. 117-122.

Diamond, W.P., LaScola, J.C., Hyman, D.M. (1986) Results of Direct Method Determination of the Gas Content of U. S. Coalbeds. *Report No. IC 9067*, U.S. Department of Interior, Bureau of Mines: Washington, DC.

Dryden, I.G.C. (1963) In Chemistry of Coal Utilization; Lowry, H.H., (ed.); *Wiley*: New York; pp. 232-295.

Dubinin, M.M. (1960) The potential theory of adsorption of gases and vapors. for adsorbents with energetically nonuniform surface. *Chem. Rev.*, Vol. 60, pp. 235-241

Eddy, G.E., Rightmire, C.T., Byren, C.W. (1982) Relationship of methane content of coal rank and depth: theoretical vs. observed. *Society of Petroleum Engineers, Department of Interior, Proceedings, Unconventional Gas Symposium*, Pittsburgh, PA, SPE/DOE 10800, pp. 117-122.

Engelder, T., Geiser, P. (1980) On the Use of Regional Joint Sets as Trajectories of Paleostress Fields During Development of the Appalachian Plateau. *Journal of Geophysical Research*, Section B, Vol. 85, New York, pp. 6319-6341.

Ertekin, T., King, G.R., Schwerer, F.C. (1986) Dynamic Gas Slippage: A Unique Dual-Mechanism Approach to the Flow of Gas in Tight Formations. *SPE Formation Evaluation, SPE 12045.*

Ertekin, T., Sung, W. (1986) Production Performance Analysis of Horizontal Drainage Wells for the Degasification of Coal Seams. *SPE 15453, Ann. Tech. Conf. And Exhibition,* New Orleans, LA, 5-8 October.

Ettinger, I., Eremin, I., Zimakov, B., Yanovskaya, M. (1966) Natural factors influencing coal sorption properties: I. Petrography and the sorption properties of coals. *Fuel*, Vol. 45, pp. 267-275.

Every, R.L., Dell'osso, L., Jr. (1972) CIM Bull., pp. 143-150.

Elektrik Üretim Anonim Şirketi, EÜAŞ (Electricity Production Company) (accessed 2007) *http://www.euas.gov.tr.*

Faiz, M.M., Aziz, N.I., Hutton, A.C., Jones, B.G. (1992) Porosity and gas sorption capacity of some eastern Australian coals in relation to coal rank and composition. *Coalbed Methane Symposium*, Townsville, pp. 9-15.

Faiz, M.M., Hutton, A.C. (1995) Geological controls on the distribution of CH_4 and CO_2 in coal seams of the southern coalfield, NSW, Australia. *International Symposium cm Workshop on Management and Control of High Gas Emissions and Outbursts*, Wollongong, pp. 375-383.

Fick, A (1855) *Ann. Physik*, Vol. 59, pp. 170.

Fievez, P., Mostade, M. (1998) Underground coal gasification (UCG)-coal bed methane recovery (CBM)-CO_2 sequestration in coal seam. *European Study Committee for Revaluation and Chemical Valorisation of Coal*, Symposium at the European Parliament.

Forrest, A.G. (1985) Oil and Gas Reserves Classification, Estimation, and Evaluation. *Journal of Petroleum Technology.*

Forrester, S.D., Giles, C.H. (1971) The origins of the surface film balance. *Chem. & Ind.*, 831.

Fyfe, W.S., Leveille, R., Zang, W., Chen, Y. (1996) Is CO_2 disposal possible?, *ACS Div. Fuel Chem. Preprints*, Vol. 41, 212th National Meeting, Orlando, FL, USA, pp. 1433-1435.

Fylling, A. (2002) Quantification of Petrophysical Uncertainty and Its Effect on In-Place Volume Estimates: Numerous Challenges and Some Solutions. *SPE 77637, Ann. Tech. Conference and Exhibition*, San Antonio, Texas, 29 September-2 October.

Fujioka, Y., Ozaki, M., Takeuchi, K., Shindo, Y., Herzog, H.J. (1997) Cost comparisons of various carbon dioxide ocean disposal options. *Energy Convers. Mgmt.*, Vol. 38, pp. 273-277.

Gale, J., Freund, P. (2001) Coal-bed Methane Enhancement with CO_2 Sequestration Worldwide Potential. *Environmental Geosciences*, Vol. 8, pp.210-217.

Gamson, P.D., Beamish, B.B., Johnson, D.P. (1993) Coal microstructure and micropermeability and their effects on natural gas recovery. *Fuel,* Vol. 72, pp. 87-99.

Gamson, P.D. (1994) Sorption behaviour and microstructure of coals, the effect of secondary mineralisation and the prospects for its removal. Coalbed Methane Extraction. *An Analysis of UK and European Resources and Potential for Development. IBC Technical Services*, London, 26 pp.

Gamson, P.D., Beamish, B., Johnson, D. (1996) Coal microstructure and secondary mineralization; their effect on methane recovery. Coalbed methane and coal geology., Gayer, R., Harris, I. (Eds.) *Geological Society of London*, London, U.K., pp. 165-179.

Gash, B.W. (1991) Measurement of Rock Properties in Coal for Coalbed Methane Production. *SPE 22909, Annual Tech. Conf. and Exhibition*, Dallas, Texas, 6-9 October.

Gash, B.W., Volz, R.F., Potter, G., Corgan, J.M. (1993) The Effects of Cleat Orientation and Confining Pressure on Cleat Porosity, Permeability, and Relative Permeability. *SPE 9321*, *Journal of Petroleum Technology*, Vol. 34, No. 3, pp. 635-644.

Gan, H., Nandi, S.P., Walker, P.L., Jr. (1972) Nature of the Porosity in American Coals. *Fuel*, Vol. 51, pp. 272-277.

Grimston, M.C., Karakoussis, V., Fouquet, R., van der Vorst, R., Pearson, P., Leach, M. (2001) The European and global potential of carbon dioxide sequestration in tackling climate change. *Climate Policy*, Vol. 1, pp. 155-171.

Gentzis, T. (2000) Subsurface sequestration of carbon dioxide — an overview from an Alberta (Canada) perspective. *International Journal of Coal Geology*, Vol. 43, pp. 287-305.

Gilman, J.R., Kazemi, H. (1983) Improvements in simulation of naturally fractured reservoirs. *SPE 10511*, *SPE Journal*, Vol. 23, No. 4, pp. 695-707.

Gray, I. (1987) Reservoir Engineering in Coal Seams: Part 1—The Physical Process of Gas Storage and Movement in Coal Seams. *SPE Reservoir Engineering,* pp. 28-34.

Greenstone, M.H. (2002) Greenhouse Gas Mitigation: The Biology of Carbon Sequestration. Bioscience, Vol. 52, No 4, pp. 323.

Gunter, W.D., Gentzis, T., Rottenfusser, B.A., Richardson, R.J.H. (1997) Deep coalbed methane in Alberta, Canada: a fossil fuel resource with the potential of zero greenhouse gas emissions. *Energy Convers. Mgmt.*, Vol. 38, pp. 217-222.

Gunter, W.D., Wong, S., Cheel, D.B., Sjostrom, G. (1998) Large CO_2 Sinks: Their role in the mitigation of greenhouse gases from an international, national (Canadian) and provincial (Alberta) perspective. *Applied Energy*, Vol. 61, pp. 209-227.

Gurdal, G. (1998) The controlling parameters of gas storage in coals of the Zonguldak basin (in Turkish). *Ph.D. Thesis*, Istanbul Technical University, Turkey, 237 p.

Hall, F.E., Zhou, C., Gasem, K.A.M. (1994) Adsorption of Pure Methane, Nitrogen, and Carbon Dioxide and Their Binary Mixtures on Wet Fruitland

Coal. *In Proceedings of the Eastern Regional Conference & Exhibition of the Society of Petroleum Engineers, SPE 29194,* Charleston, WV, pp. 329-344.

Harpalani, S. Pariti, U.M. (1993) Study of Coal Sorption Isotherms Using a Multicomponent Gas Mixture. *SPE 9356, presented at the 1993 International Coalbed Methane Symposium,* The University of Alabama, Tuscaloosa, Vol. 1, pp. 151-160.

Harpalani, S., Chen, G. (1993) Gas Slippage and Matrix Shrinkage Effects on Coal Permeability. *Presented at the 1993 International Coalbed Methane Symposium,* The University of Alabama, Tuscaloosa, Vol. 1, pp. 285-294.

Hendriks, C.A., Blok, K. (1993) Underground storage of carbon dioxide. *Energy Convers. Mgmt.,* Vol. 34, pp. 949-957.

Hendriks, C.A. (1994) Carbon dioxide removal from coal-fired power plants. *Ph.D. Thesis,* Department of Science, Technology and Society, Utrecht University, Utrecht, The Netherlands.

Herzog, H.J., Drake, E., Adams, E. (1997) Carbon Dioxide Capture, Reuse and Storage Technologies for Mitigating Global Climate Change. *DE-AF22-96PC01257,* Massachusetts Institute of Technology, USA.

Herzog H. (1998) Understanding sequestration as a means of carbon management. *US DOE workshop on Carbon Sequestration at MIT,* Boston.

Hitchon, B., Gunter, W.D., Gentzis, T., Bailey, R.T. (1999) Sedimentary basins and greenhouse gases, a serendipitous association. *Energy Convers. Mgmt.,* Vol. 40, pp. 825-843.

Hoch, O. (2005) The Dry Coal Anomaly – The Horseshoe Canyon Formation of Alberta, Canada. *SPE 95872, presented at the Ann. Tech. Conf. and Exhibition,* Dallas, Texas, 9-12 October.

Holditch, S.A. (1983) SUGARWAT, User's Guide and Documentation. *DOE contract number DE-AC21-82MC-19239.*

Holloway, S., Savage, D. (1993) The potential for aquifer disposal of carbon dioxide in the UK. *Energy Convers. Mgmt.,* Vol. 34, pp. 925-932.

Hosgormez, H., Mann, U., Yalcin, M.N., Schaefer, R.G. (1998) Total yield and composition of hydrocarbon gases in the coal bearing units of the

Zonguldak basin. *Proceedings of the 12th International Petroleum Congress and Exhibition of Turkey,* pp. 320-328.

IEA (1995) Carbon dioxide utilisation. *Greenhouse Gas R&D Programme report.* Stoke Orchard, Cheltenham.

IEA (1996) CO2 capture and storage in the Natuna NG project. *Greenhouse Issues, Greenhouse Gas R&D Programme*, Stoke Orchard, Cheltenham.

IEA (2000) CO2 Emissions From Fuel Combustion 1971-1998. *International Energy Agency*, Paris.

IPCC (2000) Special Report on Land Use, Land-Use Change And Forestry. *Cambridge University Press*, Cambridge.

IPCC (2007) Climate Change 2007: The Physical Science Basis. Contribution of Working Group I to the Fourth Assessment Report of the Intergovernmental Panel on Climate Change.

IUPAC (1994) International Union of Pure and Applied Chemistry, *Pure Appl Chem*, Vol. 66, pp. 1739.

Jalali, J. (2004) A Coalbed Methane Simulator Designed for the Independent Producers. *M.Sc. Thesis*, University of West Virginia, Morgantown, U.S.

Jeu, S.J., Logan, T.L., McBane, R.A. (1988) Exploitation of Deeply Buried Coalbed Methane Usin Different H draulic Fracturing Techniques in the PIceance Basin, Colors! o and San J'uan Basin New Mexico. *SPE 18253, Ann. Tech. Conf. And Exhibition,* Houston, TX, 2-5 October.

Jikich, S.A., Bromhal, G.S., Sams, W.N., Gorucu, F.B., Ertekin, T, Smith, D.H. (2004) Economics for Enhanced Coalbed Methane (ECBM) and CO2 Sequestration with Horizontal Wells. *SPE 91391, Eastern Regional Meeting*, Charleston, WV, 15-17 September.

Joubert, J.I., Grein, C.T., Beinstock, D. (1973) Sorption of Methane in Moist Coal. *Fuel*, Vol. 52, pp. 181-185.

Karacan, C.O. (1998) Modeling of sorption and investigation of flow mechanisms of coalbed gas. *Ph.D. Thesis*, METU, Turkey.

Karacan, C.O., Okandan, E. (1999) Heterogeneity effects on the storage and production of gas from coal seams. *SPE 56551*, presented at the 1999 SPE Ann. Tech. Conf. and Exhibition, Houston, Texas, 3-6 October.

Karayigit, A.I. (1989) Petrographic features of the Zonguldak and Amasra coals (in Turkish). *Ph.D. Thesis,* Hacettepe University, Ankara, Turkey, 315 p.

Kelafant, J.R., Stevens, S.H., Boyer, I.I., Charles, M. (1992) Coalbed gas-2: vast resource potential exists in many countries. *Oil and Gas Journal*, pp. 80-85.

Kendall, P.F., Briggs, H. (1933) The Formation of Rock Joints and the Cleat of Coal. *Proceedings*, Royal Society of Edinburgh, Vol. 53, pp. 164-187.

Kerey, I.E. (1982) Stratigraphical and sedimentological studies of Upper Carbeniferous rocks in northwestern Turkey. *Ph.D. Thesis,* University of Keele, Staffordshire, England, 238 p.

Kerey, I.E. (1985) Facies and tectonic setting of the Upper Cretaceous rocks of northwestern Turkey, in Dixon, J.E., Robertson, A.H.F. (eds.) The geological evolution of the eastern Mediterranean. *Geologic Society Special Publication,* Vol. 17, pp. 123-128.

Kidd, J.T., Camp, B.S., Lottman, L.K., Osborne, T.E., Saulsberry, J.L., Smith, J.L., Steidl, P.F., Stubbs, P.B. (1992) Geologic Manual for the Evaluation and Development of Coalbed Methane. *Gas Research Institute Topical Report No. GRI-91/0110*, Chicago, Illinois.

Kim, A.G. (1977) Estimating methane content of bituminous coalbeds from adsorption data. *US Bureau of Mines Report of Investigations 8245*, 22 pp.

King, G.R., Ertekin, T., Schwerer, F.C. (1986) Numerical Simulation of the Transient Behavior of Coal Seam Degasification Wells. *SPE 12258, SPE Formation Evaluation.*

King, G.R., Ertekin, T. (1988) Comparative Evaluation of Vertical and Horizontal Drainage Wells for the Degasification of Coal Seams. *SPE 13091, SPE Reservoir Engineering*, Vol. 24, No. 2, pp. 720-734.

King, G.R., Ertekin, T. (1989a) A survey of mathematical models related to methane production from coal seams, part 1: empirical and equilibrium sorption model. *Coalbed Methane Symposium,* University of Alabama, Tuscaloosa.

King, G.R., Ertekin, T. (1989b) A survey of mathematical models related to methane production from coal seams, part 2: Non-equilibrium sorption models. *Coalbed Methane Symposium*, University of Alabama, Tuscaloosa.

Klinkenberg, L.J. (1941) The Permeability of Porous Media to Liquids and Gases. *Drill. and Prod. Prac.,* API, pp. 200-213.

Koide, H.G., Tazaki, Y., Noguchi, Y., Iijima, M., Ito, K., Shindo, Y. (1993a) Underground storage of carbon dioxide in depleted natural gas reservoirs and useless aquifers. *Engineering Geology*, Vol. 34, pp. 175-179.

Koide, H.G., Tazaki, Y., Noguchi, Y., Iijima, M., Ito, K., Shindo, Y. (1993b) Carbon dioxide injection into useless aquifers and recovery of natural gas dissolved in fossil water. *Energy Convers. Mgmt.*, Vol. 34, pp. 921-924.

Kolesar, J.E. (1985) In-Situ Characterization Strategies for Coalbed Methane Reservoirs. *M.Sc. Thesis,* Pennsylvania State University.

Kolesar, J.E., Ertekin, T. (1986) The Unsteady-State Nature of Sorption and Diffusion Phenomena in the Micropore Structure of Coal. *SPE 15233, Unconventional Gas Technology Symposium,* Louisville, 18-21 May.

Kolesar, J.E., Ertekin, T., Obut, S.T. (1990) The Unsteady-State Nature of Sorption and Diffusion Phenomena in the Micropore Structure of Coal: Part 1 – Theory and Matheatical Formulation. *SPE Formation Evaluation*, pp. 81-88.

Kovalev, Y.M., Kuznetsov, S.V. (1974) Filtration of Gas in a Coal Seam Being Worked in the Presence of Diffusion Desorption. *Fiziko-Tekhnicheskie Problemy Razrabotke Polezbykh Iskopaemykh,* No. 6, pp. 74-77. Translated from Russian.

Knudsen, M. (1909) The Laws of Molecular and Viscous Flow of Gases Through Tubes. *Ann. Physik,* Vol. 28, pp. 75-177.

Krooss, B.M., van Bergen, F., Gensterblum, Y., Siemons, N., Pagnier, H.J.M., David, P. (2001) High-pressure methane and carbon dioxide sorption on dry and moisture-equilibrated Pennsylvanian coals. *Int. J. Coal Geol.*, Vol. 51, pp. 69-92.

Kucuk, F., Sawer, W.K. (1980) Transient Flow in Naturally Fractured Reservoirs and Its Application to Devonian Gas Shales. *SPE 9397, Ann. Tech. Conf. and Exhibition*, Dallas, Texas, 21-24 September.

Kundt, A., Warburg, E. (1875) Ueber Reibung und Waermeleitung verduennter Gase. *Ann. Physik.*, Poggendorf, Vol. 155, pp. 337-365.

Kuuskraa, V.A., Boyer, I.I., Charles, M., Kelafant, J.A. (1992) Coalbed gas-1: hunt for quality basins goes abroad. *OGJ Special, Oil and Gas Journal*, pp. 49-54.

Lama, R.D., Bartosiewicz, H. (1982) Determination of gas content of coal seams, Hargraves, A.J. (ed.) Seam gas drainage with particular reference to the working seam. *The Australian Institute of mining and metallurgy*, Illawara Branch, University of Wollongong, pp. 36-52

Lamberson, M.N., Bustin, R.M. (1993) Coalbed methane characteristics of Gates Formation coals, Northeastern British Columbia: effect of maceral composition. *AAPG Bulletin*, Vol. 77, pp. 2062–2076.

Langmuir, I. (1916) The Evaporation, Condensation and Reflection of Molecules and the Mechanism of Adsorption. *J. Am. Chem. Soc.*, Vol. 38, 2221.

Law, B.E. (1993) The Relationship Between Coal Rank and Cleat Spacing: Implications for the Prediction of Permeability in Coal. *Presented at the International Coalbed Methane Symposium*, The University of Alabama, Tuscaloosa, Vol. 2, pp. 435-441.

Law, D.H.-S., Meer, L.G.H.v.d., Gunter, Gunter, W.D. (2002) Numerical simulator comparison study for enhanced coalbed methane recovery processes, part 1: pure carbon dioxide injection. *SPE 75669, Gas Technology Symposium*, Calgary, Alberta, Canada, 30 April – 2 May.

Laxminarayana, L., Crosdale, P.J. (1999) Role of coal type and rank on methane sorption characteristics of Bowen Basin, Australia coals. *International Journal of Coal Geology*, Vol. 40, pp. 309-325.

Laxminarayana, L., Crosdale, P.J. (2002) Controls on methane sorption capacity of Indian coals. *AAPG Bulletin,* Vol. 86, pp. 201-212.

Levine, J.R. (1993) Introduction to Coal Petrology with Applications to Coalbed Methane R & D. *Short Course presented at the 1993 International Coalbed Methane Symposium*, The University of Alabama, Tuscaloosa.

Levy, H.J., Day, S.J., Killingley, J.S. (1997) Methane capacities of Bowen Basin coals related to coal properties. Fuel, Vol. 76, pp. 813-819.

Lidine, G.D et al. (1964) Control of Methane in Coal Mines. *Israel Program for Scientific Translation,* Jerusalem, Israel. Translated from Russian.

Macary, S.M., Hassan, A. (1999) Better Understanding of Reservoir Statistics is the Key for Reliable Monte Carlo Simulation. *SPE 53264, Middle East Oil Show and Conference*, Bahrain, 20-23 February.

Mahajan, O.P. in Carr, C. Jr.(ed) (1978) Analytical Methods for Coal and Coal Products. *Academic Press*, Vol. 1, pp. 125-162.

Mahajan, O.P. (1991) CO_2 surface area of coals: the 25-year paradox. *Carbon*, Vol. 29, pp. 735-742.

Manik, J. (1999) Compositional modeling of enhanced coalbed methane recovery. *M.Sc. Thesis*, Pennsylvania State University.

Manik, J., Ertekin, T., Kohler, T.E. (2002) Development and validation of a compositional coalbed simulator. *JCPT*, Vol.41.

Mazumder, S., Plug, W.J., Bruining, H. (2003) Capillary pressure and wettability behavior of coal-water-carbon dioxide system. *SPE Annual Technical Conference and Exhibition,* Denver, Colorado, U.S.A.

McFall, K.S. et al. (1987) An Analysis of the Coal and Coalbed Methane Resources of the Piceance Basin, Colorado. *SPE 16418, Journal of Petroleum Technology,* Vol. 40, No. 6, pp. 740-748.

McGarry, D.E. (2000) Challenges in assessment, management and development of coalbed methane resources in the Powder River Basin, Wyoming: in Sakkestad, B. (ed.) The Proceeding of the 25th. *International Technical Conference on Coal Utilization and Fuel Systems*, pp. 709-720.

McGuffie, K. & Sellers A.H. (2005) A Climate Modeling Primer. *John Wiley and Sons*, 3rd Edition.

McLennan, J.D., Schafer, P.S., Pratt, T.J. (1995) A Guide to Determining Coalbed Gas Content. *Gas Research Institute Report No. GRI-94/0396*, Chicago, Illinois.

Meehl, G.A., Washington, W.M., Collins, W.D., Arblaster, J.M., Hu, A., Buja, L.E., Strand, W.G., Teng, H. (2005) How Much More Global Warming and Seal Level Rise? Science, Vol. 307, pp. 1769-1772.

Mendenhall, W., Sincich, T. (1996) A Second Course in Statistics, Regression Analysis. *Prentice-Hall Inc*, New Jersey, pp. 2-34.

Moffat, D.H., Weale, K.E. (1955) Sorption by coal of methane at high-pressures. *Fuel*, Vol. 34, pp. 449-462.

Mohaghegh, S., Ertekin, T. (1991) A Type-Curve Solution for Coal Seam Degasification Wells Producing Under Two Phase Flow Conditions. *SPE 22673, Ann. Tech. Conf. and Exhibition,* Dallas, TX, 6-9 October.

Moritis, G. (1996) New technology, Improved economics boost EOR hopes. *Oil and Gas Journal*, pp. 39-61.

M.T.A. (1992a) Zonguldak-Değirmenağzı ile Gobu Arasındaki Alanın Jeolojisi ve Kömür Varlığı. *Enerji Hammadde Etüt ve Arama Dairesi Başkanlğı*, Vol. 1, Ankara, Turkey.

M.T.A. (1992b) Elartin-Amasra Taşkömür Havzası Jeoloji Raporu. *Enerji Hammadde Etüt ve Arama Dairesi Başkanlığı*, Vol. 1, Ankara, Turkey.

M.T.A. (1994) Batı Karadeniz Karbonifer Havzası Hakkında Bilgi, *Batı Karadeniz Bolge Müdürlüğü*, Zonguldak, Turkey.

Murray, D.K. (1991) Coal bed methane; natural gas resources from coal seams. *In: Peters, D.C. (Ed.), Geology in Coal Resource Utilization, Tech Books*, United States, pp. 97-103.

Murray, D.K. (1994) Technology development in western North America can enhance the worldwide potential of coalbed gas. *Technology in the 90s-Prospering in a Changing Environment,* Calgary, Alberta, Canada, pp. 90-103.

Murtha, J.A. (2001) Using Pseudocases to Interpret P10 for Reserves, NPV, and Production Forecasts. *SPE 71789, Hydrocarbon Economics and Evaluation Symposium,* Dallas, Texas, 2-3 April.

National Oceanic & Atmospheric Administration (NOAA), Trends in Carbon Dioxide (accessed 2007) *http://www.esrl.noaa.gov/gmd/ccgg/trends/*.

Newendorp, P.D., Schuyler, J.R. (2000) Decision Analysis for Petroleum Exploration. *Planning Press TM*, Aurora, USA, pp. 248-283.

NIST/SEMATECH e-Handbook of Statistical Methods (accessed 2007) *http://www.itl.nist.gov/div898/handbook/*.

Nguyen, D.N., Allinson, W.G. (2002) The economics of CO2 capture and geological storage. *SPE 77810, Asia Pacific Oil and Gas Conference and Exhibition*, Melbourne, Australia, 8-10 October.

Nodzenski, A. (1998) Sorption and desorption of gases (CH_4, CO_2) on hard coal and active carbon at elevated pressures. *Fuel*, Vol. 77, pp. 1243-1246.

Okay, I.A.C. (1939) Petrographische und chemisch-technologische Untersuchung der Turkischen Steinkohle von Zonguldak (Floze Buyuk and Sulu): *Revue de la Faculte des Sciences de l'Universite d'Istanbul*, Vol. 4, pp. 1-17.

Okay, A.I. (1989) Tectonic units and sutures in the Pontides, northern Turkey, in Sengor A.M.C (ed.) Tectonic evolution of the Tethyan region. *NATO Advanced Study Institute (ASI) Series*, Vol. 259, pp. 109-116.

Onsager, P.R., Cox, D.O. (2000) Aquifer Controls on Coalbed Methane Development in the Powder River Basin, Wyoming. *SPE 63090, Ann. Tech. Conf. And Exhibition,* Dallas, TX, 1-4 October.

Orhan, E. (1995) General geology of Zonguldak hard coal basin and stratigraphy of the Kozlu K20/G Well, in Zonguldak Basin Research Wells 1, Kozlu K20/G. *Special publication of TUBITAK,* Marmara Research Center, 217 p.

Pacala, S. & Socolow, R. (2004) Stabilization Wedges: Solving the Climate Problem for the Next 50 Years with Current Technologies. *Science,* Vol. 305, pp. 968-972.

Palmer, I., Mansoori, J. (1996) How permeability depends on stress and pore pressure in coalbeds: a new model. *SPE 36737, Ann. Tech. Conf. and Exhibition*, Denver, Colorado, 6-9 October.

Parkash, S., Chakrabartty, S. K. (1986) Microporosity in Alberta Plains Coals. *International Journal of Coal Geology*, Vol. 6, pp. 55-70.

Parr, S.W. (1928) The Classification of Coal. *Bulletin No. 180*, Engineering Experiment Station, University of Illinois.

Paul, G.W., Sawyer, W.K., Dean, R.H. (1990) Validation of 3D Coalbed Simulators. *SPE 20733, Ann. Tech. Conf. And Exhibition,* New Orleans, LA, 23-26 September.

Penny, G.S., Conway, M.W. (1993) Coordinated Studies in Support of Hydraulic Fracturing of Coalbed Methane. *Gas Research Institute Annual Report No. GRI-93/0125*, Chicago, Illinois.

Price, H.S., Ancell, K.L. (1978) The Feasibility of Methane from Coal. *Methane Gas from Coalbeds – Development, Production, and Utilization,* MERC/SP-78/1, pp. 37-73.

Prinz, D., Pyckhout-Hintzen, W., Krooss, B., Littke, R. (2001) Investigations on the micro- and mesoporous structure of coals of varying rank: a combined small angle neutron scattering (SANS) and gas adsorption experiments study. *Proceedings, International Coalbed Methane Symposium,* Tuscaloosa, Alabama.

Prinz, D., (2004) Die Porenstruktur von Kohle (The pore structure of coals). *Dissertation*, RWTH Aachen University. 164 pp.

Puri, R., Yee, D. (1990) Enhanced Coalbed Methane Production. *SPE Paper 20732*, pp. 193-202.

Puri, R., Evanoff, J.C., Brugler, M.L. (1991) Measurement of coal cleat porosity and relative permeability characteristics. *Proc. Gas Tech. Symp.*, TX, U.S., pp. 93-104.

Reeves, S.R., Schoeling, L. (2000) Geological sequestration of CO_2 in coal seams: reservoir mechanisms field performance, and economics. In: Williams, D., Durie, B., McMullan, P., Paulson, C., Smith, A. (Eds.). *Proceedings of the Fifth International Conference on Greenhouse Control Technologies*, Cairns (Australia), pp. 593-598.

Reeves, S.R., Pekot, L. (2001) Advanced Reservoir Modeling in Desorption Controlled Reservoirs. *SPE 71090, Rocky Mountain Petroleum Tech. Conf.,* Keystone, Colorado, 21-23 May.

Reeves, S. 2002. Coal-Seq project update: Field studies of ECBM recovery/CO_2 sequestration in coalseams. *Proceedings of the Japan International Workshop on the Present Status and Perspective of CO_2 Sequestration in Coal Seam*, Tokyo, Japan, pp. 87-92.

Remner, D.J., Ertekin, T., Sung, W., King, G.R. (1986) A Parametric of Coal Seam Study of the Effects Properties on Gas Drainage Efficiency. *SPE 13366, SPE Reservoir Engineering.*

Reznik, A.A. et al. (1974) Air-Water Relative Permeability of Pittsburgh and Pocahontas Coals. *Society of Petroleum Engineers Journal,* pp. 556-562.

Rice, D.D., Law, B.E., Clayton, J.L. (1993) Coal-bed gas-an undeveloped resource. In: The future of energy gases. *US Geological Survey Professional Paper No. 1570.* Washington, DC: United States Government Printing Office, pp. 389-404.

Ribeiro, J., Henry, B. (1995) Carbon dioxide disposal and storage technologies. European commission joint research centre, institute for prospective technological studies. *Report prepared for the Directorate General for Energy (DG XVII) of the European Commission.*

Rice, D.D., Law, B.E., Clayton, J.L. (1993) Coalbed Gas: An Undeveloped Resource in the Future of Energy Gases. *U.S. Geological Survey Professional Paper No. 1570*, U. S. Government Printing Office: Washington, DC, pp 389-404.

Rightmire, C.T., Eddy, G.E., Kirr, J.N. (ed.) (1984) Coalbed Methane Resources of the United States: Studies in Geology Series 17, *AAPG*, Tulsa, Oklahoma pp. 1-12.

Rike Service Inc. (1990) Statistics and Probability. *Rike Service Inc.*, course manual, New Orleans, Louisiana.

Roadifer, R.D., Moore, T.R., Raterman, K.T., Farnan, R.A., Crabtree, B.J. (2003) Coalbed Methane Parametric Study: What's Really Important to Production and When? *SPE 84425, Ann. Tech. Conf. and Exhibition,* Denver, Colorado, 5-8 October.

Rohde A.R., Global Warming Art (accessed 2007) *http://www.globalwarmingart.com.*

Ross, J.G. (1998) The Philosophy of Reserve Estimation. *SPE 37960, Hydrocarbon Economics and Evaluation Symposium,* Dallas, Texas, 16-18 March.

Rouquerol, F., Rouquerol J., Sing K. (1999) Adsorption by Powders and Porous Solids: Principles, Methodology and Applications. Elsevier.

Ryan, B. (1992) An equation for estimation of maximum coalbed-methane resource potential: British Columbia Geological Survey, *Geological Fieldwork 1991*, *Paper 1992-1*, pp. 393-395.

Saulsberry, J.L., Schafer, P.S., Schraufnagel, R.A. (editors) (1996) A Guide to Coalbed Methane Reservoir Engineering. Gas Research Institute, Chicago, U.S.A.

Sawyer, W.K. (1982) Concepts and Applications in Modeling the Devonian Shale. *Unconventional Gas Recovery Simulation Workshop Technical Proceedings,* DOE/METC/83-45, UC-92, Morgantown, WV, pp. 53-61.

Schmidt, R.A. (1979) Coal in America: An Encyclopedia of Reserves, Production and Use. *McGraw-Hill*, USA.

Schuyler, J.R. (1998) Probabilistic Reserves Lead to More Accurate Assessments. *SPE 49032, Ann. Tech. Conf. and Exhibition,* New Orleans, Louisiana, 27-30 September.

Schwerer, F.C. (1984) Development of Coal-Gas Production Simulators and Mathematical Models for Well-Test Strategies. *Gas Research Institute Final Report No. GRI-84/0060*, Chicago, Illinois.

Scott, D.S., Dullien, F.A.L. (1962) Diffusion of ideal gases in capillaries and porous solids. AIChE Journal, Vol. 8, pp. 113-117.

Scott, A.R., Kaiser, W.R., Ayers Jr., W.B. (1994) Thermogenic and secondary biogenic gases, San Juan basin, Colorado and New Mexico—implications for coalbed gas producibility. *Am. Assoc. Pet. Geol. Bull.*, Vol. 78, pp. 1186-1209.

Seidle, J.P. (1991) Long Term Gas Deliverability of a Dewatered Coalbed. *SPE 21488, Journal of Petroleum Technology,* Vol. 45, No. 6, pp. 564-569.

Seidle, J.P., Jeansome, M.W., Erickson, D.J. Application of Matchstick Geometry to Stress Dependent Permeability in Coals. (1992) *SPE Paper 24361, Rocky Mountain Regional Meeting*, pp. 433-445.

Serpen, U., Alpkaya, E.N., Ozkan, E. (1998) Preliminary investigation of Coalbed Methane Potential of the Zonguldak Basin in Turkey, *SPE 39985, Gas Technology Symposium,* Calgary, Alberta, Canada, 15-18 March.

Sharkey, A.G., Jr, McCartney, J.T. in Elliott, M.A. (ed.) (1981) Physical Properties of Coal and Its Products. *Chemistry of Coal Utilization*, Second Supplementary Volume, John Wiley and Sons, New York, pp. 159-283.

Socolow, R.H. (editor) (1997) Fuels decarbonization and carbon sequestration. *Report of a Workshop by the Members of the Report Committee, PU/CEES Report No. 302*, Center for Energy and Environmental Studies, Princeton University Princeton, NJ.

Shi, J.Q., Durucan, S. (2003a) Gas storage and flow in coalbed reservoirs: implementation of a bidisperse pore model for gas diffusion in coal matrix. *SPE 84342, Ann. Tech. Conf. and Exhibition,* Denver, Colorado, 5-8 October.

Shi, J.Q., Durucan, S. (2003b) A bidisperse pore diffusion model for methane displacement desorption in coal by CO_2 injection. *Fuel,* Vol. 82, pp. 1219-1229.

Smith, J.W., Botz, R.W., Gould, K.W., Hart, G., Hunt, J.W., Rigby, D. (1984) Outburst and Gas Drainage Investigations. *Report No. EG/84/321*, Energy Research Development and Demonstration Program, Australia.

Smith, D.M, Williams, F.L. (1984) Diffusional Effects in the Recovery of Methane from Coalbeds. *Soc. Pet. Eng. J.*, pp. 529-535.

Spencer, S.J. et al. (1987) Numerical Simulation of Gas Drainage from Coal Seams. *SPE 16857, Ann. Tech. Conf. and Exhibition,* Dallas, Texas, 27-30 September.

Stach, E. et al. (1982) Stach's Textbook of Coal Petrology. Third Edition, Borntreager, Stuttgart, and Berlin.

Stanton, R., Flores, R., Warwick, P.D., Gluskoter, H. (2001) CO_2 sequestration in low rank coals. *Proceedings of the First National Conference on carbon Sequestration*, Washington, DC, USA.

Stevens, S.H., Kuuskraa, J.A., Schraufnagel, R.A. (1996) Technology spurs growth of U.S. coalbed methane. *Oil and Gas Journal,* Vol. 94, pp. 56-63.

Stevens, S.H., Riemer, P. (1998) Enhanced Coalbed Methane Recovery Using CO2 Injection: Worldwide Resource and CO2 Sequestration Potential. *SPE 48881, International Oil and Gas Conf. and Exhibition,* Beijing, China, 2-6 November.

Stevenson, M.D. (1997) *Ph.D. thesis*, University of New South Wales, Australia.

Sung, W., Ertekin, T. (1987) An Analysis of Field Development Strategies for Methane Production from Coal Seams. *SPE 16858, Ann. Tech. Conf. and Exhibition,* Dallas, TX, 27-30 September.

Thimons, E.D., Kissell, F.N. (1973) Diffusion of methane through coal. *Fuel*, Vol. 52, pp. 274.

Tissot, B.P., Welte, D.H. (1984) Petroleum Formation and Occurrence. *Springer-Verlag*, New York, NY.

Toda, Y. (1972) Application of mercury porosimetry to coal. *Fuel*, Vol. 51, pp. 108-112.

TTK (2003) Turkish Hard Coal Enterprise, Personal Communication with Department Manager Mr. Akın ÖREK, Zonguldak.

TNO-NITG (2003) Enhanced Coalbed Methane Production: combined methane production and CO_2 disposal. *Netherlands Institute of Applied Geoscience TNO – National Geological Survey.*

Tremain, C.M., Laubach, S.E., Whitehead III, N.H. (1991) Coal fracture (cleat) patterns in Upper Cretaceous Fruitland Formation, San Juan Basin, Colorado and New Mexico: implications for coalbed methane exploration and development. In: Scwochow, S., Murray, K.D., Fahy, M.E. (Eds.), Coalbed Methane of Western North America: Rocky Mountain. *Association of Geologists*, Denver, CO, pp. 49-59.

Turkenburg W.C (1997) Sustainable development, climate change, carbon dioxide removal (CDR). *Energy Convers. Mgmt.*, Vol. 38, pp. 3-12.

Unsworth, J.F., Fowler, C.S., Jones, L.F. (1989) Moisture in coal: 2. Maceral effects on pore structure. *Fuel*, Vol. 68, pp. 18-26.

Van Krevelen, D.W. (1961) Coal-Typology, Chemistry, Physics, Constitution. *American Elsevier*, New York.

Walker, P. L., Jr., Verma, S. K.; Rivera-Utrilla, J.; Davis, A. (1988) Densities, porosities and surface areas of coal macerals as measured by their interaction with gases, vapours and liquids. *Fuel*, Vol. 67, pp. 1615-1623.

Walstrom, J.E., Mueller, T.D., McFarlane, R.C. (1967) Evaluating Uncertainty in Engineering Calculations. *Journal of Petroleum Technology*.

Wanless, H.R., Shepard, F.P. (1936) Sea Level and Climatic Changes Related to Late Paleozoic Cycles. *Geological Society of America Bulletin,* Vol. 47, pp. 1177-1206.

Warren, J.E., Root, P.J. (1963) The Behavior of Naturally Fractured Reservoirs. *Society of Petroleum Engineers Journal*, pp. 245-255.

Watson, R.T., Zinyowera, M.C., Moss, R.H. (editors) (1996) Climate change 1995 - impacts, adaptations and mitigation of climate change: scientific-technical analyses. Contribution of working group II to the second assessment report of the Intergovernmental Panel on Climate Change. *Cambridge University Press*, Cambridge.

WEC/IIASA (1998) Global Energy Perspectives. *Cambridge University Press*, UK.

Wei, X.R., Wang, G.X., Massarotto, P. (2005) A Review on Recent Advances in the Numerical Simulation for Coalbed Methane Recovery Process. *SPE 93101, Asia Pacific Oil and Gas Conf. and Exhibition,* Jakarta, Indonesia, 5-7 April.

Williamson, I.A. (1967) Coal Mining Geology. *Oxford University Press*, London.

Wong, S., MacLeod, K., Wold, M., Gunter, W.D., Mavor, M.J., Gale, J. (2001) CO2-Enhanced Coalbed Methane Recovery Demonstration Pilot – A Case for Australia. *International Coalbed Methane Symposium*, Alabama.

Wright, I.W., Lee, A., Middleton, P., Lowe, C., Imbus, S.W., Miracca, I. (2004) CO2 Capture Project: Initial Results. *SPE 86602, International Conf. on Health,*

Safety, and Environment in Oil and Gas Exploration and Production, Calgary, Alberta, Canada, 29-31 March.

Wyckoff, R.D., Botset, H.D., Muskat, M, Reed, D.W. (1933) The Measurement of the Permeability of Porous Media for Homogeneous Fluids. *Review of Scientific Instruments,* Vol. 4, pp. 394-405.

Wong, S., Foy, C., Gunter, B., Jack, T. (1998) Injection of CO2 for enhanced gas recovery: Coalbed methane versus oil recovery. *Proceedings of the Fourth Int. conference on Greenhouse Gas Control technologies,* Interlaken, published by Elsevier Science, pp. 175-180.

Yalcin, M.N. (1991) Geology and coal occurrences of Zonguldak basin as a potential source for coalbed methane. *AAPG Bulletin,* Vol. 75, pp. 697.

Yalcin, E., Durucan S. (1991a) Methane Desorption Characteristics of Zonguldak Coal. *Mining Science and Technology*, Vol. 13, pp. 207-214.

Yalcin, E., Durucan S (1991b) Methane Capacities of Zonguldak Coals and the Factors Affecting Methane Adsorption. *Mining Science and Technology*, Vol. 13, pp. 215-222.

Yalcin, M.N., Schenk, H.J., Schaefer, R.G. (1994) Modeling of gas generation in coals of the Zonguldak basin (NW Turkey). *International Journal of Coal Geology,* Vol. 25, pp. 195-212.

Yalcin, M.N. (1995a) Organic geochemical characterization of some Carboniferous coal seams of the Zonguldak basin (NW Turkey) in Snape, C. (ed.) *NATO Advanced Study Institute Series,* Vol. 445, pp. 461-476.

Yalcin, M.N. (1995b) Contribution of the Kozlu-K20/G well to the computer aided modeling studies in the Zonguldak basin (in Turkish) in Yalcin, M.N., Gurdal, G. (eds.) Zonguldak basin research wells-I: Kozlu K20/G. *Special publication of the Technical and Scientific Research Coouncil of Turkey (TUBITAK),* Marmara Research Center, pp. 173-196.

Yalcin, M.N. (1997) Role of basin modeling in coalbed methane resource assessment. *International Coalbed Methane Symposium,* pp. 357-364.

Yalcin, M.N., Inan S, Gurdal, G., Mann, U., Schaefer, G. (2002) Carboniferous coals of the Zonguldak basin (northwest Turkey): Implications for coalbed methane potential. *AAPG Bulletin,* Vol. 86, pp. 1305-1328.

Yang, R.T., Saunders, J.T. (1985) Adsorption of gases on coals and heat-treated coals at elevated temperature and pressure. *Fuel*, Vol. 64, pp. 616-620.

Yee, D., Seidle, J.P., Hanson, W.B. (1993) Gas sorption on coal and measurement of gas content. In: Law, B.E., Rice, D.D. (Eds.) Hydrocarbons From Coal. *American Association of Petroleum Geologists, AAPG Studies in Geology*, Chap. 9, pp. 203-218.

Young, G.B.C., Paul, G.W. (1993) Reservoir Characterization of Mary Lee and Black Creek Coals of the Rock Creek Field Laboratory, Black Warrior Basin. *Gas Research Institute Topical Report No.GRI-93/0179*, Chicago, Illinois.

Zhu, J., Jessen, K., Kovscek, A.R., Orr, Jr. F.M. (2003) Analytical Theory of Coalbed Methane Recovery by Gas Injection. *SPE 87338, SPE Journal,* Vol. 8, No. 4, pp. 371-379.

Zuber, M.D., Sawyer, W.K., Schraufnagel, R.A., Kuuskraa V.A. (1987) The Use of Simulation and History Matching to Determine Critical Coalbed Methane Reservoir Properties. *SPE 16420, SPE/DOE Low Permeability Reservoirs Symposium,* Denver, Colorado, 18-19 May.

Zuber, M. (1996) Basic Reservoir Engineering for Coal. *A Guide to Coalbed Methane Reservoir Engineering, Gas Research Institute Report GRI-94/0397,* Chicago, Illinois.

APPENDIX A

Lithologic information of the wells given by Turkish Hard Coal Enterprise (TTK) is listed in the following tables.

Table A.1. AK1

| Depth from the Surface, m | | Lithology | Depth from the Surface, m | | Lithology |
Start	End		Start	End	
0	11	Tuff	576	577	Coal
11	176	Agglomerate	577	797	Clayey Sandstone
176	210	Limestone	797	799	Coal
210	229	Sandy limestone	799	841	Clayey Sandstone
229	330	Filis	841	842	Coal
330	354	Limestone	842	843	Clayey Sandstone
354	466	Clayey Sandstone	843	844	Coal
466	467	Coal	844	859	Clayey Sandstone
467	576	Clayey Sandstone			

Table A.2. AK2

| Depth from the Surface, m | | Lithology | Depth from the Surface, m | | Lithology |
Start	End		Start	End	
0	295	Filis	410	442	Clayey Sandstone
295	308	Limestone	442	444	Coal
308	387	Clayey Sandstone	444	453	Clayey Sandstone
387	390	Coal	453	455	Coal
390	397	Clayey Sandstone	455	489	Clayey Sandstone
397	398	Coal	489	490	Coal
398	408	Clayey Sandstone	490	754	Clayey Sandstone
408	410	Coal			

Table A.3. AK3

| Depth from the Surface, m | | Lithology | Depth from the Surface, m | | Lithology |
Start	End		Start	End	
0	260	Filis	460	522	Sandstone
260	297	Limestone	522	523	Coal
297	300	Clay	523	598	Sandstone
300	301	Coal	598	599	Coal
301	303	Clay	599	646	Clayey Sandstone
303	305	Coal	646	648	Coal
305	319	Clay	648	656	Clayey Sandstone
319	321	Coal	656	658	Coal
321	331	Clay	658	672	Clayey Sandstone
331	332	Coal	672	676	Coal
332	344	Clay	676	700	Clayey Sandstone
344	345	Coal	700	703	Coal
345	459	Sandstone	703	709	Clayey Sandstone
459	460	Coal	709	848	Clayey Sandstone

Table A.4. AK4

| Depth from the Surface, m | | Lithology | Depth from the Surface, m | | Lithology |
Start	End		Start	End	
0	190	Agglomerate	720	739	Clayey Sandstone
190	220	Limestone	739	745	Coal
220	250	Sandstone	745	745	Clayey Sandstone
250	251	Coal	745	749	Coal
251	354	Sandstone	749	792	Sandstone
354	357	Coal	792	797	Coal
357	408	Clayey Sandstone	797	805	Clayey Sandstone
408	410	Coal	805	807	Coal
410	611	Clayey Sandstone	807	816	Clayey Sandstone
611	612	Coal	816	819	Coal
612	705	Clayey Sandstone	819	850	Sandstone
705	707	Coal	850	852	Coal
707	718	Sandstone	852	925	Clayey Sandstone
718	720	Coal			

Table A.5. AK5

| Depth from the Surface, m | | Lithology | Depth from the Surface, m | | Lithology |
Start	End		Start	End	
0	15	Limestone	251	271	Clayey Sandstone
15	89	Clayey Sandstone	271	272	Coal
89	91	Coal	272	302	Sandstone
91	93	Clayey Sandstone	302	304	Coal
93	94	Coal	304	410	Conglomerate
94	149	Clayey Sandstone	410	411	Coal
149	152	Coal	411	423	Sandstone
152	153	Clayey Sandstone	423	424	Coal
153	156	Coal	424	498	Sandstone
156	177	Clayey Sandstone	498	499	Coal
177	177	Coal	499	550	Clayey Sandstone
177	185	Sandstone	550	551	Coal
185	186	Coal	551	608	Sandstone
186	231	Sandstone	608	610	Coal
231	233	Coal	610	671	Sandstone
233	248	Clayey Sandstone	671	672	Coal
248	251	Coal	672	764	Sandstone

Table A.6. AK6

Depth from the Surface, m		Lithology	Depth from the Surface, m		Lithology
Start	End		Start	End	
0	118	Sandstone	560	569	Sandstone
118	119	Coal	569	570	Coal
119	132	Sandstone	570	631	Sandstone
132	133	Coal	631	633	Sandstone
133	196	Clayey Sandstone	633	638	Claystone
196	197	Coal	638	639	Coal
197	209	Clayey Sandstone	639	674	Sandstone
209	210	Coal	674	675	Coal
210	237	Sandstone	675	723	Sandstone
237	261	Clayey Sandstone	723	724	Coal
261	262	Coal	724	730	Sandstone
262	388	Clayey Sandstone	730	731	Coal
388	391	Coal	731	745	Clayey Sandstone
391	473	Clayey Sandstone	745	746	Coal
473	475	Coal	746	835	Clayey Sandstone
475	559	Clayey Sandstone	835	837	Coal
559	560	Coal	837	841	Sandstone

Table A.7. AK7

Depth from the Surface, m		Lithology	Depth from the Surface, m		Lithology
Start	End		Start	End	
0	32	Sandstone	403	436	Conglomerate
32	296	Clayey Sandstone	436	438	Coal
296	298	Coal	438	648	Clayey Sandstone
298	402	Clayey Sandstone	648	734	Sandstone
402	403	Coal			

Table A.8. AK8

Depth from the Surface, m		Lithology	Depth from the Surface, m		Lithology
Start	End		Start	End	
0	240	Agglomerate	260	596	Clayey Sandstone
240	260	Limestone	596	764	Sandstone

Table A.9. AK9

| Depth from the Surface, m | | Lithology | Depth from the Surface, m | | Lithology |
Start	End		Start	End	
0	272	Agglomerate	1146	1148	Coal
272	297	Pl. Limestone	1148	1151	Sandstone
297	351	Sandy Limestone	1151	1152	Coal
351	555	Clayey Sandstone	1152	1178	Sandstone
555	556	Coal	1178	1179	Coal
556	721	Clayey Sandstone	1179	1250	Sandstone
721	722	Coal	1250	1251	Coal
722	766	Clayey Sandstone	1251	1267	Sandstone
766	767	Coal	1267	1269	Coal
767	811	Clayey Sandstone	1269	1341	Sandstone
811	814	Coal	1341	1343	Coal
814	819	Clayey Sandstone	1343	1418	Sandstone
819	820	Coal	1418	1423	Coal
820	825	Clayey Sandstone	1423	1449	Sandstone
825	826	Coal	1449	1450	Coal
826	838	Clay	1450	1524	Conglomerate
838	839	Coal	1524	1525	Coal
839	844	Şiferton	1525	1593	Clayey Sandstone
844	847	Clay	1593	1594	Coal
847	848	Coal	1594	1604	Clayey Sandstone
848	861	Clay	1604	1607	Coal
861	862	Coal	1607	1624	Clayey Sandstone
862	879	Clayey Sandstone	1624	1625	Coal
879	881	Coal	1625	1707	Clayey Sandstone
881	916	Clayey Sandstone	1707	1712	Coal
916	917	Coal	1712	1732	Sandstone
917	990	Clayey Sandstone	1732	1733	Coal
990	991	Coal	1733	1770	Sandstone
991	1114	Sandstone	1770	1771	Coal
1114	1115	Coal	1771	1876	Clayey Sandstone
1115	1146	Sandstone			

Table A.10. AK10

Depth from the Surface, m Start	End	Lithology	Depth from the Surface, m Start	End	Lithology
0	290	Agglomerate	809	810	Clayey Sandstone
290	320	Pl. Limestone	810	812	Coal
320	336	Sandy Limestone	812	813	Clay
336	545	Clayey Sandstone	813	814	Coal
545	546	Coal	814	826	Clay
546	578	Clayey Sandstone	826	827	Coal
578	580	Coal	827	830	Clay
580	690	Clayey Sandstone	830	831	Coal
690	691	Coal	831	839	Clay
691	743	Clayey Sandstone	839	841	Coal
743	744	Coal	841	871	Clay
744	759	Conglomerate	871	873	Coal
759	762	Coal	873	907	Clayey Sandstone
762	789	Clayey Sandstone	907	908	Coal
789	793	Coal	908	924	Clayey Sandstone
793	794	Clay	924	925	Coal
794	798	Coal	925	963	Clayey Sandstone
798	809	Şiferton			

Table A.11. AK11

Depth from the Surface, m Start	End	Lithology	Depth from the Surface, m Start	End	Lithology
0	230	Agglomerate	704	706	Clay
230	258	Pl. Limestone	706	709	Coal
258	273	Sandy Limestone	709	709	Clay
273	574	Clayey Sandstone	709	710	Coal
574	575	Coal	710	725	Sandstone
575	654	Clayey Sandstone	725	727	Coal
654	656	Coal	727	731	Clay
656	660	Conglomerate	731	732	Coal
660	661	Coal	732	749	Clayey Sandstone
661	664	Clay	749	750	Coal
664	665	Coal	750	779	Clayey Sandstone
665	681	Conglomerate	779	780	Coal
681	687	Coal	780	797	Clayey Sandstone
687	703	Sandstone	797	798	Coal
703	704	Coal	798	1004	Clayey Sandstone

Table A.12. AK12

Depth from the Surface, m		Lithology	Depth from the Surface, m		Lithology
Start	End		Start	End	
0	206	Agglomerate	1170	1213	Sandstone
206	251	Pl. Limestone	1213	1215	Coal
251	288	Sandy Limestone	1215	1224	Clay
288	390	Filis	1224	1225	Coal
390	688	Clayey Sandstone	1225	1264	Conglomerate
688	689	Coal	1264	1265	Coal
689	750	Clayey Sandstone	1265	1278	Sandstone
750	751	Coal	1278	1279	Coal
751	755	Clay	1279	1290	Clay
755	756	Coal	1290	1291	Coal
756	804	Clayey Sandstone	1291	1313	Clay
804	805	Coal	1313	1314	Coal
805	831	Sandstone	1314	1365	Sandstone
831	832	Coal	1365	1367	Coal
832	835	Clay	1367	1392	Sandstone
835	838	Coal	1392	1393	Coal
838	847	Clay	1393	1466	Sandstone
847	848	Coal	1466	1467	Coal
848	976	Clayey Sandstone	1467	1615	Sandstone
976	978	Coal	1615	1617	Coal
978	1074	Conglomerate	1617	1724	Sandstone
1074	1075	Coal	1724	1725	Coal
1075	1168	Clayey Sandstone	1725	1770	Sandstone
1168	1170	Coal			

Table A.13. AK13

Depth from the Surface, m		Lithology	Depth from the Surface, m		Lithology
Start	End		Start	End	
0	317	Agglomerate	757	763	Clay
317	327	Pl. Limestone	763	765	Coal
327	337	Sandy Limestone	765	798	Sandstone
337	413	Clayey Sandstone	798	800	Coal
413	414	Coal	800	801	Clay
414	446	Clay	801	804	Coal
446	447	Coal	804	816	Clay
447	462	Clay	816	817	Coal
462	463	Coal	817	870	Clayey Sandstone
463	745	Clayey Sandstone	870	874	Şiferton
745	746	Coal	874	909	Clayey Sandstone
746	756	Clay	909	911	Coal
756	757	Coal	911	975	Clayey Sandstone

255

Table A.14. AK14

Start	End	Lithology	Start	End	Lithology
Depth from the Surface, m			*Depth from the Surface, m*		
0	334	Agglomerate	1103	1104	Coal
334	348	Pl. Limestone	1104	1139	Sandstone
348	365	Sandy Limestone	1139	1141	Coal
365	665	Clayey Sandstone	1141	1195	Sandstone
665	666	Coal	1195	1196	Coal
666	678	Conglomerate	1196	1229	Sandstone
678	680	Coal	1229	1230	Coal
680	717	Conglomerate	1230	1244	Sandstone
717	723	Coal	1244	1245	Coal
723	730	Clay	1245	1296	Conglomerate
730	734	Şiferton	1296	1298	Coal
734	772	Clay	1298	1363	Sandstone
772	773	Coal	1363	1364	Coal
773	795	Clay	1364	1415	Conglomerate
795	796	Coal	1415	1416	Coal
796	824	Clay	1416	1439	Sandstone
824	825	Coal	1439	1442	Coal
825	948	Clayey Sandstone	1442	1551	Sandstone
948	949	Coal	1551	1557	Coal
949	1042	Clayey Sandstone	1557	1580	Sandstone
1042	1043	Coal	1580	1581	Coal
1043	1103	Sandstone	1581	1682	Sandstone

Table A.15. AK15

Start	End	Lithology	Start	End	Lithology
Depth from the Surface, m			*Depth from the Surface, m*		
0	211	Agglomerate	670	675	Coal
211	225	Pl. Limestone	675	690	Sandstone
225	249	Sandy Limestone	690	691	Coal
249	550	Clayey Sandstone	691	714	Sandstone
550	551	Coal	714	715	Coal
551	630	Sandstone	715	718	Clay
630	632	Coal	718	720	Coal
632	670	Sandstone	720	750	Clay

Table A.16. AK16

Depth from the Surface, m		Lithology	Depth from the Surface, m		Lithology
Start	End		Start	End	
0	170	Agglomerate	1224	1237	Sandstone
170	204	Pl. Limestone	1237	1238	Coal
204	230	Sandy Limestone	1238	1250	Sandstone
230	370	Filis	1250	1251	Coal
370	426	Limestone	1251	1268	Sandstone
426	577	Clayey Sandstone	1268	1269	Coal
577	578	Coal	1269	1376	Sandstone
578	668	Clayey Sandstone	1376	1379	Coal
668	672	Coal	1379	1423	Sandstone
672	676	Clay	1423	1425	Coal
676	678	Coal	1425	1488	Sandstone
678	1138	Clayey Sandstone	1488	1494	Coal
1138	1140	Coal	1494	1518	Conglomerate
1140	1171	Sandstone	1518	1519	Coal
1171	1172	Coal	1519	1557	Conglomerate
1172	1182	Sandstone	1557	1558	Coal
1182	1183	Coal	1558	1695	Sandstone
1183	1223	Conglomerate	1695	1696	Coal
1223	1224	Coal	1696	1727	Sandstone

Table A.17. Amasra-43

Depth from the Surface, m		Lithology	Depth from the Surface, m		Lithology
Start	End		Start	End	
0	20	Sandstone	45	495	Sandstone
20	21	Coal	495	505	Limestone
21	45	Sandstone			

Table A.18. Amasra-50

Depth from the Surface, m		Lithology	Depth from the Surface, m		Lithology
Start	End		Start	End	
0	165	Andesite	413	470	Sandstone
165	190	Tuff-Marl	470	471	Coal
190	220	Limestone	471	720	Sandstone
220	230	Sandstone	720	721	Coal
230	231	Coal	721	755	Sandstone
231	350	Sandstone	755	756	Coal
350	352	Coal	756	930	Sandstone
352	370	Sandstone	930	931	Coal
370	372	Coal	931	965	Sandstone
372	405	Sandstone	965	967	Coal
405	406	Coal	967	1450	Sandstone
406	411	Sandstone	1450	1453	Coal
411	413	Coal	1453	1578	Sandstone

Table A.19. Askersuyu-31

Depth from the Surface, m		Lithology	Depth from the Surface, m		Lithology
Start	End		Start	End	
0	25	Limestone	241	250	Clayey Sandstone
25	60	Sandstone	250	251	Coal
60	125	Filis	251	275	Sandstone
125	140	Conglomerate	275	277	Coal
140	150	Clayey Sandstone	277	287	Clayey Sandstone
150	180	Sandstone	287	293	Coal
180	181	Coal	293	310	Sandstone
181	240	Clayey Sandstone	310	315	Coal
240	241	Coal	315	561	Sandstone

Table A.20. Bedesten-21

Depth from the Surface, m		Lithology	Depth from the Surface, m		Lithology
Start	End		Start	End	
0	130	Limestone	350	351	Coal
130	140	Sandstone	351	890	Sandstone
140	142	Coal	890	891	Coal
142	160	Clayey Sandstone	891	990	Sandstone
160	162	Coal	990	993	Coal
162	210	Clayey Sandstone	993	997	Sandstone
210	211	Coal	997	998	Coal
211	350	Clayey Sandstone	998	1063	Sandstone

Table A.21. Bedesten-45

Depth from the Surface, m		Lithology	Depth from the Surface, m		Lithology
Start	End		Start	End	
0	260	Sandstone	310	375	Sandstone W.B.
260	280	Sandstone W.C.	375	376	Coal
280	281	Coal	376	390	Sandstone W.B.
281	310	Sandstone W.C.	390	410	Limestone

Table A.22. Bedesten-83

Depth from the Surface, m		Lithology	Depth from the Surface, m		Lithology
Start	End		Start	End	
0	40	Alluvium	521	530	Clayey Sandstone
40	420	Filis	530	534	Coal
420	470	Limestone	534	540	Clayey Sandstone
470	520	Clayey Sandstone	540	542	Coal
520	521	Coal	542	765	Clayey Sandstone

Table A.23. Bostanlar-36

Depth from the Surface, m		Lithology	Depth from the Surface, m		Lithology
Start	End		Start	End	
0	180	Andezite-Tuff	603	640	Sandstone
180	240	Limestone	640	648	Coal
240	515	Clayey Sandstone	648	665	Sandstone
515	516	Coal	665	667	Coal
516	600	Sandstone	667	718	Sandstone
600	603	Coal			

Table A.24. Bostanlar-37

Depth from the Surface, m		Lithology	Depth from the Surface, m		Lithology
Start	End		Start	End	
0	260	Andezite-Tuff	590	670	Sandstone
260	350	Limestone	670	675	Conglomerate
350	440	Sandstone	675	760	Sandstone
440	490	Clayey Sandstone	760	761	Coal
490	500	Sandstone	761	815	Sandstone
500	590	Clayey Sandstone			

Table A.25. Bostanlar-38

Depth from the Surface, m		Lithology	Depth from the Surface, m		Lithology
Start	End		Start	End	
0	300	Andezite-Tuff	350	590	Clayey Sandstone
300	350	Limestone	590	900	Sandstone

Table A.26. Bostanlar-K17

Depth from the Surface, m		Lithology	Depth from the Surface, m		Lithology
Start	End		Start	End	
0	61	Agglomerate	425	426	Coal
61	93	Limestone	426	462	Clayey Sandstone
93	371	Clayey Sandstone	462	463	Coal
371	372	Coal	463	491	Clayey Sandstone
372	407	Clayey Sandstone	491	492	Coal
407	409	Coal	492	575	Clayey Sandstone
409	412	Clayey Sandstone	575	576	Coal
412	414	Coal	576	804	Clayey Sandstone
414	425	Clayey Sandstone	804	890	Clayey Sandstone

Table A.27. Çamlık-16A

Depth from the Surface, m		Lithology	Depth from the Surface, m		Lithology
Start	End		Start	End	
0	28	Andezite	897	908	Sandstone
28	95	Tuff-Marl	908	909	Coal
95	270	Agglomerate	909	916	Clayey Sandstone
270	319	Andezite-Tuff	916	919	Coal
319	351	Limestone	919	934	Sandstone
351	816	Sandstone	934	936	Coal
816	819	Coal	936	939	Clayey Sandstone
819	895	Clayey Sandstone	939	940	Coal
895	897	Coal	940	1488	Sandstone

Table A.28. Çamlık-56

Depth from the Surface, m		Lithology	Depth from the Surface, m		Lithology
Start	End		Start	End	
0	80	Limestone	1045	1046	Coal
80	200	Andezite	1046	1050	Clayey Sandstone
200	260	Tuff-Marl	1050	1051	Coal
260	440	Agglomerate	1051	1060	Clayey Sandstone
440	480	Limestone	1060	1061	Coal
480	1045	Clayey Sandstone	1061	1291	Sandstone

Table A.29. Çamlık-77

Depth from the Surface, m		Lithology	Depth from the Surface, m		Lithology
Start	End		Start	End	
0	100	Andezite	310	400	Limestone
100	170	Tuff-Marl	400	980	Clayey Sandstone
170	250	Agglomerate	980	983	Coal
250	310	Andezite-Tuff	983	1370	Clayey Sandstone

Table A.30. Çömlekkıran-65

Depth from the Surface, m		Lithology	Depth from the Surface, m		Lithology
Start	End		Start	End	
0	30	Andezite-Tuff	713	715	Coal
30	240	Limestone	715	880	Sandstone (Nam.)
240	272	Conglomerate	880	881	Coal
272	273	Coal	881	914	Clay
273	300	Clayey Sandstone	914	915	Coal
300	713	Sandstone (Nam.)			

Table A.31. Çömlekkıran-66

Depth from the Surface, m		Lithology	Depth from the Surface, m		Lithology
Start	End		Start	End	
0	150	Andezite-Tuff	512	560	Clayey Sandstone
150	200	Limestone	560	561	Coal
200	510	Clayey Sandstone	561	750	Sandstone
510	512	Coal			

Table A.32. Dökük-23

| Depth from the Surface, m | | Lithology | Depth from the Surface, m | | Lithology |
Start	End		Start	End	
0	90	Limestone	200	300	Sandstone (W.A.)
90	135	Sandstone (W.C.)	300	500	
135	175	Sandstone (W.A.)	500	515	
175	200	Sandstone (W.C.)			

Table A.33. Fermitkadı-55

| Depth from the Surface, m | | Lithology | Depth from the Surface, m | | Lithology |
Start	End		Start	End	
0	45	Tuff-Marl	897	1020	Sandstone
45	160	Andezite	1020	1023	Coal
160	210	Tuff-Marl	1023	1060	Sandstone
210	275	Agglomerate	1060	1062	Coal
275	860	Limestone	1062	1250	Sandstone
860	895	Sandstone	1250	1251	Coal
895	897	Coal	1251	1255	Sandstone

Table A.34. Gömü-27

| Depth from the Surface, m | | Lithology | Depth from the Surface, m | | Lithology |
Start	End		Start	End	
0	50	Sandstone (W.D.)	360	410	Sandstone (W.A.)
50	51	Coal	410	411	Coal
51	90	Sandstone (W.C.)	411	530	Sandstone (W.A.)
90	93	Coal	530	531	Coal
93	95	Sandstone	531	760	Sandstone
95	96	Coal	760	763	Coal
96	195	Sandstone (W.C.)	763	856	Sandstone
195	360	Sandstone (W.B.)			

Table A.35. Gömü-28

| Depth from the Surface, m | | Lithology | Depth from the Surface, m | | Lithology |
Start	End		Start	End	
0	50	Sandstone	240	290	Sandstone (W.C.)
50	110	Limestone	290	462	Sandstone (Nam.)
110	240	Sandstone (W.D.)			

Table A.36. Gömü-29

| Depth from the Surface, m | | Lithology | Depth from the Surface, m | | Lithology |
Start	End		Start	End	
0	80	Sandstone (W.D.)	320	321	Coal
80	90	Sandstone (W.C.)	321	330	Sandstone (W.A.)
90	93	Coal	330	331	Coal
93	105	Sandstone (W.C.)	331	460	Sandstone (W.A.)
105	107	Coal	460	515	Sandstone (W.B.)
107	120	Sandstone (W.C.)	515	516	Coal
120	123	Coal	516	560	Sandstone (W.B.)
123	215	Sandstone (W.C.)	560	800	Sandstone (W.B.)
215	320	Sandstone (W.A.)			

Table A.37. Gömü-80

Start	End	Lithology	Start	End	Lithology
Depth from the Surface, m			*Depth from the Surface, m*		
0	80	Sandstone	665	667	Coal
80	81	Coal	667	720	Clayey Sandstone
81	460	Clayey Sandstone	720	721	Coal
460	461	Coal	721	814	Sandstone
461	665	Clayey Sandstone			

Table A.38. Gömü-81

Start	End	Lithology	Start	End	Lithology
Depth from the Surface, m			*Depth from the Surface, m*		
0	25	Limestone	25	700	Sandstone

Table A.39. Gömü-84

Start	End	Lithology	Start	End	Lithology
Depth from the Surface, m			*Depth from the Surface, m*		
0	40	Sandstone	175	550	Sandstone
40	175	Limestone	550	751	Sandstone (Nam.)

Table A.40. Gömü-85

Start	End	Lithology	Start	End	Lithology
Depth from the Surface, m			*Depth from the Surface, m*		
0	170	Limestone	460	470	Sandstone
170	180	Sandstone	470	472	Coal
180	182	Coal	472	750	Sandstone
182	460	Sandstone (Nam.)			

Table A.41. Gömü-86

Start	End	Lithology	Start	End	Lithology
Depth from the Surface, m			*Depth from the Surface, m*		
0	15	Limestone	191	260	Sandstone
15	130	Sandstone	260	262	Coal
130	132	Coal	262	470	Clayey Sandstone
132	180	Sandstone	470	471	Coal
180	182	Coal	471	540	Sandstone
182	190	Sandstone	540	750	Sandstone (Nam.)
190	191	Coal			

Table A.42. Gömü-K24

| Depth from the Surface, m | | Lithology | Depth from the Surface, m | | Lithology |
Start	End		Start	End	
0	21	Filis	304	305	Coal
21	181	Limestone	305	483	Clayey Sandstone
181	249	Clayey Sandstone	483	486	Coal
249	250	Coal	486	830	Clayey Sandstone
250	273	Clayey Sandstone	830	834	Coal
273	275	Coal	834	1003	Clayey Sandstone
275	304	Clayey Sandstone			

Table A.43. Gömü-K27

| Depth from the Surface, m | | Lithology | Depth from the Surface, m | | Lithology |
Start	End		Start	End	
0	26	Limestone	488	489	Coal
26	331	Clayey Sandstone	489	534	Clayey Sandstone
331	332	Coal	534	535	Coal
332	391	Clayey Sandstone	535	586	Clayey Sandstone
391	392	Coal	586	587	Coal
392	478	Clayey Sandstone	587	598	Clayey Sandstone
478	480	Coal	598	601	Coal
480	488	Clayey Sandstone	601	644	Clayey Sandstone

Table A.44. Gömü-K32

| Depth from the Surface, m | | Lithology | Depth from the Surface, m | | Lithology |
Start	End		Start	End	
0	10	Limestone	407	408	Clayey Sandstone
10	126	Clayey Sandstone	408	409	Coal
126	128	Coal	409	415	Clayey Sandstone
128	158	Clayey Sandstone	415	417	Coal
158	159	Coal	417	421	Clayey Sandstone
159	178	Clayey Sandstone	421	423	Coal
178	179	Coal	423	435	Clayey Sandstone
179	368	Clayey Sandstone	435	439	Coal
368	369	Coal	439	764	Clayey Sandstone
369	388	Clayey Sandstone	764	765	Coal
388	391	Coal	765	828	Clayey Sandstone
391	394	Clayey Sandstone	828	830	Coal
394	395	Coal	830	942	Clayey Sandstone
395	398	Clayey Sandstone	942	944	Coal
398	400	Coal	944	995	Clayey Sandstone
400	405	Clayey Sandstone	995	996	Coal
405	407	Coal	996	1006	Clayey Sandstone

Table A.45. Gömü-K37

| Depth from the Surface, m | | Lithology | Depth from the Surface, m | | Lithology |
Start	End		Start	End	
0	39	Sandstone	300	301	Coal
39	41	Coal	301	471	Sandstone
41	72	Clayey Sandstone	471	472	Coal
72	73	Coal	472	676	Clayey Sandstone
73	152	Clayey Sandstone	676	677	Coal
152	153	Coal	677	745	Sandstone
153	223	Clayey Sandstone	745	747	Coal
223	224	Coal	747	853	Sandstone
224	268	Clayey Sandstone	853	855	Coal
268	269	Coal	855	981	Sandstone
269	300	Conglomerate			

Table A.46. K10

| Depth from the Surface, m | | Lithology | Depth from the Surface, m | | Lithology |
Start	End		Start	End	
0	375	Agglomerate	723	749	Sandstone
375	398	Pl. Limestone	749	750	Coal
398	417	Sandy Limestone	750	759	Clay
417	664	Sandstone	759	760	Coal
664	666	Coal	760	765	Clay
666	668	Clay	765	766	Coal
668	670	Coal	766	822	Sandstone
670	683	Clay	822	823	Coal
683	685	Coal	823	852	Sandstone
685	713	Sandstone	852	853	Coal
713	716	Coal	853	865	Sandstone
716	721	Clay Coal	865	866	Coal
721	723		866	1040	Sandstone (W.C.)

Table A.47. K11

| Depth from the Surface, m | | Lithology | Depth from the Surface, m | | Lithology |
Start	End		Start	End	
0	284	Agglomerate	753	760	Clay
284	297	Pl. Limestone	760	762	Coal
297	321	Sandy Limestone	762	768	Clay
321	589	Sandstone	768	771	Coal
589	590	Coal	771	782	Clay
590	638	Sandstone	782	785	Coal
638	639	Coal	785	803	Clayey Sandstone
639	723	Sandstone	803	806	Coal
723	724	Coal	806	825	Clayey Sandstone
724	751	Sandstone	825	826	Coal
751	753	Coal	826	855	Clayey Sandstone

Table A.48. K13

Depth from the Surface, m		Lithology	Depth from the Surface, m		Lithology
Start	End		Start	End	
0	351	Agglomerate	759	763	Coal
351	363	Pl. Limestone	763	775	Clayey Sandstone
363	382	Sandy Limestone	775	778	Coal
382	724	Clayey Sandstone	778	787	Clayey Sandstone
724	725	Coal	787	788	Coal
725	730	Clay	788	794	Clayey Sandstone
730	732	Coal	794	795	Coal
732	736	Clayey Sandstone	795	838	Clayey Sandstone
736	738	Coal	838	842	Şiferton
738	759	Clayey Sandstone	842	868	Clayey Sandstone

Table A.49. K14

Depth from the Surface, m		Lithology	Depth from the Surface, m		Lithology
Start	End		Start	End	
0	85	Tuff	678	680	Coal
85	425	Agglomerate	680	703	Clayey Sandstone
425	431	Pl. Limestone	703	706	Coal
431	454	Sandy Limestone	706	717	Clayey Sandstone
454	654	Clayey Sandstone	717	718	Coal
654	655	Coal	718	750	Clayey Sandstone
655	660	Clay	750	751	Coal
660	661	Coal	751	816	Clayey Sandstone
661	678	Clayey Sandstone			

Table A.50. K15

Depth from the Surface, m		Lithology	Depth from the Surface, m		Lithology
Start	End		Start	End	
0	65	Tuff	650	662	Clayey Sandstone
65	393	Agglomerate	662	665	Coal
393	405	Pl. Limestone	665	684	Clayey Sandstone
405	420	Sandy Limestone	684	686	Coal
420	509	Sandstone	686	696	Clayey Sandstone
509	510	Coal	696	697	Coal
510	562	Sandstone	697	725	Clayey Sandstone
562	563	Coal	725	726	Coal
563	627	Sandstone	726	743	Clayey Sandstone
627	628	Coal	743	744	Coal
628	648	Clayey Sandstone	744	756	Clayey Sandstone
648	650	Coal			

Table A.51. K16

Depth from the Surface, m		Lithology	Depth from the Surface, m		Lithology
Start	End		Start	End	
0	105	Tuff	720	724	Coal
105	367	Agglomerate	724	727	Clayey Sandstone
367	380	Pl. Limestone	727	729	Coal
380	393	Sandy Limestone	729	755	Clayey Sandstone
393	672	Sandstone	755	756	Coal
672	673	Coal	756	770	Clayey Sandstone
673	677	Clay	770	771	Coal
677	678	Coal	771	779	Clayey Sandstone
678	689	Clay	779	780	Coal
689	692	Coal	780	828	Sandstone
692	720	Clayey Sandstone			

Table A.52. K18

Depth from the Surface, m		Lithology	Depth from the Surface, m		Lithology
Start	End		Start	End	
0	122	Tuff	673	676	Coal
122	404	Agglomerate	676	689	Clayey Sandstone
404	414	Pl. Limestone	689	691	Coal
414	437	Sandy Limestone	691	709	Clayey Sandstone
437	653	Sandstone	709	711	Coal
653	654	Coal	711	724	Clayey Sandstone
654	655	Clay	724	726	Coal
655	656	Coal	726	809	Sandstone
656	673	Clayey Sandstone			

Table A.53. K20

Depth from the Surface, m		Lithology	Depth from the Surface, m		Lithology
Start	End		Start	End	
0	71	Tuff	712	721	Clay
71	352	Agglomerate	721	722	Coal
352	365	Pl. Limestone	722	725	Clay
365	420	Sandy Limestone	725	726	Coal
420	523	Permian	726	744	Clay
523	704	Sandstone	744	745	Coal
704	705	Coal	745	773	Clayey Sandstone
705	711	Clay	773	774	Coal
711	712	Coal	774	950	Sandstone

Table A.54. K21

Depth from the Surface, m		Lithology	Depth from the Surface, m		Lithology
Start	End		Start	End	
0	118	Tuff	543	544	Coal
118	389	Agglomerate	544	735	Clayey Sandstone
389	390	Pl. Limestone	735	736	Coal
390	419	Sandy Limestone	735	858	Clayey Sandstone
419	543	Clayey Sandstone			

Table A.55. K30

| Depth from the Surface, m | | Lithology | Depth from the Surface, m | | Lithology |
Start	End		Start	End	
0	40	Tuff	751	766	Clay
40	326	Agglomerate	766	767	Coal
326	349	Pl. Limestone	767	772	Clay
349	367	Sandy Limestone	772	773	Coal
367	688	Clayey Sandstone	773	791	Clay
688	689	Coal	791	792	Coal
689	746	Clayey Sandstone	792	794	Clay
746	751	Coal			

Table A.56. K34

| Depth from the Surface, m | | Lithology | Depth from the Surface, m | | Lithology |
Start	End		Start	End	
0	12	Pl. Limestone	808	811	Coal
12	36	Sandy Limestone	811	839	Clayey Sandstone
36	300	Filis	839	842	Coal
300	398	Clayey Sandstone	842	844	Clay
398	399	Coal	844	848	Coal
399	645	Clayey Sandstone	848	900	Clayey Sandstone
645	646	Coal	900	904	Şiferton
646	737	Clayey Sandstone	904	917	Clayey Sandstone
737	738	Coal	917	918	Coal
738	808	Clayey Sandstone	918	961	Clayey Sandstone

Table A.57. Kaman-10

| Depth from the Surface, m | | Lithology | Depth from the Surface, m | | Lithology |
Start	End		Start	End	
0	97	Andezite	391	396	Coal
97	140	Tuff-Marl	396	609	Clayey Sandstone
140	280	Agglomerate	609	611	Coal
280	329	Andezite-Tuff	611	1130	Clayey Sandstone
329	361	Limestone	1130	1131	Coal
361	391	Clayey Sandstone	1131	1226	Sandstone

Table A.58. Kaman-14

| Depth from the Surface, m | | Lithology | Depth from the Surface, m | | Lithology |
Start	End		Start	End	
0	57	Tuff-Marl	635	639	Coal
57	230	Agglomerate	639	641	Clayey Sandstone
230	263	Andezite-Tuff	641	645	Coal
263	395	Limestone	645	650	Clayey Sandstone
395	553	Clayey Sandstone	650	651	Coal
553	555	Coal	651	1000	Clayey Sandstone
555	635	Clayey Sandstone			

Table A.59. Kaman-39

Depth from the Surface, m		Lithology	Depth from the Surface, m		Lithology
Start	End		Start	End	
0	90	Limestone	390	650	Limestone
90	200	Andezite	650	680	Clayey Sandstone
200	250	Tuff-Marl	680	682	Coal
250	360	Agglomerate	682	1000	Clayey Sandstone
360	390	Andezite-Tuff			

Table A.60. Kaman-53

Depth from the Surface, m		Lithology	Depth from the Surface, m		Lithology
Start	End		Start	End	
0	90	Tuff-Marl	265	385	Agglomerate
90	195	Andezite	385	850	Limestone
195	265	Tuff-Marl	850	1000	Sandstone

Table A.61. Kaman-58

Depth from the Surface, m		Lithology	Depth from the Surface, m		Lithology
Start	End		Start	End	
0	90	Andezite	612	720	Clayey Sandstone
90	140	Tuff-Marl	720	723	Coal
140	280	Agglomerate	723	735	Clayey Sandstone
280	300	Andezite-Tuff	735	736	Coal
300	460	Limestone	736	740	Sandstone
460	610	Clayey Sandstone	740	741	Coal
610	612	Coal	741	1000	Sandstone

Table A.62. Kaman-60

Depth from the Surface, m		Lithology	Depth from the Surface, m		Lithology
Start	End		Start	End	
0	60	Tuff-Marl	460	810	Clayey Sandstone
60	165	Andezite	810	811	Coal
165	220	Tuff-Marl	811	970	Sandstone
220	350	Agglomerate	970	971	Coal
350	390	Andezite-Tuff	971	1001	Clayey Sandstone
390	460	Limestone			

Table A.63. Kaman-61

Depth from the Surface, m		Lithology	Depth from the Surface, m		Lithology
Start	End		Start	End	
0	40	Tuff-Marl	415	418	Coal
40	140	Andezite	418	425	Sandstone
140	190	Tuff-Marl	425	428	Coal
190	320	Agglomerate	428	490	Sandstone
320	350	Andezite-Tuff	490	491	Coal
350	380	Limestone	491	1000	Sandstone
380	415	Sandstone			

Table A.64. Kaman-75

Depth from the Surface, m		Lithology	Depth from the Surface, m		Lithology
Start	End		Start	End	
0	25	Andezite	220	450	Limestone
25	85	Tuff-Marl	450	750	Sandstone
85	200	Agglomerate	750	754	Coal
200	220	Andezite-Tuff	754	1002	Sandstone

Table A.65. Karaçay-9

Depth from the Surface, m		Lithology	Depth from the Surface, m		Lithology
Start	End		Start	End	
0	50	Andezite	150	859	Limestone
50	82	Tuff-Marl	859	910	Clayey Sandstone
82	132	Agglomerate	910	911	Coal
132	150	Andezite-Tuff	911	1000	Sandstone

Table A.66. Karaçay-11

Depth from the Surface, m		Lithology	Depth from the Surface, m		Lithology
Start	End		Start	End	
0	13	Alluvion	822	823	Coal
13	70	Agglomerate	823	903	Clayey Sandstone
70	80	Tuff-Marl	903	906	Coal
80	452	Limestone	906	936	Clayey Sandstone
452	584	Clayey Sandstone	936	937	Coal
584	588	Coal	937	975	Clayey Sandstone
588	796	Clayey Sandstone	975	977	Coal
796	797	Coal	977	998	Sandstone
797	822	Clayey Sandstone			

Table A.67. Karaçay-K29

Depth from the Surface, m		Lithology	Depth from the Surface, m		Lithology
Start	End		Start	End	
0	17	Andezite	584	585	Coal
17	57	Agglomerate	585	614	Clayey Sandstone
57	326	Limestone	614	615	Coal
326	394	Sandstone	615	661	Clayey Sandstone
394	398	Coal	661	662	Coal
398	520	Clayey Sandstone	662	769	Clayey Sandstone
520	521	Coal	769	770	Coal
521	545	Clayey Sandstone	770	953	Clayey Sandstone
545	546	Coal	953	955	Coal
546	584	Sandstone	955	1028	Clayey Sandstone

Table A.68. Kazpınar-7

Depth from the Surface, m		Lithology	Depth from the Surface, m		Lithology
Start	End		Start	End	
0	91	Andezite	826	827	Coal
91	148	Tuff-Marl	827	903	Clayey Sandstone
148	380	Agglomerate	903	904	Coal
380	410	Andezite-Tuff	904	921	Clayey Sandstone
410	458	Limestone	921	922	Coal
458	725	Clayey Sandstone	922	1075	Clayey Sandstone
725	726	Coal	1075	1076	Coal
726	743	Clayey Sandstone	1076	1082	Clayey Sandstone
743	745	Coal	1082	1083	Coal
745	793	Clayey Sandstone	1083	1098	Sandstone
793	794	Coal	1098	1099	Coal
794	822	Clayey Sandstone	1099	1242	Clayey Sandstone
822	823	Coal	1242	1243	Coal
823	826	Clayey Sandstone	1243	1275	Sandstone

Table A.69. Kazpınar-18

Depth from the Surface, m		Lithology	Depth from the Surface, m		Lithology
Start	End		Start	End	
0	134	Andezite-Tuff	703	704	Coal
134	183	Limestone	704	963	Sandstone
183	436	Sandstone	963	964	Coal
437	438	Coal	964	1001	Sandstone
438	703	Sandstone			

Table A.70. Kazpınar-20

Depth from the Surface, m		Lithology	Depth from the Surface, m		Lithology
Start	End		Start	End	
0	119	Andezite	525	527	Sandstone
119	170	Tuff-Marl	527	528	Coal
170	350	Agglomerate	528	771	Sandstone
350	384	Andezite-Tuff	771	773	Coal
384	411	Limestone	773	782	Sandstone
411	524	Clayey Sandstone	782	783	Coal
524	525	Coal	783	1000	Sandstone

Table A.71. Kazpınar-51

Depth from the Surface, m		Lithology	Depth from the Surface, m		Lithology
Start	End		Start	End	
0	15	Tuff-Marl	715	717	Coal
15	280	Agglomerate	717	740	Sandstone
280	310	Andezite-Tuff	740	741	Coal
310	560	Clayey Sandstone	741	805	Sandstone
560	561	Coal	805	807	Coal
561	715	Clayey Sandstone	807	1000	Sandstone

Table A.72. Kazpınar-62

Depth from the Surface, m Start	End	Lithology	Depth from the Surface, m Start	End	Lithology
0	95	Tuff-Marl	422	575	Sandstone
95	275	Agglomerate	575	576	Coal
275	305	Andezite-Tuff	576	586	Sandstone
305	325	Limestone	586	587	Coal
325	420	Sandstone	587	920	Sandstone
420	422	Coal			

Table A.73. Kazpınar-63

Depth from the Surface, m Start	End	Lithology	Depth from the Surface, m Start	End	Lithology
0	140	Agglomerate	563	640	Sandstone
140	170	Andezite-Tuff	640	641	Coal
170	200	Limestone	641	695	Sandstone
200	450	Sandstone	695	696	Coal
450	453	Coal	696	825	Sandstone
453	560	Sandstone	825	826	Coal
560	563	Coal	826	1000	Sandstone

Table A.74. Kazpınar-64

Depth from the Surface, m Start	End	Lithology	Depth from the Surface, m Start	End	Lithology
0	80	Agglomerate	686	710	Sandstone
80	200	Andezite-Tuff	710	712	Coal
200	240	Limestone	712	740	Sandstone
240	465	Sandstone	740	741	Coal
465	466	Coal	741	965	Sandstone
466	640	Sandstone	965	967	Coal
640	643	Coal	967	970	Sandstone
643	685	Sandstone	970	971	Coal
685	686	Coal	971	980	Sandstone

Table A.75. Kazpınar-69

Depth from the Surface, m Start	End	Lithology	Depth from the Surface, m Start	End	Lithology
0	60	Andezite	820	821	Coal
60	110	Tuff-Marl	821	870	Conglomerate
110	350	Agglomerate	870	873	Coal
350	360	Limestone	873	950	Conglomerate
360	635	Sandstone	950	951	Coal
635	636	Coal	951	1000	Conglomerate
636	820	Sandstone			

Table A.76. Kazpınar-78

Depth from the Surface, m		Lithology	Depth from the Surface, m		Lithology
Start	End		Start	End	
0	80	Andezite	541	670	Clayey Sandstone
80	130	Tuff-Marl	670	674	Coal
130	320	Agglomerate	674	740	Clayey Sandstone
320	380	Andezite-Tuff	740	741	Coal
380	410	Limestone	741	1160	Clayey Sandstone
410	510	Clayey Sandstone	1160	1161	Coal
510	512	Coal	1161	1170	Clayey Sandstone
512	540	Clayey Sandstone	1170	1171	Coal
540	541	Coal	1171	1235	Clayey Sandstone

Table A.77. Kazpınar-K1

Depth from the Surface, m		Lithology	Depth from the Surface, m		Lithology
Start	End		Start	End	
0	66	Andezite	483	484	Coal
66	112	Limestone	484	521	Sandstone
112	322	Agglomerate	521	522	Coal
322	346	Limestone	522	663	Clayey Sandstone
346	393	Sandstone	663	664	Coal
393	397	Coal	664	710	Clayey Sandstone
397	433	Sandstone	710	713	Coal
433	434	Coal	713	791	Clayey Sandstone
434	445	Clayey Sandstone	791	793	Coal
445	447	Coal	793	981	Clayey Sandstone
447	483	Sandstone			

Table A.78. Kazpınar-K2

Depth from the Surface, m		Lithology	Depth from the Surface, m		Lithology
Start	End		Start	End	
0	20	Andezite	374	606	Clayey Sandstone
20	112	Limestone	606	607	Coal
112	284	Agglomerate	607	629	Clayey Sandstone
284	310	Limestone	629	631	Coal
310	373	Clayey Sandstone	631	865	Sandstone
373	374	Coal			

Table A.79. Kazpınar-K3

Depth from the Surface, m		Lithology	Depth from the Surface, m		Lithology
Start	End		Start	End	
0	218	Agglomerate	613	618	Clayey Sandstone
218	245	Limestone	618	620	Coal
245	348	Clayey Sandstone	620	650	Clayey Sandstone
348	349	Coal	650	651	Coal
349	446	Clayey Sandstone	651	679	Clayey Sandstone
446	447	Coal	679	745	Sandstone
447	508	Clayey Sandstone	745	746	Coal
508	510	Coal	746	953	Clayey Sandstone
510	546	Sandstone	953	954	Coal
546	548	Coal	954	1085	Sandstone
548	612	Clayey Sandstone	1085	1086	Coal
612	613	Coal	1086	1105	Sandstone

Table A.80. Kazpınar-K4

Depth from the Surface, m		Lithology	Depth from the Surface, m		Lithology
Start	End		Start	End	
0	90	Andezite	545	547	Coal
90	130	Limestone	547	592	Clayey Sandstone
130	368	Agglomerate	592	593	Coal
368	381	Limestone	593	616	Clayey Sandstone
381	423	Sandstone	616	617	Coal
423	424	Coal	617	674	Clayey Sandstone
424	444	Sandstone	674	676	Coal
444	445	Coal	676	682	Clayey Sandstone
445	513	Sandstone	682	684	Coal
513	514	Coal	684	1057	Clayey Sandstone
515	545	Clayey Sandstone			

Table A.81. Kazpınar-K5

Depth from the Surface, m		Lithology	Depth from the Surface, m		Lithology
Start	End		Start	End	
0	117	Andezite	662	667	Coal
117	170	Limestone	667	878	Clayey Sandstone
170	375	Agglomerate	878	880	Coal
375	398	Limestone	880	1003	Clayey Sandstone
398	399	Coal	1003	1004	Coal
399	662	Clayey Sandstone	1004	1081	Clayey Sandstone

Table A.82. Kazpınar-K6

Depth from the Surface, m		Lithology	Depth from the Surface, m		Lithology
Start	End		Start	End	
0	15	Limestone	575	576	Coal
15	290	Agglomerate	576	583	Clayey Sandstone
290	315	Limestone	583	585	Coal
315	339	Sandstone	585	641	Clayey Sandstone
339	341	Coal	641	641	Coal
341	566	Clayey Sandstone	641	799	Clayey Sandstone
566	568	Coal	799	801	Coal
568	575	Clayey Sandstone	801	908	Clayey Sandstone

Table A.83. Kazpınar-K12

Depth from the Surface, m		Lithology	Depth from the Surface, m		Lithology
Start	End		Start	End	
0	12	Limestone	668	687	Clayey Sandstone
12	340	Agglomerate	687	690	Coal
340	380	Limestone	690	699	Clayey Sandstone
380	525	Clayey Sandstone	699	700	Coal
525	526	Coal	700	729	Clayey Sandstone
526	628	Clayey Sandstone	729	730	Coal
628	629	Coal	730	734	Clayey Sandstone
629	635	Clayey Sandstone	734	735	Coal
635	636	Coal	735	908	Clayey Sandstone
636	649	Clayey Sandstone	908	909	Coal
649	653	Coal	909	1077	Clayey Sandstone
653	664	Clayey Sandstone	1077	1078	Coal
664	668	Coal	1078	1087	Clayey Sandstone

Table A.84. Kazpınar-K19

Depth from the Surface, m		Lithology	Depth from the Surface, m		Lithology
Start	End		Start	End	
0	72	Andezite	774	775	Coal
72	157	Limestone	775	806	Clayey Sandstone
157	383	Agglomerate	806	807	Coal
383	418	Limestone	807	940	Clayey Sandstone
418	774	Clayey Sandstone	940	968	Clayey Sandstone

Table A.85. Kazpınar-K22

Depth from the Surface, m		Lithology	Depth from the Surface, m		Lithology
Start	End		Start	End	
0	77	Andezite	725	726	Coal
77	124	Limestone	726	795	Clayey Sandstone
124	369	Agglomerate	795	796	Coal
369	401	Limestone	796	806	Clayey Sandstone
401	645	Clayey Sandstone	806	807	Coal
645	647	Coal	807	1035	Clayey Sandstone
647	675	Clayey Sandstone	1035	1038	Coal
675	677	Coal	1038	1088	Clayey Sandstone
677	684	Clayey Sandstone	1088	1090	Coal
684	686	Coal	1090	1102	Clayey Sandstone
686	725	Clayey Sandstone			

Table A.86. Kazpınar-K23

Depth from the Surface, m		Lithology	Depth from the Surface, m		Lithology
Start	End		Start	End	
0	68	Limestone	450	817	Clayey Sandstone
68	113	Andezite	817	819	Coal
113	183	Limestone	819	839	Clayey Sandstone
183	425	Agglomerate	839	840	Coal
425	450	Limestone	840	981	Clayey Sandstone

Table A.87. Kazpınar-K25

Depth from the Surface, m		Lithology	Depth from the Surface, m		Lithology
Start	End		Start	End	
0	89	Andezite-Tuff	428	443	Clayey Sandstone
89	115	Limestone	443	445	Coal
115	311	Agglomerate	445	777	Clayey Sandstone
311	386	Tuff	777	778	Coal
386	411	Limestone	778	783	Clayey Sandstone
411	427	Clayey Sandstone	783	784	Coal
427	428	Coal	784	900	Clayey Sandstone

Table A.88. Kazpınar-K28

Depth from the Surface, m		Lithology	Depth from the Surface, m		Lithology
Start	End		Start	End	
0	72	Andezite	390	427	Limestone
72	120	Limestone	427	767	Clayey Sandstone
120	283	Agglomerate	767	768	Coal
283	390	Tuff	768	906	Clayey Sandstone

Table A.89. Kazpınar-K31

Depth from the Surface, m		Lithology	Depth from the Surface, m		Lithology
Start	End		Start	End	
0	80	Andezite	426	704	Clayey Sandstone
80	130	Tuff-Marl	704	706	Coal
130	283	Agglomerate	706	722	Clayey Sandstone
283	400	Tuff	722	723	Coal
400	426	Limestone	723	841	Clayey Sandstone

Table A.90. Kazpınar-K33

Depth from the Surface, m		Lithology	Depth from the Surface, m		Lithology
Start	End		Start	End	
0	20	Tuff-Marl	550	552	Coal
20	304	Agglomerate	552	635	Clayey Sandstone
304	337	Limestone	635	637	Coal
337	338	Coal	637	658	Clayey Sandstone
338	360	Clayey Sandstone	658	662	Coal
360	370	Coal	662	748	Clayey Sandstone
370	393	Sandstone	748	752	Coal
393	396	Coal	752	766	Clayey Sandstone
396	409	Clayey Sandstone	766	767	Coal
409	410	Coal	767	771	Clayey Sandstone
410	432	Clayey Sandstone	771	772	Coal
432	434	Coal	772	812	Clayey Sandstone
434	498	Clayey Sandstone	812	814	Coal
498	500	Coal	814	829	Clayey Sandstone
500	536	Clayey Sandstone	829	831	Coal
536	537	Coal	831	917	Clayey Sandstone
537	550	Clayey Sandstone	550	552	Coal

Table A.91. Kuşkayası-32

Depth from the Surface, m		Lithology	Depth from the Surface, m		Lithology
Start	End		Start	End	
0	230	Andezite-Tuff	378	555	Sandstone
230	240	Limestone	555	557	Coal
240	241	Coal	557	760	Sandstone
241	300	Sandstone	760	761	Coal
300	301	Coal	761	800	Sandstone
301	310	Sandstone	800	803	Coal
310	313	Coal	803	855	Sandstone
313	375	Sandstone	855	858	Coal
375	378	Coal	858	997	Sandstone

Table A.92. S6

| Depth from the Surface, m | | Lithology | Depth from the Surface, m | | Lithology |
Start	End		Start	End	
0	25	Agglomerate	813	814	Coal
25	75	Tuff	814	896	Sandstone
75	363	Agglomerate	896	897	Coal
363	380	Pl. Limestone	897	905	Sandstone
380	396	Sandy Limestone	905	906	Coal
396	500	Sandstone	906	946	Clay
500	599	Sandstone	946	947	Coal
599	600	Coal	947	1067	Sandstone
600	738	Sandstone	1067	1068	Coal
738	739	Coal	1068	1153	Clay
739	801	Sandstone	1153	1156	Coal
801	813	Clay	1156	1174	Clay

Table A.93. S12

| Depth from the Surface, m | | Lithology | Depth from the Surface, m | | Lithology |
Start	End		Start	End	
0	102	Agglomerate	788	869	Sandstone
102	106	Pl. Limestone	869	870	Coal
106	130	Sandy Limestone	870	1085	Clayey Sandstone
130	175	Permian	1085	1087	Coal
175	783	Clayey Sandstone	1087	1253	Sandstone
783	788	Coal			

Table A.94. S33

| Depth from the Surface, m | | Lithology | Depth from the Surface, m | | Lithology |
Start	End		Start	End	
0	61	Tuff	656	657	Coal
61	316	Agglomerate	657	681	Sandstone
316	324	Pl. Limestone	681	683	Coal
324	344	Sandy Limestone	683	719	Clayey Sandstone
344	550	Clay	719	977	Sandstone
550	656	Sandstone			

Table A.95. S34

| Depth from the Surface, m | | Lithology | Depth from the Surface, m | | Lithology |
Start	End		Start	End	
0	210	Agglomerate	601	663	Sandstone
210	230	Pl. Limestone	663	666	Coal
230	250	Sandy Limestone	666	717	Sandstone
250	415	Sandstone	717	725	Coal
415	418	Coal	725	739	Sandstone
418	434	Sandstone	739	740	Coal
434	435	Coal	740	789	Sandstone
435	598	Sandstone	789	789	Coal
598	601	Coal	789	833	Sandstone

Table A.96. S35

Depth from the Surface, m		Lithology	Depth from the Surface, m		Lithology
Start	End		Start	End	
0	320	Agglomerate	747	761	Clay
320	338	Pl. Limestone	761	795	Sandstone
338	365	Sandy Limestone	795	796	Coal
365	400	Clay	796	818	Sandstone
400	735	Sandstone	818	819	Coal
735	736	Coal	819	850	Sandstone
736	744	Clay	850	851	Coal
744	747	Coal	851	887	Sandstone

Table A.97. S40

Depth from the Surface, m		Lithology	Depth from the Surface, m		Lithology
Start	End		Start	End	
0	20	Pl. Limestone	464	465	Coal
20	103	Sandy Limestone	465	471	Clay
103	384	Filis	471	472	Coal
384	439	Limestone	472	762	Sandstone
439	464	Clay			

Table A.98. S41

Depth from the Surface, m		Lithology	Depth from the Surface, m		Lithology
Start	End		Start	End	
0	155	Filis	376	379	Clay
155	215	Limestone	379	389	Coal
215	239	Conglomerate	389	438	Sandstone
239	240	Coal	438	439	Coal
240	249	Clay	439	453	Clay
249	251	Coal	453	455	Coal
251	257	Clay	455	551	Sandstone
257	259	Coal	551	555	Coal
259	280	Conglomerate	555	587	Clay
280	283	Coal	587	589	Coal
283	290	Clay	589	595	Clay
290	291	Coal	595	598	Coal
291	353	Sandstone	598	614	Clay
353	357	Coal	614	615	Coal
357	370	Clay	615	623	Clay
370	372	Coal	623	628	Coal
372	374	Clay	628	682	Sandstone
374	376	Coal			

Table A.99. S47

Depth from the Surface, m		Lithology	Depth from the Surface, m		Lithology
Start	End		Start	End	
0	130	Filis	708	711	Coal
130	200	Limestone	711	713	Sandstone
200	279	Sandstone	713	716	Coal
279	281	Coal	716	747	Sandstone
281	350	Sandstone	747	748	Coal
350	351	Coal	748	823	Sandstone
351	414	Sandstone	823	824	Coal
414	415	Coal	824	855	Sandstone
415	574	Sandstone	855	856	Coal
574	575	Coal	856	867	Sandstone
575	624	Sandstone	867	869	Coal
624	626	Coal	869	904	Sandstone
626	708	Sandstone			

Table A.100. S71

Depth from the Surface, m		Lithology	Depth from the Surface, m		Lithology
Start	End		Start	End	
0	83	Tuff	825	826	Coal
83	365	Agglomerate	826	850	Clay
365	385	Pl. Limestone	850	851	Coal
385	405	Sandy Limestone	851	914	Clayey Sandstone
405	504	Clayey Sandstone	914	915	Coal
504	505	Coal	915	938	Sandy Limestone
505	575	Clay	938	939	Coal
575	576	Coal	939	1035	Sandstone
576	622	Clayey Sandstone	1035	1036	Coal
622	623	Coal	1036	1051	Clayey Sandstone
623	654	Conglomerate	1051	1052	Coal
654	655	Coal	1052	1108	Clayey Sandstone
655	668	Sandstone	1108	1146	Sandstone
668	671	Coal	1146	1148	Coal
671	714	Sandstone	1148	1181	Sandstone
714	720	Coal	1181	1182	Coal
720	730	Clay	1182	1201	Clayey Sandstone
730	734	Şiferton	1201	1202	Coal
734	737	Clay	1202	1237	Clayey Sandstone
737	738	Coal	1237	1238	Coal
738	756	Clay	1238	1261	Clayey Sandstone
756	757	Coal	1261	1263	Coal
757	774	Clay	1263	1275	Clayey Sandstone
774	775	Coal	1275	1276	Coal
775	825	Clayey Sandstone	1276	1302	Clayey Sandstone

Table A.101. S74

Depth from the Surface, m		Lithology	Depth from the Surface, m		Lithology
Start	End		Start	End	
0	26	Agglomerate	815	816	Coal
26	86	Tuff	816	859	Sandstone
86	403	Agglomerate	859	860	Coal
403	418	Pl. Limestone	860	895	Sandstone
418	440	Sandy Limestone	895	896	Coal
440	652	Sandstone	896	939	Sandstone
652	653	Coal	939	940	Coal
653	675	Sandstone	940	1044	Sandstone
675	677	Coal	1044	1045	Coal
677	695	Sandstone	1045	1099	Sandstone
695	698	Coal	1099	1100	Coal
698	710	Sandstone	1100	1130	Sandstone
710	712	Coal	1130	1132	Coal
712	724	Sandstone	1132	1167	Sandstone
724	726	Coal	1167	1168	Coal
726	746	Sandstone	1168	1194	Sandstone
746	747	Coal	1194	1195	Coal
747	815	Sandstone	1195	1203	Sandstone

Table A.102. S89

Depth from the Surface, m		Lithology	Depth from the Surface, m		Lithology
Start	End		Start	End	
0	20	Tuff	895	896	Coal
20	297	Agglomerate	896	907	Clayey Sandstone
297	317	Pl. Limestone	907	908	Coal
317	332	Sandy Limestone	908	924	Clayey Sandstone
332	696	Clayey Sandstone	924	925	Coal
696	697	Coal	925	1018	Sandstone
697	717	Clayey Sandstone	1018	1019	Coal
717	719	Coal	1019	1078	Sandstone
719	745	Clayey Sandstone	1078	1079	Coal
745	750	Coal	1079	1112	Sandstone
750	766	Clayey Sandstone	1112	1115	Coal
766	767	Coal	1115	1146	Sandstone
767	772	Clayey Sandstone	1146	1147	Coal
772	773	Coal	1147	1162	Sandstone
773	795	Clayey Sandstone	1162	1163	Coal
795	796	Coal	1163	1201	Clayey Sandstone
796	834	Sandstone	1201	1202	Coal
834	835	Coal	1202	1206	Clayey Sandstone
835	875	Sandstone	1206	1207	Coal
875	876	Coal	1207	1232	Sandstone
876	895	Sandstone			

Table A.103. Sondaj-13

Depth from the Surface, m Start	End	Lithology	Depth from the Surface, m Start	End	Lithology
0	140	Agglomerate	537	539	Coal
140	173	Andezite-Tuff	539	605	Clayey Sandstone
173	272	Limestone	605	606	Coal
272	405	Sandstone	606	660	Sandstone
405	406	Coal	660	662	Coal
406	449	Sandstone	662	749	Clayey Sandstone
449	452	Coal	749	750	Coal
452	537	Sandstone	750	1000	Sandstone

Table A.104. Şah-Mah-42

Depth from the Surface, m Start	End	Lithology	Depth from the Surface, m Start	End	Lithology
0	240	Claystone	330	869	Sandstone
240	330	Limestone			

Table A.105. Şıbben-48

Depth from the Surface, m Start	End	Lithology	Depth from the Surface, m Start	End	Lithology
0	15	Limestone	821	960	Clayey Sandstone
15	105	Andezite	960	962	Coal
105	160	Tuff-Marl	962	1150	Clayey Sandstone
160	245	Agglomerate	1150	1151	Coal
245	260	Andezite-Tuff	1151	1240	Clayey Sandstone
260	300	Limestone	1240	1241	Coal
300	820	Sandstone	1241	1297	Clayey Sandstone
820	821	Coal			

Table A.106. Tarlaağzı-22

Depth from the Surface, m Start	End	Lithology	Depth from the Surface, m Start	End	Lithology
0	35	Limestone	726	785	Sandstone
35	590	Sandstone	785	786	Coal
590	592	Coal	786	1010	Sandstone
592	725	Sandstone	1010	1012	Coal
725	726	Coal	1012	1050	Sandstone

Table A.107. Tarlaağzı-26

Depth from the Surface, m Start	End	Lithology	Depth from the Surface, m Start	End	Lithology
0	130	Sandstone (W.C.)	554	600	Sandstone
130	330	Sandstone (W.B.)	600	601	Coal
330	550	Sandstone (W.A.)	601	760	Sandstone
550	554	Coal			

281

Table A.108. Uğurlar-1

| Depth from the Surface, m | | Lithology | Depth from the Surface, m | | Lithology |
Start	End		Start	End	
0	150	Agglomerate	744	745	Coal
150	188	Andesite-tuff	745	965	Clayey sandstone
188	240	Limestone	965	966	Coal
240	537	Clayey sandstone	966	970	Clayey sandstone
537	538	Coal	970	972	Coal
538	744	Clayey sandstone	972	1060	Clayey sandstone

Table A.109. Uğurlar-2

| Depth from the Surface, m | | Lithology | Depth from the Surface, m | | Lithology |
Start	End		Start	End	
0	225	Agglomerate	622	625	Coal
225	247	Andezite-Tuff	625	652	Clayey Sandstone
247	276	Limestone	652	654	Coal
276	367	Clayey Sandstone	654	682	Clayey Sandstone
367	368	Coal	682	684	Coal
368	587	Clayey Sandstone	684	736	Clayey Sandstone
587	588	Coal	736	737	Coal
588	607	Clayey Sandstone	737	876	Sandstone
607	608	Coal	876	878	Coal
608	617	Clayey Sandstone	878	918	Clayey Sandstone
617	618	Coal	918	920	Coal
618	622	Clayey Sandstone	920	986	Sandstone

Table A.110. Uğurlar-3

| Depth from the Surface, m | | Lithology | Depth from the Surface, m | | Lithology |
Start	End		Start	End	
0	50	Agglomerate	911	917	Coal
50	82	Andezite-Tuff	917	920	Clayey Sandstone
82	129	Limestone	920	921	Coal
129	645	Clayey Sandstone	921	1003	Clayey Sandstone
645	646	Coal	1003	1004	Coal
646	905	Clayey Sandstone	1004	1129	Clayey Sandstone
905	906	Coal	1129	1131	Coal
906	911	Clayey Sandstone	1131	1230	Clayey Sandstone

Table A.111. Uğurlar-4

| Depth from the Surface, m | | Lithology | Depth from the Surface, m | | Lithology |
Start	End		Start	End	
0	160	Agglomerate	1079	1096	Clayey Sandstone
160	188	Andezite-Tuff	1096	1098	Coal
188	215	Limestone	1098	1296	Clayey Sandstone
215	509	Sandstone (Perm.)	1296	1298	Coal
509	1078	Clayey Sandstone	1298	1299	Sandstone
1078	1079	Coal			

Table A.112. Uğurlar-73

| Depth from the Surface, m | | Lithology | Depth from the Surface, m | | Lithology |
Start	End		Start	End	
0	10	Andezite	245	320	Andezite-Tuff
10	85	Tuff-Marl	320	345	Limestone
85	245	Agglomerate	345	1415	Sandstone

Table A.113. Uğurlar-K26

| Depth from the Surface, m | | Lithology | Depth from the Surface, m | | Lithology |
Start	End		Start	End	
0	86	Andezite	703	707	Coal
86	131	Limestone	707	806	Clayey Sandstone
131	703	Clayey Sandstone			

Table A.114. Uzunöz-15

| Depth from the Surface, m | | Lithology | Depth from the Surface, m | | Lithology |
Start	End		Start	End	
0	70	Andezite-Tuff	706	708	Coal
70	137	Limestone	708	848	Sandstone
137	190	Clayey Sandstone	848	851	Coal
190	190	Coal	851	976	Sandstone
190	372	Clayey Sandstone	976	977	Coal
372	374	Coal	977	1148	Sandstone
374	616	Sandstone	1148	1151	Coal
616	617	Coal	1151	1200	Sandstone
617	706	Sandstone			

Table A.115. Uzunöz-82

| Depth from the Surface, m | | Lithology | Depth from the Surface, m | | Lithology |
Start	End		Start	End	
0	10	Limestone	960	1040	Sandstone
10	90	Andezite	1040	1041	Coal
90	140	Tuff-Marl	1041	1055	Clayey Sandstone
140	160	Agglomerate	1055	1057	Coal
160	170	Andezite-Tuff	1057	1460	Clayey Sandstone
170	960	Limestone			

APPENDIX B

Lithologic information of the wells were visualized using Macromedia Flash program and given in the following figures.
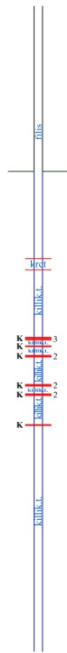
Figure B.1. AK1   Figure B.2. AK2   Figure B.3. AK3   Figure B.4. AK4
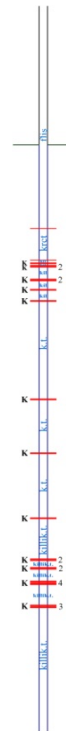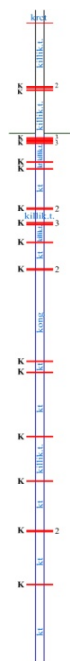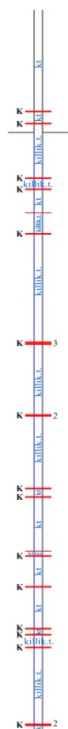
Figure B.5. AK5　　**Figure B.6. AK6**　　**Figure B.7. AK7**　　**Figure B.8. AK8**
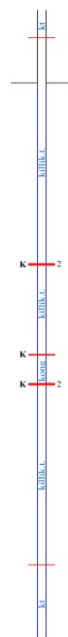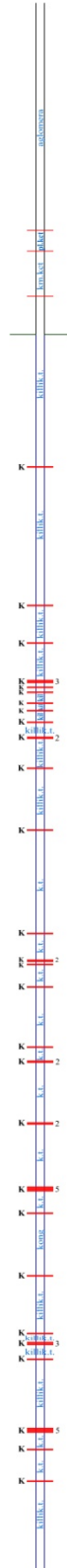
Figure B.9. AK9　　**Figure B.10. AK10**　　**Figure B.11. AK11**　　**Figure B.12. AK12**
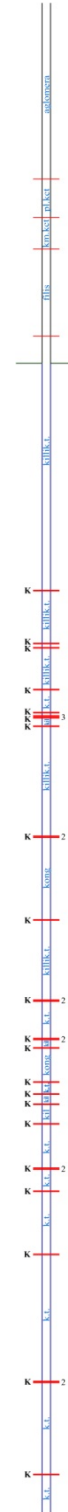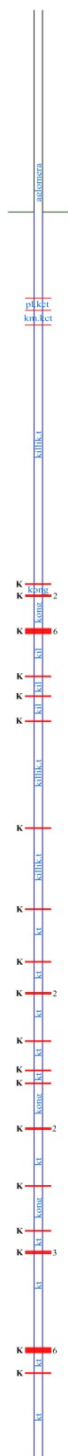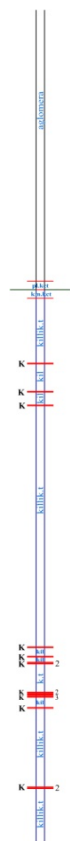
Figure B.13. AK13 **Figure B.14. AK14** **Figure B.15. AK15** **Figure B.16. AK10**
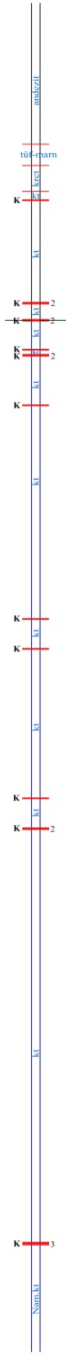
Figure B.17. AK11 **Figure B.18. AK12** **Figure B.19. Askersuyu-31** **Figure B.20. Bedesten-21**
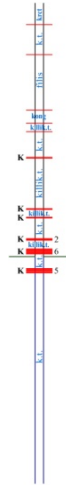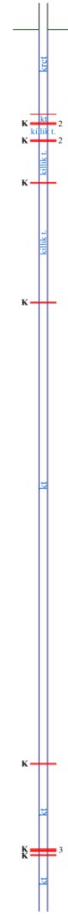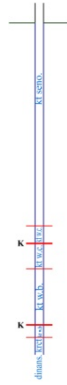
Figure B.21.
Bedesten-45
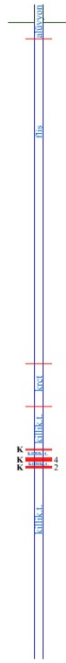
Figure B.22.
Bedesten-83

Figure B.23.
Bostanlar-36
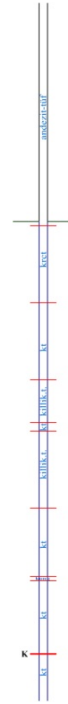
Figure B.24.
Bostanlar-37

Figure B.25.
Bostanlar-38
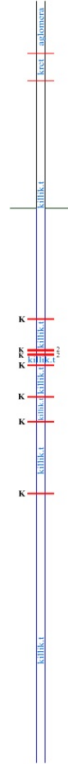
Figure B.26.
Bostanlar-K17

Figure B.27.
Çamlık-16A

Figure B.28.
Çamlık-56

Figure B.29.
Çamlık-77

Figure B.30.
Ç.Kıran-65

Figure B.31.
Ç.Kıran-66

Figure B.32.
Dökük-23

Figure B.33.
Fermitkadı-55
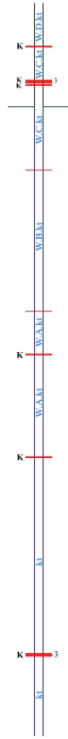
Figure B.34.
Gömü-27

Figure B.35.
Gömü-28

Figure B.36.
Gömü-29

Figure B.37.
Gömü-80

Figure B.38.
Gömü-81

Figure B.39.
Gömü-84

Figure B.40.

Gömü-85

Figure B.41.
Gömü-86
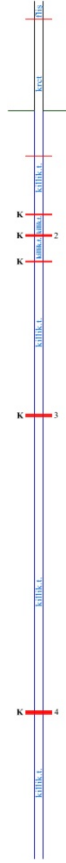
Figure B.42.
Gömü-K24
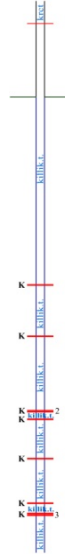
Figure B.43.
Gömü-K27

Figure B.44.
Gömü-K32
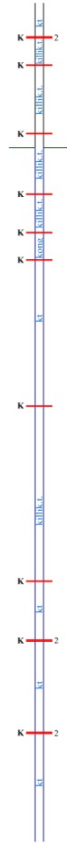
Figure B.45.
Gömü-K37

Figure B.46. K10

Figure B.47. K11

Figure B.48. K13
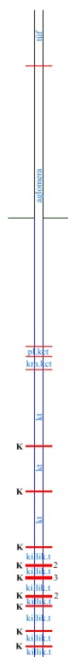
Figure B.49. K14   **Figure B.50. K15**   **Figure B.51. K16**   **Figure B.52. K18**
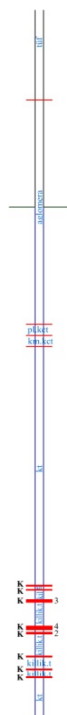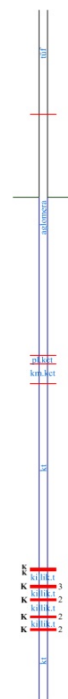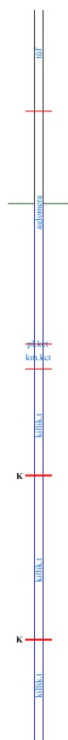
Figure B.53. K20 **Figure B.54. K21** **Figure B.55. K30** **Figure B.56. K34**

Figure B.57.
Kaman-10

Figure B.58.
Kaman-14

Figure B.591.
Kaman-39
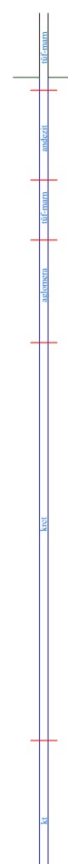
Figure B.60.
Kaman-53

Figure B.61.
Kaman-58
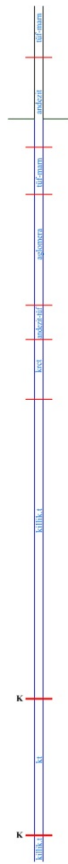
Figure B.62.
Kaman-60
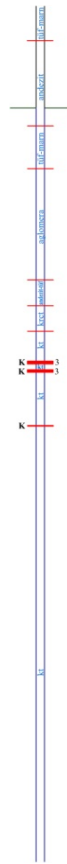
Figure B.63.
Kaman-61

Figure B.64.
Kaman-75

Figure B.65.
Karaçay-9

Figure B.66.
Karaçay-11
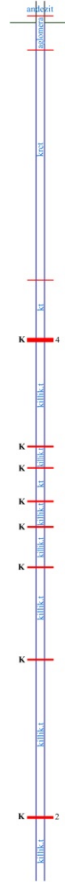
Figure B.67.
Karaçay-K29

Figure B.68.
Kazpınar-7

Figure B.69.
Kazpınar-18
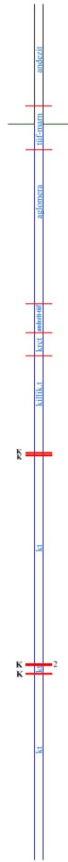
Figure B.70.
Kazpınar-20

Figure B.71.
Kazpınar-51
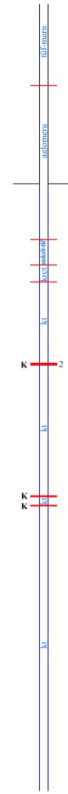
Figure B.72.
Kazpınar-62

Figure B.73.
Kazpınar-63
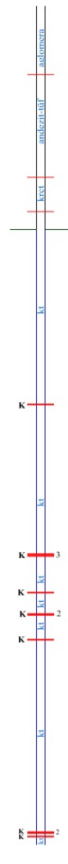
Figure B.74.
Kazpınar-64

Figure B.75.
Kazpınar-69

Figure B.76.
Kazpınar-78
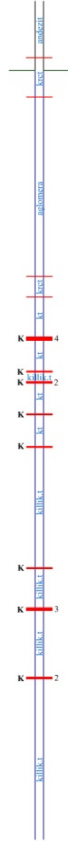
Figure B.77.
Kazpınar-K1
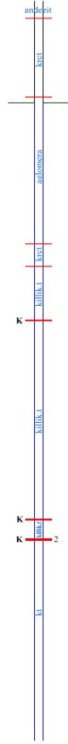
Figure B.78.
Kazpınar-K2
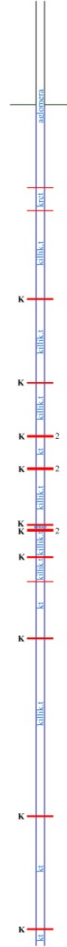
Figure B.79.
Kazpınar-K3
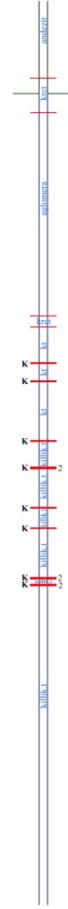
Figure B.80.
Kazpınar-K4

Figure B.81.
Kazpınar-K5

Figure B.82.
Kazpınar-K6
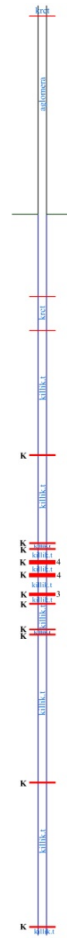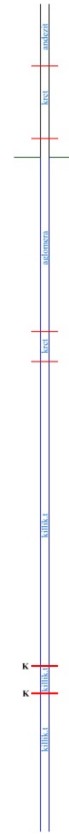
Figure B.83.
Kazpınar-K12

Figure B.84.
Kazpınar-K19

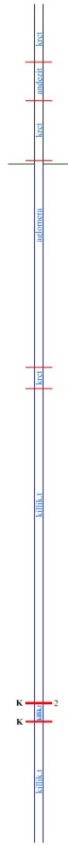**Figure B.85. Kazpınar-K22**
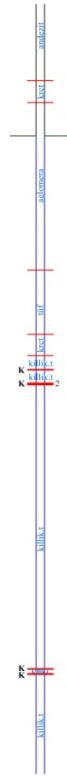
Figure B.86. Kazpınar-K23
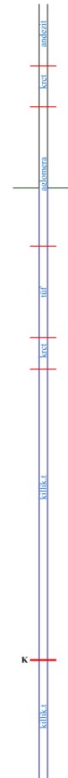
Figure B.87. Kazpınar-K25

Figure B.88. Kazpınar-K28
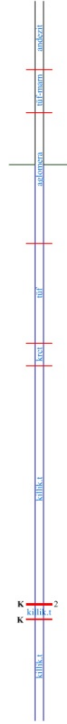
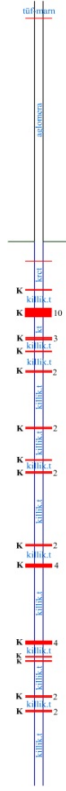**Figure B.89. Kazpınar-K31**

Figure B.90. Kazpınar-K33

Figure B.91. Kuşkayası-32
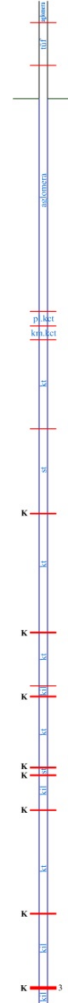
Figure B.92. S6

Figure B.93. S12   Figure B.94. S33   Figure B.95. S34   Figure B.96. S35
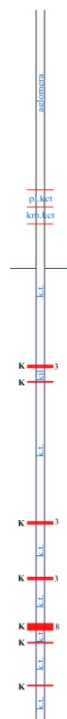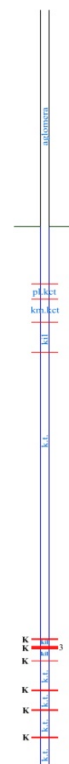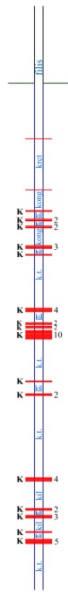
Figure B.97. S40 **Figure B.98. S41** **Figure B.99. S47** **Figure B.100. S71**
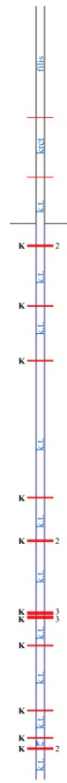
308
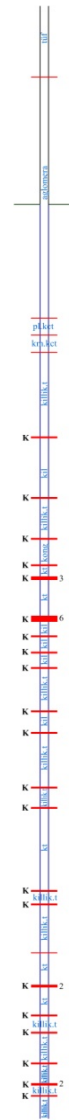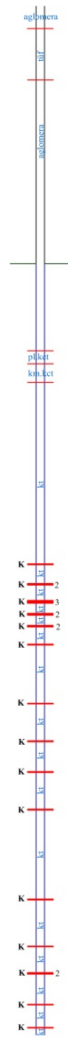
Figure B.101. S74

Figure B.102. S89

**Figure B.103.
Sondaj-13**

**Figure B.104.
Şah-Mah-42**

Figure B.105.
Şıbben-48
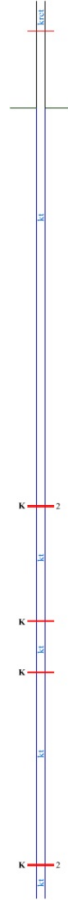
Figure B.106.
Tarlaağzı-22

Figure B.107.
Tarlaağzı-26
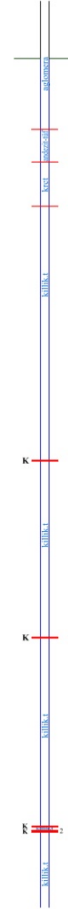
Figure B.108.
Uğurlar-1

Figure B.109.
Uğurlar-2
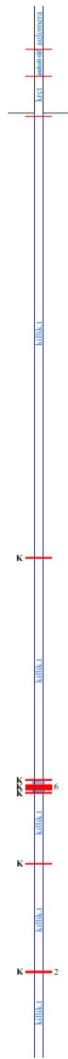
Figure B.110.
Uğurlar-3

Figure B.111.
Uğurlar-4

Figure B.112.
Uğurlar-73

311

Figure B.113.
Uğurlar-K26
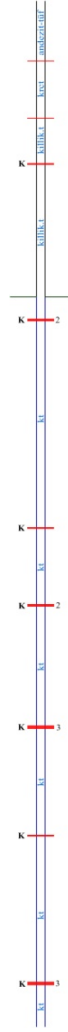
Figure B.114.
Uzunöz-15

Figure B.115.
Uzunöz-82

Correlations between coal seams can be seen in the following figures.
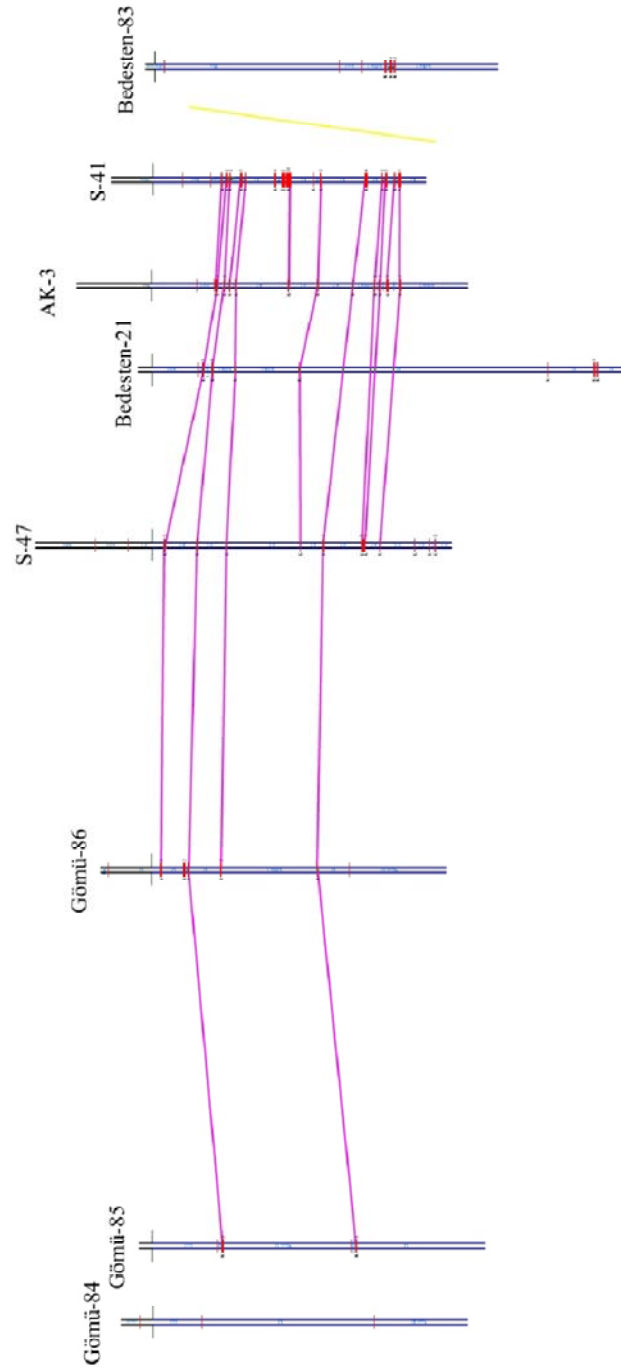
Figure C.1. Correlation of the Seams found on the Horizontal Area 1
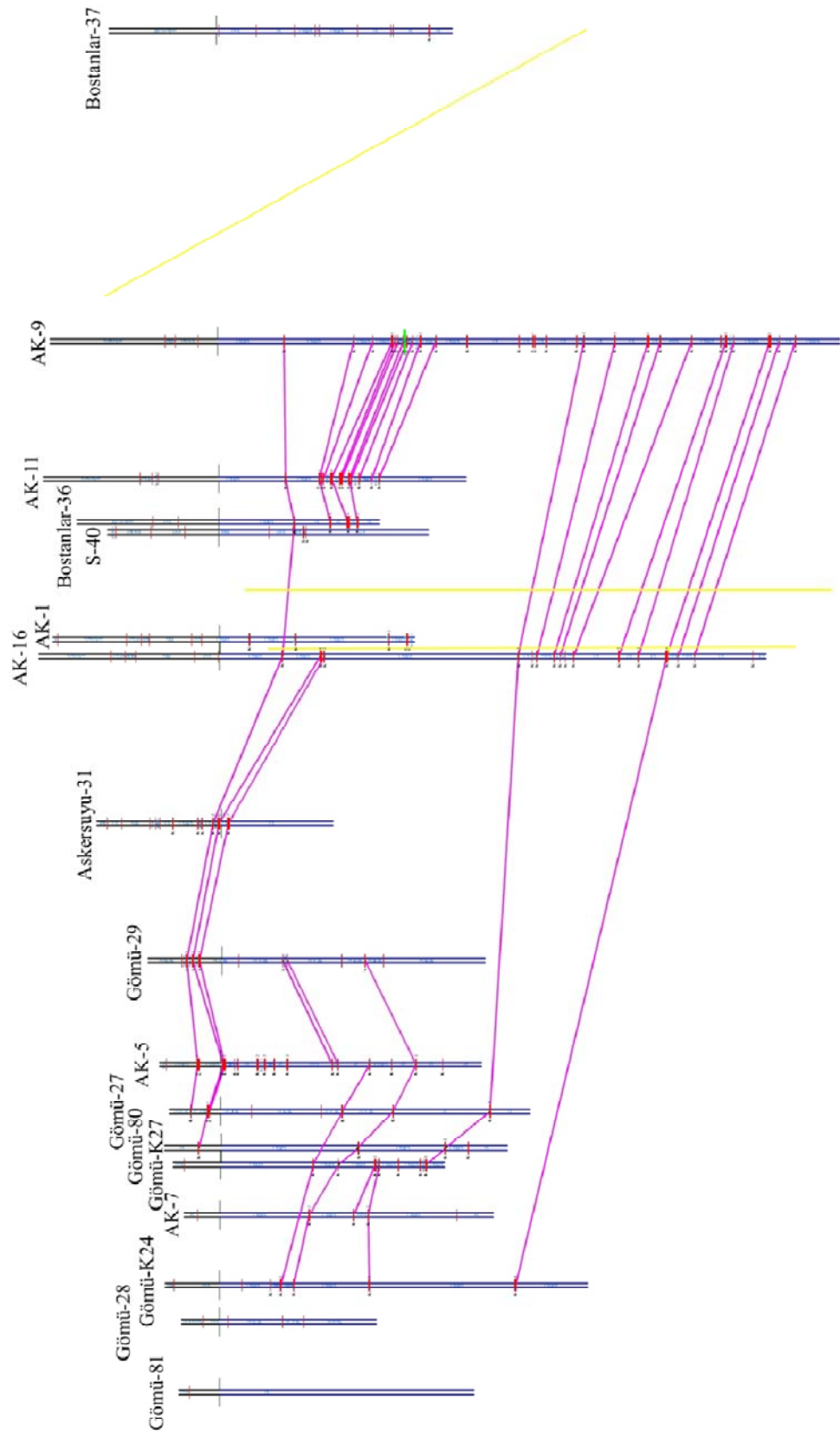
Figure C.2. Correlation of the Seams found on the Horizontal Area 2

314
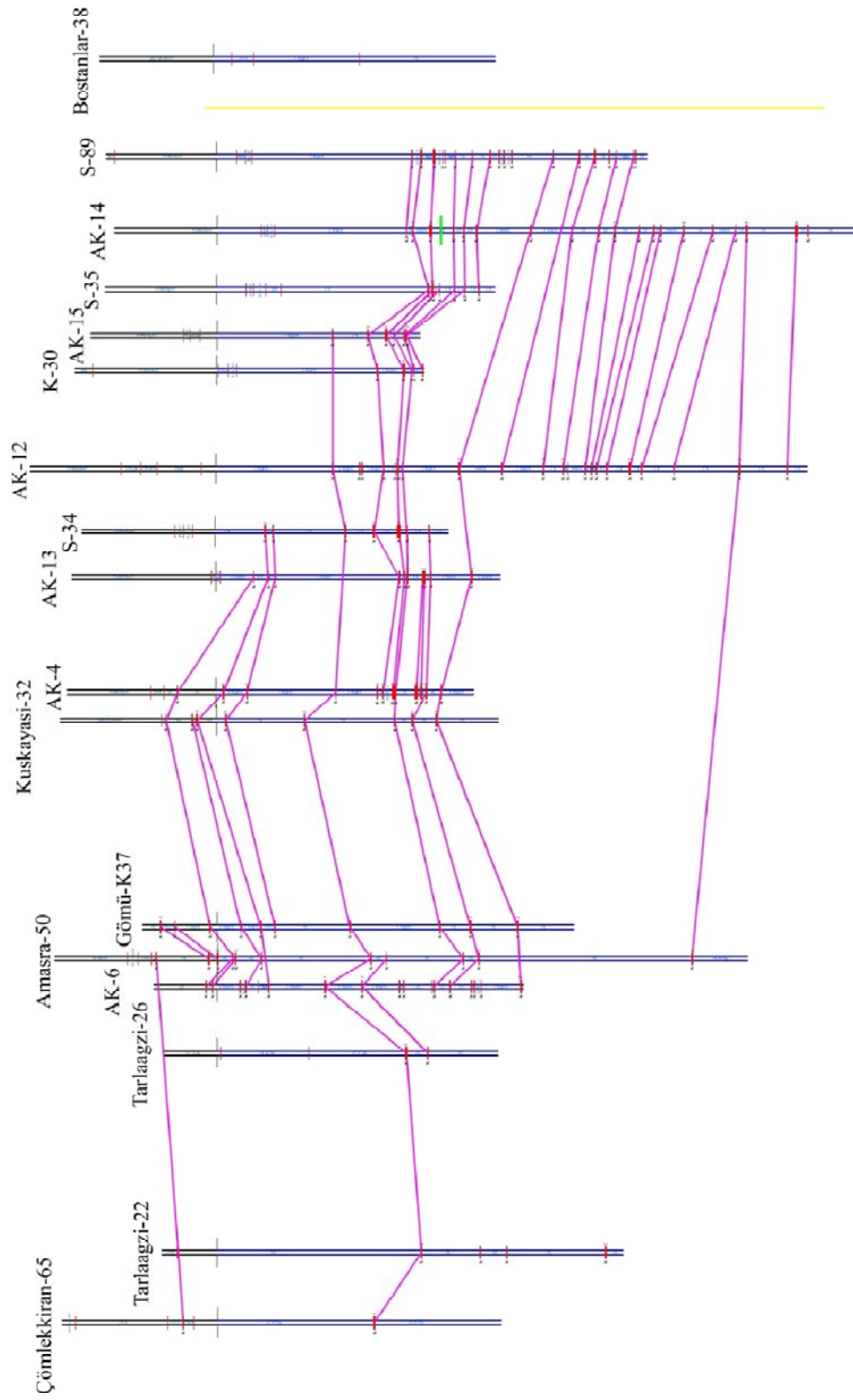
Figure C.3. Correlation of the Seams found on the Horizontal Area 3

315
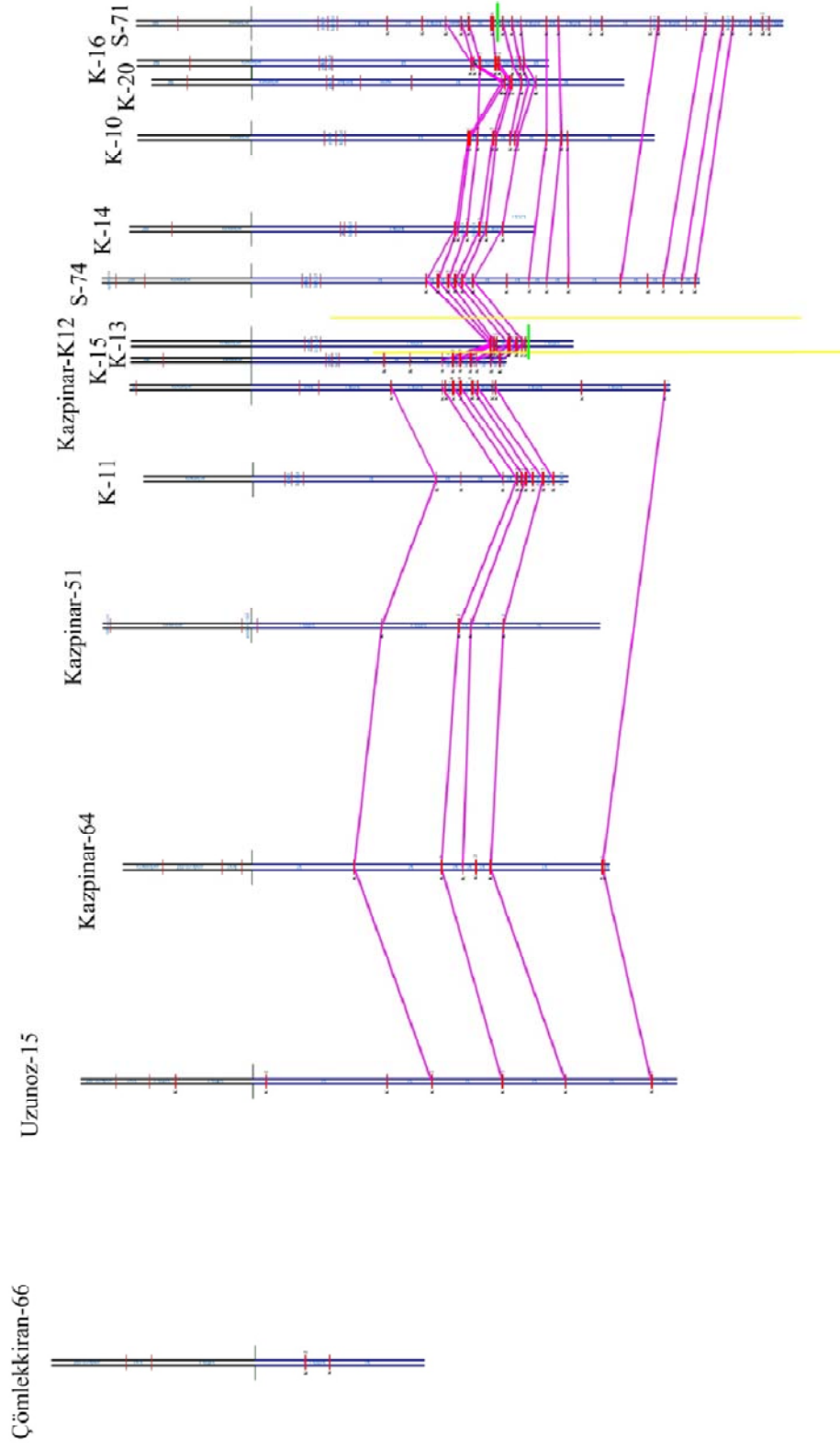
Figure C.4. Correlation of the Seams found on the Horizontal Area 4

316
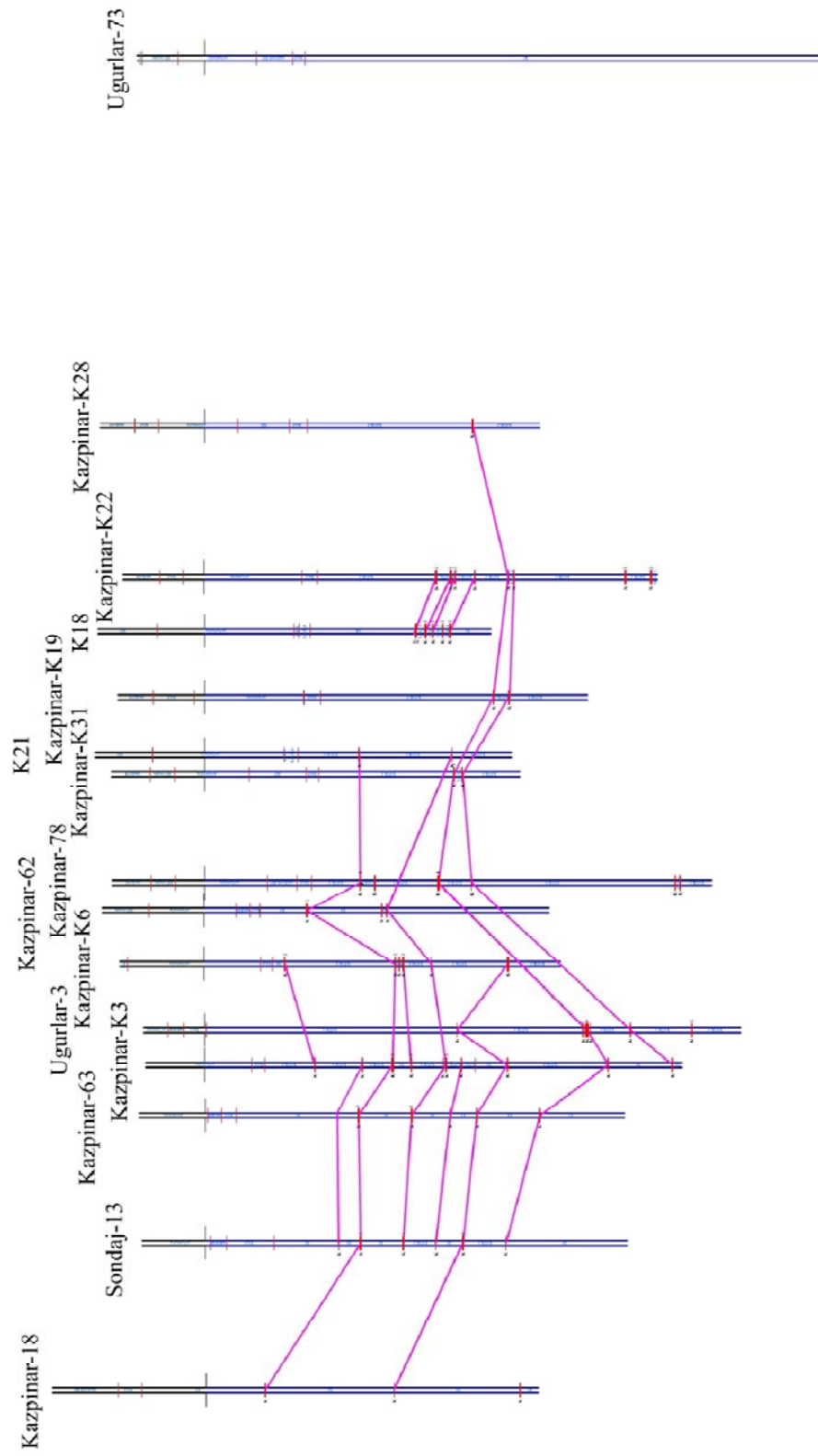
Figure C.5. Correlation of the Seams found on the Horizontal Area 5

317
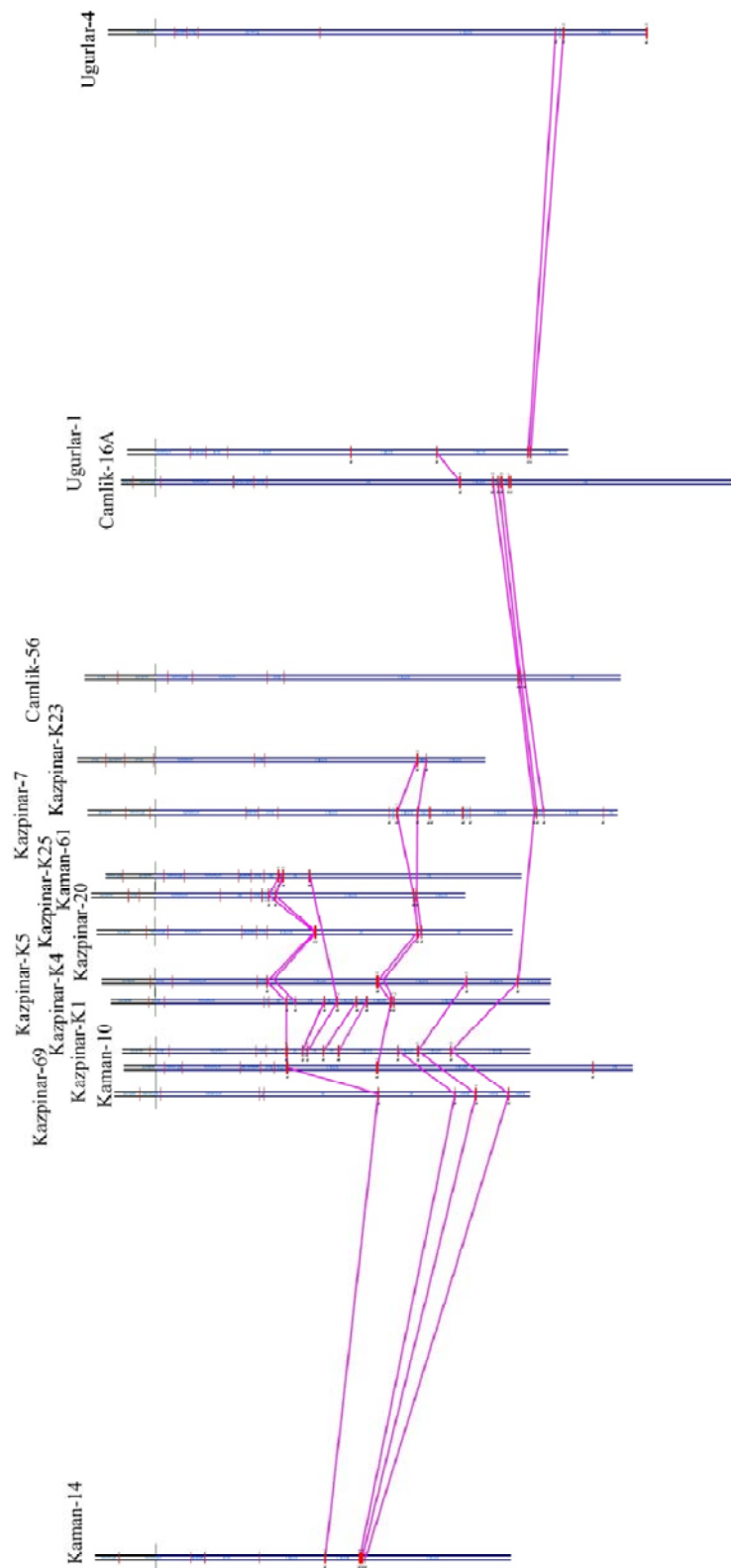
Figure C.6. Correlation of the Seams found on the Horizontal Area 6
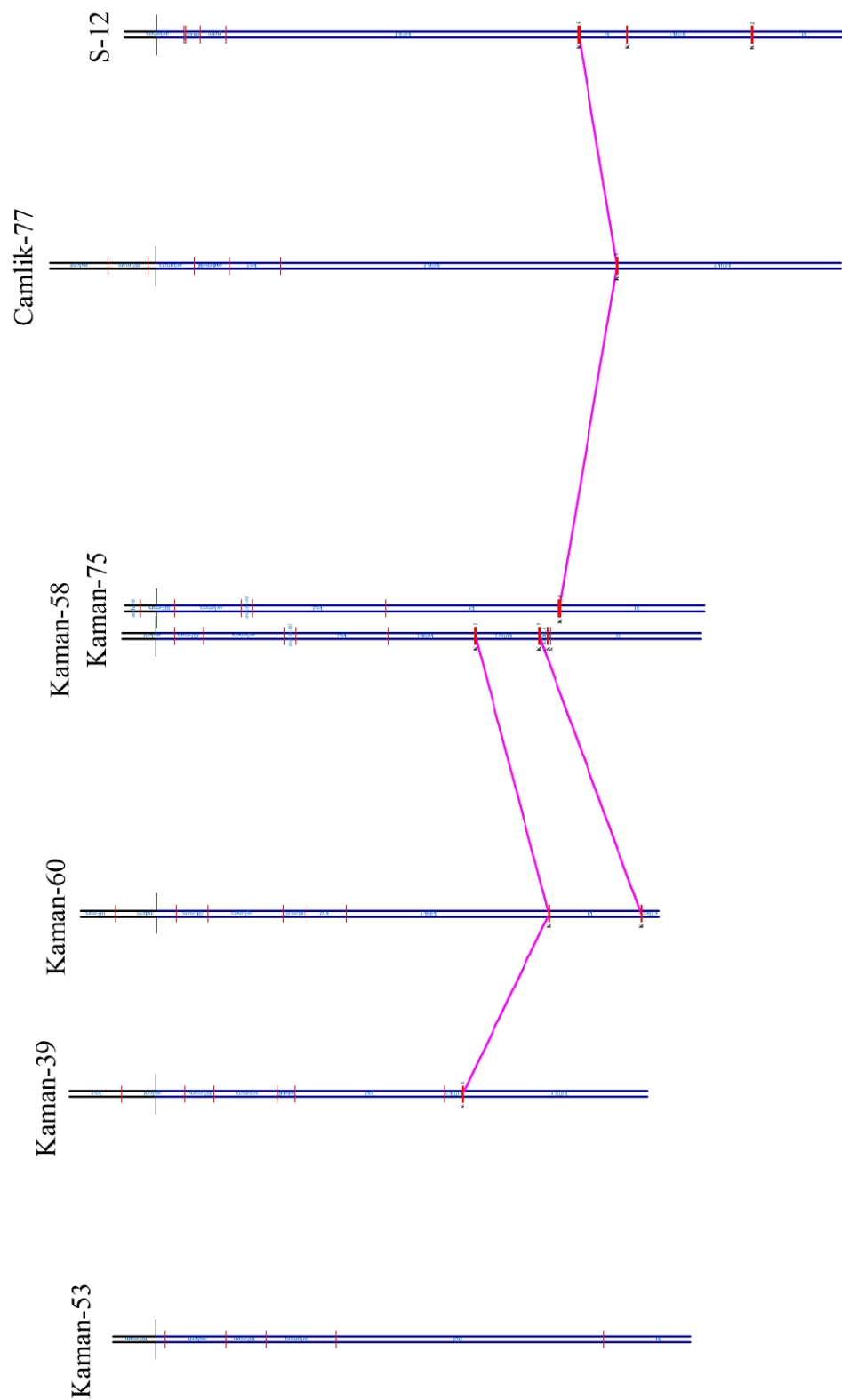
Figure C.7. Correlation of the Seams found on the Horizontal Area 7
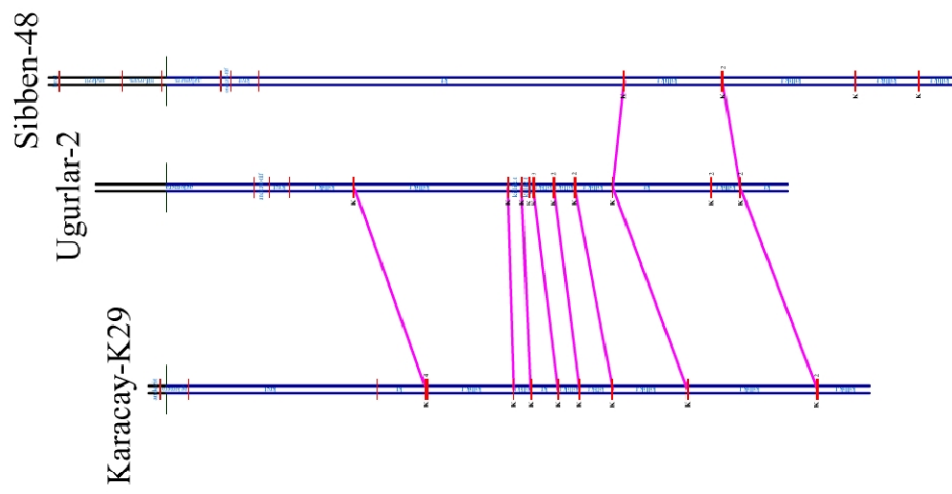
Figure C.8. Correlation of the Seams found on the Horizontal Area 8

320
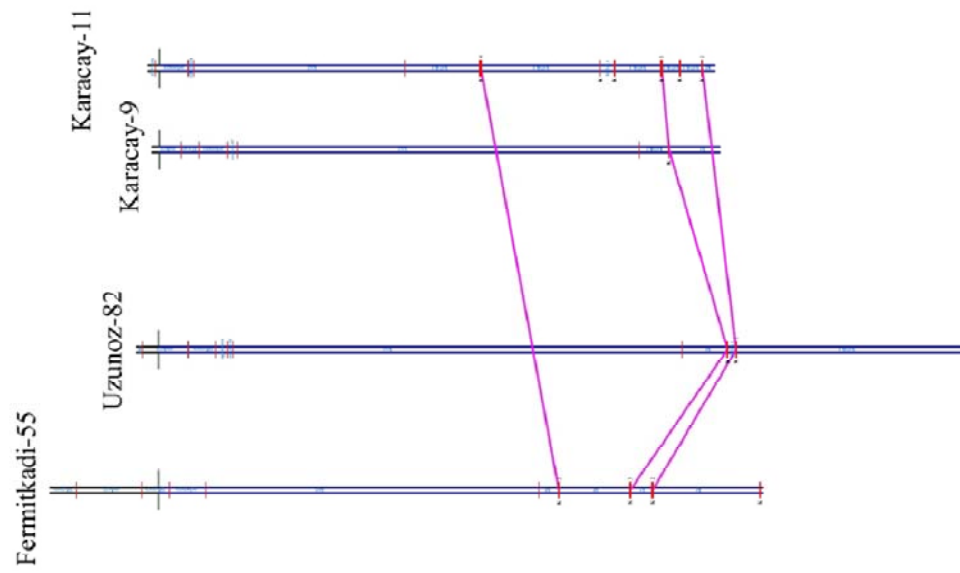
Figure C.9. Correlation of the Seams found on the Horizontal Area 9

321
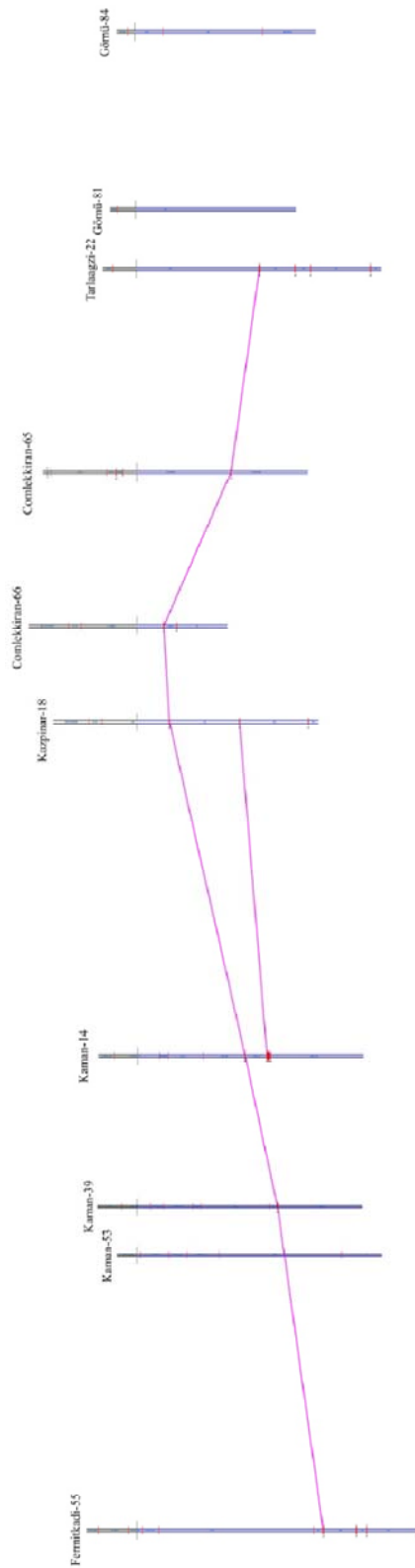
Figure C.10. Correlation of the Seams found on the Vertical Area 1

Figure C.11. Correlation of the Seams found on the Vertical Area 2

323
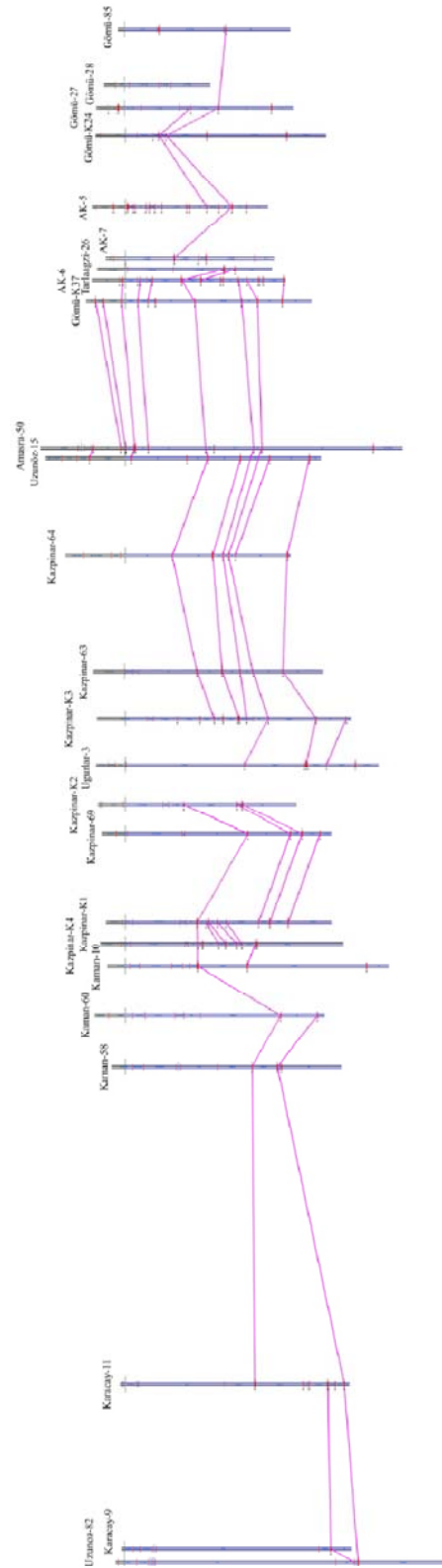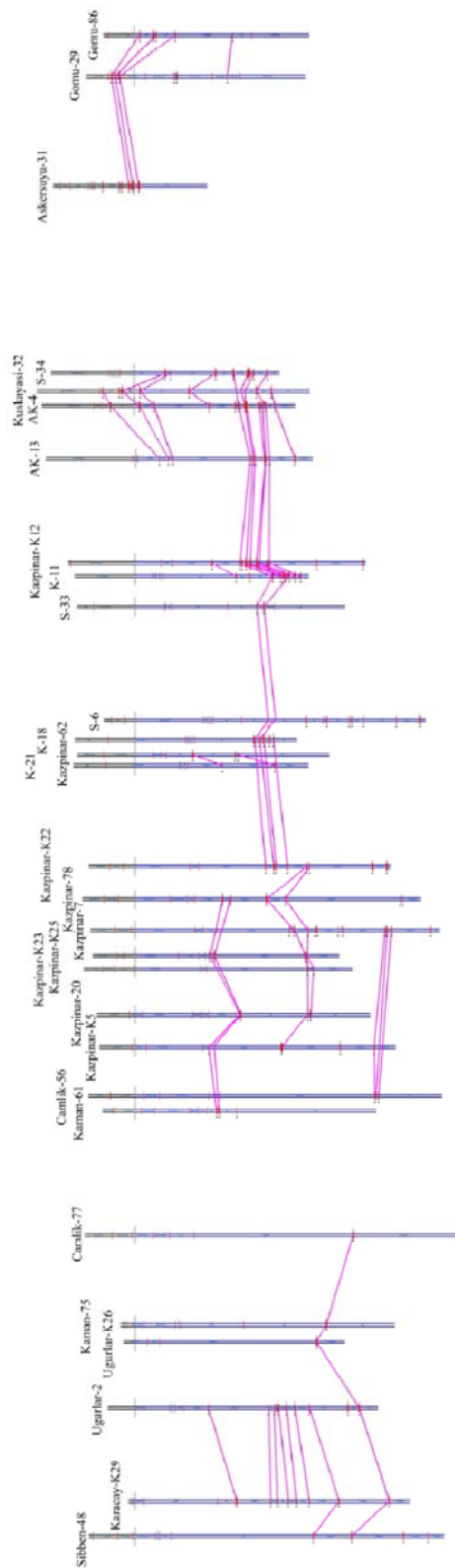
Figure C.12. Correlation of the Seams found on the Vertical Area 3
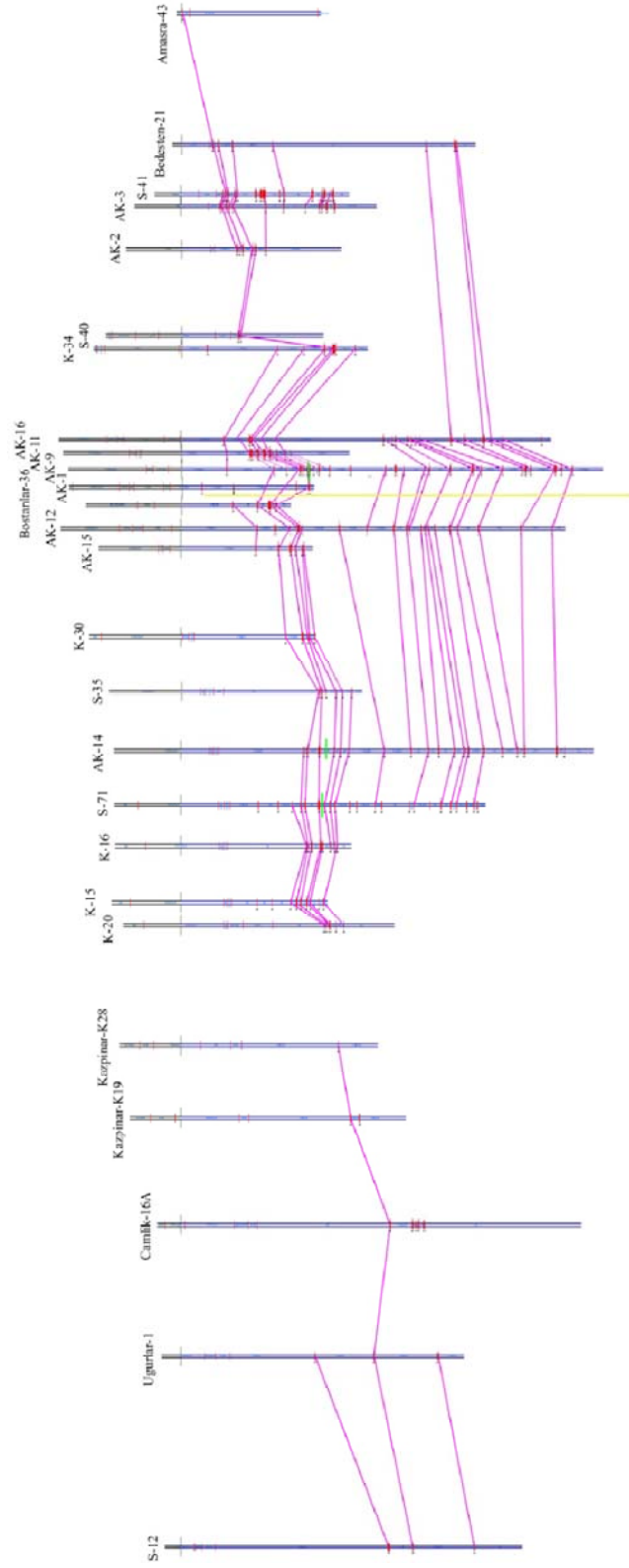
Figure C.13. Correlation of the Seams found on the Vertical Area 4

325
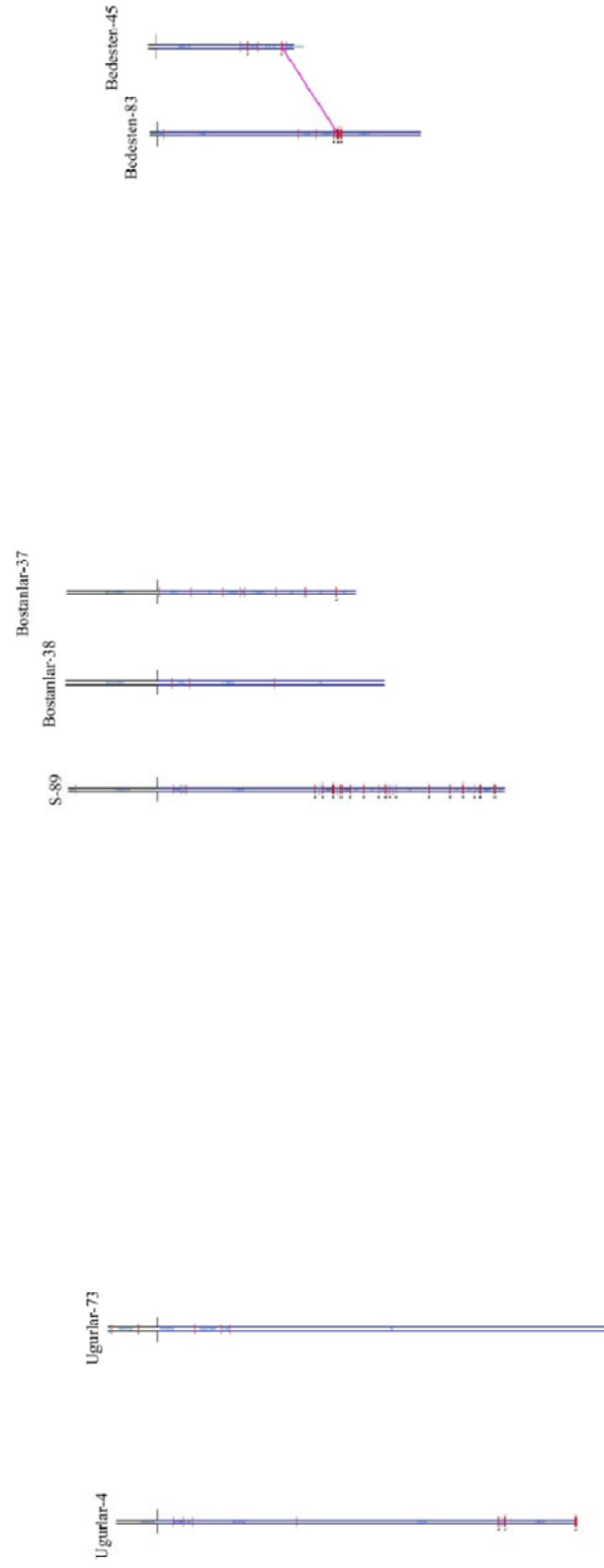
Figure C.14. Correlation of the Seams found on the Vertical Area 5

326

APPENDIX D

Results of the correlation studies are given in following tables.

Table D.1. Coal Layer#1

Hor. Area 1	Hor. Area 2	Ver. Area 3	Ver. Area 4
Gömü-85 – I	Gömü-80 – I	Askersuyu-31 – V	AK2 – III
Gömü-86 – III	Gömü-27 – II	Gömü-29 – II	AK3 – III
S47 – II	AK5 – III	Gömü-86 – III	S41 – III
Bedesten-21 – II	Gömü-29 – II		Bedesten-21 – II
AK3 – III	Askersuyu-31 – V		K34 – IV
S41 - III	AK16 – II		AK16 – II
	S40 – I		AK11 – V
	AK11 – V		AK9 – IV
	AK9 – IV		

Table D.2. Coal Layer#2

| Hor. Area 3	Hor. Area 4	Ver. Area 3	Ver. Area 4
AK4 - VII	S71 - VI	S34 - V	Bostanlar 36 - III
AK13 - V	K16 - IV	AK4-VII	AK 12 - VI
S34 - V	K20 - III	AK13-V	AK 15 - III
AK12 - VI	K10 - IV		K30 - II
K30 - II	K14 - IV		S35 - II
AK15 - III	S74 - IV		AK14 - III
S35 - II	K13 - IV		S71 - VI
AK14 - III	K15 - VI		K16 - IV
S89 - III			K15 - VI
			K20 - III

Table D.3. Coal Layer#3

Hor. Area 1	Hor. Area 2	Ver. Area 2	Ver. Area 3	Ver. Area 4
Gömü 85 - II	Gömü K24 - III	AK 7 - I	Gömü 86 - V	S 41 - XII
Gömü 86 - V	AK 7 - I	AK 5 - XV	Gömü 29 - VI	AK 3 - VIII
S 47 - V	Gömü K27 - II	Gömü K24 - III		
AK 3 - VIII	Gömü 80 - II	Gömü 27 - V		
S 41 - XII	Gömü 27 - V	Gömü 85 - II		
	AK 5 - XV			
	Gömü 29 - VI			

Table D.4. Coal Layer#4

Hor. Area 1	Hor. Area 2	Ver. Area 3	Ver. Area 4
Gömü 86 - I	Gömü 27 - I	Gömü 86 - I	Amasra 43 - I
S 47 - I	AK 5 - I	Gömü 29 - I	Bedesten 21 - I
Bedesten 21 - I	Gömü 29 - I	Askersuyu 31 - IV	S 41 - II
AK 3 - II	Askersuyu 31 - IV		AK 3 - II
S 41 - II	AK 16 - I		AK 2 - I
Bedesten 83 - II	AK 11 - I		AK 16 - I
	AK 9 - I		AK 9 - I
			AK 11 - I

Table D.5. Coal Layer#5

Hor. Area 1	Hor. Area 2	Ver. Area 3	Ver. Area 4
Gömü 86 -IV	Gömü 27 - III	Gömü 86 - IV	AK9 - VI
S 47 - III	AK 5 - IV	Gömü 29 - III	AK11 - VII
Bedesten 21 - III	Gömü 29 - III	Askersuyu 31 - VI	AK16 - III
AK 3 - V	Askersuyu 31 - VI		S40 -I
S 41 - V	AK 16 - III		AK2 - IV
	AK 11 - VII		AK3 - V
	AK 9 - VI		S41 - V
			Bedesten 21 - III

Table D.6. Coal Layer#6

Hor. Area 1	Ver. Area 4
S 47 - IV	Bedesten 21 - IV
Bedesten 21 - IV	S 41 - XI
AK 3 - VII	AK 3 - VII
S 41 - XI	

Table D.7. Coal Layer#7

Hor. Area 1	Ver. Area 4
S 47 - VI	S 41 - XIII
AK 3 - IX	AK 3 - IX
S 41 - XIII	

Table D.8. Coal Layer#8

Hor. Area 1	Ver. Area 4
S 47 - VII	S 41 - XIV
AK 3 - X	AK 3 - X
S 41 - XIV	

Table D.9. Coal Layer#9

Hor. Area 1	Ver. Area 4
S 47 - VIII	S 41 - XVI
AK 3 - XII	AK 3 - XII
S 41 - XVI	

Table D.10. Coal Layer#10

Hor. Area 1	Ver. Area 4
AK 3 - VI	AK 2 - VI
S 41 - IX	AK 3 - VI
	S 41 - IX

Table D.11. Coal Layer#11

Hor. Area 2	Ver. Area 2
Gömü K24 - II	Gömü 27 - IV
Gömü K27 - I	AK 5 - XIII
Gömü 27 - IV	Gömü K24 - II
AK 5 - XIII	

Table D.12. Coal Layer#12

Hor. Area 2
Gömü K24 - IV
AK 7 - III
Gömü K27 - IV

Table D.13. Coal Layer#13

Hor. Area 2	Ver. Area 4
Gömü K24 - V	AK 16 - XIII
AK 16 - XIII	Bedesten 21 - VI
AK 9 - XXVI	AK 9 - XXVI

Table D.14. Coal Layer#14

Hor. Area 3	Ver. Area 4
AK 12 - XX	AK 12 - XX
AK 14 - XVII	AK 14 - XVII
Amasra 50 - XI	

Table D.15. Coal Layer#15

Hor. Area 2	Ver. Area 4
Gömü K27 - VII	AK 16 - IV
Gömü 80 - III	AK 9 - XVIII
Gömü 27 - VI	
AK 16 - IV	
AK 9 - XVIII	

Table D.16. Coal Layer#16

Hor. Area 2	Hor. Area 3	Hor. Area 4	Ver. Area 4
AK 9 - XIX	AK 12 - XIV	S 71 - XVI	AK 9 - XIX
	AK 14 - XI	S 74 - XIII	AK 12 - XIV
			AK 14 - XI
			S 71 - XVI

Table D.17. Coal Layer#17

Hor. Area 2	Hor. Area 3	Ver. Area 4
AK 9 - XX	AK 12 - XVII	AK 9 - XX
	AK 14 - XIV	AK 12 - XVII
		AK 14 - XIV
		S 71 - XX

Table D.18. Coal Layer#18

Hor. Area 2	Hor. Area 3	Ver. Area 4
AK 16 - VIII	AK 12 - XVIII	AK 16 - VIII
AK 9 - XXI	AK 14 - XV	AK 9 - XXI
		AK 12 - XVIII
		AK 14 - XV

Table D.19. Coal Layer#19

Hor. Area 2	Hor. Area 3	Ver. Area 4
AK 16 - X	AK 12 - XIX	AK 16 - X
AK 9 - XXII	AK 14 - XVI	AK 9 - XXII
		AK 12 - XIX
		AK 14 - XVI

Table D.20. Coal Layer#20

Hor. Area 2	Ver. Area 4
AK 16 - XI	AK 16 - XI
AK 9 - XXIV	AK 9 - XXIV
	Bedesten 21 - V

Table D.21. Coal Layer#21

Hor. Area 2	Ver. Area 4
AK 16 - XIV	AK 16 - XIV
AK 9 - XXVII	AK 9 - XXVII
	Bedesten 21 - VII

Table D.22. Coal Layer#22

Hor. Area 2	Hor. Area 3	Ver. Area 4
AK 16 - XV	AK 12 - XXI	AK 16 - XV
AK 9 - XXVIII	AK 14 - XVIII	AK 9 - XXVIII
		AK 12 - XXI
		AK 14 - XVIII

Table D.23 (a). Coal Layer#23

Hor. Area 2	Hor. Area 3	Hor. Area 4	Hor. Area 5
Bostanlar 36 - IV	AK 12 - VII	Kazpınar K12 - V	Kazpınar 63 - III
AK 11 - VIII	S 34 - VI	K11 - VI	Kazpınar K3 - VII
AK 9 - VII	AK 13 - VI	Kazpınar 51 - III	Sondaj 13 - IV
	AK 4 - VIII	Kazpınar 64 - III	
	K 30 - III		
	AK 15 - IV		
	S 35 - III		
	Kuskayası 32 - VI		
	Gomu K37 - VIII		
	Amasra 50 - IX		
	AK 6 - X		

Table D.23 (b). Coal Layer#23

Vor. Area 2	Ver. Area 3	Ver. Area 4
Gomu K37 - VIII	S34 - VI	AK 9 - VII
AK 6 - X	Kuskayası 32 - VI	AK 11 - VIII
Amasra 50 - IX	AK 4 - VIII	Bostanlar 36 - IV
Kazpınar 64 - III	AK 13 - VI	AK 12 - VII
Kazpınar 63 - III	Kazpınar K12 - V	AK 15 - IV
Kazpınar K3 - VII	K 11 - VI	K30 - III
		S35 - III

Table D.24 (a). Coal Layer#24

Hor. Area 2	Hor. Area 3	Hor. Area 4	Hor. Area 5
Bostanlar 36 - II	AK 12 - IV	S 71 - V	K 18 - I
AK 11 - II	K 30 - I	K 16 - III	Kazpınar K22 - I
AK 9 - II	AK 15 - II	K 10 - III	
	S 35 - I	K 14 - III	
	AK 14 - II	S 74 - III	
	S 89 - II	K 13 - III	
	S 34 - IV	K 15 - V	
	AK 13 - IV	Kazpınar K12 - II	
	AK 4 - VI	K 11 - III	

Table D.24 (b). Coal Layer#24

Ver. Area 3	Ver. Area 4
S 34 - IV	Bostanlar 36 - II
AK 4 - VI	AK 9 - II
AK 13 - IV	AK 11 - II
Kazpınar K12 - II	AK 12 - IV
K 11 - III	AK 15 - II
S 33 - I	K 30 - I
S 6 - I	S 35 - I
K 18 - I	AK 14 - II
Kazpınar K22 - I	S 71 - V
	K 16 - III
	K 15 - V

Table D.25. Coal Layer#25

Hor. Area 3	Ver. Area 2
Çömlekkıran 65 - I	Amasra 50 - I
Amasra 50 - I	Uzunoz 15 - I

Table D.26 (a). Coal Layer#26

Hor. Area 3	Hor. Area 4	Hor. Area 5	Hor. Area 6
Çomlekkıran 65 - II	Uzunoz 15 - IV	Kazpinar 18 - I	Kaman 14 - I
Tarlaagzi 22 - I	Kazpinar 64 - I	Sondaj 13 - II	Kazpinar 69 - I
Tarlaagzi 26 - I	Kazpinar 51 - I	Kazpinar 63 - I	Kaman 10 - I
AK 6 - VI	K11 - I	Kazpinar K3 - III	Kazpinar K1 - I
Amasra 50 - VII	Kazpinar K12 - I	Kazpinar K6 - II	Kazpinar K4 - I
Gomu K37 - VII		Kazpinar 62 - I	Kazpinar K5 - I
Kuskayasi 32 - V		K21 - I	Kazpinar 20 - I
AK 4 - IV		Kazpinar 78 - I	Kazpinar K25 - I
S 34 - III			Kaman 61 - I
AK 12 - I			
AK 15 - I			

Table D.26 (b). Coal Layer#26

Hor. Area 7	Hor. Area 9
Kaman 39 - I	Fermitkadi 55 - I
Kaman 60 - I	Karacay 11 - I
Kaman 58 - I	

Table D.26 (c). Coal Layer#26

Ver. Area 1	Ver. Area 2	Ver. Area 3	Ver. Area 4
Çomlekkıran 65 - II	Tarlaagzi 26 - I	Kuskayasi 32 - V	AK 12 - I
Tarlaagzi 22 - I	AK 6 - VI	AK 4 - IV	AK 15 - I
Çomlekkıran 66 - I	Gomu K37 - VII	S 34 -III	
Kazpinar 18 - I	Amasra 50 - VII	K21 - I	
Kaman 14 - I	Uzunoz 15 - IV	Kazpinar 62 - I	
Kaman 39 - I	Kazpinar 64 - I	Kaman 61 - I	
Fermitkadi 55 - I	Kazpinar 63 - I	Kazpinar K5 - I	
	Kazpinar K3 -III	Kazpinar 20 - I	
	Kazpinar K2 - I	Kazpinar K25 - I	
	Kazpinar 69 - I	Kazpinar 78 - I	
	Kazpinar K1 - I	K11 - I	
	Kazpinar K4 - I	Kazpinar K12 - I	
	Kaman 10 - I		
	Kaman 60 - I		
	Kaman 58 - I		
	Karacay 11 - I		

Table D.27. Coal Layer#27

Hor. Area 3	Ver. Area 2
Tarlaagzi 26 - II	Tarlaagzi 26 - II
AK 6 - VII	AK 6 - VII
Amasra 50 - VIII	

Table D.28. Coal Layer#28

Hor. Area 3	Ver. Area 2	Ver. Area 3
AK 6 - II	Uzunoz 15 - II	Kuskayasi 32 - I
Amasra 50 - V	Amasra 50 - V	AK 4 - I
Gomu K37 - III	Gomu K37 - III	AK 13 - I
Kuskayasi 32 - I	AK 6 - II	
AK 4 - I		
AK 13 - I		

Table D.29. Coal Layer#29

Hor. Area 3	Ver. Area 2
AK 6 - IV	AK 6 - IV
Amasra 50 - VI	Amasra 50 - VI
Gomu K37 - IV	Gomu K37 - IV
Kuskayasi 32 - II	

Table D.30. Coal Layer#30

Hor. Area 3	Ver. Area 2	Ver. Area 3
AK 6 - V	AK 6 - V	Kuskayasi 32- III
Gomu K37 - V	Gomu K37 - V	AK 4 - II
Kuskayasi 32- III		AK 13 - II
AK 4 - II		S 34 - I
AK 13 - II		
S 34 - I		

Table D.31 (a). Coal Layer#31

Hor. Area 3	Hor. Area 4	Hor. Area 5	Hor. Area 6
AK 6 - XI	Kazpinar K12 - IX	Kazpinar 18 - II	Kaman 14 - II
Amasra 50 - X	K 11 - IX	Sondaj 13 - V	Kazpinar 69 - II
Gomu K37 - IX		Kazpinar 63 - IV	Kazpinar K1 - VI
Kuskayasi 32 - VII		Kazpinar K3 - VIII	
AK 4 - XI		Ugurlar 3 - I	
AK 13 - IX		Kazpinar K6 - VI	
S 34 - VII			

Table D.31 (b). Coal Layer#31

Ver. Area 1	Ver. Area 2	Ver. Area 3
Kazpinar 18 - II	AK 6 - XI	Kuskayasi 32 - VII
Kaman 14 - II	Gomu K37 - IX	S 34 - VII
	Amasra 50 - X	AK 4 - XI
	Kazpinar 64 - IV	AK 13 - IX
	Kazpinar 63 - IV	Kazpinar K12 - IX
	Kazpinar K3 - VIII	K 11 - IX
	Ugurlar 3 - I	
	Kazpinar K2 - II	
	Kazpinar K1 - VI	
	Kazpinar 69 - II	

Table D.32. Coal Layer#32

Hor. Area 3	Ver. Area 2	Ver. Area 3	Ver. Area 4
AK 6 - XV	AK 6 - XV	Kuskayasi 32 - VIII	AK 12 - VIII
Gomu K37 - X	Gomu K37 - X	AK 4 - XII	AK 14 - VII
Kuskayasi 32 - VIII		AK 13 - X	S 71 - XII
AK 4 - XII			
AK 13 - X			
AK 12 - VIII			
AK 14 - VII			
S 89 - XII			

Table D.33. Coal Layer#33

Hor. Area 3	Ver. Area 3
Gomu K37 - VI	Kuskayasi 32 - IV
Kuskayasi 32 - IV	S 34 - II
AK 4 - III	AK 4 - III
AK 13 - III	AK 13 - III
S 34 - II	

Table D.34. Coal Layer#34

Hor. Area 3	Hor. Area 4	Hor. Area 5	Ver. Area 3
AK 4 - IX	Kazpınar K12 - VI	K 18 - III	AK 4 - IX
AK 13 - VII	K11 - VII	Kazpınar K22 - II	AK 13 - VII
			Kazpınar K12 - VI
			K 11 - VII
			S 33 - II
			K 18 - III
			Kazpınar K22 - II

Table D.35. Coal Layer#35

Hor. Area 3	Hor. Area 4	Ver. Area 2	Ver. Area 3
AK 4 - X	Kazpınar K12 - VII	Kazpınar 64 - V	AK 4 - X
AK 13 - VIII	K 11 - VIII	Uzunoz 15 - VI	AK 13 - VIII
	Kazpınar 51 - IV		Kazpınar K12 - VII
	Kazpınar 64 - V		K 11 - VIII
	Uzunoz 15 - VI		

Table D.36. Coal Layer#36

Hor. Area 3	Hor. Area 4	Ver. Area 4
K 30 - IV	S 71 - VII	K 30 - IV
AK 15 - V	K 16 - VI	AK 15 - V
S 35 - IV	K 20 - V	S 35 - IV
AK 14 - IV	K 10 - VI	AK 14 - IV
S 89 - VI		S 71 - VII
		K 16 - VI

Table D.37. Coal Layer#37

Hor. Area 3	Hor. Area 4	Ver. Area 4
K30 - V	S 71 - VIII	K 30 - V
AK 15 - VI	K 16 - VII	AK 15 - VI
S 35 - V	K 10 - VII	S 35 - V
AK 14 - V		AK 14 - V
S 89 - VII		S 71 - VIII
		K 16 - VII

Table D.38. Coal Layer#38

Hor. Area 3	Ver. Area 4
AK 12 - IX	AK 12 - IX
S 89 - XIII	AK 9 - XIII

Table D.39. Coal Layer#39

Hor. Area 3	Ver. Area 4
AK 12 - X	AK 12 - X
AK 14 - VIII	AK 9 - XVI
S 89 - XIV	AK 14 - VIII

Table D.40. Coal Layer#40

Hor. Area 3	Hor. Area 4	Ver. Area 4
AK 12 - XI	S 71 - XV	AK 12 - XI
AK 14 - IX	S 74 - XI	AK 9 - XVII
S 89 - XVI		AK 14 - IX
		S 71 - XV

Table D.41. Coal Layer#41

Hor. Area 3	Ver. Area 4
AK 12 - XIII	AK 12 - XIII
AK 14 - X	AK 14 - X
S 89 - XVII	

Table D.42. Coal Layer#42

Hor. Area 3	Hor. Area 4	Ver. Area 4
AK 12 - XV	S 71 - XVII	AK 12 - XV
AK 14 - XII	S 74 - XIV	AK 14 - XII
		S 71 - XVII

Table D.43. Coal Layer#43

Hor. Area 3	Hor. Area 4	Ver. Area 4
AK 12 - XVI	S 71 - XVIII	AK 12 - XVI
AK 14 - XIII	S 74 - XV	AK 14 - XIII
		S 71 - XVIII

Table D.44. Coal Layer#44

Hor. Area 3	Hor. Area 4	Ver. Area 4
S 35 - VI	S 71 - IX	S 35 - VI
AK 14 - VI	K 16 - VIII	AK 14 - VI
S 89 - VIII	K 20 - VI	S 71 - IX
	K 10 - VIII	K 16 - VIII
	K 14 - VI	K 15 - IX
	S 74 - VI	K 20 - VI
	K 15 - IX	

Table D.45. Coal Layer#45

Hor. Area 3	Hor. Area 4	Ver. Area 4
AK 14 - I	S 71 - IV	AK 14 - I
S 89 - I	K 16 - II	S 71 - IV
	K 20 - II	K 16 - II
	K 10 - II	K 15 - IV
	K 14 - II	K 20 - II
	S 74 - II	
	K 15 - IV	

Table D.46. Coal Layer#46

Hor. Area 4	Hor. Area 5	Ver. Area 2	Ver. Area 3
Uzunoz 15 - V	Kazpınar 63 - II	Uzunoz 15 - V	K 11 - IV
Kazpınar 64 - II	Sondaj 13 - III	Kazpınar 64 - II	Kazpınar K12 - IV
Kazpınar 51 - II	Kazpınar K3 - VI	Kazpınar 63 - II	Kazpınar 62 - III
K 11 - IV	Kazpınar K6 - V	Kazpınar K3 - VI	K 21 - II
Kazpınar K12 - IV	Kazpınar 62 - III		
	K21 - II		

Table D.47 (a). Coal Layer#47

Hor. Area 4	Hor. Area 5	Hor. Area 6
Uzunoz 15 - VII	Kazpınar 63 - V	Kazpınar 7 - II
Kazpinar 64 - VI	Sondaj 13 - VI	Kazpınar K23 - I
Kazpinar K12 - XI	Kazpınar K3 - IX	Kazpınar K25 - III
	Ugurlar 3 - III	Kazpınar 20 - III
	Kazpınar 78 - III	Kazpınar K5 - II
	Kazpınar K31 - I	Kazpınar K4 - VII
	Kazpınar K19 - I	Kaman 10 - II
	Kazpınar K22 - V	Camlık 16A - I
	Kazpınar K28 - I	Ugurlar 1 - II

Table D.47 (b). Coal Layer#47

Ver. Area 2	Ver. Area 3	Ver. Area 4
Uzunoz 15 - VII	Kazpınar 78 - III	Kazpınar K28 - I
Kazpinar 64 - VI	Kazpınar K22 - V	Kazpınar K19 - I
Kazpınar 63 - V	Kazpınar 7 - I	Camlik 16A- I
Kazpınar K3 - IX	Kazpınar K25 - III	Ugurlar 1 - II
Ugurlar 3 - III	Kazpınar K23 - I	S12 - II
Kazpınar K4 - VII	Kazpınar 20 - III	
Kaman 10 - II	Kazpınar K5 - II	

Table D.48. Coal Layer#48

Hor. Area 4	Ver. Area 4
K 15 - III	K 15 - III
S 74 - I	K 20 - I
K 14 - I	K 16 - I
K 10 - I	S 71 - III
K 20 - I	
K 16 - I	
S 71 - III	

Table D.49. Coal Layer#49

Hor. Area 4	Ver. Area 4
K 15 - VII	K 15 - VII
S 74 - V	K 20 - IV
K 14 - V	K 16 - V
K 10 - V	
K 20 - IV	
K 16 - V	

Table D.50. Coal Layer#50

Hor. Area 4
S 74 - VIII
K 10 - IX
S 71 - X

Table D.51. Coal Layer#51

Hor. Area 4
S 74 - IX
K 10 - X
S 71 - XI

Table D.52. Coal Layer#52

Hor. Area 5	Hor. Area 6	Ver. Area 2	Ver. Area 3
Kazpınar K3 - X	Kazpınar 7 - III	Kazpınar K3 - X	Kazpınar 78 - IV
Ugurlar 3 - V	Kazpınar K23 - II	Ugurlar 3 - V	Kazpınar K22 - VI
Kazpınar 78 - IV	Kazpınar K25 - IV		Kazpınar 7 - III
Kazpınar K31 - II	Kazpınar 20 - IV		Kazpınar K25 - IV
Kazpınar K19 - II	Kazpınar K4 - VIII		Kazpınar K23 - II
Kazpınar K22 - VI			Kazpınar 20 - IV

Table D.53. Coal Layer#53

Hor. Area 6	Ver. Area 2
Kaman 14 - III	Kazpınar 69 - III
Kazpınar 69 - III	Kazpınar K2 - III
Kazpınar K1 - VII	Kazpınar K1 - VII
Kazpınar K5 - III	

Table D.54. Coal Layer#54

Hor. Area 6	Ver. Area 2	Ver. Area 3
Kaman 14 - IV	Kazpınar 69 - IV	Kazpınar K5 - IV
Kazpınar 69 - IV	Kazpınar K1 - VIII	Camlık 56 - I
Kazpınar K1 - VIII		Kazpınar 7 - VIII
Kazpınar K5 - IV		
Kazpınar 7 - VIII		
Camlık 56 - I		
Camlık 16A - II		

Table D.55. Coal Layer#55

Hor. Area 6	Ver. Area 2
Kazpınar K1 - III	Kazpınar K1 - III
Kazpınar K4 - IV	Kazpınar K4 - IV
Kaman 61 - III	

Table D.56. Coal Layer#56

Hor. Area 6	Ver. Area 3
Kazpınar K4 - II	Kazpınar 20 - II
Kazpınar 20 - II	Kazpınar K25 - II
Kazpınar K25 - II	Kaman 61 - II
Kaman 61 - II	Kazpınar 78 - II

Table D.57. Coal Layer#57

Hor. Area 6	Ver. Area 3
Kazpınar 7 - IX	Kazpınar 7 - IX
Camlık 56 - II	Camlık 56 - II
Camlık 16A - III	

Table D.58. Coal Layer#58

Hor. Area 6	Ver. Area 3
Kazpınar 7 - X	Kazpınar 7 - X
Camlık 56 - III	Camlık 56 - III
Camlık 16A - IV	

Table D.59. Coal Layer#59

Hor. Area 6	Ver. Area 4
Ugurlar 1 - IV	Ugurlar 1 - IV
Ugurlar 4 - II	S 12 - III

Table D.60. Coal Layer#60

Hor. Area 7	Hor. Area 9	Ver. Area 2
Kaman 60 - II	Karacay 11 - VI	Kaman 60 - II
Kaman 58 - II	Uzunoz 82 - II	Kaman 58 - II
	Fermitkadı 55 - III	Karacay 11 - VI
		Uzunoz 82 - II

338

Table D.61. Coal Layer#61

Hor. Area 7	Hor. Area 8	Ver. Area 3	Ver. Area 4
Kaman 75 - I	Ugurlar 2 - X	Kaman 75 - I	S12 - I
Camlik 77 - I	Sibben 48 - II	Camlık 77 - I	Ugurlar 1 - I
S 12 - I	Karacay K29 - VIII	Ugurlar K26 - I	
		Ugurlar 2 - X	
		Karacay K29 - VIII	
		Sibben 48 - II	

Table D.62. Coal Layer#62

Hor. Area 8	Ver. Area 3
Karacay K29 - VII	Karacay K29 - VII
Ugurlar 2 - VIII	Ugurlar 2 - VIII
Sibben 48 - I	Sibben 48 - I

Table D.63. Coal Layer#63

Hor. Area 9	Ver. Area 2
Fermitkadı 55 - II	Uzunoz 82 - I
Uzunoz 82 - I	Karacay 9 - I
Karacay 9 - I	Karacay 11 - IV
Karacay 11 - IV	

CURRICULUM VITAE

ADDRESS

- Home: Vadikent Sitesi, Gumussehir Apt. No:11/1, Cayyolu, Ankara, TURKEY
- Office: Petroleum Research Center (PAL), LPG Laboratories, Middle East Technical University (METU), 06531 Ankara, TURKEY
- Tel: (Home) (+90) (312) 242 05 25 (Office) (+90) (312) 210 56 59
- E-mail caglars@metu.edu.tr, caglar@sinayuc.com

PERSONAL INFORMATION

- Date of Birth: 30th of May, 1975
- Place of Birth: Ankara, TURKEY
- Nationality: Turkish
- Marital Status: Married and has a son.
- Gender: Male

EDUCATION HISTORY

- PhD: METU – Petroleum & Natural Gas Engineering Department
  'Modelling of Enhanced Coalbed Methane Recovery from Amasra Coalbed in Zonguldak Basin', July 2007, CGPA: 3.36/4.00.
- MSc: METU – Petroleum & Natural Gas Engineering Department
  'Prediction of the Phase Behavior of a Gas-Condensate System: Computer Modeling Study', September 2001, CGPA:3.86/4.00.
- BSc: METU – Petroleum & Natural Gas Engineering Department
  June, 1998, CGPA: 3.28/4.00, First rank in the class.
- High School: Ankara Anatolian High School - French Division
  June, 1993.

WORK EXPERIENCE

2001-present: Petroleum Research Center (PAL), METU, Ankara, TURKEY

- LPG Laboratory Lab Coordinator (2001 – present), first LPG Lab in Turkey has been established,
- Quality Manager (2003 – present), Petroleum Research Center has been accredited according to ISO 17025 standard.

1998-2001: Petroleum & Natural Gas Engineering Department, METU, Ankara, TURKEY

- Research and Teaching Assistant, METU Petroleum and N.G. Eng. Dept.
- Lab Assistant, PETE 216, Reservoir Rock and Fluid Properties
- Course Assistant, PETE 441, Petroleum Reservoir Engineering II
- Course Assistant and Recitation Lecturer, PETE 461, Natural Gas Engineering

1996 Summer:

Trainee, Schlumberger Wireline and Testing, Shukheir, EGYPT, A report on "Mechanical Plug Back Tool" has prepared and presented.

1995 Summer:

Trainee, TPAO, Adiyaman, TURKEY, Drilling of "Ozan Sungurlu 6" well has observed.

SKILLS

Computer:

- Computer Modelling Group – Generalized Equation-of-State Model Compositional Reservoir Simulator (GEM) Module
- Palisade @Risk Risk Analysis Tool
- Basic, Fortran, C, C++, C# Programming
- Microsoft Visual Studio.net
- Microsoft Office Applications (Word, Excel, PowerPoint, Access)
- Macromedia Applications (Flash, Dream weaver)
- SQL

Language:

- Turkish (Native)
- English (Fluent)
- French (Good)
- Russian (Poor)

PAPERS & PROCEEDINGS

- Sinayuc, C., Gumrah, F.: "Modeling of Enhanced Coalbed Methane Recovery in a Coalbed at Zonguldak Basin", 16th International Petroleum Congress and Exhibition of Turkey, May 29-31, 2007 ANKARA
- Sinayuc, C., Gumrah, F.: "Predicting the Critical Properties of Heptanes-Plus in Gas-Condensates: Genetic Algorithms as an Optimization Tool", 5th Canadian International Petroleum Conference, 6-8 October 2004, Calgary, Canada.
- Sinayuc, C., Gumrah, F.: "Model for Gas-Condensate Phase Equilibria for Estimating C7+ Critical Properties Using Genetic Algorithm", Transport in Porous Media, Vol. 55, pp. 201-214, 2004.
- Okandan, E, Sınayuç, Ç.: "Otogaz'da Kalite", LPG ve CNG Uygulamaları Sempozyumu, 14 Aralık 2002, ANKARA.
- Sınayuç, Ç., Gumrah, F.:"Gaz Kondensat Faz Davranışlarının Tahmin Edilmesi", 13th International Petroleum Congress and Exhibition of Turkey, June 04-06, 2001 ANKARA
- Sınayuç, Ç., Küçükekşi M.S., Gümrah, F.: "Bir Yeraltı Gaz Deposu Rezervuarından Gaz Üretiminin Optimizasyonu", Türkiye 8. Enerji Kongresi, May 08-12, 2000 ANKARA
- Sinayuc, C., Kucukeksi M.S., Gumrah, F.:"Optimization of Energy Production from an Underground Gas Storage Reservoir", Energy Sources, Vol:22, No.5, June 2000

PROJECTS ATTENDED

- Carbon dioxide Capture and Storage, TUBITAK, 2007 - In Progress.

- Natural Gas Demand Modelling & Projection for Turkish Market, BOTAS Company, 2002-2004, done by PAL, METU, Ankara.

- NATO CCMS Short Term AD-HOC Project: Environmental Security of Hazardous Substances involved in Oil & Gas Transportation in Black Sea & Caspian Regions, 2001, done by PAL, METU, Ankara.

HOBBIES

- Chess, Table Tennis, Swimming, Billiards